Characterising embryonic stem cell-derived tenocytes and determining the changing role of scleraxis during tendon development

Yasmin Zoe Paterson

Department of Veterinary Medicine

University of Cambridge

This thesis is submitted for the degree of

Doctor of Philosophy

Darwin College

October 2020

This dissertation is dedicated to my loving family.

Preface

This dissertation is the result of my own work and includes nothing which is the outcome of work done in collaboration except as declared in the preface and specified in the text. It is not substantially the same as any work that has already been submitted before for any degree or other qualification except as declared in the preface and specified in the text. It does not exceed the prescribed word limit of 60,000 words, exclusive of figures, tables, footnotes, bibliography, and appendices as set by the Degree Committee.

On the 23rd of March 2020, during the final year of this PhD, the Prime Minister placed the United Kingdom on a police-enforced lockdown to prevent the spread of Coronavirus (COVID19). This lockdown was enforced for several months, and as a result of the financial pressure arising as a result of the pandemic, my host institute the Animal Health Trust closed from the 23rd of March, entering compulsory liquidation on the 31st July 2020. As such some aspects of the thesis were not completed.

However, the majority of the work presented on the transcriptomic differences between adult, fetal and ESC-derived tenocytes described in chapter 3 has been published in (Paterson et al. 2020; *Stem Cell Research & Therapy*). Likewise, the bulk of the work describing the effect of knocking down scleraxis in adult, fetal and ESC-derived tenocytes outlined in chapter 4 & 5 has been published in (Paterson et al. 2020; *Mechanisms of Development*), with both manuscripts being written by myself under the guidance of my supervisor.

Yasmin Zoe Paterson

October 2020

Acknowledgements

There are many people who deserve thanks for their numerous and varied contributions to this thesis. First and foremost, I would like to thank Dr Debbie Guest for accepting me on this PhD, for her continual advice and guidance, and for performing the initial research which made this work possible. Your incredible support and encouragement throughout my time at the Animal Health Trust (AHT) has been invaluable and I thank you for helping me mature into the scientist that I am today. Many thanks also go to everyone at the AHT, past and present, for making me feel so welcome and to those who have helped with techniques and ideas along the way. In particular, Alyce McClellan for not only her support in the laboratory, but also for providing invaluable emotional support and friendship; you will always be my number one "walkies" buddy.

I would also like to thank my AHT mentor, Dr Sally Ricketts, for providing lots of help and advice during our coffee catchups. To Dr Fran Henson, my initial secondary supervisor at Cambridge University, I thank you for your support and encouragement, as well as Dr Barbara Blacklaws for stepping in at the last minute to take over my supervision. I would also like to express my gratitude to Dr Adam Cribbs and Ellen Schofield, for all your help and advice with the RNA-sequencing analysis and for being so patient with me during the learning process. To Emma Goodfellow for collecting the tissue samples used throughout this thesis, thank you.

Importantly, I would like to express my endless gratitude to my amazing family who have supported me throughout my studies. In particular to my parents, brother and sister-in-law, thank you for always being there at the other end of the phone and for all your love and well wishes. Very special thanks go to my partner, Joji, for being by my side in everything I do, for your constant encouragement throughout my studies, without which this wouldn't have been possible. Also, thanks go to Denise and Naoki for your incredible kindness and support.

Thanks finally go to the BBSRC-DTP programme and the PetPlan Charitable Trust for funding this work and to Mind the Graph for supplying the infographics used throughout this thesis.

Abstract

Tendon injuries occur commonly in equine athletes. Adult tendons undergo poor natural regeneration, resulting in scar-tissue which is prone to re-injury. Fetal tendons however are capable of completely scar-less regeneration, a property which is intrinsic to the fetal cells themselves. Novel cell therapies should therefore try to recapitulate this scar-less fetal tendon regeneration. This thesis builds on previous research into the use of horse embryonic stem cells (ESCs) to aid tendon regeneration. The aim of this thesis was to determine if tendon cells derived from ESCs were more similar to fetal or adult tendon cells, as well as try to understand if scleraxis (SCX), an essential gene in tendon formation, has different roles at different stages of tendon development.

Equine adult, fetal and ESC-derived tenocytes were cultured in a three-dimensional environment, with histological, morphological and transcriptomic differences compared. Additionally, the effects on gene expression of culturing adult and fetal tenocytes in either conventional two-dimensional monolayer culture or three-dimensional culture was compared using RNA-sequencing. No qualitative differences in three-dimensional tendon constructs generated from adult, fetal and ESCs were found using histological and morphological analysis. However, genome wide transcriptomic analysis using RNA-sequencing revealed that ESC-derived tenocytes transcriptomic profile more closely resembled fetal tenocytes as opposed to adult tenocytes. Furthermore, this thesis adds to the growing evidence that monolayer cultured cells gene expression profiles converge, with adult and fetal tenocytes having only 10 differentially expressed (DE) genes when cultured in this manner. In contrast, when adult and fetal tenocytes were cultured in three-dimensional culture, large distinctions in gene expression between these two developmental stages were found, with 542 genes being DE.

The effects of knocking down the expression of SCX on gene expression in adult, fetal and ESC-derived tenocytes was then determined using RNA-sequencing and qPCR. SCX knockdown had a larger effect on gene expression in fetal tenocytes, affecting 477 genes in comparison to the 183 genes effected in adult tenocytes, indicating that scleraxis-dependent processes differ in these two developmental stages. Gene ontology, network and pathway analysis revealed an overrepresentation of extracellular matrix (ECM)

remodelling processes within both comparisons. These included several matrix metalloproteinases, proteoglycans and collagens, some of which were also investigated in SCX knockdown tenocytes from young postnatal foals. Using chromatin immunoprecipitation, novel genes that SCX differentially interacts with in adult and fetal tenocytes were identified. SCX knockdown in ESCs resulted in upregulation of cartilage markers, a result which still needs to be confirmed in further biological replicates.

In summary, the data presented in this thesis provides an unprecedented insight into some of the differences between fetal regenerative and adult reparative tenocytes. It also indicated that ESC-derived tenocytes are more similar to fetal rather than adult tenocytes, highlighting their potential as a therapeutic cell source. The results presented also indicate a role for SCX in modulating ECM synthesis and breakdown and provides a useful dataset for further study into SCX gene regulation. Taken together this data is likely to be important for the future development of novel cellular or pharmacological therapeutics.

Contents

Abbreviations

Abbreviation	Description
2D	Two-dimensional
3D	Three-dimensional
ASC	Adipose derived mesenchymal stem cell
AT	Achilles tendon
bHLH	Basic helix-loop-helix
BMSC	Bone marrow derived mesenchymal stem cell
bp	Base pair
cDNA	Complementary DNA
ChIP	Chromatin immunoprecipitation
CMV	Cytomegalovirus
Ct	Cycle threshold
CTGF	Connective tissue growth factor
DE	Differentially expressed
DMEM	Dulbecco's Modified Eagle's Medium
DMSO	Dimethyl sulphoxide
DNA	Deoxyribonucleic acid
DNase	Deoxyribonuclease
dNTPs	Deoxynucleotide triphosphate
E	Embryonic day (e.g. E10)
E-box	Enhancer box
ECM	Extracellular matrix
EDTA	Ethylene-diamine-tetraacetic acid
EF1a	Elongation factor 1 alpha
ESC	Embryonic stem cell
FBS	Fetal bovine serum
FDP	Flexor digitorum profundum
FDR	False discovery rate
FGF	Fibroblastic growth factor
FITC	Fluorescein isothiocyanate
GAG	Glycosaminoglycans
GAPDH	Glyceraldehyde 3-phosphate dehydrogenase
GDF	Growth differentiation factor
GF	Growth factor
GFP	Green fluorescent protein

GMP	Good manufacturing practice
GO	Gene ontology
H&E	Haematoxylin and eosin
HA	Hyaluronic acid
hESC	Human embryonic stem cell
HRP	Horse radish peroxidase
HSC	Haematopoietic stem cell
IGF	Insulin growth factor
IL	Interleukin
IP	Immunoprecipitation
iPSC	Induced pluripotent stem cell
Kb	Kilobase pair
kDa	kiloDaltons
KO	Knockout
LIF	Leukaemia inhibitory factor
lncRNA	Long non-coding RNA
Log2FC	Log 2-fold change
L-Q	L-glutamine
M	Molar
MEF	Mouse embryonic fibroblast
mESC	Mouse embryonic stem cell
MHC	Major histocompatibility complex
miRNA	Micro-RNA
MKX	Mohawk
MLR	Mixed lymphocyte reaction
MMC	Mitomycin C
MMP	Matrix metalloproteinase
MRL	Murphy Roth large mice
mRNA	Messenger RNA
MSC	Mesenchymal stem cell
NGS	Next generation sequencing
NK	Natural killer cell
NT	Non-target
nt	Nucleotide
ORI	Origin of replication
P	Passage (e.g. P3)
p	p-value
p.adj	Adjusted p-value
P/S	Penicillin-streptomycin
PBMC	Peripheral blood mononuclear cell

PBS	Phosphate buffered saline
PCA	Principal component analysis
PCR	Polymerase chain reaction
PDGF	Platelet derived growth factor
PE	Paired end
PGA	Poly(glycolic acid)
PGE2	Prostaglandin E2
PGK	Phosphoglycerate kinase
PRP	Platelet rich plasma
Q	Phred score
qPCR	quantitative PCR
RNA	Ribonucleic Acid
RNA-seq	RNA-sequencing
RNAse	Ribonuclease
rRNA	Ribosomal RNA
SBS	Sequencing by synthesis
scRNA-seq	Single cell RNA-sequencing
SCX	Scleraxis
s.d.	Standard deviation
SDFT	Superficial digital flexor tendon
SE	Single end
SEM	Standard error of the mean
Shh	Sonic hedgehog
shRNA	Short hairpin RNA
shSCX	Short hairpin RNA against scleraxis
sno-RNA	Small nucleolar RNA
SOLiD	Sequencing by oligonucleotide ligation and detection
TAE	Tris-Acetate-EDTA
TALE	Three-amino acid loop
TF	Transcription factor
TGF	Transforming growth factor
Tm	Melting temperature
TMM	Trimmed mean of M-values
TSC	Tendon stem/progenitor cells
UCB	Umbilical cord blood
UCT	Umbilical cord tissue
VEGF	Vascular derived growth factor
VST	Variance-stabilizing transformation
WPRE	Woodchuck hepatitis virus post-transcriptional regulatory element
WT	Wild type

List of Figures

List of Tables

Chapter 1 – Introduction

Orthopaedic injuries are the most common cause of wastage in the performance horse accounting for 82% of injuries in horses competing in National Hunt and flat races (1–3). Of these 46% are involved in overstrain and traumatic tendon and ligament injuries, with the superficial digital flexor tendon (SDFT) being particularly at risk (3). Current treatment methodologies are unsatisfactory, resulting in incomplete recovery and high re-injury rates. Tendon injuries therefore remain a significant clinical challenge.

1.1 Tendon structure and function

1.1.1. Tendon composition

Tendons are highly organised, dense, fibrous tissue structures which serve to transmit contractile forces from skeletal muscle to bone. The composition of the tendon is not homogeneous along the entire tendon axis, having different cellular and structural properties at both the interface between muscle (myotendinous junction) and between bone (enthesis) (4). Here however, I will focus on the tendon proper or tendon mid-substance.

Type I collagen fibrils are the predominant component of the tendon proper, making up 65-80% of its dry weight (5). These fibrils are composed of a triple helix made up of two α 1 chains and one α 2 chain of molecules which align uniformly in the direction of force (6). The collagen molecules, encoded by the *COL1A1* and *COL1A2* genes, are organised into distinct hierarchical levels (Figure 1.1) and are stabilised by intermolecular crosslinks, primarily composed of proteoglycans (2). Decorin (DCN), hyaluronan (HA), lumican (LUM), biglycan (BGN) and fibromodulin (Fmod) are just some of the proteoglycans present. These proteoglycans have specialised carbohydrate glycosaminoglycan (GAG) side chains which allows them to link to other proteoglycans in order to maintain collagen fibril diameter and fibril distances, thereby providing

structural strength (7–9). The synthesis of these extracellular matrix (ECM) components is conducted by a small population of resident tendon fibroblasts (referred to as tenocytes), which make up 95% of the cells within the tendon (10,11). Tenocytes in adults, although not a homogenous population, are predominantly characterised as elongated, spindle-shaped cells, whose large cytoplasmic extensions allow them to link to each other via gap junctions to form extensive communicative networks within the ECM (2,12,13). In general these tenocytes primary function is to remodel and control ECM production by producing collagens, proteoglycans and matrix metalloproteinases (MMPs) in response to mechanical stimulus (14).

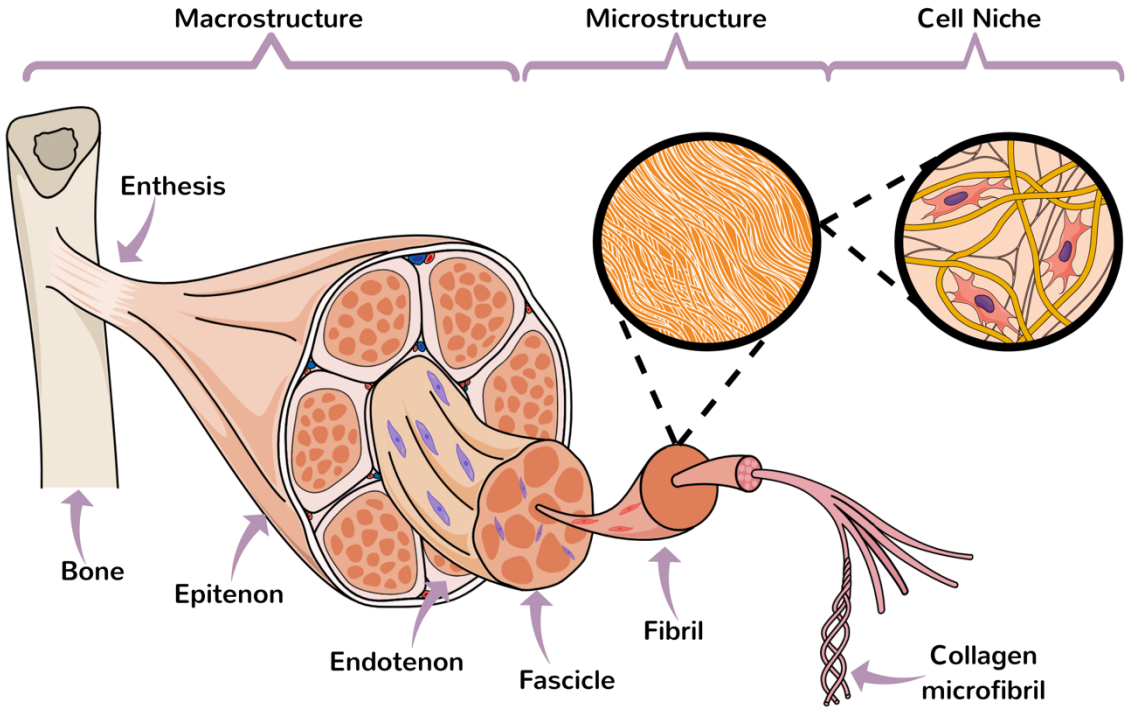

Figure 1.1. Tendon architecture. Structure of the tendon showing the interface between the tendon and bone (enthesis) moving into the tendon proper or tendon midsection. The tendon proper is composed of a hierarchical structure which spans from a single collagen fibre up to fibrils, fascicles and whole tendon. These collagen fibres arrange in parallel in the orientation of the applied force as displayed in the microstructure insert. Looking closer at the tendon microstructure (displayed in the cell niche insert), resident tenocytes populations (pink) are situated between the collagen fibres (yellow) and associate with proteoglycans (grey) which help to maintain the structural strength. The cellular population is however not homogeneous and other cell types are found between collagen fascicles and within the endotenon although they are not well characterised.

The remaining 5% of cells include endothelial cells, chondrocytes and tendon stem/progenitor cells (TSCs) (10). TSCs are believed to differ from their terminally differentiated tenocyte counterparts by having multi-differentiation potential and self-renewal capabilities, and have been identified in human, mouse, rabbit and equine tendons (15–17). However, the concept of tenocytes as being terminally differentiated is being challenged, with studies showing tendon-derived fibroblasts can also differentiate into chondrocytes, adipocytes and osteocytes suggesting instead that tenocytes may have trans-differentiation potential (18,19). This trans-differentiation potential is not unique to tenocytes, with fibroblasts derived from other tissues including the skin, lungs, heart as well as many others having also been demonstrated to have multilineage potential as outlined in Ichim *et al.,* 2018 (20).

Thorough comparison of tendon cell populations, in particular between tenocytes and TSCs, are scarce within the literature, with those that have been conducted showing conflicting results (21). One study in rabbits showed large differences in TSCs and tenocytes isolated from patellar and Achilles tendons, with TSCs having expression of stem cell markers octamer binding transcription factor-4 (OCT4), stage specific embryonic antigen-4 (SSEA4) and nucleostemin, which were absent in tenocytes (19). Similarly, a study comparing mouse TSCs and tenocytes showed increased expression of stem cell markers (*Nanog* and cluster of differentiation-73 (*CD73)*) in TSCs, although these were different markers than that observed in the rabbit study (21). In contrast comparison between TSCs and tenocytes isolated from the equine SDFT showed few differences in stem and tenogenic gene expression (22). Taken together, the lack of consensus data and molecular markers available to allow precise identification and isolation of tendon cell subsets at present impedes our understanding of their exact locations and functions.

1.1.2. Tendon function

The force transmitting SDFT shares remarkable similarities with the human Achilles tendon (AT) in terms of its composition and function (23,24). These tendons serve not only to connect skeletal muscle to bone, but also provide a means of energy-storing to facilitate high-speed locomotion. In simple terms, this system works by storing the potential and kinetic energy generated during the loading phase (i.e. as the foot hits the

ground). This stored energy is then released back as elastic energy when the foot leaves the ground (i.e. the elastic recoil phase), thus reducing the muscular effort required (23). As such, these tendons are often referred to as biomechanical springs and in the galloping horse this elastic energy saving results in an up to 36% recovery of mechanical work (25). The efficiency of this energy return system has been calculated to be approximately 93%, with around 5% of energy being lost as heat (hysteresis) (23,26). This rise in temperature in the tendon core can reach up to 46ºC, a temperature in which fibroblasts from other locations would not survive (12,27). As the tendon is relatively avascular this heat is then very slowly dissipated. The tendon is therefore subjected to some of the most intense mechanical demands in the body (28), with strains of up to 16% in the equine SDFT having been recorded from horses at a gallop. This degree of strain is extremely close to the *in vitro* calculated tendon failure rate of 15-17% (2,29). However caution should be taken when comparing calculated strains from *in vivo* and *in vitro* experiments as they do not always corroborate (30). Regardless, the exposure of such high strains can put tendon tissue at risk of damage.

1.2 Tendon injury and repair

1.2.1. Pathogenesis of tendon injury

Overstrain injuries are the most common form of tendon injury and occur either by a sudden overloading of the tendon or more frequently by a progressive build-up of microdamage due to repetitive exposure to high strains (12). Whilst it is not fully understood when these micro-degenerative changes progress into macroscale damage, this gradual weakening eventually overwhelms its structural integrity leading to irreversible damage (31). In the SDFT this damage most commonly presents in the central core region, which can be visualised ultrasonographically as a centrally located ‘hole’ (12).

Modelling overstrain injuries has been conducted to try and explore the impacts of cyclic mechanical loading on tendon ECM and inflammatory protein production. Applying cyclic loading from 2-12% uniaxial strain to isolated equine SDFTs results in increased expression of interleukin-6 (IL-6) and cyclooxygenase-2 (COX2) inflammatory

mediators, collagen degradation markers C1 and C2 as well as MMP13, albeit at relatively low levels (32). Similarly, loaded *ex vivo* bovine tendons exposed to cyclic strain from 1-10% show collagen fibre disruption as well as increased expression of IL-6, COX2, MMP-1, 3 and 13 (33). Cell culture models echo these results, with human tenocytes exposed to 3.5% cyclic strain for 2 hours showing upregulation of MMP3 and interleukin 1 beta (IL1-β), a cytokine which can induce MMP expression (34). Such evidence suggests that it is this increased production of matrix degrading enzymes and low levels of inflammation, resulting from cyclic overloading of the tendon that ultimately results in the degenerative changes seen in tendinopathies.

1.2.2. Tendon repair process

Once the tendon presents with clinical injury the healing process is thought to comprise of three main stages (Figure 1.2). Firstly there is an acute and local inflammatory response, where inflammatory cells such as macrophages, monocytes and neutrophils are attracted to the injury via signalling from pro-inflammatory cytokines (35). Recruited inflammatory cells secrete growth factors which in turn activate tenocytes (36). In adults, there is then rapid cellular proliferation and a delayed but excessive accumulation of unorganised ECM, composed predominantly of type III collagen. Remodelling of the tissue then occurs over a number of weeks and months to consolidate the tissue, through gradually decreasing cellularity and increasing the fibrous matrix by replacing collagen type III with type I. Finally the maturation stage occurs, to stiffen and restore the tendons tensile strength (35). However, this newly remodelled scar tissue is functionally inferior in comparison to that of normal tendon. Although it tends to be on the whole stronger than that of the original tissue it is much stiffer, with this stiffness leading to reduced efficiency of the tendon acting as a spring which results in substantial risk of re-injury of up to 67% in racehorses and 31% in human athletes (23,37–39).

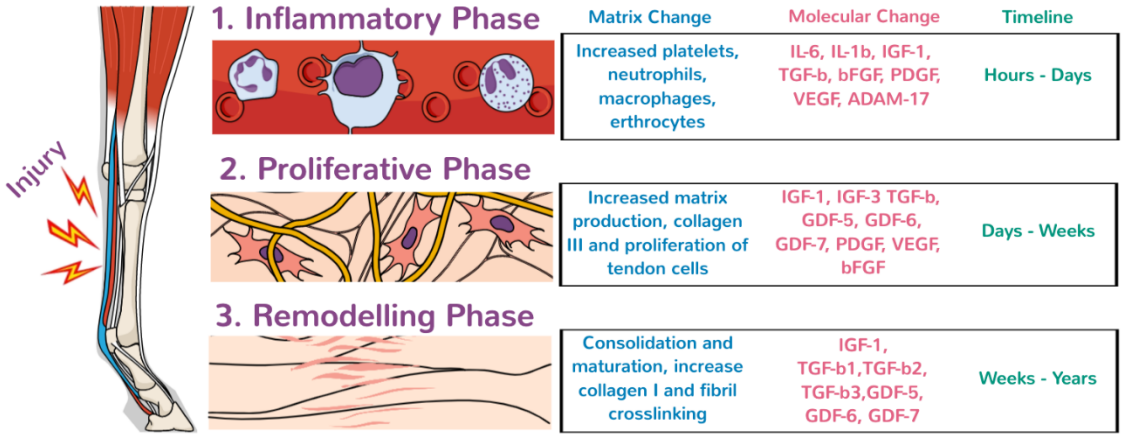

Figure 1.2. Adult tendon repair process. Tendon healing passes through three main overlapping stages. Some of the most commonly cited matrix and molecular changes are listed in the figure above which is adapted from Schneider *et al*., 2018 (40).

In contrast, fetal tendon wounds regenerate with non-disrupted collagen ECM through simultaneous proliferation and synthesis of organised collagen (41). Although the exact mechanisms of fetal scar-less healing are unknown, various studies suggest this difference in regenerative ability is partly explained by intrinsic differences between adult and fetal fibroblasts themselves. Comparative studies have indicated that differences in the migratory activity, inflammatory responses, cellular mediated expression of chemokine, cytokines and growth factors, and deposition of components of the ECM may play a vital role (41–44). The concept of fetal regeneration will be explored further in chapter 3.

1.3 Therapies for tendon injury

Many proposed treatments for tendon injuries have been developed and tested over the years, with most showing indistinguishable or even damaging results (12). The standard treatment for tendon injuries however remains to subject the horse to lengthy periods of confinement and controlled exercise programmes, which may be required for up to 12 months post injury (45,46). Some alternative treatments are discussed below.

1.3.1. Surgical intervention

Surgical interventions during the acute inflammatory stage can be conducted in the horse, such as by percutaneous tendon splitting. Here a puncture is created with a scalpel or needle and typically intratendinous polysulfated glycosaminoglycans, a pharmacological agent which *in vitro* has been shown to inhibit prostaglandin E2 (PGE2) production, is injected in to reduce the pressure in the wound and promote vascularisation (47). This therapy has been shown to more rapidly decrease the lesion size in the tendon core, however functionally the tendon is not vastly improved in comparison to controlled exercise alone (47,48). Similarly, desmotomy of the accessory ligaments is often performed in conjunction with tendon splitting to allow lengthening of the SDFT muscle/tendon unit which is thought to protect the repairing SDFT from peak strain. However, although initial evidence suggested a beneficial effect by increasing the rate of return to racing, others have demonstrated it also results in an increased incidence of suspensory ligament strains and desmitis (47,49–51).

1.3.2. Growth factors and biologics

Newer treatment methods are starting to emerge focusing on enhancing tendon regeneration through the delivery of various growth factors. Growth factors are important signalling molecules that play a role in tendon healing and development, with growth factors such as insulin growth factor-1 (IGF-1), transforming growth factor beta (TGF-β), basic fibroblastic growth factor (bFGF), platelet derived growth factor (PDGF), vascular endothelial growth factor (VEGF), to name a few, being of particular interest therapeutically (35,52). Typically these are applied by local injection, or by implanting biomaterial scaffolds or even suture material to allow for a more sustained release (35,52–54). Overall, growth factor treatments appear to provide some beneficial effects for tendon healing. For example, treatment with PDGF has been shown to increase collagen production and crosslinking as well as hyaluronic acid content leading to improved functional movement in a canine model of intrasynovial flexor tendon repair (55). Similarly, bFGF has been shown to accelerate wound closure through stimulation of cell proliferation in rat patellar tendon injury models (56). Likewise the addition of IGF-1, bFGF and PDGF in rabbit flexor tendon injuries also resulted in a marked increase in cell

proliferation rates (57). However, for many of these treatments the long-term benefits still remain to be seen, with mixed success being reported (58).

Platelet rich plasma (PRP) treatment has gained much popularity in the last decade. This involves drawing peripheral blood from the patient and, using centrifugation or gravity filtration, red blood cells are removed, and the resulting concentrated plasma/platelet mix is then injected into the tendon. This PRP mix contains a rich source of growth factors which are believed to stimulate cell proliferation and ECM production (12). Evidence regarding PRP's effectiveness is developing, however of the clinical trials conducted thus far, many include study biases with multiple factors contributing to this lack of evidence. Study biases and issues include the significant patient to patient variability in the constitution of PRP produced, differences in how vendors isolate PRP as well as the delivery method used, all of which make it difficult to draw strong conclusions (52). Systematic reviews on PRP have therefore failed to find solid evidence of its efficacy (59).

1.3.3. Cell-based therapies

The use of growth factors and biologics may be inadequate if the resident tendon cells cannot be manipulated to reduce the scarring. As such this has led to research into cell-based therapies, to harness the powers of cells which do potentially possess such regenerative properties. One such strategy is the use of adult derived mesenchymal stromal cells (MSCs), which have the capacity to differentiate into tenocytes (Figure 1.3). To date the most commonly investigated MSC source is bone marrow-derived MSCs (BMSCs), which are increasingly being used in the veterinary field for transplantation into injured tendons and ligaments (60). This therapy has shown promising results, with one study showing a reduction in re-injury rates from 56% down to 18% following autologous implantation of BMSCs into injured SDFTs (61), with others showing similar reductions (39). However, the true efficacy of these studies is difficult to assess. Many clinical trials do not include adequate control animals, which likely reflects the reluctance of horse owners to enrol valuable horses into controlled studies where they may only receive a placebo. Similarly, comparisons between studies is difficult due to the many differences in the treatment itself such as whether the MSCs have been combined with

other biologics such as serum, the number of MSCs injected, the age of the horses treated, the treatment follow up time and the post treatment recovery plan.

Although the results from clinical trials of MSCs is encouraging there is still a number of limitations to their use. Firstly, each patient has to undergo an invasive tissue isolation procedure, typically bone marrow aspiration of the sternum, in order to collect the required cells. Of this aspirate only 0.001-0.01% of the total cell population contains BMSCs, which then need to be expanded in culture for 2-4 weeks before sufficient numbers are obtained for therapeutic use, which can result in loss of stemness (35). This long delay therefore prevents the immediate treatment of acute injury. Several clinical trials in surgical or collagenase induced tendon lesions in rats, rabbits and horses have demonstrated improved rates of healing and maturation as a result of BMSC treatment (62–65). However, in many small animal models ectopic bone formation was also described (66–68). In comparison to date, no ectopic bone formation has been described following MSC injection in the horse, highlighting that small animal studies often act as poor models for the horse (69). Similarly, the long-term effects on tendon strength and functional performance post injury remain unclear and proper follow up studies are required.

Adipose tissue derived MSCs (ASCs) and umbilical cord blood (UCB) or tissue (UCT) MSCs have also been investigated as potential therapeutics. Adipose tissue in particular present as a much more accessible, abundant source of MSCs. Trials in equine collagenase induced SDFT injury have shown increased collagen fibre organisation as a result of ASC treatment (70). Peripheral blood is equally becoming an increasingly popular source of MSCs, which using techniques such as gradient separation, can lead to isolation of fibroblastic cells which display mesenchymal differentiation potential. Equine peripheral blood-derived MSCs have however been demonstrated to be more restricted in their differentiation potential compared to BMSCs (71). Similarly, studies using ASCs, UCB/UTC and peripheral blood MSCs are limited, and again like any autologous therapy, age, patient to patient variability and expansion time are a concern.

Due to the various practical limitations related to autologous MSC treatments, investigations have been conducted into the use of allogeneic MSCs (i.e. those derived from a different horse than the recipient), with previous work from our group and others showing that MSCs are immune privileged *in vitro* (72–75). These *in vitro* studies have

typically used mixed lymphocyte reactions (MLRs) to show that allogeneic MSCs inhibit the proliferation of major histocompatibility complex (MHC) mismatched lymphocytes, demonstrating also that MSCs secrete a variety of immunomodulatory cytokines in order to modulate this effect (76). In a clinical setting, MSC therapy has generally been regarded as safe following systematic reviewing of clinical trial data (77), however adverse clinical events such as cytotoxicity and allograft rejection has been observed in several horse, mouse, pig and macaques *in vivo* studies (78–86). This discrepancy is likely due to the fact that few clinical studies properly control for MHC matched or mismatched molecule expression or conduct a thorough immune response analysis, such as cell-mediated functional assays, humoral assays and *in vivo* imaging to track MSC survival (76).

Regardless, many companies are now offering "off the shelf" sources of MSCs to be used allogeneically in horses, including Arti-Cell® (of which the MSC source is not stated) and HorStem (UCT- derived MSCs) (87–89). However, questions regarding their efficacy in tendon injuries remain, with the concept of how exogenously applied MSCs function in the injured tendon changing considerable over the years (90). Where MSCs were first thought to migrate to the injury site, differentiate into functional tendon cells and engraft into the injured tissue, cell tracking techniques and follow up studies have disproven this theory. The survival rate of injected MSCs is in fact very poor (91–93) and as such it is now hypothesised that rather than actively contributing to tissue regeneration, MSCs may instead work via modulation of the inflammatory environment (72,94). As well as their ability to modulate the immune system response, *in vivo* studies have also demonstrated their ability to promote the growth and differentiation of resident progenitor and immune cells at the wound site (76,95,96). It is likely that in order for exogenous MSCs to have a full therapeutic effect via these indirect mechanisms, treatment would be best given during the acute inflammatory stage of tendon injury and further studies to assess the potential of allogeneic MSCs is needed.

1.4 Pluripotent stem cells[1]

Embryonic Stem Cells (ESCs) may offer an alternative solution to the drawbacks encountered when using MSCs for tissue repair. Here I will briefly discuss their history as well as the characteristics which make them an interesting candidate for tendon injury repair.

1.4.1. A brief history of ESCs

Although it is difficult to pinpoint when and who first discovered what we now call "stem cells", the first scientists to thoroughly define their key characteristics were Ernest McCulloch and James Till in the 1960s. Their work led them to discover the blood-forming stem cell, the haemopoietic stem cell (HSC), a cell type which could self-renew in culture and give rise to multiple cell types (98). This discovery would ultimately lead to the clinical application of bone marrow transplantations for haematopoietic disorders (98). This, and other key advancements in the field, led to the isolation and characterisation of many different stem cell types. The differentiation potential of stem cells is very dependent on the stage of embryonic development and are highlighted in Figure 1.3.

[1] Section modified and/or reprinted from Y Z Paterson, C Kafarnik and D J Guest, Characterization of Companion Animal Pluripotent Stem Cells, 137-148, © 2018, with permission from Wiley Online Library. https://onlinelibrary.wiley.com/doi/full/10.1002/cyto.a.23163.

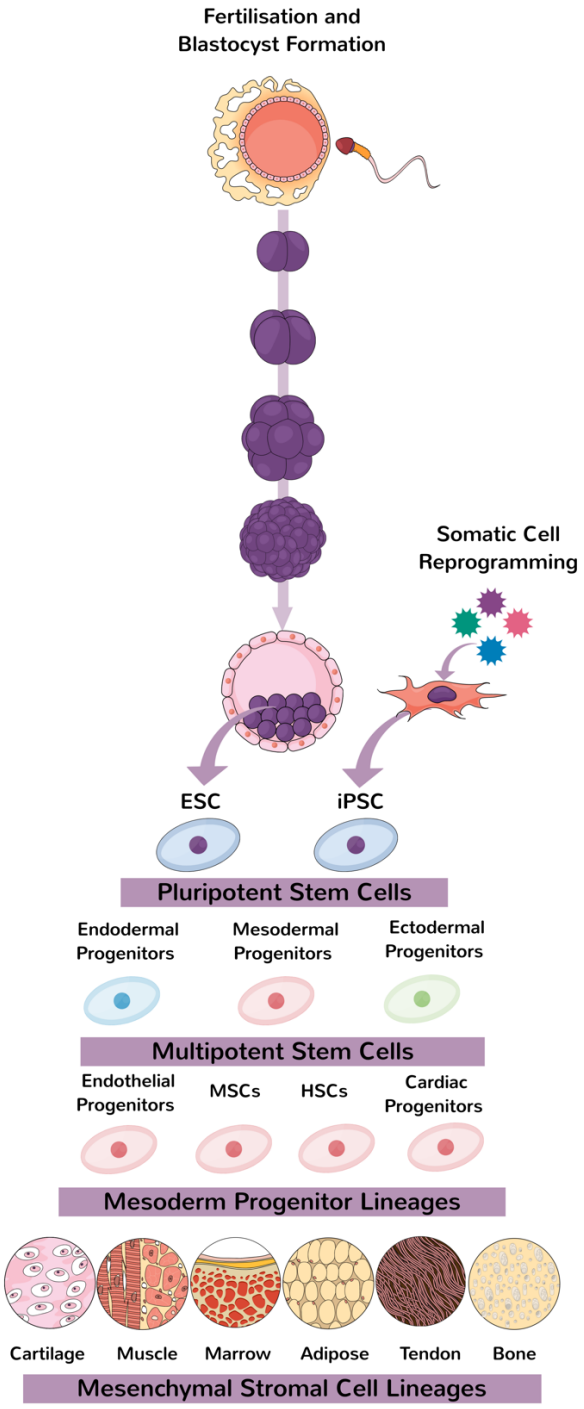

Figure 1.3. Stem cell differentiation pathway. At the base of the stem cell hierarchy is the fertilised oocyte, which is totipotent, having the ability to differentiate into extra-embryonic tissue as well as the embryo itself. Following this, during the initial days of mammalian embryonic development the first stem cells arise, derived from the inner cell mass of the pre-implantation embryo. These cells are termed embryonic stem cells (ESCs) and are pluripotent in nature, being able to differentiate into any cell type that arises from the three embryonic germ layers – endoderm, mesoderm and ectoderm. Fibroblasts can also be reprogrammed back into a state of pluripotency by introducing a number of reprogramming factors such as Oct4, sex determining region Y-box2 (Sox2), Kruppel-like factor-4 (Klf4) and cMyc (Yamanaka factors). The mesodermal lineage then gives rise to a number of progenitor lineages including MSCs which are multipotent, being able to give rise to a restricted number of specialised lineages.

One of the major advancements was the discovery of pluripotent embryonic stem cells which were first cultured in mice in 1981 and in humans 17 years later (99–101). These cells, unlike those derived from adults, can differentiate into derivatives of all three germ layers, be propagated extensively in culture (102–104), and have a degree of immune privilege (72,105–107). Pluripotent stem cells were later obtained from inducing adult somatic cells back into a state of induced pluripotency through a process termed as cell reprogramming (108). Similarly to ESCs, these induced pluripotent cells (iPSCs) are capable of self-renewal and differentiation into derivatives of all three germ layers and also provide a more ethical approach to studying pluripotency without the need to destroy an embryo (102).

To date human and mouse ESCs are still the most commonly used and studied pluripotent stem cell source, providing the standard against which all other species are compared. Much of our current knowledge on the molecular basis of pluripotency, differentiation and self-renewal has been drawn from the murine model. The core triad of transcription factors Oct4, Sox2 and Nanog, markers which are expressed in all pluripotent stages and are required for the maintenance of pluripotency and self-renewal, have been demonstrated to be highly conserved between species, giving credit to the continued use of murine models in aiding our understanding of pluripotency across species (97). However, some clear differences do exist, with variations in molecular signalling pathways, morphology and developmental potential occurring (109). Murine ESCs (mESCs), originally derived from the blastocyst of early embryos, can be easily isolated and maintained in a naïve state, express the cell surface markers SSEA-1 and SSEA-3, are karyotypically stable and are unable to differentiate into trophectoderm (109). In comparison, human ESCs (hESCs), similarly derived from the preimplantation embryo, have marked characteristic deviations from mESCs being isolated and maintained in a primed pluripotent state meaning that they are in a later stage of pluripotency compared to their naïve counterparts. Accordingly they express the cell surface markers SSEA-3, SSEA-4, TRA-1-60 and TRA-1-81, are karyotypically less stable than mESCs, and can differentiate into trophectoderm (109). Such differences highlight the need to continue research on species specific pluripotent cells alongside that of murine models.

1.4.2. Equine pluripotent stem cells

Deriving and studying pluripotent cells in other species has lagged somewhat behind that of mice and humans and there are only limited numbers of reports on their derivation. The first equine derived ESC-like cells were reported in 2002 (110). These cells were maintained *in vitro* for more than 56 passages and could be induced to differentiate into neural, haematopoietic and endothelial precursors (110). This was later replicated by two further independent groups in 2006 and 2010 (111,112). Although the aforementioned equine ESCs displayed many of the key characteristics of pluripotency, unlike in human and mouse studies they have not yet been shown to be capable of forming interspecies chimeras such as described in human cells (113), nor do they form teratomas following injection of putative stem cells into immunodeficient mice. Although teratoma assays are a common measure of pluripotency, there are several limitations to their use. Such limitations include the lack of consistency between laboratories in terms of inoculation site, number of cells injected, mouse strain used, number of injections per animal and time *in vivo,* all of which affect whether or not a teratoma will form (114–116). Given the aforementioned limitations it is therefore difficult to interpret if the negative results displayed are the result of experimental variations or truly due to an inability of the cells to form a teratoma.

The stark number of publications on equine ESC derivation is in complete contrast to the large numbers of publications researching the application of adult stem cells for their regenerative potential in horses. This difference likely reflects the difficulties in both equine ESC isolation and culture, as well as the ethical concerns regarding embryo destruction required in order to isolate ESCs. Not only this, research using horses is particularly expensive and breeding is seasonal, therefore having access to sufficient numbers of horse embryos with which to successfully isolate ESCs can be a limitation. Similar to the success rates of deriving ESCs from human embryos (117), our group has found that only up to 20% of horse embryos will successfully give rise to an ESC line which further highlights these difficulties.

Following the successful derivation of human (118) and mouse iPSCs (119), investigation into the derivation of equine iPSCs commenced as a means to remove the aforementioned limitations. The first report of equine iPSCs was in 2011 where a piggyback transposon system was used, containing murine Oct4, Sox2, Klf4, and Myc reprogramming factors

(120). Several other publications have followed this, the majority of which have used viral expression vectors to mediate genome integration of the reprogramming gene sequences (121–127). In order for an iPSC treatment to be deemed clinically safe it is important that the viral transgenes which are integrated during reprogramming are silenced (128). However, in many of the equine iPSCs generated to date, continued variable expression of the transgenes remain. In the first publication on the generation of equine iPSCs transgenes were required to be constitutively expressed to maintain pluripotency (120,122–125), with only one other study demonstrating that the transgenes were silenced (127). Although the equine iPSCs reported share many of the features of equine ESCs and iPSCs reported in other species, their differentiation potential has been shown to be limited in their ability to differentiate down the tendon lineage (121). Further research to understand this is required before iPSCs can be considered as a therapeutic for tendon regeneration.

1.4.3. ESCs as a therapeutic

ESCs could provide an unlimited source of allogeneic cells for treating tendon injuries. However, what makes ESCs so favourable for clinical use also brings a note of caution. Whether ESCs will succumb to immune rejection when used therapeutically has proven controversial. MHC cell surface proteins are important components of the immune system. The expression of MHC antigens on cellular surfaces mediate the outcome of alloantigen-specific T-cell responses. There are two classes, class I molecules which activate $CD8^+$ (cluster of differentiation 8 positive) cytotoxic T-cells, and class II molecules which activate $CD4^+$ (cluster of differentiation 4 positive) helper T-cells (129). Mouse ESCs have been shown to have no MHC class I or class II gene expression (130,131), whereas both human and equine ESCs express low levels of MHC class I but no MHC class II gene expression (132,133). Several studies have shown that both human and equine ESCs do not trigger a T-cell response *in vitro* or *in vivo* (72,91,97,106,134,135), highlighting their potential low immunogenicity.

However, despite this lack of T-cell response, immune rejection has been demonstrated in several studies, with allogeneic natural killer (NK) cells being shown to be capable of eliminating mouse and human ESCs using chromium release and cytotoxicity assays (129,136,137). Kofidis *et al.,* 2005 (138), also found that following injection of labelled

undifferentiated mESCs into damaged myocardium of allogeneic recipients, a strong immune response was generated with 75% of injected cells dying within 48 hours. Likewise, transplantation of undifferentiated mESCs into allogeneic hosts resulted in infiltration of immune cells and subsequent rejection within 28 days of intramuscular injection (139).

Contrary to this, our group has shown that injecting labelled equine ESCs into mechanically induced SDFT injuries has a different effect, with ESCs being found after 10, 30, 60 and 90 day periods at the injection site and other distant induced mechanical lesions (91). Injected ESCs were found to take on the correct orientation and tendon morphology and had a high survival rate of at least 60% (91,140). A gradual decrease in leukocyte numbers at the injection site was noted, and that coupled with the ESCs high survival rate suggests that the ESCs did not induce immune cell stimulation. Although no other studies to date have been performed to look at the immune-privileged status of horse ESCs, several other studies using human ESCs have similarly shown a lack of inflammatory response and tolerance to ESC engraftment following injection into immunocompetent mice (141,142).

It is difficult to know whether ESC survival and immunogenicity is species specific or a result of the particular environment in which they are injected. Evidence of this site specific immune-privilege can be found in the eye, where stem cell grafts in the subretinal space of the rat eye show much better cell integration and migration compared to that of the vitreous cavity (143,144). However, it must be noted that in a diseased state even so called immune privileged sites are often compromised due to breakdown of blood-tissue barriers (145). Further research on the effects of differentiation and the specific host tissue receiving the cells under a diseased state is therefore required.

Another limitation is that current clinical trials using ESCs have only been monitored short term, with trials in horse tendons having only been monitored for up to 90 days post injection (91). The long term survival/rejection of these cells is therefore unknown, and studies in human and mouse models have indicated a high likelihood of teratoma formation based on injection into other transplantation sites (146). To avoid this risk, strategies to induce human and mouse ESCs towards the appropriate lineage prior to clinical application have been investigated (147–152). One preliminary report on the use of human ESCs differentiated retinal pigment epithelium cells for the treatment of

macular degeneration showed no apparent rejection, tumorigenicity or ectopic tissue formation after 4 months of injection with some improvements to vision noted (153). Similarly, human ESC differentiated cardiac progenitors embedded in fibrin scaffolds and surgically delivered to infarct areas of the heart have shown no adverse immune effects or tumour formation after a 3-month period. Yet, again here long term follow up data is not available in either case. Moving pluripotent cells to the clinic will therefore require robust assessment of *in vitro* differentiation and long term monitoring to ensure that the differentiated cells are functional (121,124,154).

1.5 Transcription factors in tendon development

In order to decipher the most robust methods for ESCs differentiation *in vitro,* it is first important to have a better understanding of the mechanisms and transcription factors involved in tendon development. Better understanding of basic tendon biology should lead to better identification of effective treatments.

1.5.1. Scleraxis

Unlike in skeletal muscle or cartilage, to date the master tendon regulator or regulators have not been identified. At present, scleraxis (SCX), a basic helix-loop-helix transcription factor, is the most widely studied tendon marker, upon which much of the information regarding tendon development and tenocyte behaviour has been built (155). SCX gene expression is first detected between mouse embryonic day (E) 10 and 11, in which SCX positive cells condense to form a complex structure between developing cartilage and muscle tissue by E12.5 (155–157). This induction occurs through the interplay between fibroblastic growth factors (FGFs) and sonic hedgehog (Shh) signalling (Figure 1.4) and later by TGF-β in the developing limbs (155,158–160). By E14.5 embryonic tendons are distinctly characterised by SCX expression, which continues into late development as well as postnatally, also being upregulated during adult injury repair (155,156,161,162).

Although not exclusively expressed in tendons, being expressed in other ECM rich tissues such as the heart, periodontal ligaments and muscle, SCX has an indispensable role in the development of force transmitting and intramuscular tendons, which are severely

disrupted in SCX knockout mice (163). Interestingly, short-range anchoring tendons are only moderately affected by SCX absence (163). Upon examination of the flexor digitorum profoundum (FDP) of SCX knockout mice, ECM organisation, as visualised by electron microscopy and histological staining, was severely disrupted with a complete loss of collagen alpha-1(XIV) (*COL14A1)* and tenomodulin (*TNMD)* expression and disorganised microfibrils being apparent (163). SCX therefore, although not a single, master regulator of tendon development, clearly plays an important role in differentiation down the tenogenic lineage as well as in ECM structural organisation in the tendon.

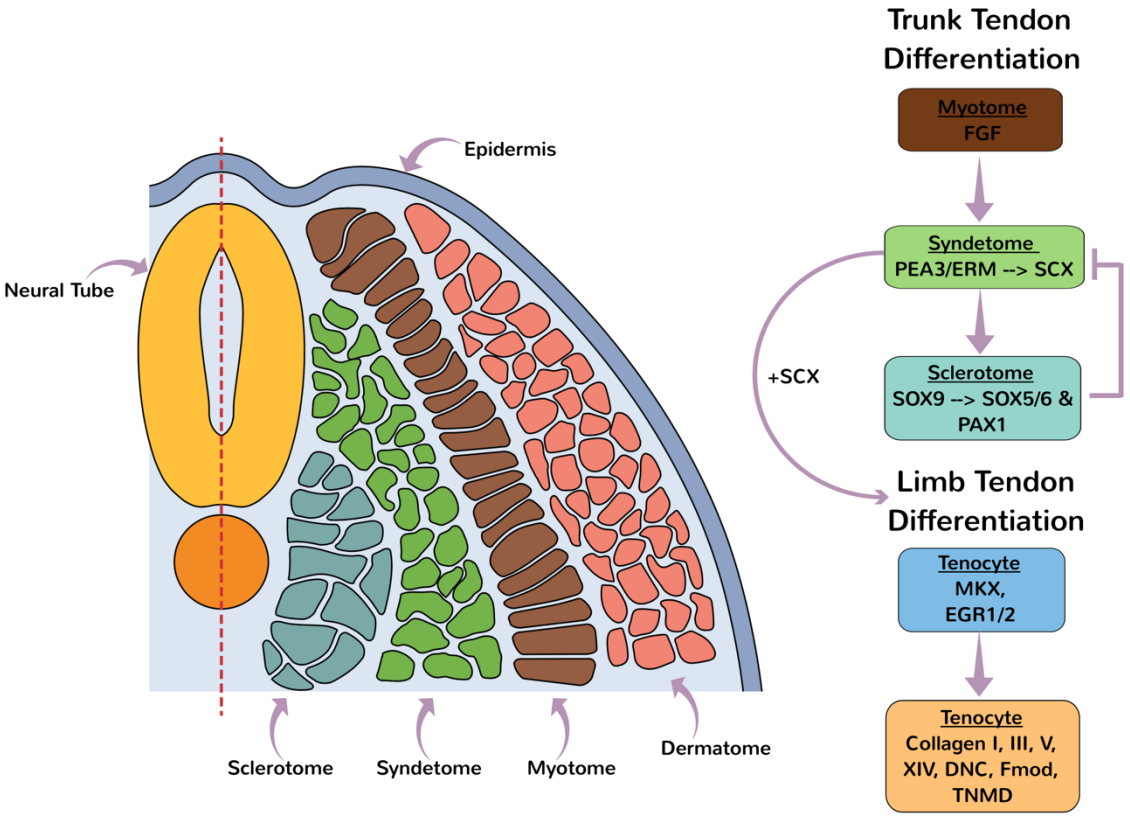

Figure 1.4. Embryonic limb tendon development. FGF signalling in the myotome activates the inducers PEA3/ERM (polyoma enhancer activator protein-3 & ezrin radixin moesin proteins respectively) to upregulate SCX which induces cells of the sclerotome to become tendon cells. Inhibition of SCX occurs via SOX9 upregulation of the sclerotomal factors SOX5/6 and paired box protein-1 (PAX1), which allows cartilage to develop. In the limb, SCX is the first signal for tendon progenitor cell initiation. Mohawk (MKX), early growth response-1 and 2 (Egr1/2) are secondary signals required for tendon differentiation and maturation leading to eventual expression of ECM molecules at various stages of tendon development. Figure adapted from Liu *et al*., 2011 (58).

1.5.2. Mohawk

Mohawk (MKX) is a member of the three-amino acid loop (TALE) superclass of atypical homeobox genes whose expression is first detected in E12.5 mouse limb and tail tendons (164). It is however, most robustly expressed during E13.5 to E14.5 when tendon progenitors begin to condense and differentiate, with it then dramatically decreasing by E16.5 (165). Although MKX is expressed postnatally, it is much weaker than during embryonic development, being mostly localised to the cells of the limb tendon sheath (165). Interestingly like SCX, MKX has been shown to be mechanosensitive and is upregulated in adult mice subjected to mechanical loading, leading to increased collagen fibrinogenesis and collagen cross-linking (166,167). MKX mutant knockout mice have also demonstrated that MKX is essential for normal tendon morphology and function of the forelimbs, tail and trunk, with knockout mice displaying smaller, paler, hypoplastic tendons which have decreased tensile strength (165,168,169). Tendon gene expression is also significantly altered, with E16.5 mice displaying reduced *COL1A1*, *TNMD*, *Fmod, LUM* and *DCN* expression, with many of these genes being required to regulate collagen fibril growth (165,168,169). Histologically, MKX knockout tendons had an overall lower density of collagen fibres, as determined using aniline blue staining and electron microscopy, compared to the wildtype control (168). Similarly, MKX null tendons had decreased total soluble collagen and decreased collagen I protein content, as determined by soluble collagen assays and western blotting techniques (168).

Interestingly, when comparing SCX to MKX knockout mice no direct interaction is apparent, as the lack of one gene does not affect the expression of the other throughout embryonic tendon development (163,164). It therefore appears that SCX and MKX take part in distinct signalling cascades during tendon development, with MKX having a more pronounced role in collagen fibril growth and regulation. MKX expression, like SCX, is not restricted to tendons, being expressed in progenitor populations of cartilage, skeletal muscle and bone in early somites (164). Studies utilising MKX gain and loss of function techniques in mice and zebrafish have highlighted MKX's ability to suppress myoblast determination protein-1 (*MyoD)* transcription, thereby inhibiting muscle differentiation and development suggesting a role of MKX in promoting tendon differentiation via repression of muscle development (4,164,170,171). Further work is required to validate

this however, as MKX knockout mice do not display any clear skeletal muscle changes (169).

1.5.3. Early growth response 1 and 2

Early growth response 1 and 2 (Egr1 and Egr2) are members of the early growth response family of zinc finger transcription factors which have been implicated in tendon development (172). Egr1 is first detected at E12.5 in the developing mouse forelimb tendons at the attachment between the tendon and muscle tissue, whereas Egr2 is first detected at E14.5 in all limb tendon regions (172). Activation of both Egr1 and Egr2 occurs through FGF4, via unknown mechanisms during vertebrate tendon development (172). Upon activation both proteins are capable of transactivating the tendon regulatory regions of the *COL1A1* proximal promoter, with Egr1 also directly binding to the *COL1A2* promoter to regulate gene expression (172,173). Although both Egr1 and Egr2 are expressed during tendon development and regulate *COL1A1*, Egr1 seems to play the leading role. Egr1 knockout mice display significantly reduced expression of key tendon markers, *SCX,* and *TNMD,* as well as a variety of tendon associated collagens (*COL1A1, COL1A2, COL14A1, COL3A1* and *COL5A1*) and tendon associated ECM components (*BGN*) (172,173). These mice also display defects in collagen fibrils, which are present in smaller numbers, with smaller diameters and reduced function, leading to a lower ultimate tensile strength compared to their wild type (WT) littermate controls (172,173). Egr1 and Egr2 may also function to maintain *SCX* expression during embryonic development, as overexpression of both induces *SCX* expression in ectoderm and mesoderm-derived tissue (172). However, the mechanisms of *SCX* and *TNMD* activation are not well defined, as Egr1 does not directly transactivate these genes. It is thought that Egr1 may activate expression through the known downstream binding partner *TGF-β2*, which is consistent with the recognised role of TGF-β signalling in tendon gene expression (Figure 1.5) (174,175).

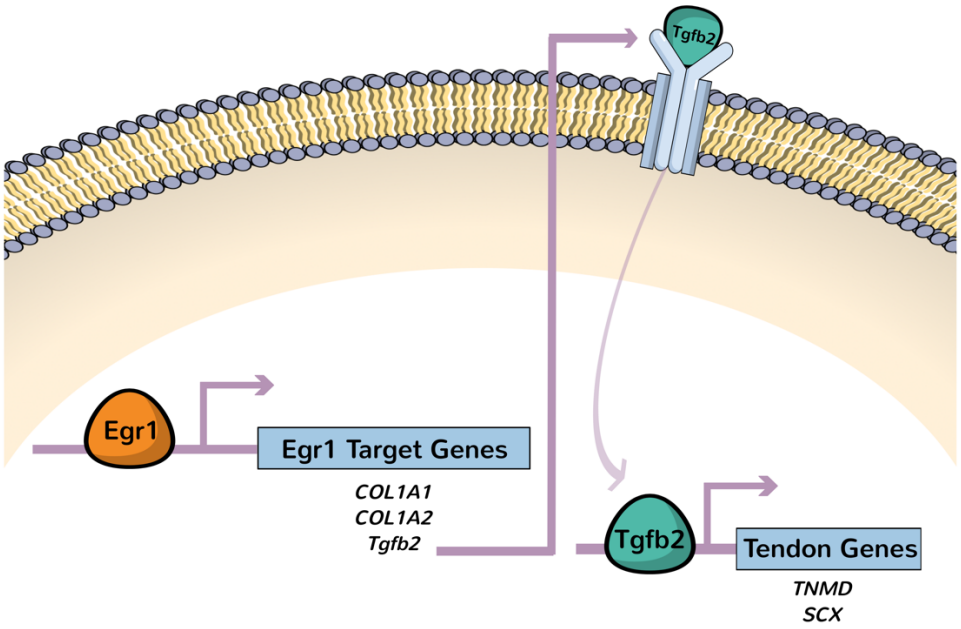

Figure 1.5. Proposed Egr1 signalling cascade in tendon cells. Diagrammatic representation of the Egr1 downstream regulation of tendon gene expression through proposed downstream binding partner *TGF-β2 (Tgfb2)*. Adapted from Havis et al., 2020 [131].

1.6 Strategies for tenogenic differentiation *in vitro*

1.6.1. Transcription factors

As previously described, it is likely that stem cells may need to be pre-differentiated *in vitro* prior to clinical application. Transcription factors identified as key for tendon development *in vivo* have been investigated as a means to facilitate this process.

Forced expression of SCX for example, has been used to differentiate human BMSCs to TSCs (176). In doing so tendon-related gene expression (*COL1A1*, *DCN*, *Fmod*, *LUM*, *TNMD* and alpha smooth muscle actin (*α-SMA)*) increased, with the resulting cells having decreased self-renewal potential and restricted multipotentiality (176). Similarly, human ESCs have also been shown to be capable of stepwise differentiation down the tendon-lineage (177). ESCs were first differentiated into MSCs via the replacement of pluripotency medium with 20% serum medium, the resulting ESC derived MSCs were then subjected to SCX-overexpression via lentiviral infection (177). Resulting cells displayed tenocyte morphology and had upregulated *COL1A1* and tenascin C (*TNC)* tendon gene expression and downregulated SOX9 (cartilage gene) and alkaline

phosphatase (ALP) (pluripotency gene) expression (177). *In vivo* studies have also shown that SCX transduced MSCs, when used to treat rat supraspinatus induced tendon injuries, improved the tendons overall tensile strength compared to the non-transduced MSC controls suggesting SCX induction leads to improved regeneration (178). Taken together this suggests that SCX has a role in promoting tendon differentiation *in vitro,* the mechanisms of which will be further explored in chapters 4 and 5.

MKX overexpression has also been shown to induce tenogenic gene expression in MSC, showing upregulation of several tendon-associated genes including *COL1A1, TNMD* and *TNC* (179,180). Moreover, ectopic MKX overexpression in MSCs was found to be more efficient at promoting tenogenesis than SCX overexpression, showing significantly greater expression of tenogenic genes and improved collagen fibril growth (180). They also showed that MKX indirectly regulated *SCX* expression via *TGF-β2* expression, much like that of Egr1 as previously described in section 1.5.3. It therefore appears that maintenance of *SCX* expression during tendon development is achieved in part via transcriptional activation of the TGF-β signalling pathway. Using MKX to induce tendon differentiation has also been conducted in equine BMSCs and iPSCs resulting in increased expression of *SCX, Egr1, COL1A2, COL14A1, DCN,* elastin *(ELN), Fmod* and *TNC*.

Similarly, Egr1 has also been tested as a strategy to induce tendon differentiation in MSCs. Following its forced expression cells have a reduced capacity to differentiate into fat and bone lineages as well as an increased expression of several tendon-associated molecules including *COL1A1, TNMD* and *TNC* (173). This result has been further demonstrated in rabbit tendon stem cells, with forced Egr1 expression leading to increased tendon gene expression and an inhibition of non-tenocyte differentiation (181).

1.6.2. Growth factors

Growth factors are produced throughout tendon development and differentiation as well as during tendon healing. To differentiate stem cells into bone and cartilage lineages, fairly well-defined growth factor formulations are used which produce reproducible results, however the same has not yet been achieved for tendon differentiation.

The most widely reported growth factors used come from the transforming growth factor beta family, which forms part of the most significantly upregulated signalling pathway expressed during embryonic limb development (159). TGF-β1, 2 and 3 have all been investigated, and show robust induction of *SCX* both *in vitro* and *in vivo,* as well as other tendon-related marker genes. Its suitability can be drawn from studies in which TGF-β signalling is disrupted in the mesenchyme of mouse limb buds, which leads to prevention of tendon formation (175). Similarly, TGF-β signalling also appears to be required for the continuous maintenance of the tendon cell fate, as without this tenocytes revert into a more stem/progenitor like state which can be rescued by its reintroduction (182).

A whole host of other growth factors and growth factor combinations, including connective tissue growth factors (CTGFs), growth differentiation factors (GDFs), basic fibroblastic growth factors (bFGFs) and insulin growth factors (IGFs) have been utilised in tenogenic induction protocols. However, a consensus on the optimal combination has not been reached, which likely comes from the lack of definitive markers to define the different tendon cell populations. Table 1.1 summarises some of the current *in vitro* growth factor strategies that have been used for tenogenic differentiation

Table 1.1. Growth factor strategies for tendon differentiation. Adapted and updated from Zhang *et al*., 2018 and Shojaee *et al*.,2019 (60,183). Acronyms not previously defined are:- cartilage oligomeric matrix protein (COMP), thrombospondidn-4 (THBS4), fibronectin (FN), vimentin (VIM), aggrecan (ACAN), mothers against decapentaplegic homolog-8 (SMAD8).

Growth Factor	Target Cell	Optimal Concentration	Other Modifications	Treatment Time	Outcome	Reference
TGF-β1	Mouse flexor tendon tenocyte	10 or 100 ng/ml	3D collagen gel	24, 48 hours	⇧*SCX, MKX, BGN, COL V, COL XII, Serpine1* ⇩*MMP16, DCN* gene expression	(184)
	Horse ESC	20 ng/ul		7 to 14 days	⇧COLIA1, COMP, TNC, TNMD, THBS4 protein expression	(140)
	Horse BMSC	5 ng/ml	3D collagen gel	10 days	⇧*SCX* gene expression	(185)
	Human ASC	50 ng/ml	50 µg/ml Ascorbic Acid	14 days	⇧*SCX, MKX, COMP, THBS4, TNC, COL1A1, COL1A2, COL3A1* gene expression	(186)
TGF-β2	Mouse MSC	20 ng/ml	3D collagen culture	1, 24 hours	⇧*COLIA1*, *SCX* gene expression	(173)
	Horse ESC	20 ng/ml		7 to 14 days	⇧COLIA1, COMP, TNC, TNMD, THBS4 protein expression	(140)
	Mouse TSC and MSC	20 ng/ml	Culture in cell sheets	12, 24, 48 hours	⇧*COLIA1*, *SCX, COL5A1* gene expression	(180)
TGF-β3	Human bone marrow derived mononuclear cells	20 ng/ml	3D fibrin gel	7 days	Synthesis of collagen fibrils and appearance of fibripositors	(187)

	Horse ESC	20 ng/ml		1, 2, 3, 7, 14 days	⇧*SCX, TNC, COMP* gene expression between 24 -72 hours of induction ⇧COLIA1, COMP, TNC, TNMD, THBS4 protein expression	(140)
	Human BMSC	10 ng/ml	Cultured on aligned chitosan-poly caprolactone nanofibers	24 hours, 5, 10 days	⇧*COL1A1, TNMD* gene expression ⇧COL I protein production	(188)
	Horse ESC	20 ng/ml	3D collagen gel	1, 2, 3, 7, 14 days	⇧*COL1A1, COMP* and induction of *THBS4, TNMD gene expression* ⇧SCX, COLIA1, COMP, TNC, TNMD, THBS4 protein expression	(154)
	Horse iPSC	20 ng/ml	2D or 3D collagen gel	1, 3, 7, 14 days	⇧*COL1A1, COMP, SCX* gene expression ⇧COLIA1, COMP, TNC, protein expression	(121)
CTGF	Human BMSC	100 ng/ml	50 µg/ml Ascorbic Acid	4 weeks	⇧*COLI*, *TNC* gene expression	(189)
	Human BMSC	100 ng/ml	50 µg/ml Ascorbic Acid	4 weeks	⇧*COLI, COLIII, TNC, FN, VIM, MMP1,* gene expression ⇧COLI and TNC protein expression	(190)
	Rat TSC	25 ng/ml	25 µM/L Ascorbic Acid Culture in cell sheet	2 weeks	⇧*COL1A1, SCX, THBS4, TNMD, ELN, DCN, BGN* gene expression ⇧TNMD, COL1, COLIII protein expression	(191)
	Rat TSC	25 ng/ml	25 µM/L Ascorbic Acid Culture in cell sheet		⇧*COL1A1, TNMD* ⇩*ACAN, COL2A1, ALP* gene expression	(192)

GDF-5 (BMP14)	Rat ASC	100 ng/ml		3, 6, 9, 12 days	⇧*COLI, DCN, ACAN, SCX, TNMD, TNC* gene expression and ⇧TNMD, TNC, SMAD8, MMP13 protein expression	(193)
	Human BMSC	10 ng/ µl		14 days	⇧*DCN, COLIII, TNC* gene expression ⇧TNC, DCN, COL1, COL III protein expression	(194)
	Human BMSC	100 ng/ml		4 days	⇧*COLI, SCX, TNC* gene expression	(195)
	Human BMSC	Dosed released – variable concentrations	Synthetic 3D environment	3 days	⇧*COL1A1, COL3A1 DCN, SCX, TNC* gene expression	(196)
	Rat BMSC	50 ng/ml		2, 5, 7 days	⇧*COLI, COLIII SCX* gene expression	(197)
GDF-6 (BMP13)	Mouse BMSC	100 nM		3 days	⇧*COLI, THBS4* gene expression	(198)
	Rat BMSC	20 ng/ml		2 weeks	⇧*SCX, TNMD* gene expression ⇧TNMD protein expression	(199)
GDF-7 (BMP12)	Horse BMSC	50 ng/ml		14-21 days	⇧DCN, *TNMD* gene expression	(200)
	Mouse BMSC	100 nM		3 days	⇧*COLI, THBS4* gene expression	(198)
	Rat BMSC	10 ng/ml	2D or 3D collagen scaffolds	12 hours	⇧*COLI, TNMD, TNC, SCX* gene expression	(201)
	Rat BMSC	50 ng/ml		2 weeks	⇧ *TNMD, TNC, SCX* gene expression ⇧TNMD protein expression	(202)

	Dog/Mouse ASC	50 ng/ml		2 weeks	⇧TNMD, SCX gene and protein expression	(203)
	Horse amniotic fluid MSC	50 ng/ml		14 days	⇧TNMD, DCN gene and protein expression	(204)
	Horse UCB-MSC	50 ng/ml		10 days	⇧*TNMD, MKX, SCX, COL1A1, DCN* gene expression ⇧TNMD, DCN protein expression	(205)
	Rat TSC	50 ng/ml		14 days	⇧TNMD, SCX, COLI, TNC gene and protein expression	(206)
	Human ASC	100 ng/ml		7 days	⇧*SCX, MKX* gene expression ⇧MKX, COLI protein expression	(207)
	Horse BMSC	5 ng/ml	3D collagen gel	10 days	⇧*SCX, DCN, COLIII g*ene expression	(185)
	Human ASC	50 ng/ml	50 µg/ml Ascorbic Acid	14 days	⇧*SCX, MKX, COMP, THBS4, DCN* gene expression	(186)
FGF-2 (bFGF)	Human BMSC	3 ng/ml		14 days	⇧*COLI, COLIII, FN* gene expression	(208)
	Rabbit BMSC	Dosed released – variable concentrations	Nanofiber scaffold	10, 14 days	⇧*COLI, COLIII* gene expression ⇧TNC, COLI, COLIII protein expression	(209)
	Human BMSC	10 ng/ µl		14 days	⇧*SCX, DCN, COLI, COLIII, TNC* gene expression ⇧TNC, DCN, COL1, COL III protein expression	(194)
IGF-1	Human BMSC	10 ng/ µl		14 days	⇧*SCX, DCN, TNC, COLIII* gene expression ⇧TNC, DCN protein expression	(194)

	Horse TSC	100 ng/ml	Acellular tendon matrix	7 days	Increase proliferation with COL and GAG synthesis increased	(210)
	Horse BMSC	10 ng/ml	3D collagen gel	10 days	⇧*SCX, TCN, DCN, COLIII* gene expression	(185)
TGF-β3, bFGF2	Horse peripheral blood MSC	10 ng/ml	Low-level laser therapy	5 days	⇧*Egr1, DCN, TNC* gene expression	(211)
GDF-5, GDF-6, GDF-7	Horse ASC	10 ng/µl GDF-5 & 6, 100 ng/µl GDF-7	3D collagen gel in bioreactor	21 days	⇧*COL1, COLIII* gene expression	(212)
GDF-6, GDF7	Human ESC	10 ng/ml		40 days	⇧*COL1A2, TCN, COL3A1, THBS4, TNMD, DCN* gene expression and ⇧TNMD protein expression	(213)
GDF-7, CTGF, TGF-β3	Human ASC	50 ng/ml GDF-7, 100 ng/ml CTFC, 10 ng/ml TGF-β3	50 µg/ml Ascorbic Acid, collagen coated plates	1, 3, 7 and 14 days	⇧*SCX, COL1A1, COL3A1, COMP, MMP3, MMP13* gene expression ⇧SCX, TNMD protein expression	(214)
TGF-β1, CTGF	Rat BMSC	10 ng/ml	50 µg/ml Ascorbic Acid, stepwise approach	7 days with TGF-β1, 7 days with CTGF	⇧*SCX, COL1, Egr1, COMP, TNC, THBS4, Fmod, TNMD* gene expression	(215)
TGF-β2, TGF-β3	Mouse MSC	20 ng/ml		24, 48 hours	⇧*COL1A1, SCX* gene expression	(159)

1.6.3. Three-dimensional culture and mechanical stimulation

As suggested in Table 1.1 the use of scaffolds and three-dimensional (3D) cell culture is commonly utilised to assist in tendon differentiation. Tension and mechanical stimuli is a major part of the tendon cell niche, with mechanical stimulation controlling the formation of all musculoskeletal tissue during embryonic development (4,216). Tendons are particularly mechanosensitive, and tendon tissue does not form in the absence of muscle (155,217). Similarly *in vitro,* tenocytes are said to de-differentiate when cultured in traditional two-dimensional (2D) monolayer culture, with loss of tension in tenocyte culture being associated with apoptosis (218,219). In contrast, when tenocytes are exposed to mechanical force or strain, tendon related gene expression is promoted and cell proliferation increases (220–226). Due to the clear importance of mechanical stimulation, researchers sought to try to improve tenogenic differentiation by designing ECM-like scaffolds and 3D culture methods to better recapitulate the *in vivo* environment. In doing so both cell alignment and migration can be better observed, as well as changes to the ECM organisation and ECM protein deposition.

Culturing cells in 3D constructs was first reported in 1972, here fibroblasts were seeded into a collagen gel which contracted over time down to $1/10^{th}$ of its original size by rearranging the collagen matrix (227). Since its publication, collagen gels have become a popular scaffold for studying tendon development, differentiation and wound healing (63,154,173,184,185,201,212,228). For these gels collagen I is typically used, due to it being the most abundant collage in the native tendon. The gels are then grown either under “static” tension (121,154,177,187,229,230), where tension is applied by suspending the gel between two fixed point and intrinsic force applied by the matrix of cell themselves (140), “uniaxial applied tension” (231), where a constant one dimensional tension is applied externally, or under “cyclic tension”, (231), where a recurrent cycling tension is applied externally (229,232,233). Fibrin (prepared from fibrinogen and thrombin) alone or in combination with hyaluronan or collagen is another popular scaffold system used to produce tendon-like constructs (187,222,234). Utilising these methods has been reported to enhance tenogenic differentiation in comparison to 2D culture, with 3D culture alone being a potent driver of ESC and MSC differentiation towards the tendon cell fate (140,229,235).

New bioengineering strategies including electrospun collagen scaffolds, de-cellularised tendon hydrogels, poly(glycolic acid) (PGA) scaffolds, knitted silk and collagen matrices are also being investigated, and may provide a more "*in vivo*" like environment for tendon differentiation and culture (236). However further research, as well as thorough characterisation of cells grown in these culture systems is required.

1.7 Determining tendon differentiation

1.7.1. Tendon associated markers

As described in section 1.6 a huge array of methods have been proposed to differentiate stem cells down the tenogenic lineage, with no clear consensus on the most efficient and robust protocol. One of the main reasons for this is the clear lack of definitive markers defining the tendon cell lineage, unlike that of cartilage, muscle and bone. Typically, for tendon differentiation studies only a small panel of tendon-related genes are investigated in order to evaluate the efficiency of the protocol as highlighted in Table 1.1. However, caution needs to be taken with this approach as many of the common markers, including *COMP, TNC, Fmod, BGN* are highly expressed in both cartilage and tendon tissue (237–240). Similarly, *SCX, TNMD* and *THBS4* which are often regarded as the most specific tendon markers are widely expressed in a variety of tissue fibroblasts (241,242). Therefore, it is equally possible that many *in vitro* differentiation protocols, which only assess a small number of candidate genes, result in the generation of other cell types. This highlights the need for more global high throughput gene expression approaches to be taken in order to identify the best tenocyte differentiation protocols. Such global techniques, including their inception and development will be discussed below.

1.7.2. From microarrays to next generation sequencing

High throughput transcriptomics first became possible with the invention of the microarray in the 1990s (243). These small analytical devices, typically composed of a glass chip printed with thousands of microscopic spots of known DNA sequence at defined positions (probes), allowed genomic exploration of vast numbers of genes at high speed. Microarrays work by first converting sample RNA into complementary DNA

(cDNA) labelled with fluorescent tags. Molecules in the fluorescent sample then bind to complementary probes on the microarray through a process called hybridization leading to emission of light upon stimulation with a laser, the intensity of which is proportional to the level of gene expression (243). Microarrays are particularly useful in clinical research and drug development due to their ability to rapidly assess gene expression in thousands of different samples at relatively low cost. However, microarrays are only capable of detecting known sequences, with chips needing to be constantly updated in order to contain the latest sequence information, which limits their ability to detect novel transcripts (244). Similarly, the hybridization process can often result in background, with probe saturation interference making low and high-level detection more difficult. Although microarray technology continues to evolve, with regards to dyes, probes, platforms, algorithms etc, RNA-sequencing (RNA-seq) is now considered the leader in high throughput technologies for transcriptome analysis. A comparison of microarray and RNA-seq techniques is displayed in Figure 1.6.

The power of RNA-seq lies in the fact that it provides a method for both mapping and quantifying entire transcriptomes all in a single assay. RNA-seq generally works by first converting an RNA sample into cDNA fragments, otherwise known as a cDNA library. Adapter sequence containing functional elements required for the sequencing are added to the ends of each fragment in the cDNA library before subjecting it to next generation sequencing (NGS). The principle behind NGS is similar to that of Sanger sequencing, in which capillary electrophoresis is used, with different companies offering different sequencing methods from pyrosequencing to sequencing by ligation (SOLiD). Illumina sequencing however, which uses a sequencing method adapted from Sanger sequencing called sequencing by synthesis (SBS), has dominated the sequencing industry and is described in Figure 1.6. One of the key benefits RNA-seq has over microarrays include the fact than no prior knowledge of the reference genome is required, which opens the technology up to scientists working on unusual model organisms allowing them to construct de novo transcriptomes without the need for a sequenced genome (245). Similarly, unlike microarrays, minimal background signal occurs, allowing greater detection of low abundance transcripts if the sequencing is done at a high enough depth. RNA-seq also does not have an upper limit for quantifying highly expressed genes meaning it has a much broader range of detection. Finally, RNA-seq requires very little starting material and has also been shown to be extremely robust, producing reproducible

results for both technical and biological replicates. Taken together it is clear why this technology has become so popular, becoming widely used in place of microarrays.

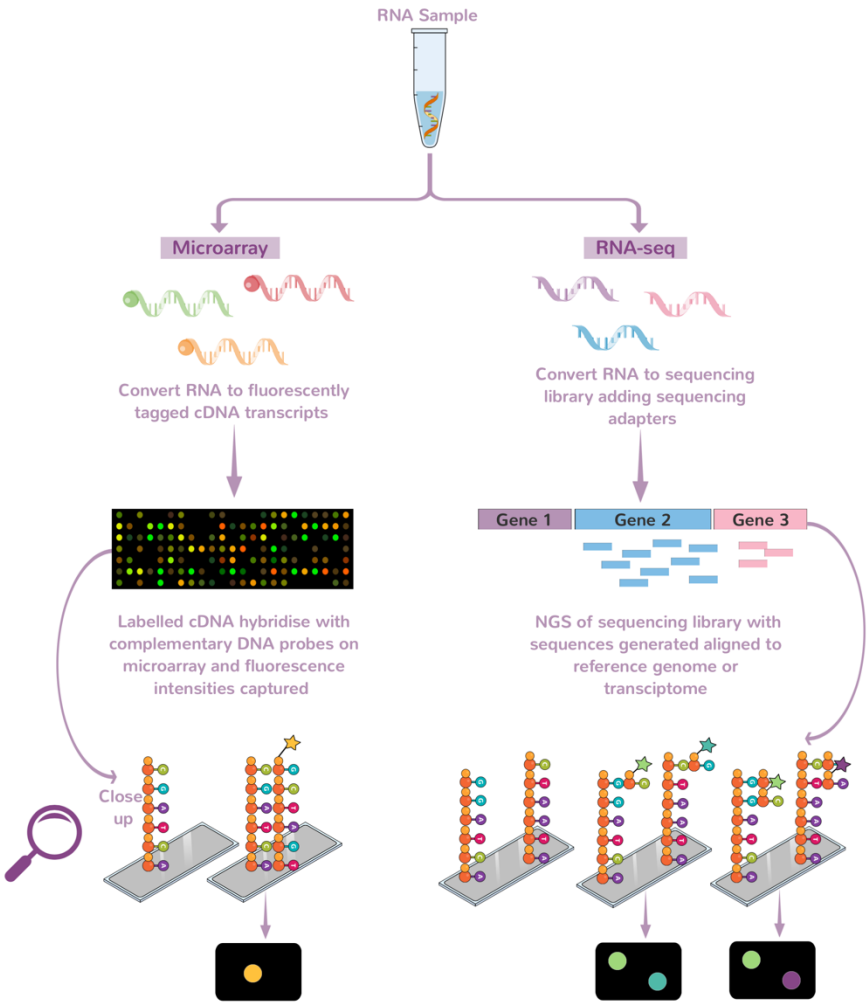

Figure 1.6. Comparison of microarrays and RNA-sequencing technologies. For microarrays the RNA sample is reverse transcribed to produce cDNA incorporating a fluorescent tag. The labelled cDNA is then added to the DNA microarray where it hybridises with cDNA probes that are attached to the microarray slide. Following a series of wash steps to remove unbound fragments, a laser is used to excite the bound fluorescently labelled target sequences and a fluorescent signal emitted. The intensity of signal represents the amount of target sample bound to each probe, which is subsequently quantified to give the level of gene expression. For RNA-seq the RNA sample is again fragmented and converted into cDNA, this time with the addition of adapters on both sides of the fragments. Bridge PCR is then used to amplify the cDNA library, which is performed on the flow cell, with each fragment being linked to it via the adapters. This results in clusters of identical DNA fragments which act as primers for the sequencing reaction. During the sequencing reaction each of the four nucleotides, each linked with different fluorescent tags, and a terminator group is added alongside polymerase. These nucleotides then bind to their complementary nucleotide and due to the terminator sequence further synthesis is not possible. A picture is then captured of the flow cell and the colour of the probe detected. The tag and terminator are then cleaved, and the process repeats until each sequence of nucleotides is determined. The sequences generated are then aligned to a reference genome or transcriptome to determine gene expression.

1.7.3. RNA-sequencing experimental design

Before any RNA-seq experiment is performed it is crucial that good experimental planning is conducted to ensure the biological question of interest can be properly answered. This can include how many replicates are required, library type, sequencing depth as well as how the data will be analysed. The first aspect to consider is the RNA-extraction protocol used. Typically for differential gene expression studies it is the messenger RNA (mRNA) that we are interested in, rather than the more abundant ribosomal RNA (rRNA) (1-2% versus > 90% of the total RNA) (246). The right RNA-extraction protocol therefore needs to be considered in order to enrich the mRNA from the rRNA. This can be in the form of poly(A) selection, which is typically performed on samples which have high RNA integrity or by rRNA depletion which is more suitable for samples which have decreased RNA integrity. With poly(A) selection a greater exonic coverage is obtained versus RNA depletion methods, with fewer pre-mRNA reads generated. However it does mean that any non-poly(A) transcripts, including small nucleolar RNAs (sno-RNAs), microRNAs (miRNAs) and some long non-coding (lncRNAs) are not detected and so poly(A) selection should not be used if these components are of interest (246).

Another factor which should be considered is read length. This can be particularly important for large transcriptomes, such as the horse being composed of 59,087 gene transcripts, in which if reads are too short they may map to multiple locations in the genome (247). Therefore, careful consideration needs to be taken on whether the cheaper single-end (SE) shorter reads or the longer more expensive pair-end (PE) read method is chosen. Similarly, the depth of sequencing coverage is an important consideration which has implications on the overall cost. In general the greater the sequencing depth the more coverage provided, with more complex transcriptomes requiring more sequencing depth in order to provide adequate coverage (247). Finally, one key aspect of experimental design is the number of replicates used. The number of replicates required will depend on how much technical variability there is in the RNA-seq procedure as well as the amount of biological variability in your system. Power calculations are typically used to determine how many replicates are needed, which work by making inferences from publicly available prototype data in order to calculate the best trade-off between replicate number and sequencing depth in order to detect your chosen power.

1.7.4. Data analysis

With transcriptomic analysis rapidly becoming standard practice in life science research this has led to a tremendous amount of data being generated. In order to turn this data into something with biological meaning it has meant that computational tools have had to be developed and updated at an exceptional rate to keep up (248). As such there is a whole host of different software available to analyse RNA-seq data. However, regardless of the software chosen the general principles remain the same. These include firstly quality control checking and pre-processing the generated reads, assembling the reads into a transcriptome either using a reference genome, reference transcriptome or by *de novo* assembly, a quantification step to estimate gene and transcript expression, and a statistical analysis step such as conducting differential gene expression analysis (245).

Describing these steps in more detail, firstly when sequencing reads are generated, they are assigned a Phred score (Q), this is a measure of the accuracy of base calling (245). Similarly, GC content, PCR duplicates, untrimmed adapter sequence and other PCR artifacts or contamination all need to be assessed prior to analysis to prevent inaccuracies in the downstream analysis and data interpretation (245). Once this is determined software can be used to trim or remove low quality sequence and remove any contaminating sequence or adapters. Once trimmed, reads then need to be aligned and assembled into transcripts. If a reference genome is available, this will typically involve aligning the reads onto the reference genome or transcriptome (246). This is clearly computationally challenging, considering that RNA-seq reads are relatively short and have the potential to map to multiple location within the reference genome or transcriptome with many spanning exon-exon junctions (249). To solve this, two main algorithmic approaches can be taken. Firstly, an unspliced read aligner can be used, which aligns reads without any large gaps, meaning only known exonic regions are considered as alignment is done to reference cDNA (transcriptome) rather than genomic DNA (genome). This method is computationally quicker and useful if you are only interested in quantifying known genes. The second option is to use a spliced aligner, which instead aligns reads to the entire genome, including intron spanning reads (249). This therefore allows the identification of novel splice sites. However, if no reference sequence is available then *de novo* assembly is performed, which involves constructing transcripts

directly from overlapping reads, and typically needs to be performed with longer PE reads with high sequencing depth in order to generate a reliable assembly.

Once the reads are assembled into transcripts, gene expression can be estimated. To do so several sources of variability need to be taken into account, with read counts needing to be properly normalised to minimise the effects of these variables. Firstly, there is the variability caused by the fragmentation process during library construction where longer transcripts will generate more reads than shorter ones regardless of whether they have the same abundance in the sample (249). Secondly, the number of reads generated and the length of reads for each sample, as well as the GC content between genes can fluctuate and must be taken into consideration. Several normalisation methods including the trimmed mean of M-values (TMM) normalisation factor, total count normalisation factor and median of ratio normalisation factor can be used to account for these biases (245).

Once the normalisation factor is chosen and transcript expression is quantified, typically the next step is to determine how these expression values differ between experimental conditions. Many different tools have been developed to detect differentially expressed genes, which continue to be made at an expeditious rate. In its simplest form, these methods use a test statistic to identify genes which have statistically significant changes in gene expression in one sample condition compared to another. Different differential expression analysis tools do so by using various statistical models based on, for example, Poisson distribution or normal or negative binomial distributions in order to accommodate the count-based nature of RNA-seq data (249). Which tool and model is best is not clear and depends on the biological variability, number of conditions and number of samples per condition; with multiple studies having been performed to compare available tools (250–253). As such no one standard protocol is used for RNA-seq analysis which can make data less comparable across platforms (244).

Once a list of generated differentially expressed (DE) genes is obtained, a number of tools can be utilised in order to gain some biological insight into what biological pathways are up or downregulated between comparisons. This includes the use of biological gene ontology analysis, pathway and network analysis software, which allow for the investigation of the biological processes and pathways that are enriched within your list of DE genes.

RNA-seq techniques and methodologies continue to evolve, playing an indispensable role for studying gene expression. Although I have focused on bulk RNA-seq techniques here, newer techniques such as single cell RNA-seq (scRNA-seq) are starting to push to the forefront, with ever more sensitive and automated methods being developed. With time, such techniques will become more accessible and should allow for a more robust understanding of many aspects of biology, including studies into stem cell differentiation.

1.8 Research aims

In summary, tendon injuries occur commonly in human and equine athletes. Adult tendons undergo poor natural regeneration, resulting in scar-tissue which is prone to re-injury. Novel cell therapies are being developed to facilitate adult tendon healing. However, for a cell-based therapy to be effective it is important that the cells used represent a viable regenerative cell type.

Fetal tendon injuries undergo completely scar-less regeneration (254). This regenerative ability is intrinsic to the fetal cells themselves, as fetal tendons, once transplanted into an adult environment, retain their regenerative capacity (255–259). Although fetal tenocytes are being considered as a cellular therapy (260), accessing fetal tissue is an issue when considering their use in clinical practice. Stem cell therapies are therefore being considered as stem cells can turn into tenocytes, however, during normal adult tendon repair there is already an influx of tenocytes into the injury site which result in scarring. It is therefore important that stem cell therapies mimic fetal regenerative tenocytes and recapitulate the properties of fetal scar-less healing.

This thesis builds on previous research into the use of horse ESCs to aid tendon regeneration. It will determine if tendon cells derived from ESCs represent the fetal or adult stage of tendon development and begin to determine if scleraxis, an essential gene in tendon formation, has different roles at different stages of development. To achieve this the following specific objectives were set:

1) To determine if ESCs differentiate into tenocytes which represent the fetal or adult stage of development by comparing their global gene expression profiles with those of adult and fetal tenocytes.

2) To identify and compare how gene expression is affected by knocking-down the tendon-related gene scleraxis in adult, fetal and ESC-derived tenocytes.

3) To identify novel genes which are the direct targets of scleraxis regulation in adult, fetal and ESC-derived tenocytes.

Chapter 2 - Materials and Methods

2.1 Tissue isolation

2.1.1. Tendon and tenocyte isolation

Tenocytes used in this study were either freshly isolated from tendon tissue or obtained from previously derived cryopreserved stocks. Equine (*Equus caballus*) tissue was harvested with the approval of the Animal Health Trust ethical review committee (AHT02_2012). Tendon tissue was collected from healthy SDFTs of eight adult Thoroughbred horses (aged 2-10 years) and three Thoroughbred foals (aged 54 days – 84 day postpartum), euthanised for reasons unrelated to this project, and from seven spontaneously aborted Thoroughbred fetuses which were 271, 289, 316, 319, 320, 321 and 340 days through gestation (full term = 322-387 days). As the sex was not determined at the time of tissue collection, polymerase chain reaction (PCR) was conducted using primers specific for the SRY gene (sex-determining gene on the Y chromosome) and sex chromosome-encoding zinc finger ZFX-ZFY genes (261) as described in section 2.4. Tendon tissue was collected in tenocyte culture medium (Dulbecco's Modified Eagle's Medium (DMEM) (Gibco, Invitrogen, Carlsbad, CA, USA) containing 10% Fetal Bovine Serum (FBS) (Gibco), 2 mM L-glutamine (L-Q) (Gibco) and 1% penicillin-streptomycin (P/S) (Gibco)), supplemented with 2.5 μg/ml of fungizone (Gibco). Tenocytes were isolated from the mid-metacarpal region of the SDFT, ensuring the peritenon was removed and only the central tendon core was used (Figure 2.1). Dissected tendon tissue was then cut into small pieces and digested in 1 mg/ml type I collagenase produced by *Clostridium histolyticum* (Sigma, Poole, Dorset, UK) in tenocyte culture medium at 37°C overnight. The culture digest was then pelleted by centrifugation (161 x g, 5minutes) and washed three times before re-plating in fresh tenocyte culture medium.

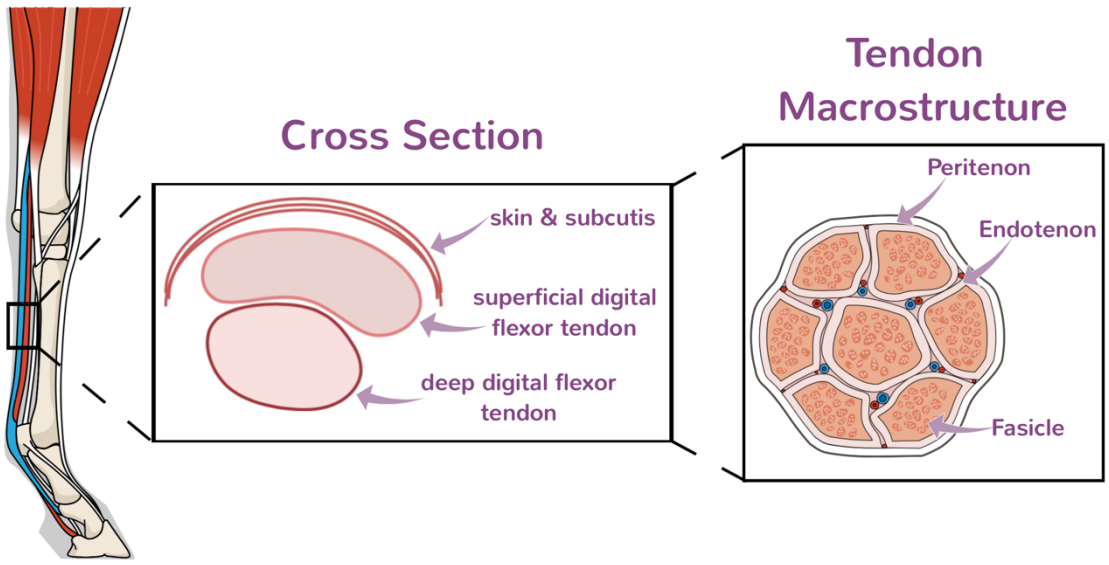

Figure 2.1. Tendon dissection and tenocytes isolation. Tendon tissue from the mid-metacarpal region of the equine forelimb was obtained. The SDFT, identified as the semi-circular tendon located laterally, was extracted and the peritenon removed. The central core was then digested in order to extract the tenocytes.

2.1.2. Cartilage isolation

Articular cartilage was harvested with the approval of the Animal Health Trust ethical review committee (AHT02_2012) under sterile conditions from both forelimb fetlock joints of one warmblood mare aged approximately 10 years. The horse was euthanised for reasons unrelated to this project, and no joint disease was detected. Both forelimb fetlock joints were disarticulated, and the cartilage removed from the articular surfaces using a scalpel blade before storing in RNA*later*® stabilization solution (Invitrogen, Renfrewshire, UK) at -20°C.

2.2 Tenocyte cell culture

2.2.1. Two-dimensional culture

Tenocyte medium composed of DMEM containing 10% FBS, 2 mM L-Q and 1% P/S (all Gibco) was used for tenocyte cellular expansion and culture, with conditions being maintained at 37°C in 5% CO_2. Medium was replaced every 2-3 days with cells being passaged using 0.25% trypsin/EDTA (Sigma) once they reached 80% confluency. When

required cells were cryopreserved in tenocyte medium supplemented with 10% tissue culture grade dimethyl-sulfoxide (DMSO) (Sigma). Cells were frozen gradually in CoolCell® cryogenic freezing containers (Sigma) at -70°C for 24 hours before transferal to liquid nitrogen. To thaw, cells were partly thawed in a 37°C water bath before transferring to pre-warmed culture medium, centrifuging for 5 minutes at 161 x g and re-plating in a new culture dish with fresh medium.

2.2.2. Serial passaging of tenocytes

Three lines of adult tenocytes were isolated and passaged ten times in 2D culture as described in section 2.2.1, with RNA extracted (see section 2.7.1) at every passage to measure *COL1A1, COL1A2*, *COL3A1, SCX*, *THBS4* and *TNMD* gene expression via qPCR as described in section 2.8.

2.2.3. Three-dimensional culture

Three-dimensional cell culture was conducted using pairs of 0.2 mm-diameter minutien pins (Interfocus fine science tools) embedded at 15 mm distances into silicon-coated six-well plates (Sylgard 184 Silicone elastomer; Dow Corning) (Figure 2.2). Tenocytes were suspended at a concentration of 4 x 10^5 cells/ml in a mixture of eight parts chilled PureCol (Bovine collagen type I; Advanced Biomatrix, Carlsbad, CA, USA) to 2 parts chilled cell culture medium (pH adjusted with 1 M sodium hydroxide from a reading of 7.2 to a reading of 7.6). Live cell counts were performed using trypan blue (Sigma) exclusion staining and a haemocytometer. The chilled cell suspension mix (200 μl) was pipetted around each pair of pins and the plate sealed with parafilm, before allowing to set for 60-90 minutes at 37°C. Once fully set, 3 ml of tenocyte medium was added per well with the medium changed every 3-4 days during the 14-day culture period. Images were obtained throughout the culture period and contraction analysis was conducted using ImageJ software (National Institutes of Health), with results being displayed as a percentage of the Day 0 value. For each time point from day 0 to 14, contraction analysis was carried out on 3-18 constructs per biological line. Cell survival assays were also performed by digesting 3D constructs in 1 mg/ml type 1 collagenase produced by *C. histolyticum* (Sigma) in tenocyte medium for 1-2 hours at 37°C. Survivals were carried out on days 3, 7 and 14 of culture. Live cell counts using trypan blue exclusion staining (Sigma) were

performed, with cell counts determined using a haemocytometer. Cell survival was calculated as a percentage of the number of cells originally seeded and were carried out on three to six constructs per time point for each biological line.

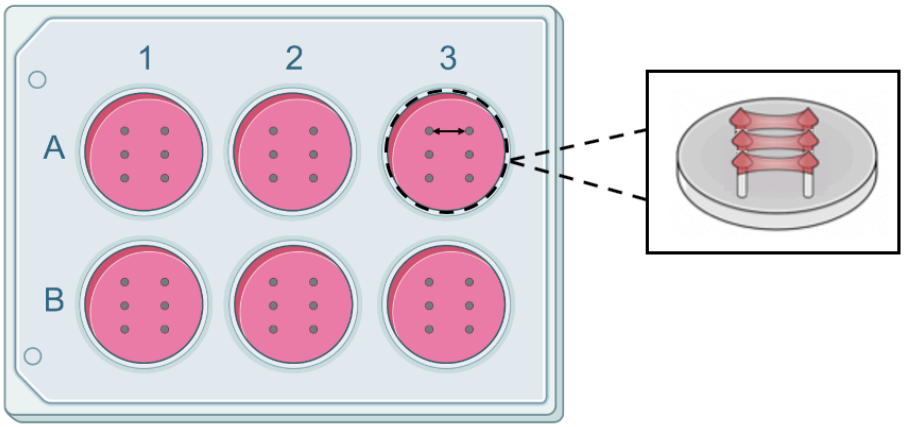

Figure 2.2. Three-dimensional cell culture set-up. A 6-well plate depicting location of 0.2 mm-diameter minutien pins depicted as grey dots, embedded in silicon coated plate. Pins are placed 15 mm apart (black arrow), and the collagen/cell suspension is pipetted around and between each pair of pins.

2.3 Embryonic stem cell culture

2.3.1. Feeder cell production

Active MF1 mouse embryonic fibroblasts (MEF), which had been tested for both bacterial and fungal contamination, were obtained at passage 0 from the Cambridge Stem Cell Institute Tissue Culture facility (Cambridge, UK). Cells obtained on dry ice were thawed and plated at a density of 8.5-10000 cells per cm^2 of tissue culture plastic and were maintained in DMEM containing 10% FBS, 2 mM L-Q and 1% P/S (all Gibco). Once 60-70% confluency was reached cells were passaged using 0.25% trypsin/EDTA (Sigma) and re-plated at the same density to increase the stock. This process was repeated up to the fifth passage. Cells were then inactivated using 10 μg/ml of mitomycin C (MMC) (Sigma) for 2 hours at 37°C, washed in culture medium and subsequently cryopreserved, as described in section 2.2.1, at a concentration of $1.6x10^6$ cells per cryovial. Each cryovial was then thawed onto 1 x 6 well plate at least one day before cells were used for ESC co-culture.

2.3.2. Undifferentiated ESC culture

Three lines of previously characterised ESCs (111,132), isolated from three different embryos were used. ESCs were maintained at 37°C in 5% CO_2 on a mitotically inactivated MEF layer as previously described (111,132). Briefly, cells were cultured in Dulbecco's modified Eagle medium/F12 (DMEM/F12 (Gibco)) containing 15% FBS (Gibco), 2 mM of L-Q (Gibco), 1% non-essential amino acids, 1 mM of sodium pyruvate, 0.1 of mM 2-mercaptoethanol (all from Invitrogen), and 1000 U/ml of human leukaemia inhibitory factor (LIF) (Cambridge University, Biochemistry Department, UK). ESCs were passaged mechanically (See Figure 2.3) every 5-7 days in the presence of 2 µM Thiazovivin (StemGent, Cambridge, MA, USA) with the medium replaced daily. Only those colonies which displayed characteristic morphology, i.e. compact, multicellular colonies characterised by a distinct border, were passaged. Any areas of spontaneous differentiation were removed throughout the culture period using a cell picker (glass pipette flamed at the end into a fine point), with the medium containing the removed areas of spontaneous differentiation replaced.

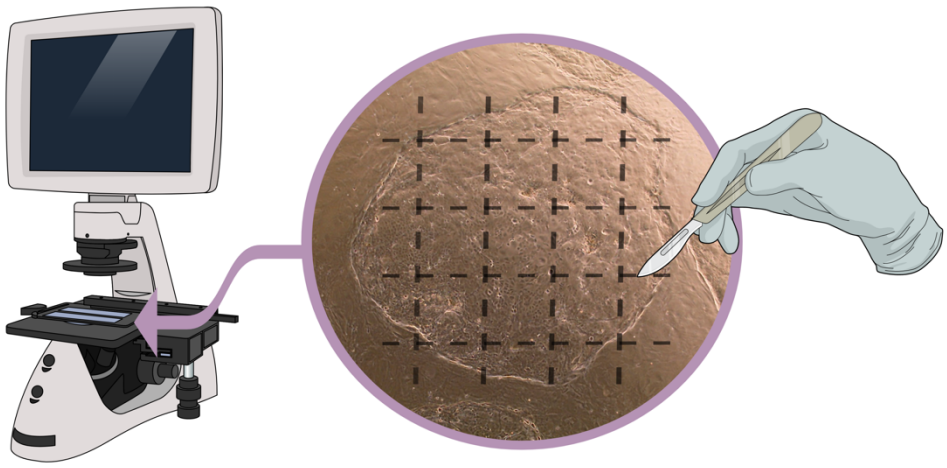

Figure 2.3 Mechanical passaging of ESCs. Using an EVOS XL Core Cell Imaging System (ThermoFisher), once colonies reached approximately 70% confluency mechanical passaging was conducted by cutting the colonies into small squares of approximately 50 - 100 µm in size (containing approximately 50 - 200 cells) using a scalpel blade. Cut colonies were then lifted using a cell picker, collected into a 15 ml falcon tube and allow to settle by gravity. The medium above the gravity separated cell pellet was removed to ensure no single cells remained and the process repeated with fresh medium. Cell aggregates were then re-plated at a 1:2 splitting ratio onto a new plate of inactivate MEFs' (thawed one day prior to ESC passaging).

2.3.3. Two-dimensional ESC tenocyte differentiation

Differentiation of the ESCs in 2D was induced by passaging the cells into feeder-free conditions in ESC medium without LIF. Cells were allowed to attach for 24 hours before the addition of 20 ng/ml of TGF-β3 (Peprotech, London, UK). Differentiation was conducted for 14 days with the medium being replaced every 3 days with fresh TGF-β3 added.

2.3.4. Three-dimensional ESC tenocyte differentiation

Mechanically passaged clumps of ESCs (see section 2.3.2) were isolated, and an aliquot dissociated into single cells using TrypLE™ Select (Invitrogen), by incubating for 8-10 minutes at 37°C, in order to conduct representative cell counts. Non-dissociated colonies of ESCs were then suspended at the same cell density and prepared in the same way as tenocyte constructs (see section 2.2.3) but using ESC medium without LIF. Contraction analysis and cell survival assays were performed as stated previously (see section 2.2.3).

2.4 Sexing cell lines

Genomic DNA from all cell lines used was extracted from $1x10^6$ cells using the QIAamp DNA mini kit (Qiagen, Valencia, CA) according to manufacturer's instruction. Primers were designed to amplify the SRY and ZFX-ZFY genes using Primer3 (http://primer3.ut.ee/) ensuring they had a GC content between 40-80%, were of length 18-24 bases, with the primers in a pair having a Tm within 5°C of each other, and avoided primer secondary structures as determined by the programme mfold (262). Primers are found in Table 2.1.

Table 2.1. PCR primers for sexing cell lines.

Primer Name	Sequence (5'→ 3')	PCR Product (bp)	Melting Temperatures
SYR Forward	TGCTATGTCCAGAGTATCCAACA	Male: 714	58°C
SYR Reverse	TGAGAAAGTCCGGAGGGTAA	Female: 0	58°C
ZFX/Y Forward	AAATCAAAACCTTCATGCCAAT	Male: 604 + 553	53°C
ZFX/Y Reverse	TTCCGGTTTTCAATTCCATC	Female: 604	53°C

The One*Taq*® DNA polymerase (NEB) was used for amplification of the PCR products from genomic DNA in accordance with the manufacturer's instructions. Briefly, for each, 1.5 µl of genomic DNA (diluted to give approximately 50 ng), 10 µM of each primer, 10 µl of 5x One*Taq*® Standard Buffer, 10 mM of deoxynucleotide triphosphate (dNTPs), 0.25 µl of One*Taq*® Hot Start DNA Polymerase (all NEB) and distilled water were mixed to obtain a final volume of 50 µl. For the amplification the BioRad T100™ Thermal Cycler was used and set to a program of: 94°C for 30 seconds, 30 cycles of denaturation at 94°C for 30 seconds, primer annealing at either 55°C for the SYR primers or 48°C for the ZFX/Y primers for 1 minute, extension at 65°C for 1 minute and a final elongation step of 65°C for 10 minutes. Amplified PCR products were then run on 1% agarose gel and visualised as described in section 2.6.1.

2.5 Lentiviral infection of cells

2.5.1. Packaging cell culture

HEK293T, a human embryonic kidney cell line that expresses a mutant version of the SV40 large T antigen was used as a packaging cell. These cells were used due to their known ability to produce high lentiviral titers by allowing transfected plasmid DNAs that carry the SV40 origin of replication (ORI) to replicate within them (263). HEK293T cells were maintained in DMEM containing 10% FBS, 2 mM of L-Q and 1% P/S (all Gibco). Once 80% confluency was reached cells were passaged using 0.25% trypsin/EDTA, with care being taken to ensure cells did not become overconfluent as this can affect their growth rate and the subsequent lentiviral titer produced. Prior to transfection, HEK293T lines were passaged 3-4 times after thawing in order to give the cells time to recover from the thawing process and return to their normal growth rate.

2.5.2. Lentiviral production and target cell infection

TRC2-pLKO.1-puro vector plasmids containing a short hairpin RNA (shRNA) specific for human SCX (95.24% identity to the equine SCX sequence) (clone NM_001008271.1-95s21c1; Sigma) (shSCX), a non-target, scrambled (NT) shRNA sequence (SHC202; Sigma) and a Turbo-GFP shRNA (SHC203; Sigma) were utilised for stable cell line

generation. For visualisation of the Turbo-GFP shRNA (SHC203; Sigma) in ESCs the plasmid was modified as described in section 2.6. One microgram of the pLKO.1 plasmid alongside 750 ng of psPAX2 (#11260; Addgene, Cambridge, MA) and 250 ng of pMD2.G (#12259; Addgene) were transfected into HEK293T packaging cells, using the FuGENE® 6 transfection reagent (Promega, Hampshire, UK) as described in Figure 2.4.

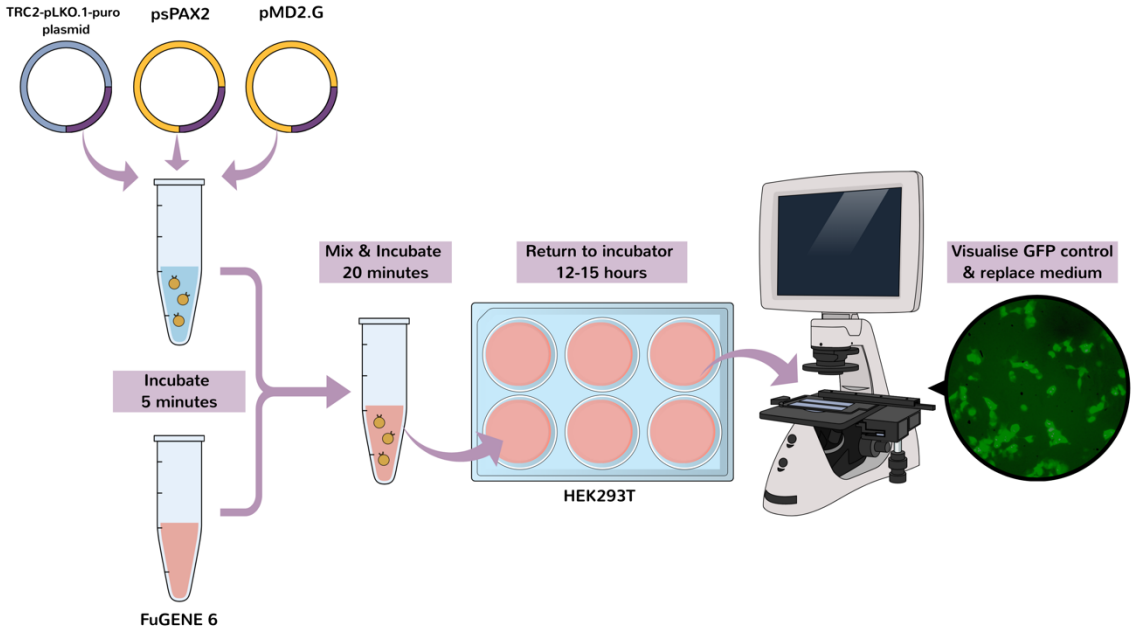

Figure 2.4. HEK transfection. To an Eppendorf tube the psPAX2 and pMD2.G packaging plasmids, as well as either the shSCX, NT or Turbo-GFP plasmid previously described were added, and the volume adjusted with Opti-MEM reduced serum medium (Gibco) to give a 20 µl final volume per reaction. In a second Eppendorf tube, 6 µl of FuGENE® 6 transfection reagent was added to 74 µl of Opti-MEM per reaction. Both Eppendorf tubes were incubated for 5 minutes at room temperature before mixing and incubating for a further 20 minutes. The 100 µl of plasmid/FuGENE® mix was then added dropwise per well of HEK293T cells, which were plated at $1x10^5$ cells per well one day prior. Cells were returned to the incubator for 12-15 hours, before qualitative visualisation of transfection efficiency using the green fluorescent protein (GFP) control on the Olympus IMT2-SFR inverted microscope.

Packaging cell supernatant containing infectious lentiviral material was then collected 48-, 72- and 96-hours post transfection, filtered through a 0.45 µm filter (Millipore, Billerica, MA, USA) to remove cellular debris and frozen at -70°C. Target cells were seeded at $1x10^5$ cells per well of a 6-well plate 24-hours before infection with $1x10^7$ IU/ml of virus. Puromycin (Sigma) antibiotic selection was then carried out at a concentration of 4 µg/ml (determined optimal based on an antibiotic kill curve of non-infected cells). The qPCR Lentivirus Titration Kit (LV900) from abm (Applied Biological Materials Inc, Richmond, CA) was used to calculate the viral titer of the frozen preparations as described

in section 2.5.3. Lentiviral infection was optimised using titers varying from $5x10^5$ IU/ml to $1x10^8$ IU/ml, with $1x10^7$ IU/ml obtaining the best viral efficiency with limited cytotoxic effects and optimal copy number integration (see section 2.5.4).

All SCX knockdown and paired NT control lines generated were expanded in culture with cryopreserved stocks made as described in section 2.2.1. RNA was extracted from each line (see section 2.7.1) and similarly coverslips of all SCX knockdown and paired NT control lines set up and fixed (as described in section 2.11.1) ready for subsequent analysis. Six biological replicates of SCX knockdown and paired NT control lines were generated in adult and fetal tenocytes, four of which (i.e. four adult and four fetal tenocyte lines) were used in RNA-seq experiments (see section 2.9). All adult and fetal tenocyte shSCX and NT lines used in subsequent experiments were between passage (P)5 and P10. SCX knockdown in young postnatal foal tenocytes was conducted in three biological replicates, with cells being used between P5 and P9 in all subsequent experiments. For the undifferentiated ESCs, SCX knockdown was conducted in one biological line, with the knockdown being performed in three independent technical replicates. SCX knockdown ESCs were used between P19 and P22 in subsequent experiments.

2.5.3. Lentiviral titer

The abm qPCR Lentivirus Titration Kit was used to determine the titer of frozen viral preparations according to the manufacturer's instructions. Briefly, viral supernatant was centrifuged at 2000 x g for 5 minutes to remove any remaining cellular debris. Viral lysis was then conducted by adding 2 µl of viral supernatant to 18 µl of Viral Lysis Buffer (abm), which was incubated at room temperature for 3 minutes. A qPCR reaction was then set up containing 12.5 µl of SensiMix SYBR No-ROX supermix (Bioline, London, UK), 10 µl of reagent-mix (abm) and 2.5 µl of either the viral lysate, standard 1, standard 2 or distilled water added to give a final reaction volume of 25 µl. Each reaction was set up in triplicate and run as described in section 2.8.2. The sample titer was then calculated using the abm High Titer Lentivirus Calculator (http://www.abmgood.com/High-Titer-Lentivirus-Calculation.html).

2.5.4. Lentiviral copy number integration

Genomic DNA was extracted from $1x10^6$ lentiviral infected cells using the QIAamp DNA mini kit (Qiagen, Valencia, CA) according to manufacturer's instruction. Transgene copy number was quantified using a combination of the protocols described in Joshi et al., 2008 and Barczak et al., 2014 (264,265). Briefly qPCR was conducted using 100 ng of DNA per 25 µl reaction using SensiMix SYBR No-ROX (Bioline). Primers were designed for the detection of the Woodchuck Hepatitis Virus Post-Transcriptional Regulatory Element (WPRE) sequence, a lentiviral specific fragment, and the 18s rRNA housekeeping gene (Table 2.4). All reactions were conducted using the cycling conditions described in section 2.8.2. The mass of one copy of the SCX shRNA, NT shRNA and Turbo-GFP shRNA plasmids were calculated using the formula below: -

$$m = \frac{M}{N_A}$$

Where m = mass of one copy, M = molecular weight of the plasmid (Dalton) calculated based on the length (bp) of the plasmid and the molecular weight of nucleotide (650 Daltons/base pair) and N_A = Avogadro's number (6.02×10^{23} copies/mole).

It was calculated that each copy of the SCX shRNA and NT shRNA had a mass of 5.7 ag and 1 ng of plasmid therefore had approximately 1.23×10^9 copies of WPRE transgene. Each copy of GFP shRNA had a mass of 9.5 ag and 1 ng of plasmid therefore had approximately 1.23×10^9 copies of WPRE transgene. Plasmid concentrations were quantified using the Quant-iT™ PicoGreen™ dsDNA assay kit (Invitrogen) according to the manufacturer's instructions. A standard curve was constructed by carrying out serial dilutions of each plasmid, containing the relevant sequence (WPRE), from 1 pg to 10 ag allowing quantification of unknown samples. All dilutions were made in the presence of 10 ng/µl carrier DNA from WT equine tenocytes (not containing the WPRE transgene) in order to increase the stability of the dilutions. The number of transgene lentiviral integrating events in 100 ng of DNA was calculated from their respective C_T (cycle threshold) value using a linear equation calculated from each plasmid standard curve. WPRE copy number per diploid cell was then calculated based on an average DNA yield of 28.33 µg obtained from $1x10^6$ cells as shown in the equation below: -

$$Average\ number\ of\ cells\ per\ 100\ ng\ DNA = \frac{28.33\ \mu g}{100\ ng} = 283.3\ ng$$

$$= \frac{1x10^6}{283.3} = 353\ cells$$

Therefore, it was calculated that 100 ng of DNA contains the DNA from approximately 353 diploid cells.

2.6 Modification of Turbo-GFP shRNA plasmid

To facilitate the expression of the green fluorescent protein (GFP) in ESCs the Turbo-GFP shRNA (SHC203; Sigma) control cytomegalovirus (CMV) promoter, which did not have transcriptional activity in equine ESCs, was replaced with either the human phosphoglycerate kinase (PGK) or elongation factor 1 alpha (EF1a) ubiquitous promoter sequence. To do so, the Turbo-GFP shRNA plasmid (Figure 2.5) was cut using the restriction enzymes KpnI and NehI in order to remove the CMV promoter. Restriction enzyme digests were typically performed using 10 units of restriction enzyme (NEB) per 1µg of DNA in the appropriate buffer for 1 hour at 37°C. The cut plasmids were dephosphorylated using FastAP Thermosensitive Alkaline Phosphatase (Thermo) according to the manufacturer's instructions, in order to prevent self-ligation. Linearized plasmids were run on an agarose gel (see section 2.6.1) and the backbone of the vector, minus the CMV insert, excised and purified (see section 2.6.2).

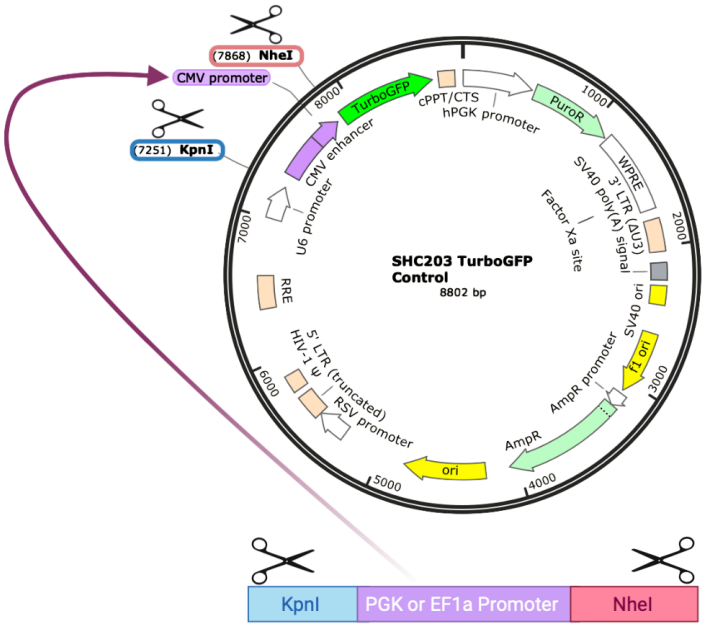

Figure 2.5. SHC203 Turbo-GFP modification. Scissors highlight the restriction enzyme cut sites used during the cloning process to remove the CMV promoter from the Turbo-GFP shRNA control plasmid, for replacement with either the PGK or EF1a PCR amplified promoters. Plasmid maps visualised in SnapGene® (v.5.1).

Using modified primers containing recognition sequences for the restriction enzymes that were used to remove the CMV promoter, KpnI and NehI at the 5' and 3' end respectively (Table 2.2), the PGK promoter from the NT shRNA plasmid (SHC202; Sigma) and the EF1a promoter from the pLV-EF1a-IRES-Blast (a gift from Tobias Meyer – Addgene) were amplified by PCR as described in section 2.6.3. PCR products were then purified (see section 2.6.2) and cut using the restriction enzymes KpnI and NehI to create the complementary base pair overhangs. Cut PCR products were ligated to the linearized plasmid backbone using T4 ligase (NEB) in accordance with the manufacturer's instructions. The ratio of vector to insert was calculated using the NEBioCalculator™ (v1.10.1). Ligation products were transformed into competent cells (see section 2.6.4), alongside no insert and no T4 ligase internal controls (see section 2.6.4). Eight resistant colonies were then picked from each successful ligation and seeded into LB broth containing 50 µg/ml ampicillin, and subsequently small-scale plasmid DNA isolations performed as described in section 2.6.4. Restriction enzyme test digests were used to initially verify correct insertion of the new promoter before sanger sequencing (see section 2.6.5). Plasmids with correctly inserted promoters were then isolated using large-scale DNA isolation as described in section 2.6.4.

Table 2.2. Primer sequences used for PCR. Capitalised sequence text represents the binding region. Green lowercase text indicates additional base pairs added before the restriction enzyme digest site. Blue lowercase text indicates the addition of a KpnI restriction digest site. Pink lowercase text indicated the addition of a NheI restriction digest site.

Primer Name	Sequence (5'→ 3')	PCR Product (bp)	Melting Temperature
PGK-KpnI Forward	tgaggtaccTTGCGCCTTTTCCAAGGCAG	PGK: 519	67°C
PGK-NheI Reverse	ttagctagcCTGGGGAGAGAGGTCGGTG		67°C
EF1a-KpnI Forward	tgaggtaccCGATGAGGCCCTTTCGTCT	EF1a: 1124	68°C
EF1a-NheI Reverse	cgagctagcGGATCCTCACGACACCTGAAAT		68°C

2.6.1. Agarose gel electrophoresis

The appropriate percentage agarose gel (1.0% for effective separation of 400–8000 bp, 1.5% for 200-3000 bp or 2% for 100-2000 bp) was prepared by melting Ultra-Pure Agarose (Invitrogen) in 1x TAE (Tris-Acetate-EDTA)(Sigma). GelRed® Nucleic Acid Gel Stain (Biotium, Fremont, CA) was added to the molten agarose at a 1x final concentration. Orange DNA Loading Dye (6X) (ThermoFisher, Loughborough, UK) was added to the DNA before loading alongside either the Quick-Load Purple 100bp or 1Kb DNA Ladder (NEB). Electrophoresis was performed in 1x TAE at 100 volts for the time required for optimal separation (typically 45 minutes). UV light on a transilluminator was used to visualise the DNA and gels were photographed using the Alpha Innotech Alphalmager 2200 Gel Image Analysis System.

2.6.2. Plasmid DNA and PCR purification

Plasmid DNA and products obtained from polymerase chain reactions (PCR) were purified using the Monarch® PCR & DNA Cleanup Kit (New England BioLabs (NEB), UK) according to the manufacturer's instructions. DNA extraction from agarose gel was conducted by excising the appropriately sized band from the gel using a scalpel blade and purifying using the Monarch® DNA Gel Extraction Kit (NEB, UK) according to the manufacturer's instructions. DNA concentration was calculated from the absorbance at 260 nm measure using a Nanodrop™ One Microvolume UV-vis Spectrophotometer

(ThermoFisher). A 50 µg/ml solution of double-stranded DNA and a 33 µg/ml solution of single stranded DNA have an absorbance of 260nm of 1.0.

2.6.3. Using PCR to amplify plasmid promoter regions

Primers were designed using Primer3 (http://primer3.ut.ee/) ensuring they had a GC content between 40-80%, were of length 18-24 bases, with the primers in pairs having a Tm within 5°C of each other and avoided primer secondary structures as determined by the programme mfold (262).

The Phusion™ High-Fidelity DNA polymerase (ThermoFisher), a Pyrococcus-like proofreading polymerase and fused DNA-binding domain, was used to amplify the PGK and EF1a promoters (see section 2.6) from plasmid DNA in accordance with the manufacturer's instructions. Briefly, for each, 1 µl of plasmid DNA (diluted to approximately 2 ng/µl), 0.5 µM of each primer, 10 µl of HF Buffer, 10 mM of dNTPs, 0.5 µl of Phusion DNA Polymerase (all ThermoFisher) and distilled water were mixed to obtain a final volume of 50 µl. For the amplification the BioRad T100™ Thermal Cycler was used and set to a program of: 98°C for 30 seconds, 35 cycles of denaturation at 98°C for 10 seconds, primer annealing at 60°C for 30 seconds, extension at 72°C for 30 seconds and a final elongation step of 72°C for 10 minutes.

2.6.4. Bacterial transformation

All bacterial work was carried out near a Bunsen burner on the blue flame, with the lids of glass bottles and L-shaped bent glass pipettes used for spreading transformations flamed and treated with 70% ethanol.

E.coli DH5α competent cells (Invitrogen) were used for transformations, using the heat shock method. Briefly, 50 µl of competent cells were thawed on ice and 5 µl of ligation reaction or 1 µl of plasmid DNA (approximately 50 ng) added and incubated for 10 minutes on ice. Following incubation, the reaction was transferred to a 42°C water bath for 30 seconds before re-incubating on ice for a further 2 minutes. A volume of 900 µl of LB broth, made by adding 5 g of Tryptone, 2.5g of. yeast extract and 2.5 g of NaCl (all Sigma) to 500 ml of distilled water which is then autoclaved, was added to the competent cells and incubated at 37°C for 30 minutes with gentle shaking. LB agar plates were made

by adding 5 g of Tryptone, 2.5 g of yeast extract, 2.5 g of NaCl and 7.5g of bactoagar (all Sigma), made up to 500 ml with distilled water which is then autoclaved before 50 μg/ml ampicillin was added, and the liquid poured into petri dishes. Bacterial transformations were then plated onto LB agar plates and incubated upside-down at 37°C overnight.

Resulting colonies were picked and seeded into 2 ml of LB broth for small scale plasmid DNA isolation or 250 ml for large scale plasmid DNA isolation. Small scale plasmid DNA isolation were performed using the Monarch® Plasmid Miniprep Kit (NEB) according to the manufacturer's instructions. Large scale plasmid DNA isolation were performed using the HiSpeed® Plasmid Maxi Kit (Qiagen) according to the manufacturer's instructions.

2.6.5. Sanger sequencing of modified plasmids

Sanger dideoxynucleotide sequencing (266) was carried out in-house. Briefly, sequencing reactions were set up containing 5 μl of sequencing buffer (final concentration 80mM TRIS-HCl pH 9.0, 2mM $MgCl_2$), 1 μl of Big Dye™ Terminator mix version 3.1 (Applied Biosystems), 1.5 μl of sequencing primer (0.08 μM final concentration, primers found in Table 2.3), 2.5 μl of purified plasmid (at 50 ng/μl) and water to a final volume of 20 μl. Reactions were run on a Biddy Scientific™ Techne™ TC-512 gradient thermo cycler (ThermoFisher) using the following program: denaturation at 96°C for 15 seconds, primer annealing at 50°C for 10 seconds, and extension at 60°C for 2 minutes, which was repeated 25 times. Sequencing products were purified by precipitation by adding 2 μl of 3M sodium acetate (pH 4.6) and 50 μl of 100% ethanol and incubating for 15 minutes at room temperature. Precipitated products were then centrifuged at 3500 x g for 30 minutes before removing the liquid and adding 125 μl of 70% ethanol and incubating for a further 15 minutes. Precipitated products were centrifuged again, and the ethanol removed. For the sequencing step, 10 μl of HiDi buffer (Applied Biosystems), was added to each precipitated sample and denatured for 1 minute at 96°C, before being placed on ice. Sample electrophoresis and analysis was performed on an ABI Prism 3100XL Genetic Analyser (Applied Biosystems). Resulting sequencing data was analysed in SnapGene® (v.5.1).

Table 2.3. Primers for sanger sequencing.

Primer Name	Sequence (5'-3')
U6 Region Forward	GACTATCATATGCTTACCGT
GFP Region Reverse	CATCTTGTTGGTCATGCGGC

2.7 RNA extraction

2.7.1. RNA isolation from cells and 3D constructs

RNA was harvested into 1 ml of Tri-reagent (Sigma) per 10 cm plate for 2D cultured cells or per six to nine gel constructs for 3D cultured cells and stored at -70°C until required. When ready to use, samples were thawed and incubated at room temperature for 5 minutes, 300 µl of chloroform (Sigma) added, vortexed for 15 seconds, incubated for a further 5 minutes and then centrifuged at 12,000 x g for 15 minutes at 4°C. The aqueous layer was then isolated and 700 µl of 70% ethanol added. For 3D cultured cells, the aqueous layer of between 9 and 35 gel constructs (harvested from the same biological line and experimental set up) were pooled. RNA was then extracted using a RNeasy mini kit (Qiagen) according to the manufacturer's instructions. DNase treatment was then conducted using the DNA-free™ kit (Ambion, Texas, USA) as per the manufacturer's instructions. RNA concentrations were calculated using a Nanodrop™ One Microvolume UV-vis Spectrophotometer, using an absorbance of 260 nm and ensuring the 260:280 ratio lay within 1.8 and 2.2 indicating high purity RNA.

2.7.2. RNA isolation from cartilage

Using a liquid nitrogen cooled pestle and mortar, warmblood cartilage stored in RNA*later*® (see section 2.1.2) was ground into a powder. The resulting powder was collected in PBS (phosphate buffered saline), centrifuged at 161 x g for 5 minutes and resuspended in 1 ml of Tri-reagent (Sigma) and stored at -70°C until later use. RNA-extraction was conducted as described in section 2.7.1.

2.7.3. cDNA synthesis

One microgram of total RNA was reverse transcribed using the SensiFAST cDNA Synthesis Kit (Bioline, London, UK). Samples were prepared and underwent thermo cycling on a BioRad T100™ Thermal Cycler. Briefly, 4 µl of TransAmp Buffer and 1 µl of Reverse Transcriptase were added to the RNA and made up to 20 µl with DNase/RNase free water before cycling as follows: primer annealing at 25°C for 10 minutes, reverse transcription at 42°C for 15 minutes, optional step at 48°C for 15 minutes and inactivation at 85°C for 5 minutes. Reactions lacking the reverse transcriptase were also carried out to ensure no genomic DNA contamination. Following thermocycling reactions were diluted in DNase/RNase free water to a final volume of 50 µl, which assuming 100% efficient cDNA synthesis, resulted in a final concentration of 20 ng/µl of cDNA. All products were then stored at -20°C until qPCR was carried out.

2.8 Quantitative PCR (q-PCR)

2.8.1. Primer design for qPCR

Equine gene specific primers were designed using NCBI Primer-Blast (https://www.ncbi.nlm.nih.gov/tools/primer-blast/) and are found in Table 2.4. The programme mfold (262) was used to ensure each amplicon (50-150 bp in size) had a Tm of between 58-62°C, a GC content between 40-80% and were devoid of secondary structure at Tm 60°C. All primers were ordered from Sigma and were designed to span an intron where possible in order to ensure amplicons were devoid of contaminating genomic DNA. The efficiency of each primer set was determined by generating a standard curve of known quantities of appropriate equine cDNA (40 ng, 20 ng, 10 ng, 5 ng, 2.5 ng and 1.25 ng), ensuring the efficiency lay between 85% and 115%, with reactions being set up as described in section 2.8.2. The efficiency was calculated using the equation

$$\text{Efficiency} = 10^{(-1/\text{slope})} - 1$$

Where the slope is derived from the Cycles to Threshold (Ct) values plotted against the Log10 of the template amount. The size of all products was also confirmed using agarose

gel electrophoresis (see section 2.6.1), and the products Tm confirmed via the melt curve (see section 2.8.2).

Table 2.4. qPCR primers.

Gene	Forward Primer (5'-3')	Reverse Primer (5'-3')	Product Melting Temp (Tm)
18s rRNA	CCCAGTGAGAATGCCCTCTA	TGGCTGAGCAAGGTGTTATG	78°C
ACAN	GCGGTACGAGATCAACTCCC	GCGACAAGAAGAGGACACCA	88 C
ACTB	CCAGCACGATGAAGATCAAG	GTGGACAATGAGGCCAGAAT	80°C
CDK1	CTGGGCAGTTCATGGATTCT	CAATCCCTTGTAGGATTTGG	74°C
CNMD	GGGAACAACTTGGAGACCTT	TTCTCTCCTCCAGCAAAACG	75°C
COL1A1	TGCGAAGACACCAAGAACTG	GACTCCTGTGGTTTGGTCGT	85°C
COL1A2	GTGCCTAGCAACATGCCAAT	GTCCTCTATCTCCGGTTGGG	79°C
COL2A1	TCCTGGTGTCAAAGGTCACA	TCCCTTAGCACCATCCAGAC	78°C
COL3A1	CTGGTGCTAATGGTGCTCCT	TCTCCTTTGGCACCATTCTT	77 C
COL14A1	CTTCATGTTCTGCCTACGGG	CGTCTTGGACAGGGGTGAAT	80°C
COMP	AGAACATCATCTGGGCCAAC	CGCTGGATCTCGTAGTCCTC	81°C
EYA2	GGGCTCCGTGTTTCCTATTG	GGCCGAACCTCTGCATTATC	79°C
GAPDH	CGACCACTTTGTCAAGCTCA	GTCCACCACCCTATTGCTGT	77°C
GPRIN3	AGCTTAGACTCTGAACATATGAGG	CCAGGGTCTACGTATGCAGG	78°C
IL1R1	GAAGCGCATAAAGGGCACTA	CGTGGGCCTGATTTCATCTA	76°C
IL1R2	TCTGGCACCTACATCTGCAC	CAGGGCAGCTTCTGTCTTCT	81°C
IL1RN	GCCTGTGTCAAGTCTGGTGA	CCTCCTTGTTCTTGCTCAGG	78°C
LHX9	AACAGGGCTGACCAAAAGAG	TGAATTTGGCTCGTGCGTTT	72°C
MKX	AAGGCAAAGGAACCATTCGG	TTAGCTGTCACCCTTATTGGAT	79°C
MMP2	CAGGAGGAGAAGGCTGTGTT	AGGGTGCTGGCTGAGTAGAC	77°C
MMP3	TGGACCTGGAAAAGTTTTGG	GACCAAGTTCATGAGCAGCA	80°C
MMP9	GAGATCGGGAATCATCTCCA	CCAAGAGTCGCCAGTACCTC	76°C
MMP13	GCCACTTTGTGCTTCCTGAT	CGCATTTGTCTGGTGTTTTG	77°C
SCX	CCCAAACAGATCTGCACCTT	ATCCGCCTCTAACTCCGAAT	81°C
SMAD3	ATCCCCAAATCCGATGTCCC	GCGCTGGTTCAGCTCATAGT	83°C
SOX9	GCTCTGGAGACTTCTGAACGA	GTAATCCGGGTGGTCCTTCT	86°C
SOX11	GTTCATGGTGTGGTCCAAGA	GCTGTCCTTCAGCATTTTCC	82°C
TENM4	CTGATGGGAAGACATGGAGC	GCGGTCATTCTTGTCGAACT	79°C
THBS4	GGGAAATGGGGTTACCTGTT	CGGGTAGCAGGGATGATATT	76°C
TNC	AACCCGTCCAAAGAGACCTT	GCGTGGGATGGAAGTATCAT	81°C
TNMD	GTCCCTCAAGTGAAGGTGGA	CCTCGACGGCAGTAAATACAA	79°C
VIM	GAGAGCACCCTGCAATCC	AAGGTCAAGACGTGCCAAAGA	77°C
WPRE	AGCTGACAGGTGGTGGCAAT	TGCTGACGCAACCCCCACTGGT	72°C

2.8.2. qPCR reaction

qPCR was carried out using a Biorad CFX96 Touch Real-time PCR detection machine. Each qPCR reaction was performed in duplicate and consisted of 10 µl of SensiMix

SYBR No-ROX supermix (Bioline), 1 µl of forward and reverse primers (final concentrations, 0.5 µM), 6 µl of HPLC grade water and 2 µl (40 ng) of relevant cDNA (or controls; no reverse transcription RNA and no template control). Cycling was conducted using the following program: initial denaturation at 95°C for 10 minutes, followed by 45 cycles of denaturation at 95°C for 15 seconds, annealing at 55°C for 15 seconds and elongation at 72°C for 15 seconds. The temperature was then reduced to 60°C and gradually increased by 0.5°C every 10 seconds up to 90°C, to produce a melt curve. Reactions were quantified relative to the 18s rRNA housekeeping gene, which has previously been used as a housekeeping gene in these cell types (121,140,154,267) and proved stable upon validation (see section 2.8.3). To calculate the relative gene expression the following formula was used: $2^{-\Delta\Delta CT}$, where ΔCT = average threshold cycle of the gene of interest – average threshold cycle of the housekeeping gene (268).

2.8.3. Housekeeping gene validation

cDNA samples from three independent lines of adult, fetal and ESC-derived tenocytes (cultured in 3D) used for the RNA-seq experiments were used to validate the most suitable housekeeping gene for qPCR. Seven genes were tested and normalised to three different equine specific housekeeping genes, *18s rRNA*, *ACTB* and *GAPDH* (Table 2.4). The results were then compared to that obtained from the RNA-seq experiment. The stability of the housekeeping genes was also evaluated using RefFinder (https://www.heartcure.com.au/reffinder/) which integrates the following computational housekeeping validation tools: geNorm, Normfinder, BestKeeper and the comparative deltaC_T method. As an input for this analysis the triplicate C_T values obtained from three independent lines of adult, fetal and ESC-derived tenocytes of *18s rRNA, ACTB* and *GAPDH* were used and the genes ranked from most to least stable.

2.9 RNA-sequencing

2.9.1. Power calculations

Prior to sequencing power calculations were performed, according to established protocols (269), to determine the minimum sample size required per group for RNA-seq

in order to provide an 80% power to detect a 2-fold change in gene expression at a significance level of 5%. Calculations were performed based on the following assumptions: A) an estimated co-efficient of variation (CV) in gene expression of 0.25 between sample of a single cell type. This estimate is based on RNA-seq data in human cells and tissues which report CVs' ranging from 0.2 for peripheral blood mononuclear cells (PBMCs) to 0.74 for more complex tissue samples (269). As our experiments are based on *in vitro* cell cultures, comparing tenocytes under different conditions a CV more similar to PBMCs was used. B) A mean coverage of 30X, based on obtaining 26 million reads per sample which has been shown to be sufficient to detect differential gene expression for the majority of genes (246). Based on these assumptions, 3 samples per group was calculated to be sufficient to detect a 2-fold change in gene expression at a significance level of 5% with 80% power.

2.9.2. RNA-sequencing sample integrity

Three lines of adult, fetal and ESC-derived tenocytes cultured in 3D, three lines of adult and fetal tenocytes cultured in 2D, four lines of adult shSCX and NT expressing cells and four lines of fetal shSCX and NT expressing cells were used in RNA-sequencing experiments. Adult and fetal 3D tendon constructs were between P3 and P8. ESC-derived 3D tendon constructs were between P12 and P22. Adult and fetal tenocytes 2D cultures were between P3 and P8. Adult and fetal shSCX and NT lines were between P5 and P8.

RNA quality was determined for all the aforementioned samples using the Agilent 2200 Tape station system (outsourced to Cambridge Genomics Service, Cambridge). RNA Integrity Number (RIN^e) values for all samples were between 9.3-10.

2.9.3. RNA sample library preparation and sequencing

mRNA library preparation and sequencing were performed by external providers (Edinburgh Genomics, Edinburgh, UK and Otogenetics, Atlanta, USA) using a TruSeq stranded mRNA kit (Illumina, Cambridge, UK) or Clonetech Smart cDNA kit (Clonetech laboratories, CA, USA) and the NovaSeq6000 (Illumina) and Illumina HiSeq2500 respectively. The generalised workflow of both library prep assays can be found in Figure 2.6. The size distribution, quality and quantity of the Illumina libraries were determined

using an Agilent Bioanalyser 2100, before being submitted for sequencing (paired-end 100-125 nucleotides (nt), designated 26 million reads).

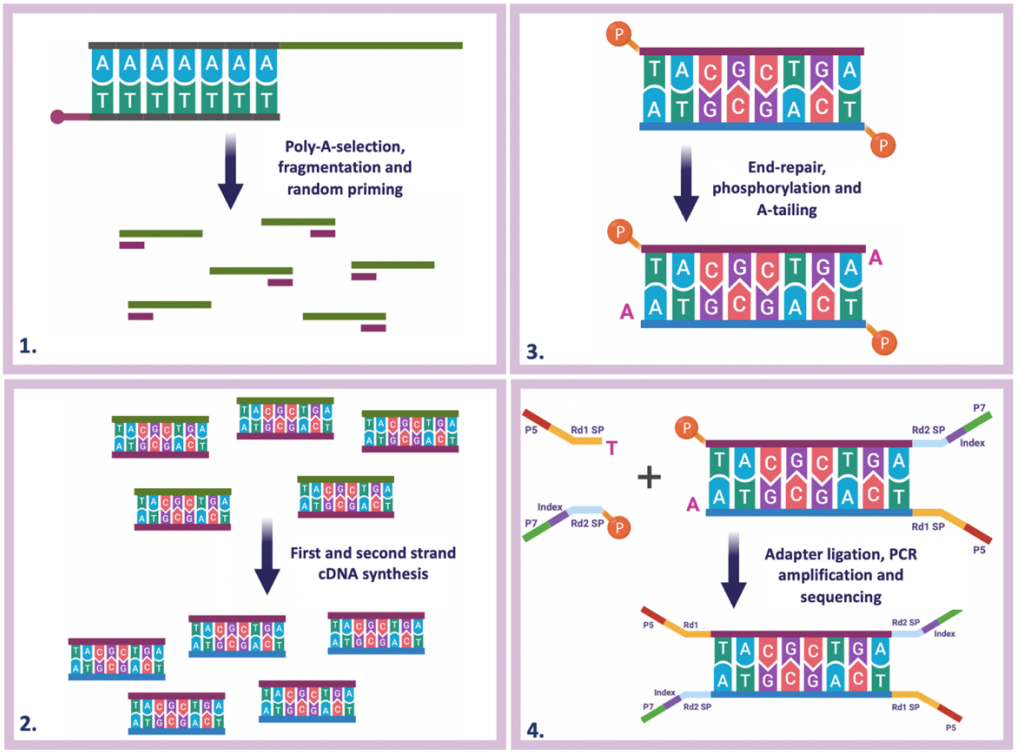

Figure 2.6. RNA-sequencing library preparation steps. (1) Poly(A) selection is used to enrich mRNA from the total RNA. This method was used instead of rRNA depletion due to the high quality of the RNA samples. mRNA is then fragmented. **(2)** Random priming is used to synthesise the first strand of cDNA, followed by synthesis of the second strand. **(3)** cDNA is end repaired, phosphorylated and A-tailed. **(4)** Adapters are ligated, and PCR amplification performed before the library is then ready for clustering and sequencing.

2.10 Bioinformatics

2.10.1. Quality control

The sequencing data generated in this thesis is available at the National Centre for Biotechnology Information Gene Expression Omnibus (NCBI GEO, www.ncbi.nlm.nih.gov/geo) under the accession numbers GSE132358, GSE145029 and GSE149570. Per sample, on average 32.3 million total read sequences, of approximately 100 base pairs in length were generated. The raw reads were quality control checked using FASTQC and FASTQC Screen (Babraham Institute, Cambridge, UK) to determine if trimming of low-quality ends (error rate < 0.05) and adapters was required.

2.10.2. Genome mapping and downstream analysis

Mapping via this method was conducted for the 3D adult, fetal and ESC-derived tenocyte construct data only. Here the resulting high quality reads were mapped to the *Equus Caballus* reference genome (EquCab 3.0, Ensembl v96) using the HISAT2 (hisat2-align-s v.2.1.0) spliced aligner (270). Resulting sequence alignment/map (SAM) files were then converted into sorted BAM files (binary version of a SAM file) using samtools (271). Next featureCounts (v.1.6.2) from the Subread package (272) was used to count how many reads were mapped to each single genomic coordinate within the genome. The counts table generated from featureCounts was then loaded into R (v.3.5.2), converted into a matrix and the R/Bioconductor DSeq2 (v.1.22.2) software used to conduct differential expression analysis as described in Love *et al*., 2014 (273). For analysis of differential expression between 3D adult, fetal and ESC-derived tenocyte constructs genes with a log 2-fold change (Log2FC) of ±2 and adjusted p-value (p-adj) of < 0.01 were considered differentially expressed (DE).

2.10.3. Transcriptome mapping and downstream analysis

Mapping via this method was conducted for the 3D adult, fetal and ESC-derived tenocyte construct data as well as for the 2D cultured adult and fetal tenocyte data and the adult and fetal shSCX and NT data. For transcriptome mapping the pseudoaligner Salmon (274) in Quasi-mapping based mode was used to align the reads to the Ensembl version v96 EquCab 3.0 transcriptome with GC-bias correction (-gcBias) applied. Gene-level abundance data was imported into R (v.3.5.2) using Tximport (275) and the R/Bioconductor DSeq2 (v.1.22.2) software used to conduct differential expression analysis as described in Love et al., 2014 (273). For analysis of differential expression between 3D adult, fetal and ESC-derived tenocyte constructs genes with Log2FC of ±2 and p-adj of < 0.01 were considered DE. For analysis of differential expression between 2D and 3D adult and fetal tenocytes genes with Log2FC of ±2 and p-adj of < 0.01 were considered DE. For analysis of differential expression between adult and fetal NT shRNA expressing versus SCX shRNA expressing cells genes with Log2FC of ±1 and p-adj of < 0.05 were considered DE. Visualisation of differential expression analysis was conducted in R (v.3.5.2). Euclidean sample-to-sample distance matrices with hierarchical clustering using VST (variance stabilizing transformation) transformed data were generated using

the R package "pheatmap" (v.1.0.12) (273). Heatmaps were also generated using the R package "pheatmap" (v.1.0.12) with dendrograms based on Pearson correlation. Euclidean principal component analysis (PCA) plots were generated in ggplot2 (v.3.1.0) using VST transformed data. The gene level summaries, including the differential expression analysis and normalized counts for all genes and samples can be found at NCBI GEO (www.ncbi.nlm.nih.gov/geo) under the accession numbers GSE132358, GSE145029 and GSE149570.

2.10.4. Gene ontology, network and pathway analysis

Gene Ontology (GO) analysis was performed using Panther (http://www.pantherdb.org/), with a false discovery rate (FDR) of < 0.05 being defined as significantly enriched. Pathway analysis was performed using GeneAnalytics from the LifeMap's GeneCards Suite (http://www.geneanalytics.genecards.org), with an entity score of > 5 being equivalent to a corrected p-value of < 0.05 and therefore defined as significantly enriched. Entity scores of > 13 were considered highly significantly enriched being equivalent to a corrected p-value of < 0.01. Network analysis was conducted using the STRING Protein network analyser plug-in of Cytoscape (v.3.7.2) (http://apps.cytoscape.org/apps/stringapp) using the human reference set. Networks were generated using a less stringent cut off of Log2FC ± 0.6 p.adj < 0.05 to encompass a larger number of DE genes.

2.11 Histology

2.11.1. Preparation of tissues and cells

Three lines of adult, fetal and ESC-tenocyte 3D constructs (P6 to P9 for adult and fetal tenocytes and P18 – 20 for ESC-tenocytes) were embedded in OCT compound (VWR) and snap frozen in liquid nitrogen cooled isopentane (Sigma). Longitudinal sections at 11 μm thick, were cut using a cryostat, fixed on glass slides for 10 minutes in 100% acetone and stored at -20°C. Four biological lines of adult and fetal NT shRNA and SCX shRNA infected (shSCX) tenocytes were cultured on gelatin-coated (Sigma) coverslips (P8 to

P10). Coverslips were fixed for 20 minutes in 3% paraformaldehyde, washed 3x in PBS and stored in PBS at 4°C.

2.11.2. Haematoxylin and eosin (H&E) staining

Previously fixed slides were placed in slide holders and transferred into Mayers haematoxylin (Sigma) for 5 minutes. "Blueing" was then carried out by placing the slides in running water for 10 minutes, before placing in eosin (Sigma) for 5 minutes. Slides were briefly rinsed in tap water before passing through an alcohol gradient of 70% ethanol, 95% ethanol, absolute ethanol twice and histoclear (National Diagnostics, Atlanta, USA) twice, shaking 5-10 times in each solution. Coverslips were then mounted on glass slides using Dpx mountant (Sigma).

2.11.3. Picro Sirius red staining

Picro Sirius red staining was conducted using the Abcam Picro Sirius Red Stain Kit according to the manufacturer's instructions. Briefly, slides were rinsed in distilled water before submerging in Picro Sirius Red Solution (Abcam) for 60 minutes. Slides were then rinsed in Acetic Acid Solution (Abcam), followed by dehydration in two changes of absolute alcohol before mounting using Dpx mountant (Sigma).

2.11.4. Immunofluorescence

For immunofluorescence, paraformaldehyde fixed 2D coverslips were permeabilized in 0.1% triton-X-100 (Sigma) for 1 hour before blocking. 3D slides or 2D coverslips were then blocked in 2.5% normal horse serum (Vector Laboratories, Peterborough, UK) for 20 minutes at room temperature. Following the blocking step, the serum was removed before incubating with primary antibodies overnight at 4°C. Following primary antibody incubation, the slides or coverslips were washed in PBS (3x 5 minutes) and subsequently incubated with fluorescently labelled secondary antibodies for 3 hours at room temperature. All primary and secondary antibodies were used at optimized concentrations in 2.5% normal horse serum (Table 2.5). Finally, all slides and coverslips were washed in PBS (3x 5 minutes), rinsed in water and mounted in VECTASHIELD® HardSet™ mounting media containing DAPI (Vector Laboratories).

Table 2.5. Primary and secondary antibodies used for immunofluorescence.

Primary Antibodies			
Antibody Target	**Species**	**Dilution**	**Company**
Actin, muscle	mouse	1:200	Dako (M0635)
BMP7	rabbit	1:100	Abcam (ab56023)
CADM1	rabbit	1:100	Abcam (ab3910)
Collagen type 1	mouse	1:100	Abcam (90395)
COMP	rabbit	1:500	Kindly provided by Professor Roger Smith, Royal Veterinary College, UK
IGF1	goat	1:50	Abcam (ab106836)
LOXL4	rabbit	1:100	Biorbyt (orb100094)
PDGFB	rabbit	1:50	Abcam (ab181341)
RUNX2	rabbit	1:50	Santa Cruz (sc10758)
SCX	rabbit	1:100	Abcam (ab58655)
SPP1	mouse	1:50	Santa Cruz (sc21742)
THBS4	rabbit	1:100	Santa Cruz (sc7657-R)
TNC	rabbit	1:100	Abcam (ab108930)
Secondary Antibodies			
Antibody Target	**Fluorescence**	**Dilution**	**Company**
Anti-mouse IgG	Alexafluor 594	1:200	Thermo Fisher (A11005)
Anti-rabbit IgG	Alexafluor 594	1:200	Thermo Fisher (A11012)
Anti-mouse IgG	FITC	1:200	Abcam (ab7064)
Anti-goat IgG	FITC	1:200	Abcam (ab7121)

2.11.5. Image acquisition

All brightfield and immunofluorescence images were acquired using the Zeiss Axioplan 2 imaging suite (Zeiss, Oberkochen, Germany). An Olympus IMT2-SFR inverted microscope, with polarizing filters was used for visualising Picro Sirius Red staining (Abcam). An EVOS XL Core Cell Imaging System (ThermoFisher) was used for visualising colorimetric images such as H&E staining. All images were processed and arranged using Microsoft PowerPoint.

2.12 Enzyme-linked immunosorbent assay (ELISA)

The Equine IL-10 ELISA Kit (ab155466; Abcam) was used to measure IL-10 levels in the supernatant from 3D cell cultures, according to the manufacturer's instructions. Cell culture supernatant from 3D constructs was collected at days 7, 9 and 14 of culture and frozen in 2 ml volumes at -20°C until required. Supernatant was either used as collected or concentrated using Amicon® Ultra-2 Centrifugal filter units (2 ml sample volume) (Millipore, Massachusetts, USA) according to the manufacturer's instructions.

To conduct the ELISA, IL-10 Equine Standard was serially diluted 8 times in 1x Assay Diluent B (Abcam) to produce a standard curve. Standards and samples, carried out in duplicate, were incubated in the equine IL-10 coated 96-well plate for 2.5 hours at room temperature to allow any IL-10 present in the sample to bind to the immobilized antibody. The wells were then washed, and a biotinylated anti-equine IL-10 antibody (Abcam) added to each well and incubated for 1 hour at room temperature with gentle shaking. The wells were then washed again to remove any unbound biotinylated antibody, and HRP-conjugated streptavidin (Abcam) added and incubated for a further 1 hour at room temperature with gentle shaking. The wells were washed to remove any unbound HRP-conjugated streptavidin and a TMB substrate solution (Abcam) added and incubated with gentle shaking in the dark for 30 minutes, with colour developing in relation to the level of bound IL-10. The reaction was then stopped using the Stop Solution (Abcam) and read immediately on a microplate absorbance reader (ThermoMax Technologies, Columbia, MD, USA) at 450 nm. Results were exported as a txt file and the data input into ElisaAnalysis.com (Leading Technology Group, Australia) in order to determine the mean sample concentration.

2.13 Chromatin immunoprecipitation (ChIP)

2.13.1. DNA-protein cross-linking

Three lines of non-transduced adult and fetal tenocytes (between P4 - P8) and one line of 2D ESC-derived tenocytes (P19) (approximately $25x10^6$ cells) were washed in PBS and fixed in 11% formaldehyde for 10 minutes at room temperature with gentle shaking.

Fixation was quenched by adding glycine at a final concentration of 125 mM. Samples were washed twice in PBS, pelleted and stored at -80°C until required.

2.13.2. Cell lysis and chromatin shearing

All subsequent steps were performed on ice. The iDeal ChIP-qPCR Kit (# C01010180; Diagenode, Seraing, Belgium) was used to prepare chromatin, conducted according to the manufacturer's instructions. Briefly, samples were thawed on ice and 1 ml cold lysis buffer iL1b (Diagenode) per million cells added and incubated for 20 minutes at 4°C under constant rotation. Samples were then pelleted at 500 x g for 5 minutes at 4°C, the supernatant removed and 600 µl of cold lysis buffer iL2 (Diagenode) added per million cells. Samples were incubated this time for 10 minutes at 4°C under constant rotation, before again pelleting and removing the supernatant. Pellets were then resuspended in 100 µl shearing buffer containing protease inhibitor cocktail (Diagenode) per 1.5 million cells and incubated for 10 minutes. Chromatin shearing was performed using the Misonix Sonicator XL2020 Ultrasonic Liquid Processor (Misonix, NT, USA) using the cup horn water bath probe. Shearing optimisation determined that a programme of 7 minutes and 40 seconds, with pulse parameters of 20 seconds on and 20 seconds off provided the most efficient shearing. Sheared chromatin was then centrifuged at 16,000 x g for 10 minutes at 4°C and stored at -80°C until required, except for a 50 µl aliquot which was taken forward for shearing analysis. For shearing analysis 2 µl of diluted RNase cocktail (Ambion) (1 µl diluted in 150 µl of ChIP grade water) was added to the sheared sample and incubated at 37°C for 1 hour. Cross-linking was then reversed by adding elution buffers (Diagenode) and incubating overnight at 65°C. DNA was then purified as described in section 2.6.2 and run on a 1.5% agarose gel as described in section 2.6.1.

2.13.3. Magnetic immunoprecipitation

Sheared chromatin was immunoprecipitated using antibody bound DiaMag Protein A-coated magnetic beads (Diagenode). Briefly beads were washed three times with 1x ice-cold 1x ChIP Buffer iC1b (Diagenode) before incubating at 4°C for 4 hours with gentle rotation with either 4 µg of anti-SCX antibody (#PA5-23943; ThermoFisher), 2 µg anti-Histone H3 antibody (#ab1791; Abcam) and either 2 µg or 4 µg of rabbit non-immune IgG (#C15410206; Diagenode), according to the iDeal ChIP-qPCR Kit instructions. Once

antibodies were bound to the beads 250 µl of sheared chromatin was added to each reaction, keeping aside 2.5 µl at 4°C to be used as an input sample, and incubated overnight at 4°C under constant rotation. Following overnight incubation samples were washed 4 times in wash buffers iW1, iW2, iW3 and iW34 (Diagenode). Input samples and immunoprecipitation (IP) samples were then treated in parallel, incubating in DIB buffer containing Proteinase K (Diagenode) at 55°C for 15 minutes, followed by 15 minutes at 100°C in order to isolate the DNA from the beads and de-cross-link. Samples were placed on a magnetic rack and the supernatant containing the DNA transferred to a freshly labelled tube and stored at -20°C for subsequent analysis.

2.13.4. ChIP-qPCR

Immunoprecipitated DNA was subjected to qPCR as previously described (see section 2.8.2). Primer generation was conducted using the sequences of equine proximal promoter regions of 11 genes in order to identify putative E-box regions (consensus sequence CANNTG (N = any nucleotide)) in which SCX may bind (Table 2.6). As promoter regions in the horse are currently not well annotated, the sequence 2 Kb upstream of the transcription start sites were used to define the "promoter" region. Some genes contained multiple E-boxes within their predicted promoter regions, therefore where necessary multiple primers were designed in order to capture these. Negative control regions included genes which had no expression in equine tenocytes, were not within a predicted promoter region and had no E-box binding sites within 250 bp either side of the primers (TEX33 and RNASE9) and intronic regions which contained no E-box binding sites within 1.5 Kb of the primers (Intronic #1 and Intronic #2). The relative amount of immunoprecipitated DNA compared to the input DNA (% recovery) was calculated using the following formula as described in the iDeal ChIP-qPCR Kit protocol (Diagenode):

$$\% \text{ recovery} = 2\text{^}((Ct_{input} - 6.64) - Ct_{sample}) * 100\%$$

Where the Ct_{input} and Ct_{sample} are the threshold cycles obtained from the exponential phase of the qPCR for the input sample and the immunoprecipitated DNA sample respectively. The amplification efficiency is 2, based on the assumption that the PCR is 100% efficient and the compensatory factor is 6.64 in order to correct the input dilution (where 1% input was used, i.e. 2.5 µl of input to 250 µl sheared chromatin per IP). Fold enrichment was

then calculated by dividing the ratio of IP-bound DNA to the average of the negative controls (TEX33, RNASE9, Intronic #1 and Intronic #2) normalised for input DNA.

Table 2.6. Primers for ChIP-qPCR.

Gene	Forward Primer (5'-3')	Reverse Primer (5'-3')	Reason for Selection
Intro #1	TTTGGGGGAGGTTTTGCTTC	AACCGAAGTCCTGATACTGC	Negative Control
Intro #2	AGAGGAGATTCAACATTCTGC	CCTTTGCAGTATTCAGTGTACC	Negative Control
RNASE9	CCAGCCCTTGAAAGATCCATT	GCTTCCAACCCTATCTTTGCT	Negative Control
TEX33	CTCACAACGATGGAGAAAGGG	CTCCTCTCAGCTCCACAACT	Negative Control
ACTA #1	CATTCCCCTTCAAAAGGTCCA	GGGAATTGCTTACATTTTGGC	RNA-seq Result
ACTA #2	TCCTCTGACCCCCATTCTG	CCTGCTGAAGCGGTTCTATTT	RNA-seq Result
CLDN16	CGTTCAGCATGAGTGACAGA	AAAGCATGGCAAAGTTGGAA	RNA-seq Result
COL1A2	CCAACAGTAGGCGTCCTC	GGTTCTGTCTGTGGAGGGTT	Positive Control
FGF9	CAATACAGCTTGCGCTTGTG	CATGTTGCATTGCGCTAGGA	RNA-seq Result
FGF19	AGCGGTTGGAGGAATAATGAG	AGGGGACTTTGGCTCAACAC	RNA-seq Result
IGF2BP1 #1	GTGAACGGCATGAAATCGTCT	TTCCTTGTGATTTTGTGTGCAG	RNA-seq Result
IGF2BP1 #2	GCTTCTCTTTGTCTCTCTCGG	GAGTTTGCCCACCCTACCTC	RNA-seq Result
KLF15	CCTCCACGCATGCTTACTTC	GATTCTGGGAAAGCTCACGA	RNA-seq Result
MMP3 #1	CAAACGAGCTCCAACCTACC	ACAACTACGCAGAGTCAAGA	RNA-seq Result
MMP3 #2	GGTAAGTAGGTGAGGTTGGTG	AGACCCTAAACATTCCCAGA	RNA-seq Result
MMP3 #3	CCTGAACTAACTGCCACCTT	AGGGTCAGATAATGGCTGGT	RNA-seq Result
NOV	CCCAAACTTCAGGCATCCTTC	CAAGCAGGGCTGCGAATGTA	RNA-seq Result
PDGFB	TTTAGCCGGCGAGTGAAGAC	CAAGAGGAAAAAGAACACGGC	RNA-seq Result
TNMD	GGTGGGGATGAAAAGTTGCC	ACAGGTTCTTTGCTCTCCTCT	Positive Control

2.14 Statistical analysis

Statistical analysis of qPCR and gel contraction data was performed using XLSTAT (version 22.1.3). Histograms were plotted to visualise the distribution of the datasets and all were confirmed to have a Gaussian distribution using the Shapiro Wilks normality test and subsequent visualisation of Q-Q plots. For comparisons of two groups the Student's *t*-test (unpaired, two-tailed) was used. For comparisons of more than two groups with equal variance ANOVA was used, followed by the Tukey's post hoc test. When unequal variance was observed (as determined by the k-sample comparison of variance test, Levene's Test) Welch's ANOVA was used, followed by the Games-Howell post hoc test. For comparisons of two groups in which two continuous variables were compared, such as in the serial passaging experiment (see section 2.2.2), linear regression analysis was

conducted, which was deemed appropriate following visualisation of diagnostic plots including Residuals vs Fitted, Normal Q-Q, Scale-Location and Residuals vs Leverage to ensure the test/model was suitable (all conducted in R (v.3.5.2)). In all cases the significance threshold was set at $P < 0.05$ and is marked with an asterisk (*). The number of independent biological replicates used for each experiment is indicated in the figure legends.

Chapter 3 - Comparison of Adult, Fetal and ESC-Derived Tenocytes

3.1 Introduction

As previously described, tendon injuries occur frequently in equine athletes. Treatment options are limited, and the prognosis is often poor with functionally deficient scar tissue resulting. Fetal tendon injuries in contrast are capable of healing without forming scar tissue. ESCs may provide a potential cellular therapeutic to improve adult tendon regeneration however, whether they can mimic the properties of fetal tenocytes is unknown. To this end, this chapter will focus on trying to better understand the unique expression profile of normal adult and fetal tenocytes, which is crucial to allow validation of ESC-derived tenocytes as a cellular therapeutic.

3.1.1. Regenerative healing in the animal kingdom

Examples of regenerative healing are abundant in the animal kingdom, the capacity of which varies considerably from species to species. Whereas more primitive vertebrates such as fish and amphibians are able to regenerate entire limbs, by contrast high level mammals have a much more limited regenerative capacity (276). Furthermore, this regenerative ability also typically declines throughout development and ageing, the most classic example of this being the shift from fetal regenerative healing to adult reparative healing in mammals, which was first explored in early human fetuses in the 1970s (277). Regeneration appears not only to be age specific, but also tissue specific, with neonatal hearts being able to undergo complete regeneration within the first week after birth, whereas other wounds such as early fetal wounds of the gut being found to still heal with scar formation (278–280).

Where at first it was believed that the amniotic fluid-rich sterile uterine environment was the reason for this fetal regenerative capability, this was later opposed with studies in marsupials showing scar-less healing up to pouch day 9 (281). Further to this it was found that regeneration is intrinsic to the fetal cells themselves, with fetal skin transplanted into an adult environment continuing to heal without scarring (43,282). In contrast, when adult skin is transplanted into a fetal environment it continues to heal in a reparative manner (43,282). Whilst the precise mechanisms which account for this regenerative fetal healing are still largely unknown, a summary of those factors identified in fetal versus adult skin wounds can be found in Table 3.1.

Table 3.1. Summary of differences found in fetal wounds as compared to adult wounds. Adapted from information provided in the following reviews:- Larson *et al*., 2010, Rolfe *et al*., 2012 and Wilgus *et al*., 2020 (41,278,283).

	Fetal Wound Healing	**Reference**
Collagen Content	Less dense, finer structure with basket-weave orientation	(43,282,284–287)
	Less crosslinking	(288)
	Higher levels of collagen III to collagen I in healthy fetal skin, lower ratio of collagen I to III in fetal wounds	(288–294)
ECM Modulators	Tenascin C earlier deposition	(287,295)
	Increased expression of some integrins	(296)
	Decreased lysyl oxidase expression	(297)
	Reduced decorin	(298–300)
	Increased MMPs, reduced TIMPs	(301)
	Increased fibromodulin levels, inhibiting fibromodulin leads to scar formation, fibromodulin addition reduces scar formation	(302,303)
Growth Factors	Lower levels of VEGF and less vascular, scar-forming phenotype induced by endogenous VEGF addition	(304)
	Lower levels of TGF-β1 and 2 in fetal wounds and no upregulation of TGF-β3 in response to injury, no TGF-β receptor expression	(305–309)
	Increased PDGF but more rapid clearance from wound, exogenous addition causes fibrosis	(310,311)

	FGF2 increased in expression, *FGF7* and *FGF10* downregulated	(312,313)
	Fetal dermal fibroblasts have lower proliferation and collagen synthesis in response to IGF-1 compared to adults	(314)
Hyaluronic Acid (HA)	High levels of HA and HA-stimulating activity (HASA)	(315–319)
	Lower levels of hyaluronidase (degrades HA), exposing to hyaluronidase leads to fibrotic response	(320–322)
Inflammation	Fewer resident inflammatory macrophages and mast cells	(323–325)
	Fewer and less activated cells of the acute immune system	(324,326–329)
	Fewer circulating inflammatory cells recruited to injury site	(284,330–333)
	Neutrophils less adherent to fetal cells	(334)
Interleukins	Diminished IL-6 production, IL-6 addition leads to scar formation	(335)
	Diminished IL-8 production	(336)
	Increased IL-10 production, IL-10 knockout fetal mice heal with scars, enhancing IL-10 reduces inflammation and scar formation	(337–340)
	Diminished IL-33 production, IL-33 addition leads to scar formation	(341)
Transcription and Gene Expression	Microarray analysis between scar free E15 murine fibroblasts and E18 fibrotic fibroblasts have differences in genes involved in cell proliferation, cell signalling, inflammatory pathways and cell-cell interactions	(342)
	Microarray analysis between scar free E16 murine fibroblasts and E18 fibrotic fibroblasts have differences in genes related to PDGF signalling and degradative enzymes for superoxide radicals	(343)
	Microarray analysis of wound healing shows rapid upregulation of groups of genes involved in cell growth and proliferation, proposed to contribute to rapid wound healing	(344)
Wound Closure	Absence of fibroblast to myofibroblast transition	(345,346)
	Basal differences in proliferation rates, migration rates and contractile ability	(347–351)
	Wounds close by actin cable	(352,353)
	Rapid upregulation of adhesion proteins stimulates cell attachment and migration	(295,296,354,355)

3.1.2. Fetal wound healing in the tendon

Models of fetal tendon wound healing have similarly demonstrated that they undergo regenerative healing. Here partial tenotomy of the lateral extensor tendon was performed in fetal sheep at 60-70% of the way through gestation and compared to those created in maternal limbs (254). Fetal tendons healed regeneratively, with no abnormalities found and complete reconstitution of the collagen architecture (254). In contrast adult wound tissue appeared granulated, with increased inflammatory cells and disorganised fibre orientation at the site of injury (254). Furthermore, it was later demonstrated that injured fetal tendon transplanted into an adult environment retained its regenerative properties, suggesting that the adult environment does not impede scar less repair, with this repair mechanism being intrinsic to the fetal tissue itself (255). Similarly studies have demonstrated that intrinsic differences exist between adult and fetal tendon cells (259). When fetal tendon fibroblast scaffolds were sutured into adult mouse Achilles tendon injuries it resulted in higher levels of collagen deposition and improved microstructure repair compared to that of adult tendon fibroblast seeded scaffolds (259). Moreover, the fetal fibroblast seeded wounds had less inflammatory cells present and increased recruitment of native fibroblast-like cells (259). The mechanisms behind this are not understood, nor is the timepoint in which fetal tendon regeneration switches to fibrotic repair. However, taken together this remarkable healing capacity of fetal cells has driven investigations into their use as a cellular therapy.

3.1.3. Understanding the fetal cell phenotype to aid therapeutics

Fetal skin progenitor cells are currently being tested in clinical trials for burns victims and show a remarkable ability to rapidly close wounds with little hypertrophy (356,357), with similar investigations also being conducted with fetal tendon progenitor cells (260). However, access to fetal tissue presents as an issue. Sources of fetal tissue are often limited, being typically obtained from aborted fetuses as a result of viral infections, bacterial infections, mycotoxins or gene mutations which may be of concern if they are to be utilised as a cellular therapy. Furthermore, in order to obtain enough cells for transplantation, cells must be serially passaged on tissue culture plastic, which can lead to an altered cellular phenotype due to *in vitro* selective pressures (358–362).

Regenerative medicine methodologies which mimic fetal-like regeneration are therefore required.

Embryonic stem cells (ESCs) may provide a potential cellular therapeutic to improve adult tendon regeneration, however whether they can mimic the properties of fetal tenocytes in unknown. Equine ESCs differentiate into tenocytes *in vitro* in response to transforming growth factor-β3 (TGF-β3) and three-dimensional (3D) culture (60,140,154). Similarly, human ESCs have been differentiated into tenocytes *in vitro* (213,230). Transplantation of differentiated human ESC derived 3D fibrin tendon gels into rat patella tendon injury models has indicated that ESC-tenocytes secrete a number of fetal tendon matrix and differentiation factors (230), highlighting the potential role ESC-tenocytes may play in tissue regeneration. However, to date a full transcriptional characterisation of ESC differentiated tenocyte progeny has not been performed.

3.1.4. Chapter aims

Understanding the unique expression profile of normal adult and fetal tenocytes is crucial to allow validation of ESC-derived tenocytes as a cellular therapeutic. Therefore, the aim of this chapter is to:-

1) Determine the transcriptional differences between equine adult, fetal and ESC-tenocytes cultured in 3D by comparing their global gene expression profiles.

2) Identify the global transcriptional effects of culturing adult and fetal tenocytes in conventional monolayer systems compared to that of a 3D culture system.

3.2 Results

3.2.1. Determining sex of cell lines

The sex of the horses from which tendon samples were obtained was not recorded at the time of collection, therefore PCR was used to determine this by amplifying sex specific sequences (Figure 3.1). Of the eight adult tenocyte cell lines used seven were determined to be male. This was demonstrated by amplification of a 714 bp region of the SYR (sex-determining region Y) gene which is located on the short branch of the Y chromosome, as well as amplification of the zinc finger protein Y-linked and X-linked genes (ZFY and ZFX) resulting in a double band at 604 bp and 553 bp. One adult tenocyte line was determined to be female, having no amplification of the SYR gene and only amplification of the ZFX gene (604 bp). Of the eight fetal tenocytes lines, two were determined to be male and six were female. Finally, of the ESC lines, one was determined to be male and the remaining two were female.

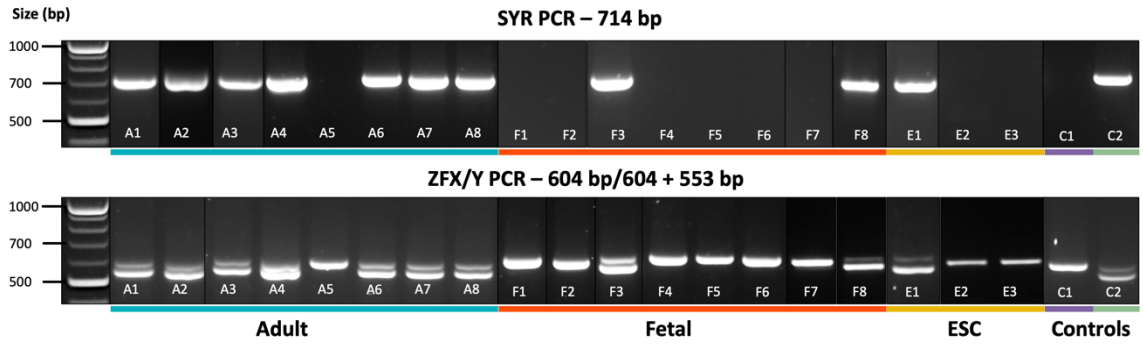

Figure 3.1. Sexing cell lines. PCR followed by agarose gel electrophoresis to amplify the SYR gene and the ZFX/Y genes in equine tenocytes and ESCs. Adult tenocyte lines are numbered from A1-A8. Fetal tenocyte lines are numbered from F1-F8 and ESC lines are numbered from E1-E3. Control known female sample (C1) and control known male samples (C2) were included as positive controls. Male samples should amplify a 714 bp fragment when SYR primers are used and both a 604bp and 714 bp fragment when ZFX/Y primers are used. Female samples should have no amplification when the SYR primers are used and a single 604 bp fragment when ZFX/Y primers are used.

3.2.2. Serial passaging alters gene expression

Due to the difficulty in obtaining large numbers of cells from primary tissue for research purposes, serial monolayer passaging is utilized to increase cell numbers. Typically, primary cells are recommended to be used in experimental studies before the tenth passage (P10) as many primary tissues have been shown to exhibit changes in cell morphology and gene expression (359–361). The effect of serial passaging on the expression of six tendon associated genes *COL1A1, COL1A2*, *COL3A1, SCX*, *THBS4* and *TNMD,* in adult equine tenocytes was therefore measured (Figure 3.2). *COL1A1* had significantly higher expression at P0 than at P3 through to P10. However, *COL1A1* levels did not significantly change beyond P3 with the further passage. *COL1A2* expression was variable with passaging, with a significant difference from P0 only being observed at P6 and P7 (p-value = 0.0256 and 0.0027 respectively). *COL3A1* was expressed at high levels at all passages, although the results showed variability between donors. No significant differences in *COL3A1* expression were observed at any passage between P0 and P10. *SCX* expression at P0 was significantly higher than from P4 through to P10 (p-values all < 0.05). However, *SCX* levels did not change beyond P4 with further passaging. *THBS4* at P0 was significantly higher than from P1 through to P10 (p-values all < 0.05). However, *THBS4* levels did not change beyond P4 with further passaging. *TNMD* at P0 was significantly higher than at P1 through to P10 (p-value = 0.009). However, TNMD expression did not change beyond P1 with further passaging.

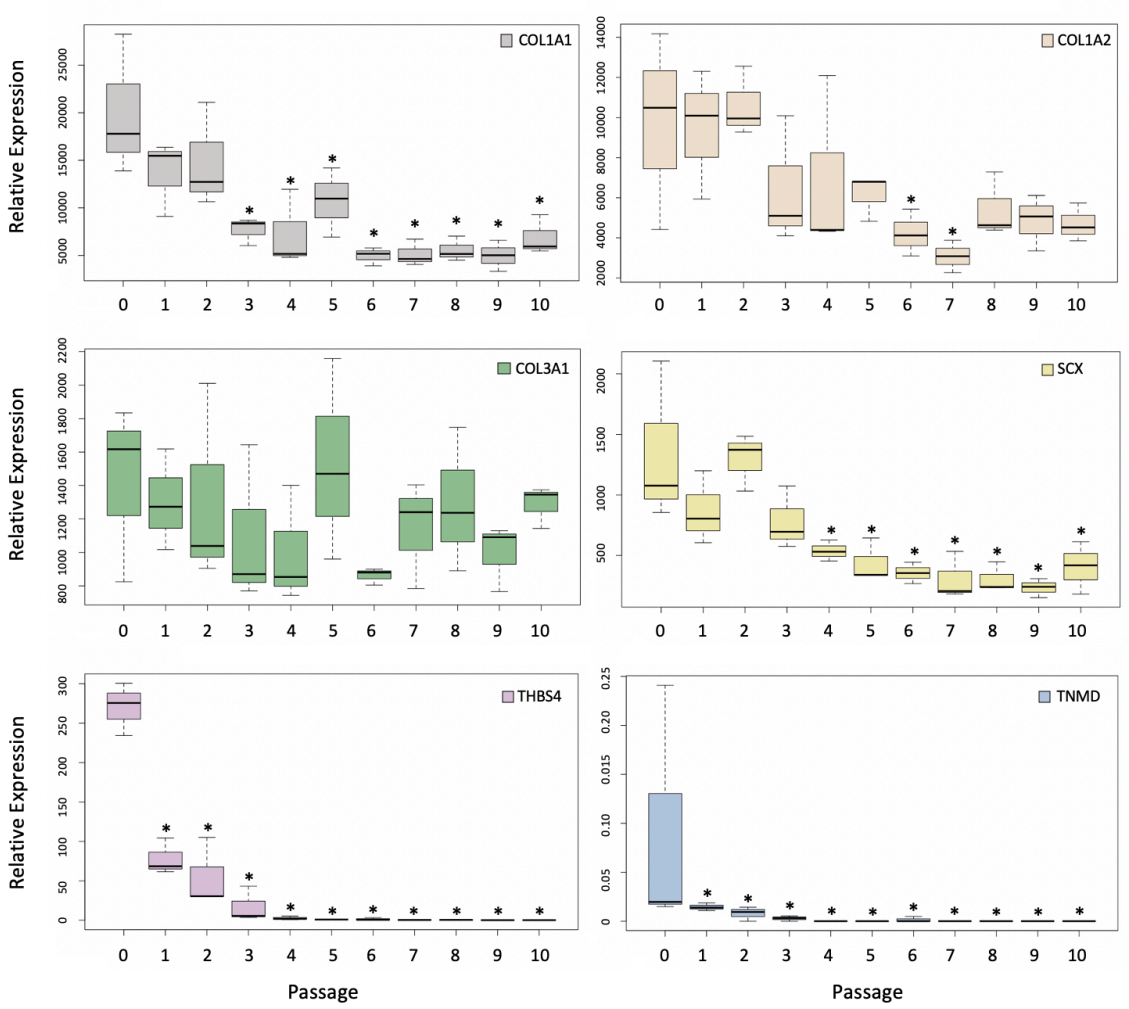

Figure 3.2. Box and whisker plots of tendon gene expression over serial passaging in adult equine tenocytes. Changes in *COL1A1*, *COL1A2*, *COL3A1*, *SCX*, *THBS4* and *TNMD* expression from freshly isolated adult tenocytes (passage 0) through 10 subsequent passages. Error bars represent the maximum and minimum relative gene expression values of three tenocyte lines derived from different donors. Statistical significance was tested using linear regression analysis in R (v.3.5.2), with an asterisk (*) denoting statistical significance using P0 as the intercept.

3.2.3. Histological characterisation of 3D constructs

Our group have previously demonstrated that equine ESCs can differentiate into tenocytes in both 2D and 3D culture, showing increased differentiation in 3D (154). To further characterise equine ESC derived tenocytes, 3D constructs cultured for 14 days were compared to that of adult and fetal seeded constructs. No significant differences in the degree of contraction was observed between the cell types during the 14 days of culture (Figure 3.3.A). Histological analysis was then performed on the 3D cultured constructs as described in (Figure 3.3.B). There were no qualitative differences in either collagen fibre alignment or cell distribution as determined by H&E staining (Figure 3.3.C). Picro Sirius Red staining similarly indicated that the relative staining of type I collagen to type III collagen was not qualitatively different between cell types (Figure 3.3.C).

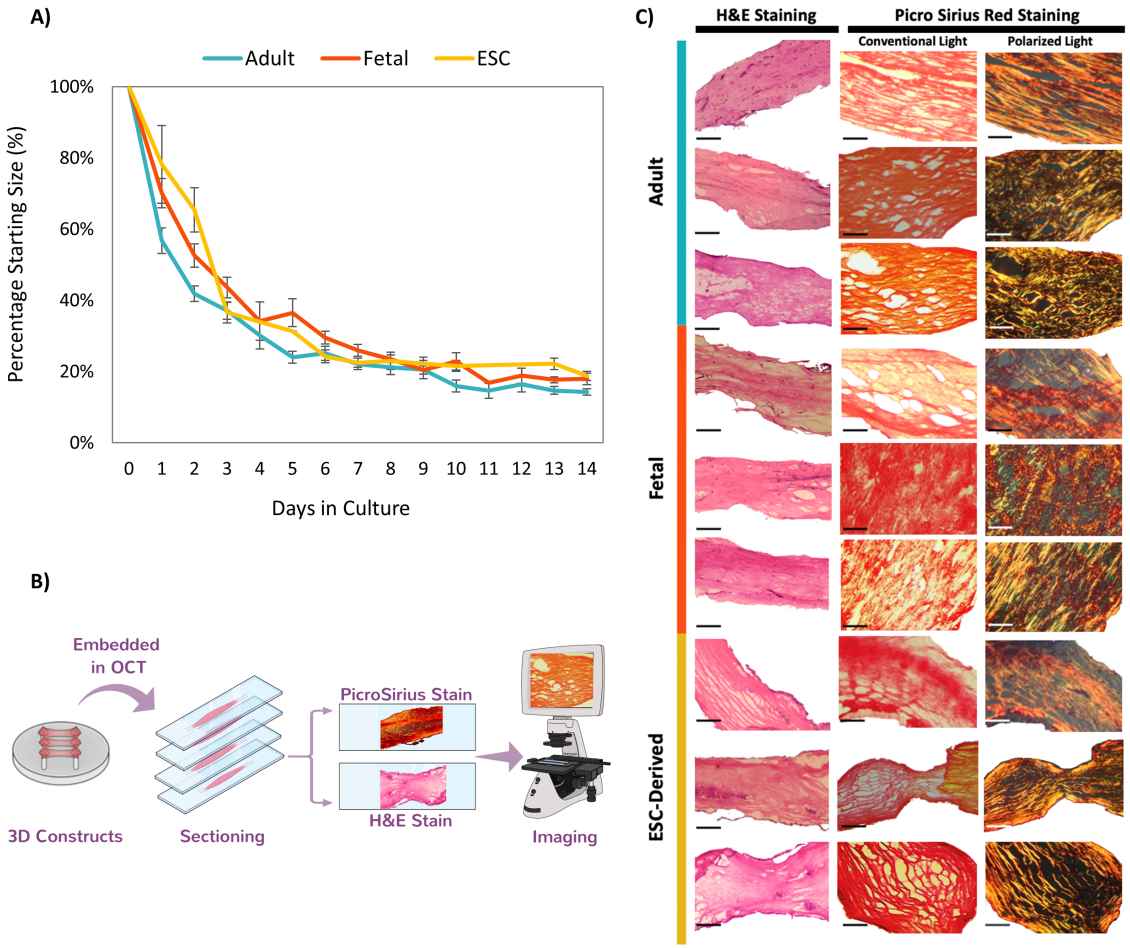

Figure 3.3. Histological characterisation of 3D constructs. A) Adult, fetal and ESC-tenocytes are capable of contracting a collagen gel to the same degree. Contraction shown as the percentage of the day 0 value. $p = > 0.05$ using ANOVA. Error bars represent the SEM of 3-7 biological replicates per condition. **B)** Overview of histology procedure for 3D constructs. **C)** H&E and Picro Sirius Red staining of three biological lines of adult, fetal and ESC-derived 3D constructs. All cell types show similar collagen fibre alignment and collagen content within the constructs after 14 days of culture. Scale bar for H&E = 0.5 mm. Scale bar for Picro Sirius Red = 250 μm. Under light microscopy all collagen fibres are red following Picro Sirius Red staining, under polarized microscopy collagen type I fibres have yellow-orange birefringence and collagen type III fibres have green birefringence.

3.2.4. Quality control and technical validation of 2D and 3D RNA-sequencing data

RNA was extracted from day 14 adult, fetal and ESC-tenocytes seeded constructs and 2D monolayer cultures of adult and fetal tenocytes for subsequent RNA-seq analysis. All 12 RNA samples passed quality control checking, using an Agilent 2200 TapeStation performed by Cambridge Genomics Services (CGS) (Figure 3.4).

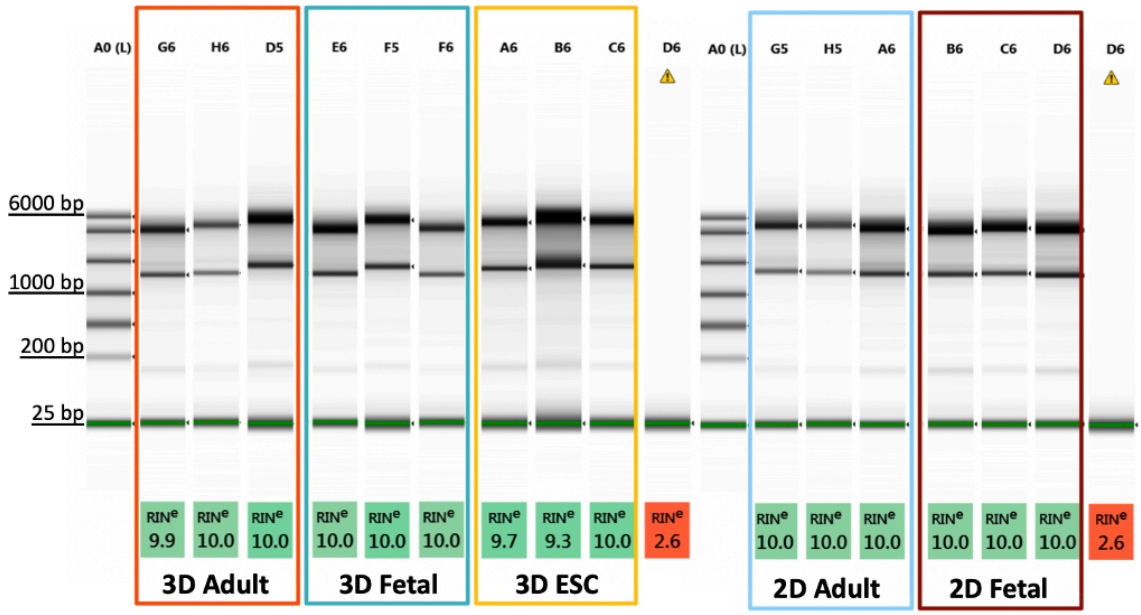

Figure 3.4. RNA Integrity Scores. RNA integrity results obtained for all the samples used in RNA-sequencing experiments in this chapter were between 9.3-10, indicating high quality RNA. Lane A0 shows the electronic ladder and D6 the no sample control. RIN^e values are obtained based on computational analysis, by generating sample electropherograms and determining degradation based upon decreasing signal intensity for the ribosomal bands 18S (1.9 Kb) and 28S (4.7 Kb) rRNAs, as well as other features, resulting from increased short fragments.

Following the RNA-seq run a total of 29.4 billion reads were generated across all the 3D cultured cell lines, with an average of 94.8 million reads per sample group (s.d. 1.17 million read pairs). For the 2D data a total of 19.3 billion reads were generated across all the 2D cultured cell lines, with an average of 96.3 million reads per sample group (s.d. 3.04 million read pairs). The average read number was 3.1 billion (1.55 billion read pairs)

for the 3D cultured adult tenocytes, 3.2 billion (1.6 billion read pairs) for the 3D cultured fetal tenocytes and 3.2 billion (1.6 billion read pairs) for the 3D cultured ESC-derived tenocytes. The average read number was 3.1 billion (1.55 billion read pairs) for the 2D cultured adult tenocytes and 3.3 billion (1.65 billion read pairs) for the 2D cultured fetal tenocytes. Detailed analysis of the 3D cultured RNA-seq data set quantity and size distribution of the Illumina sequencing run can be found in Table 3.2.

All RNA samples passed quality control (QC) carried out using FastQC and FastQC Screen. Trimming of reads was not required due to the high sequence quality and minimal adapter content. A GC content of 50-52% was obtained, with no sequences being flagged as poor quality. The RNA-seq dataset generated for this chapter is freely available in the National Centre for Biotechnology Information Gene Expression Omnibus repository (NCBI GEO, www.ncbi.nlm.nih.gov/geo) under the accession numbers GSE132358 and GSE145029.

Table 3.2. Overview of 3D and 2D cultured RNA-seq metrics. The total size and number of read pairs refers to the total read sizes and counts per group. The same applies for the median and mean values, both of which include three biological replicates. Phred score is a measurement of the quality of the nucleotide base calling. Encoding has been carried out using the Sanger format (Phred+33) where scores range from 0-41, with increasing scores corresponding to higher quality base scoring. (363,364).

	3D Adult Tenocytes	3D Fetal Tenocytes	3D ESC-Derived Tenocytes	2D Adult Tenocytes	2D Fetal Tenocytes
Total size of all reads per group (bp)	9,558,774,440	9,728,203,108	10,143,681,660	9,410,000,000	9,840,000,000
Median size of reads per sample (bp)	3,090,000,000	3,190,000,000	3,310,402,472	3,140,000,000	3,230,000,000
Mean size of reads per sample (bp)	3,186,258,147	3,242,734,369	3,381,227,220	3,136,666,667	3,280,000,000
Total number of all reads per group	93,516,740	95,330,218	95,695,110	94,100,000	98,400,000
Median number of reads per sample	30,900,000	31,900,000	31,230,212	31,400,000	32,300,000
Mean number of reads per sample	31,172,247	31,776,739	31,898,370	31,366,667	32,800,000
Mean Phred score per sample	36.06	36.16	36.03	36.12	36.08

3.2.5. Genome and transcriptome mapping comparison of the 3D cultured tenocytes

Following quality control checking of the generated RNA-seq reads, mapping was performed using two different pipelines on the data produced from the 3D cultured tenocytes (Figure 3.5.A). Figure 3.5.B shows the mapping statistics for both the alignment-based (HISAT2) and alignment-free (Salmon) methods. For the adult tenocytes the average mapping rate for HISAT2 and Salmon was 65.3% and 65.5% respectively. For the fetal tenocytes the average mapping rate for HISAT2 and Salmon was 64.3% and 64.7% respectively. For the ESC-tenocytes the average mapping rate for HISAT2 and Salmon was 61.5% and 60.9% respectively.

Gene expression profiles obtained by RNA sequencing of the entire equine transcriptome yielded 7,557 DE (DE) genes in total across the three 3-D cultured cell type comparisons (Log2FC of ±2 and p-adj of < 0.01) when using the alignment-based HISAT2 pipeline, this is in comparison to the 6,190 detected DE genes (Log2FC of ±2 and p-adj of < 0.01) when using the alignment-free Salmon pipeline. Of the 21,689 mapped genes deemed to be expressed across the three sample types as determined by both alignment methods, 554 genes were DE between the adult and fetal tenocytes, 3,562 genes were DE between the adult and ESC-tenocytes and 3,441 genes were DE between the fetal and the ESC-tenocytes when using alignment-based HISAT2 pipeline (Figure 3.5.C). In comparison, 542 genes were DE between the adult and fetal tenocytes, 2,940 genes were DE between the adult and ESC-tenocytes and 2,708 genes were DE between the fetal and the ESC-tenocytes when using the alignment-free Salmon pipeline (Figure 3.5.D). Of those genes determined as DE between adult and fetal tenocytes, 441 genes were identified using both pipelines, an additional 113 genes were identified when using HISAT2 only and an additional 101 genes were identified using Salmon only (Figure 3.5.E). The gene lists corresponding to Figure 3.5.E can be found in appendix A. The RNA sequencing data is freely available in the National Centre for Biotechnology Information Gene Expression Omnibus repository (NCBI GEO, www.ncbi.nlm.nih.gov/geo) [accession number GSE145029]. The lists of differentially expressed genes are available in full in (Paterson et al., 2020, additional file 3).

A)

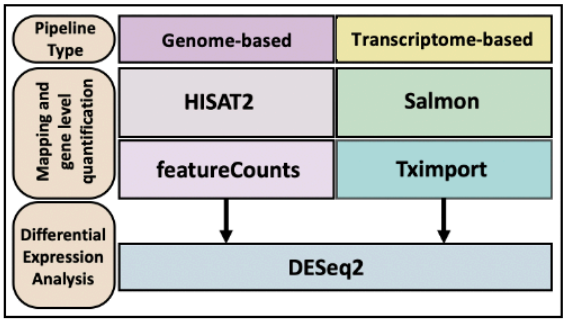

B)

	HISAT2		Salmon	
Sample	% Mapped	Million Aligned	% Mapped	Million Aligned
Adult 1	66.20%	21.2	66.10%	20.4
Adult 2	66.00%	19.1	66.00%	18.5
Adult 3	63.60%	11.3	64.40%	11.1
Fetal 1	64.50%	20.6	64.10%	19.8
Fetal 2	64.30%	21.2	65.10%	20.7
Fetal 3	64.20%	10.8	65.00%	10.6
ESC 1	61.30%	10	60.30%	9.4
ESC 2	62.00%	11.3	61.50%	10.8
ESC 3	60.80%	9.4	60.90%	9

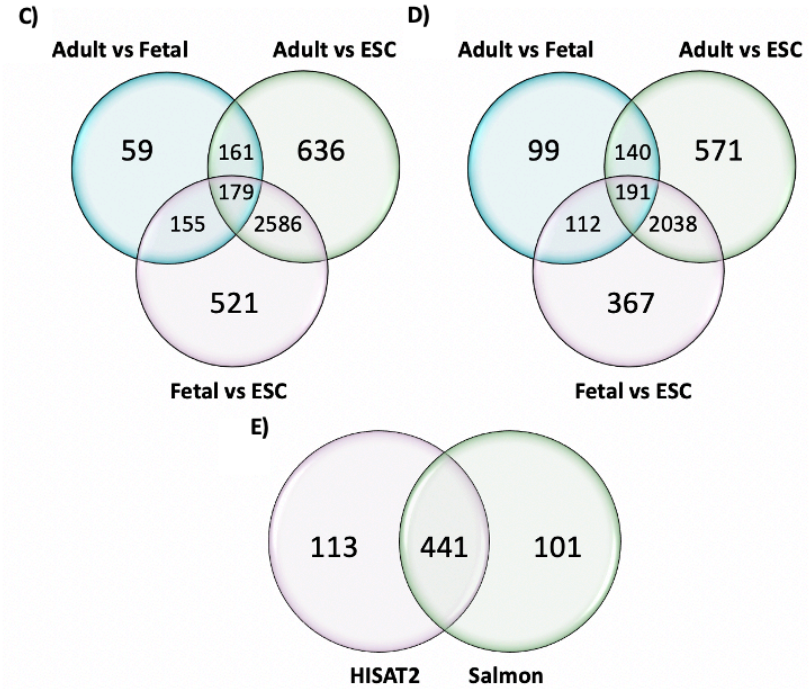

Figure 3.5. Mapping comparison overview. A) Overview of the genome alignment›‹ method, mapping using HISAT2 versus the transcriptome alignment method using Salmon. **B)** Overview of mapping statistics for HISAT2 and Salmon mapped data showing the percentage of reads mapped to exons and number aligned. **C)** Venn diagram of those genes which are significantly DE based on a p-adj of < 0.01 and ±2 Log2FC using the alignment-based HISAT2 pipeline. 179 genes are DE between all three groups. 59 are uniquely DE between adult and fetal tenocytes, 521 are uniquely DE between ESC-derived tenocytes and fetal tenocytes and 636 are uniquely DE between ESC-derived tenocytes and adult tenocytes. **D)** Venn diagram of those genes which are significantly DE based on a p-adj of < 0.01 and ±2 Log2FC using the alignment-free Salmon pipeline. 191 genes are DE between all three groups. 99 are uniquely DE between adult and fetal tenocytes, 367 are uniquely DE between ESC-derived tenocytes and fetal tenocytes and 571 are uniquely DE between ESC-derived tenocytes and adult tenocytes. **E)** Venn diagram of those genes which are significantly DE based on a p-adj of < 0.01 and ±2 Log2FC in adult and fetal tenocytes using the alignment based versus the alignment-free pipelines. 441 genes are identified as being DE in adult and fetal tenocytes using both HISAT2 and Salmon. 113 genes are identified as being DE in adult and fetal tenocytes using HISAT2 only. 101 genes are identified as being DE in adult and fetal tenocytes using Salmon only.

3.2.6. Validation of 3D RNA-sequencing results by qPCR and correlation with protein-level expression

To validate the biological significance of the RNA-seq data, several DE genes were investigated at either the RNA level, protein level or both. For qPCR validation the original samples sequenced were used alongside an additional cohort of adult (total n = 8) and fetal tenocytes (total n = 7), with the expression relative to three different housekeeping genes determined (*18s rRNA*, *GAPDH* and *ACTB*).Of the seven genes tested there was a 90.5% corroboration to that of the RNA-seq data when the *18s rRNA* housekeeping gene was used, an 85.7% corroboration when *GAPDH* was used and an 80.9% corroboration when *ACTB* was used (Figure 3.6.A-C). Using RefFinder as described in section 2.8.3 the stability of the three different housekeeping genes was then determined, with *18s rRNA* being the most stable overall across the four different stability tests (Figure 3.6.D). A further four genes (*SCX, SOX11, CDK1* and *THBS4*) were therefore assessed, with expression calculated relative to the *18s rRNA* housekeeping gene only, which resulted in an overall 79% corroboration to that of the RNA-seq data across the eleven genes tested (Figure 3.6.E-G). Corroboration of differential expression was achieved when both the required fold-change (Log_2 FC ±2) as well as the required p-value (RNAseq adj.-p <0.01; RT-qPCR p <0.05) was achieved.

A)

Gene	Adult vs Fetal: RNA-seq (p.adj)	Cohort qPCR (p-value) 18s	Cohort qPCR (p-value) GAPDH	Cohort qPCR (p-value) ACTB
COL14A1	NA	0.0634	0.9901	0.4501
IL1R1	NA	0.6424	0.5783	0.8363
IL1R2	0.2149	0.8860	0.3412	0.7556
IL1RN	NA	0.2450	0.3414	0.1151
MKX	5.13E-05	0.0019	0.2579	0.1585
MMP13	0.1134	0.2362	0.0034	0.1591
SMAD3	**0.0045	0.3045	0.5391	0.3730

B)

Gene	Adult vs ESC: RNA-seq (p.adj)	Cohort qPCR (p-value) 18s	Cohort qPCR (p-value) GAPDH	Cohort qPCR (p-value) ACTB
COL14A1	NA	0.0499	0.0614	0.1014
IL1R1	0.0487	8.85E-05	0.2139	0.0267
IL1R2	9.92E-37	1.14E-05	5.45E-07	0.0276
IL1RN	0.0023	3.87E-07	0.0004	0.0036
MKX	9.57E-07	0.0167	0.1588	0.1392
MMP13	0.0009	0.0962	0.0224	0.1435
SMAD3	0.7591	0.1171	0.4554	0.2189

C)

Gene	Fetal vs ESC: RNA-seq (p.adj)	Cohort qPCR (p-value) 18s	Cohort qPCR (p-value) GAPDH	Cohort qPCR (p-value) ACTB
COL14A1	NA	0.0987	0.1014	0.0960
IL1R1	0.0202	0.0044	0.0267	0.0750
IL1R2	3.62E-37	1.14E-05	0.0276	0.0276
IL1RN	0.0022	3.88E-07	0.0036	0.0036
MKX	0.2727	0.1826	0.1392	0.3079
MMP13	0.1454	0.3928	0.1435	0.3553
SMAD3	**0.0027	0.4301	0.2189	0.5812

D)

Tool	Housekeeping Gene Validation: 18s	GAPDH	ACTB
Delta CT	0.652	0.653	0.58
BestKeeper	0.277	0.316	0.421
Normfinder	0.511	0.514	0.272
Genorm	0.579	0.628	0.579

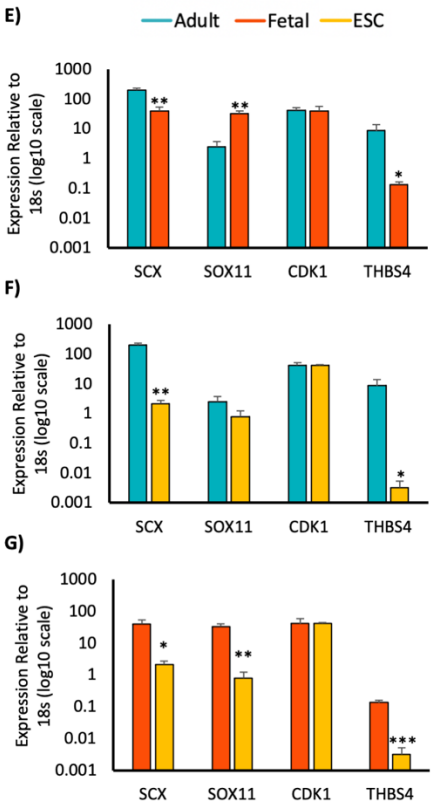

Figure 3.6. qPCR validation of RNA-sequencing results. A-C) Comparison of DE genes in three biological replicates of adult, fetal and ESC-tenocytes using RNA-seq and qPCR results using a Log2FC cut-off ± 2 for both datasets. Significance threshold for RNA-seq p-adj values < 0.01 as routinely used. Significance threshold for qPCR p-value < 0.05 as routinely used. Red shaded boxes indicate no significant difference. Yellow shaded boxes represent a significant p-adj value; but do not meet the Log2FC cut-off. Green shaded boxes indicate there is a significant difference based on both p-adj/p-value and Log2FC. NA values arise due to count outliers as detected by Cook's distance, and are therefore not significant. **D)** Housekeeping gene validation scores obtained using RefFinder for the housekeeping genes *18s rRNA*, *GAPDH* and *ACTB*. For all four tools (Delta CT, BestKeeper, NormFinder and Genorm) the lower the value the greater the stability. Green highlighted boxes represent the most stable gene, yellow boxes the intermediate and red the least stable. **E-G)** RNA-seq validation using qPCR on larger cohort of adult and fetal tenocytes (n = 8 and n = 7 respectively). For the ESC-tenocytes a larger cohort could not be assessed due to only three biological lines being available. Expression shown relative to the 18s rRNA housekeeping gene on a log 10 scale. A single asterisk (*) denotes significance detected in the RNA-seq results only (p-adj values < 0.01 & Log2FC cut-off ± 2). A double asterisk (**) denotes significance detected both in the RNA-seq results and following qPCR (p-value < 0.05 using two-tailed Student's *t*-test). A triple asterisk (***) denotes significance detected following qPCR only. Error bars represent the SEM.

Validation via immunocytochemistry, although not quantitative, showed a high consensus to that of the sequencing data, with ACTA1, IGF1, LOXL4, SCX and THBS4 having visibly higher protein expression in the adult tenocytes compared to the fetal and ESC-tenocytes as predicted from the RNA-seq data (Figure 3.7). Protein expression of PDGFB and RUNX2 did not corroborate with sequencing data, and no visible differences were observed between the three groups (Figure 3.7). BMP7 expression was expected to be absent from adult and ESC-tenocytes based on the RNA-seq data, however, protein was detectable in the ESC-tenocytes and adult tenocytes, although at a lower level than in fetal tenocytes (Figure 3.7). Note the antibodies BMP7, IGF1, LOXL4 and PDGFB were due to be tested in western blots to confirm their specificity in the horse, however as a result of the COVID19 pandemic this could not be completed (see preface). However, all antibodies were predicted to cross-react with the horse, having over 80% homology to the intended target species.

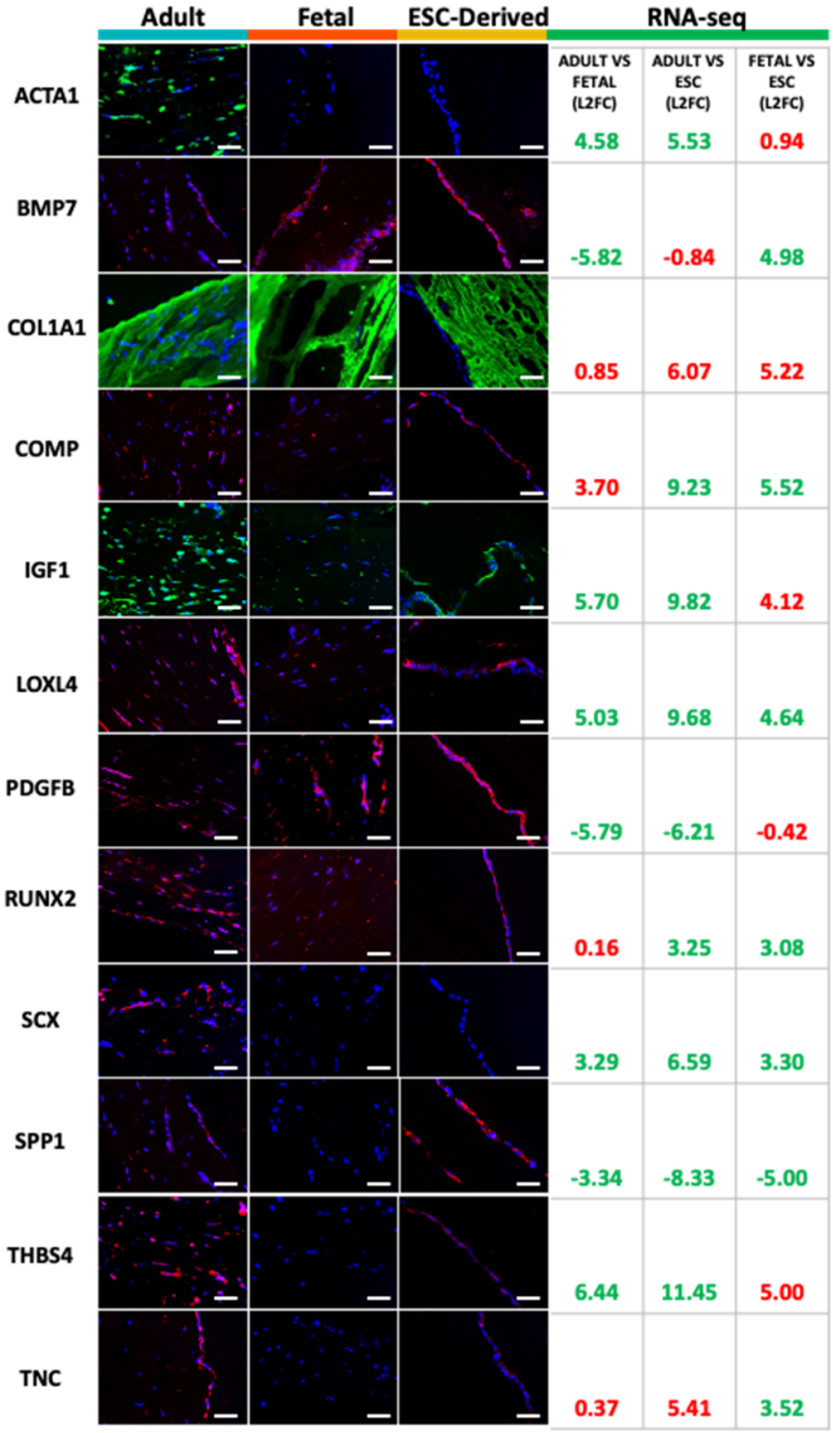

Figure 3.7. Correlation of protein level expression with RNA-sequencing results. Comparison of the corresponding proteins for 12 significantly DE genes. Images represent longitudinal sections of 3D adult, fetal and ESC seeded constructs following 14 days of culture (n = 3 for each cell type). RNA-sequencing Log2FC are listed in the adjoining tables with green text indicating significance based on p.adj value of < 0.01 and red text indicating no significant difference. Scale bar = 40 μm. DAPI staining of the nuclei is shown in blue. Anti-ACT1, COL1A1 and IGF1 are detected using the FITC secondary antibody shown in green. Anti-BMP7, COMP, LOXL4, PDGFB, RUNX2, SCX, SPP1, THBS4 and TNC are detected using the Alexa Fluor 594 secondary antibody shown in red.

The cytokine Interleukin 10 (*IL-10*) was notably decreased in adult tenocyte in comparison to both fetal and ESC-tenocytes, having over 7-fold decreased expression (p.adj 0.001 and 0.004 respectively) (Figure 3.8.A). IL-10 is a key anti-inflammatory cytokine which has been implicated in tendon wound healing, enhancing cell proliferation and migration at the wound site (365,366). In order to confirm whether adult tenocytes secrete less IL-10 protein in comparison to both fetal and ESC-tenocytes an IL-10 sandwich ELISA was conducted on both fresh and concentrated 3D culture supernatant (Figure 3.8.B). Fresh medium collected following 7, 9 and 14 days of culture had barely detectable IL-10 protein levels in adult, fetal or ESC-tenocytes. Control culture medium in which 10 ng/ml of IL-10 was added on days 3, 7 and 11 had detectable IL-10 protein as expected, however at a much lower concentration than that added (0.4 pg/ml) (Figure 3.8.C). To determine if this was due to the sample being too dilute, the proteins present in the culture medium were concentrated by ultra-centrifugation and the ELISA repeated. Again, medium collected following 7, 9 and 14 days of culture, even following concentration, had barely detectable levels of IL-10 protein in adult, fetal and ESC-tenocytes (Figure 3.8.D). Control culture medium in which IL-10 was added, following medium concentration had higher detectable levels of IL-10 (4.5 pg/ml). Again the detectable IL-10 within the day 14 culture supernatant was less that that added on day 11, this may be due to the half-life of IL-10 being 2.7 to 4.5 hours (367) resulting in a drop in concentration by day 14. The ELISA assay therefore did not corroborate the decreased IL-10 expression in adult tenocyte in comparison to both fetal and ESC-tenocytes identified by RNA-sequencing.

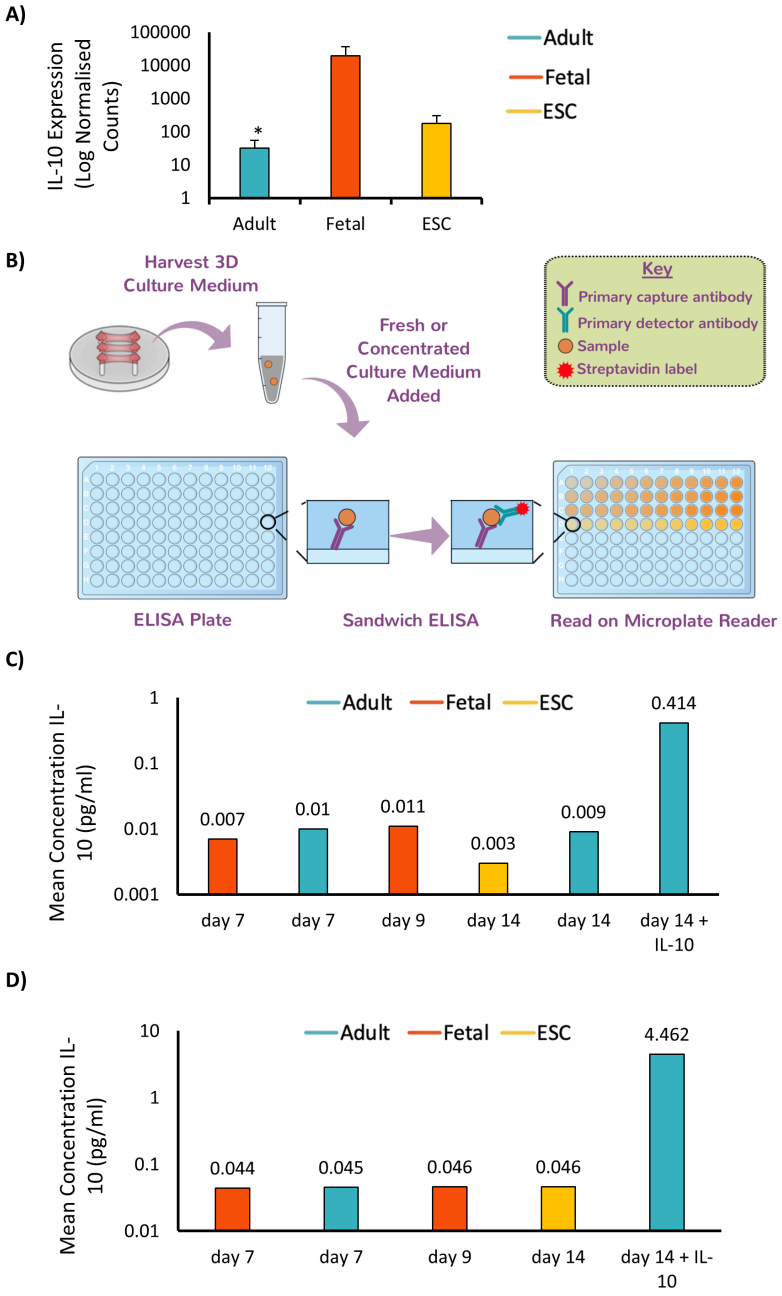

Figure 3.8. Investigating IL-10 protein expression. A) *IL-10* gene expression in adult, fetal and ESC-tenocytes. *Y*-axis shows the gene expression in terms of the log normalised RNA-seq counts. Asterisk (*) represents a significant difference between the adult tenocytes and both fetal and ESC-tenocytes (p-adj values < 0.01 & Log2FC cut-off ± 2). **B)** Outline of ELISA experiment, where 3D cultured adult, fetal and ESC-tenocyte medium was used in an IL-10 sandwich ELISA. Sample is incubated onto an ELISA plate which is coated with primary capture antibody, to which present IL-10 will bind. A primary detector antibody (biotin), followed by a streptavidin label is then added and following addition of development solution a coloured product is detected using a microplate reader and the absorbance compared to known standards. **C)** ELISA results from fresh 3D culture supernatant. Values shown as the mean concentration of IL-10 (pg/ml) in each sample based on duplicate microplate wells. **D)** ELISA results from concentrated 3D culture supernatant. Values shown as the mean concentration of IL-10 (pg/ml) in each sample based on duplicate microplate wells.

3.2.7. ESC-derived tenocytes are transcriptomically more similar to fetal than adult tenocytes when cultured in 3D

Further analysis of the RNA-seq data was conducted using the alignment-free Salmon pipeline only. Hierarchical clustering and principal component analysis (PCA) on adult, fetal and ESC-tenocytes cultured in 3D showed clear segregation of the three cell types, with the greatest variance separating the ESC-tenocytes from the adult and fetal tenocytes (Figure 3.9.A&B). To further identify the cells as being tenocytes, a panel of 28 musculoskeletal associated genes identified from the current literature (240,368–371) were specifically examined (Figure 3.9.C). ESC-tenocytes expressed all tendon associated genes, however at lower levels compared to adult and fetal tenocytes (Figure 3.9.C). Of the eight cartilage genes, only *COMP* and *THBS3* showed significant differences between the cell types, with both markers having the lowest expression in ESC-tenocytes. Of the bone genes *CD36*, *SNCG* and *SPP1* were expressed significantly more in the ESC-tenocytes, but *RUNX2* was expressed at a significantly lower level in the ESC-tenocytes.

To better understand the differences between fetal and adult tenocytes, heatmaps were constructed of the top 30 DE gene, ranked based on both the p-adj value and FDR. This resulted in dendrogram clustering of the fetal tenocytes with the ESC-tenocytes, with 21 out of the 30 genes showing a more similar expression pattern than with adult tenocytes (Figure 3.10.A). Cluster 1 highlights six genes which are highly upregulated in adult tenocytes, whereas clusters 4 and 5 show 15 genes which are highly downregulated in adult tenocytes. Two clusters, 2 and 3, consisting of 9 genes in total, show a more closely related expression pattern between ESC-tenocytes and adult tenocytes. Heatmaps of the top 100, 200 and 500 genes were also constructed and resulted in similar dendrogram clustering of the fetal tenocytes with the ESC-tenocytes, again being ranked based on both their p-adj value and FDR (Figure 3.10.B).

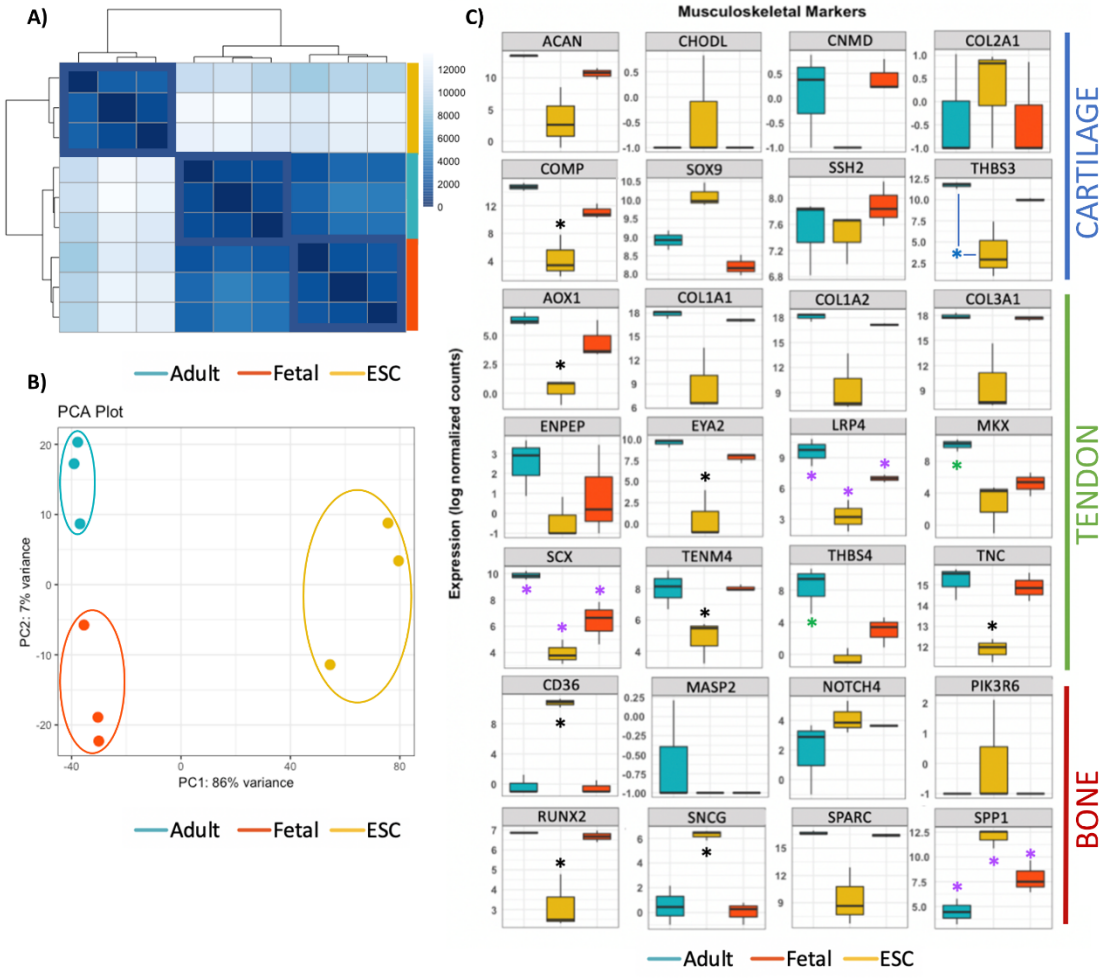

Figure 3.9. Transcriptomic comparison of adult, fetal and ESC-tenocytes. A) Euclidean sample-to-sample distance matrix with hierarchical clustering using VST transformed data across all mapped genes of three biological lines of 3D cultured adult, fetal and ESC-tenocytes. **B)** Principal component analysis of gene expression data profiling three biological lines of 3D cultured adult, fetal and ESC-tenocytes across all mapped genes. **C)** Boxplots of gene expression of cartilage, tendon and bone markers in adult (teal), fetal (orange) and ESC-tenocytes (yellow). Y-axis shows the gene expression in terms of the log normalized counts. Significant differences are depicted by an asterisk (*) with black asterisks representing a significant difference between the ESC-tenocytes and both the adult and fetal tenocytes, blue asterisks representing a significant difference between the ESC-tenocytes and adult tenocytes only, green asterisks representing a significant difference between the adult tenocytes and both the ESC and fetal tenocytes and purple asterisks representing a significant difference between all three groups.

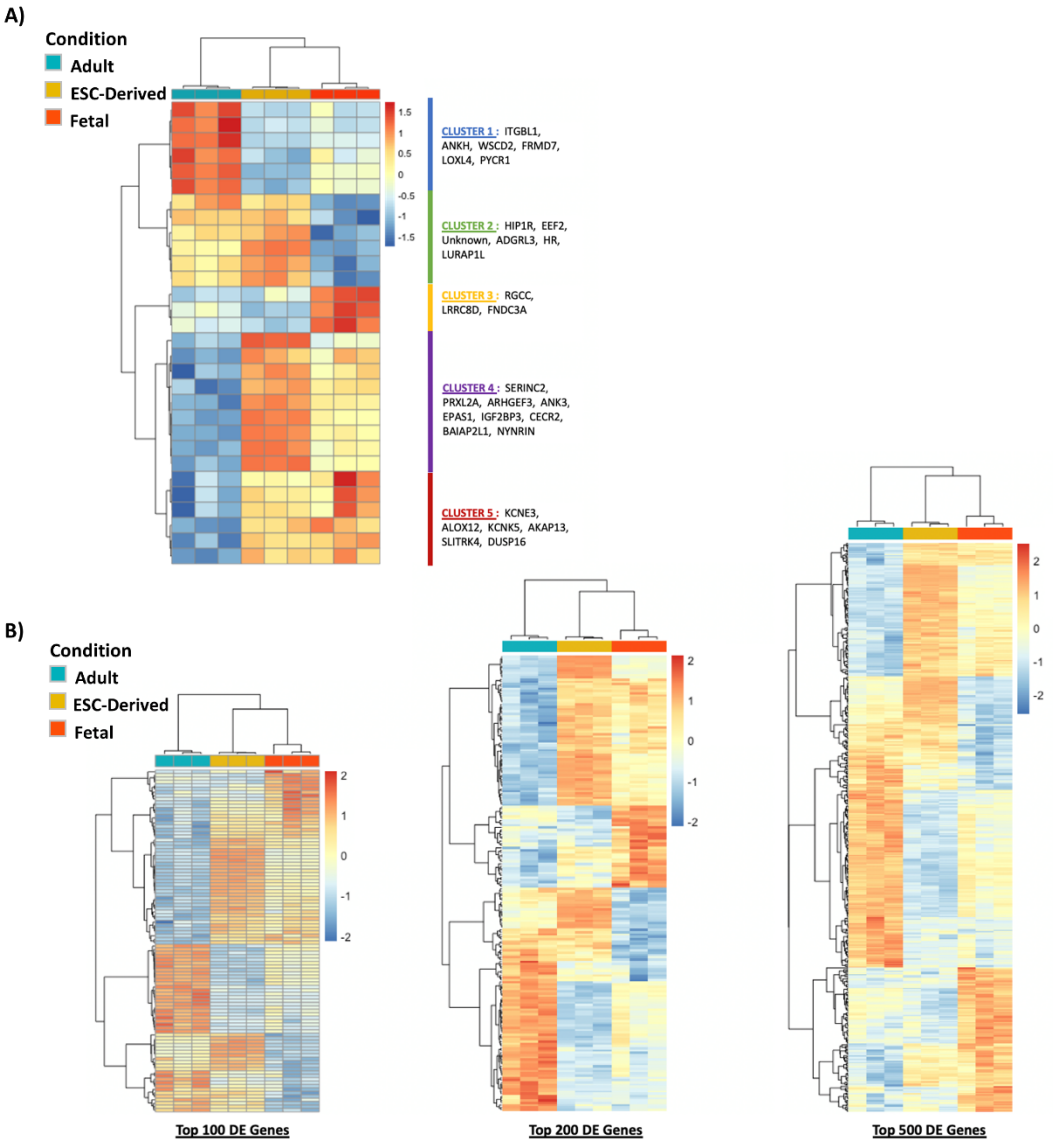

Figure 3.10. Heatmap of top DE genes comparing adult, fetal and ESC-tenocytes. A) Differential gene expression analysis for top 30 genes DE in adult and fetal tenocytes. Dendrograms are based on Pearson correlation, with red and blue colours representing up and down regulated genes respectively. Samples with intermediate expression are represented in yellow. Groups are visualized in columns, with the coloured bar above the heatmap indicating the grouping variable. Genes are represented in individual rows, with patterns of up and down regulated genes being classified into 5 clusters. **B)** Differential gene expression analysis for top 100, 200 and 500 genes DE in adult and fetal tenocytes. Dendrograms are based on Pearson correlation, with red and blue colours representing up and down regulated genes respectively. Samples with intermediate expression are represented in yellow. Groups are visualized in columns, with the coloured bar above the heatmap indicating the grouping variable. Genes are represented in individual rows, with patterns of up and down regulated genes being classified into clusters.

3.2.8. Comparison of over-represented gene ontologies and pathways in adult, fetal and ESC-derived tenocytes cultured in 3D

Gene ontology (GO) analysis was performed on the genes identified as being DE between the three different groups based on pairwise analysis. The top 10 over-enriched terms are listed in Table 3.3. Next to the more common terms (e.g. regulation of cell communication, signal transduction, cellular processes etc.), DE genes between adult and fetal tenocytes were assigned to processes involving the inflammatory response, cellular migration and motility. Chemokines, growth factors and growth factor binding proteins, all of which have been shown to play a role in cellular migration during wound healing (372–375), were amongst the genes associated with these enriched GO terms (Figure 3.11). Comparing ESC-tenocytes to adult and fetal tenocytes revealed pathways involved in organism processes, development and biological and cellular adhesions as being significantly overrepresented (Table 3.3).

Table 3.3. Gene ontology analysis. Summary of the top 10 significantly enriched GO biological process terms for each pairwise comparison of DE genes in adult, fetal and ESC-derived tenocytes. GO terms are arranged alphabetically to allow easier comparison between each group. REFLIST COUNT = number of genes in the reference list that map to the particular annotation category, INPUT COUNT = number of genes in DE gene list that map to the particular annotation, INPUT (expected) = number of genes that would be expected in the DE gene list for this category based on the reference list, INPUT (Fold Enrichment) = fold enrichment of the genes observed in the DE gene list over the expected, INPUT (FDR) = the FDR showing the probability that the number of genes observed in this category occurred by chance as determined by the reference list.

PANTHER GO-Slim Overrepresented Biological Process	REFLIST COUNT (14707)	INPUT COUNT	INPUT (expected)	INPUT (Fold Enrichment)	INPUT (FDR)
Adult vs Fetal					
Cell migration (GO:0016477)	131	20	4.27	4.69	3.45E-05
Cell motility (GO:0048870)	155	20	5.05	3.96	1.32E-04
Cellular process (GO:0009987)	4616	200	150.34	1.33	5.65E-04
Cellular response to stimulus (GO:0051716)	1506	88	49.05	1.79	4.61E-05
Defence response (GO:0006952)	98	19	3.19	5.95	3.71E-06

Inflammatory response (GO:0006954)	60	14	1.95	7.16	2.84E-05
Localization of cell (GO:0051674)	155	20	5.05	3.96	1.48E-04
Regulation of cell communication (GO:0010646)	258	27	8.4	3.21	1.10E-04
Regulation of signal transduction (GO:0009966)	258	27	8.4	3.21	9.40E-05
Signal transduction (GO:0007165)	1267	84	41.27	2.04	2.36E-06
Adult vs ESC-tenocytes					
Biological adhesion (GO:0022610)	265	86	46.61	1.84	2.83E-04
Cell adhesion (GO:0007155)	265	86	46.61	1.84	3.05E-04
Cell surface receptor signalling pathway (GO:0007166)	501	154	88.13	1.75	1.59E-06
Cellular process (GO:0009987)	4616	945	811.97	1.16	6.14E-05
Enzyme linked receptor protein signalling pathway (GO:0007167)	200	73	35.18	2.08	8.61E-05
Multicellular organism development (GO:0007275)	464	146	81.62	1.79	1.67E-06
Multicellular organismal process (GO:0032501)	897	255	157.78	1.62	3.52E-08
Signal transduction (GO:0007165)	1267	304	222.87	1.36	1.23E-04
System development (GO:0048731)	364	109	64.03	1.7	3.27E-04
Transmembrane receptor protein tyrosine kinase signalling pathway (GO:0007169)	164	60	28.85	2.08	4.86E-04
Fetal vs ESC-tenocytes					
Biological adhesion (GO:0022610)	265	85	42.61	1.99	2.13E-05
Cell adhesion (GO:0007155)	265	85	42.61	1.99	2.37E-05
Cell surface receptor signalling pathway (GO:0007166)	501	152	80.56	1.89	7.52E-08
Cellular process (GO:0009987)	4616	876	742.29	1.18	1.39E-05

Cellular response to stimulus (GO:0051716)	1506	321	242.18	1.33	1.92E-04
Enzyme linked receptor protein signalling pathway (GO:0007167)	200	68	32.16	2.11	5.28E-05
Multicellular organism development (GO:0007275)	464	134	74.61	1.8	2.32E-06
Multicellular organismal process (GO:0032501)	897	231	144.24	1.6	9.16E-08
Signal transduction (GO:0007165)	1267	306	203.74	1.5	4.64E-08
Transmembrane receptor protein tyrosine kinase signalling pathway (GO:0007169)	164	58	26.37	2.2	1.03E-04

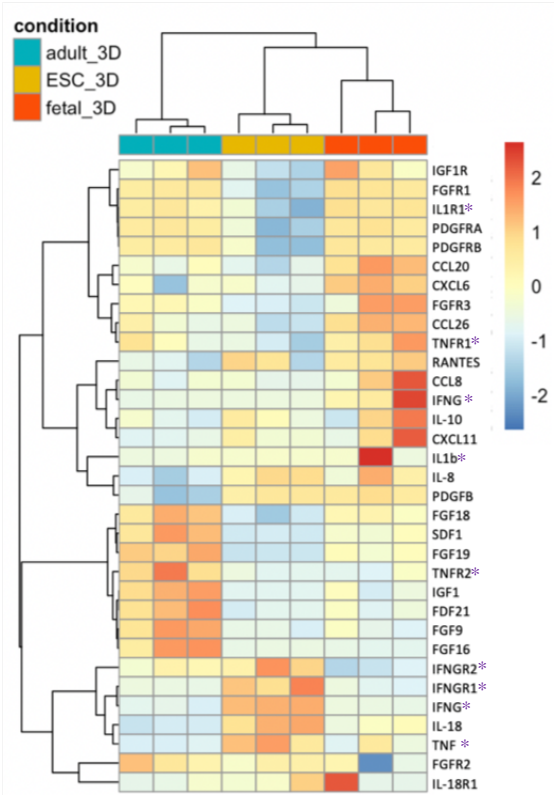

Figure 3.11. Heatmap of genes within the enriched inflammatory response, cellular migration and motility GO terms between adult and fetal tenocytes. Chemokine, cytokine and GF receptors which were expressed are also depicted. Dendrograms are based on Pearson correlation, with red and blue colours representing up and down regulated genes respectively. Samples with intermediate expression are represented in yellow. Groups are visualized in columns, with the coloured bar above the heatmap indicating the grouping variable. Genes are represented in individual rows, with patterns of up and down regulated genes being classified into clusters. Additional chemokine, cytokine and GF receptors, not belonging to an enriched category are depicted using an asterisk (*).

DE genes were then overlaid into GeneAnalytics Pathway Analysis. ERK, PAK, Akt and PI3K-Akt signalling were differentially regulated among all three groups, as was extracellular matrix (ECM) degradation (Table 3.4). In corroboration with the GO analysis cytokine signalling in the immune system was found to be differentially regulated in adult and fetal tenocytes (Table 3.4).

Table 3.4. GeneAnalytics pathway analysis. The Gene Analytics pathway analysis tool was used to determine the top 10 pathways which are upregulated for each pairwise comparison of DE genes in adult, fetal and ESC-tenocytes based on entity score. Entity Score = a SuperPath is a cluster of pathways with similarities in their associated genes, based on various data sources including KEGG, Reactome and BioSystems. The binomial distribution is used to test the null hypothesis that the input gene list is not over-represented within any SuperPath, with the higher the score the smaller the p-value. Entity scores above 13 represent a p-value smaller or equal to 0.0001. Number of Genes in SuperPath = The total number of genes listed per SuperPath. Number of Gene Matched = the number of genes in the input list that appear in the SuperPath.

GeneAnalytics Pathway Analysis	Entity Score	Number of Genes in SuperPath	Number of Genes Matched
Adult vs Fetal			
ERK Signalling	39.55	1180	60
Akt Signalling	23.78	682	35
Signalling by GPCR	22.52	2599	84
PAK Pathway	22.14	683	34
TGF-Beta Pathway	22.02	653	33
RET Signalling	21.48	972	42
PI3K-Akt Signalling Pathway	20.48	524	28
Degradation of the Extracellular Matrix	20	297	20
Microglia Activation During Neuroinflammation	19.82	71	10
Cytokine Signalling in Immune System	18.74	760	34
Adult vs ESC-Derived			
ERK Signalling	166.1	1180	257
Degradation of the Extracellular Matrix	67.19	297	103
Phospholipase-C Pathway	48.42	500	128
Akt Signalling	43.21	682	154
Integrin Pathway	41.08	568	133
Cell Junction Organization	39.2	134	51
PAK Pathway	39.18	683	150
Apoptotic Pathways in Synovial Fibroblasts	36.38	727	154
PI3K-Akt Signalling Pathway	32.34	524	117
Activation of CAMP-Dependent PKA	32.26	630	134

Fetal vs ESC-Derived			
ERK Signalling	166.1	1180	239
Degradation of the Extracellular Matrix	64.66	97	97
Phospholipase-C Pathway	53	500	125
Akt Signalling	46.29	682	149
PAK Pathway	46.12	683	149
Integrin Pathway	39.78	568	125
CREB Pathway	35.7	529	115
Activation of CAMP-Dependent PKA	34.25	630	129
PI3K-Akt Signalling Pathway	33.43	524	112
Angiogenesis (CST)	31.53	89	89

3.2.9. 2D Monolayer culture results in convergence in the expression profiles of adult and fetal tenocytes

To investigate the effect on gene expression of culturing adult and fetal tenocytes in either 2D and 3D culture RNA-seq was performed (Figure 3.12.A). Hierarchical clustering and PCA was conducted on adult and fetal tenocytes cultured in either 2D or 3D (Figure 3.12.B&C). Analysis revealed a convergence of expression profiles in 2D, with only 10 genes being DE. This is in comparison to 542 DE genes in 3D (Figure 3.5.D). When comparing adult tenocytes cultured in either 2D or 3D culture, 502 genes were DE, whereas in fetal tenocytes cultured in either 2D or 3D culture, 851 genes were DE. Of these only 183 genes were common between adult 2D versus 3D culture and fetal 2D versus 3D culture (Figure 3.12.D).

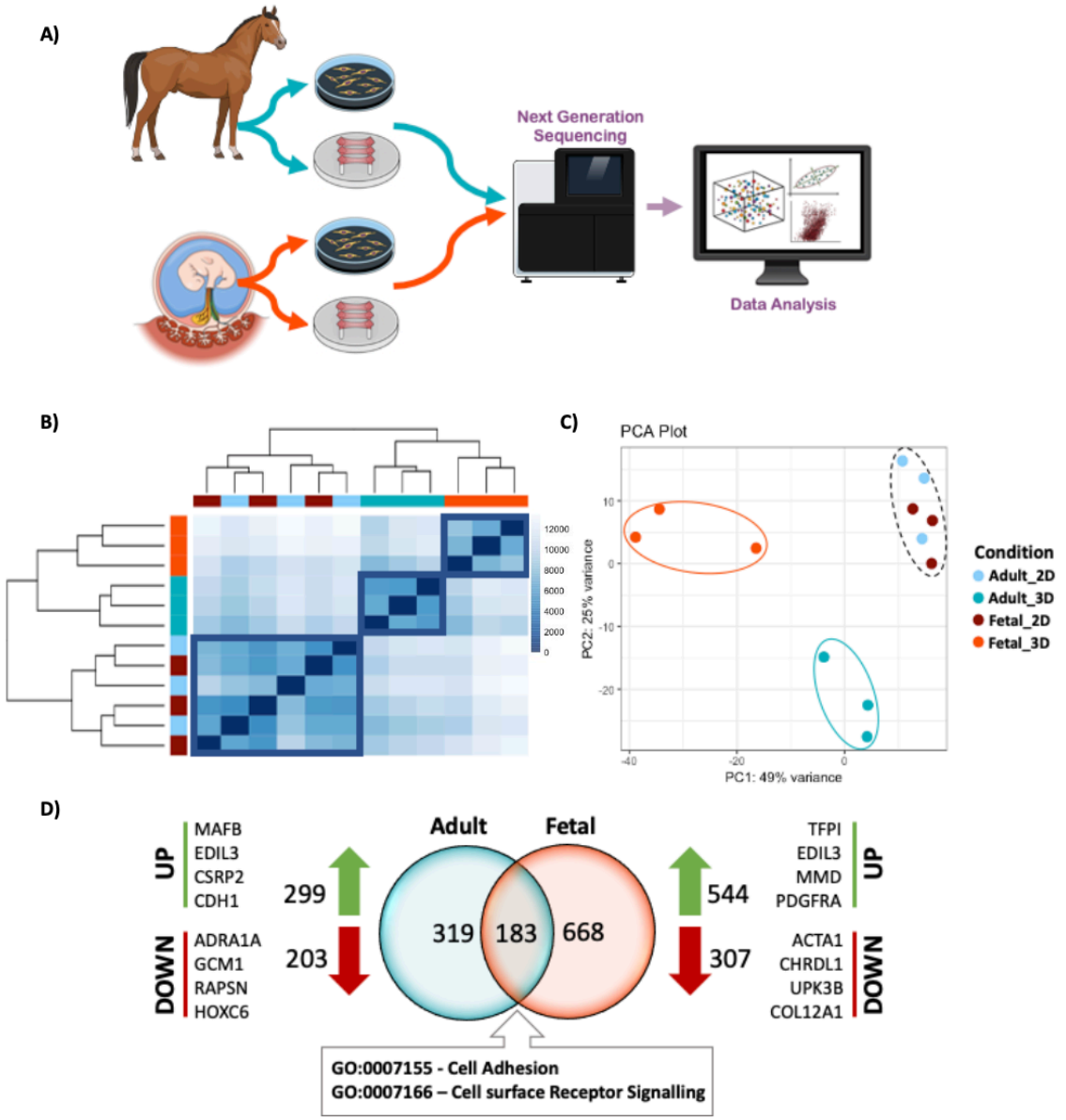

Figure 3.12. Comparison of gene expression changes upon 2D and 3D culturing of equine tenocytes. A) Comparison of RNA transcriptome profile between three biological lines of fetal and adult tenocytes cultured in either 2D or 3D. **B)** Euclidean sample-to-sample distance matrix with hierarchical clustering using VST transformed data. **C)** Principal component analysis of gene expression data profiling three biological lines of 3D versus 2D cultured adult and fetal tenocytes. **D)** Quantitative VENN diagram showing overlap of DE genes in the adult 3D versus 2D culture comparison (blue) and fetal 3D versus 2D culture comparison (orange). Top 4 upregulated genes based on their p-adj value are shown in both groups next to the green arrow and the top 4 downregulated genes value are shown in both groups next to the red arrows.

GO analysis of these 183 genes revealed cell adhesion (GO:0007155) and cell surface receptor signalling (GO:0007166) as key overrepresented biological processes (Table 3.5).

Table 3.5. GO analysis of DE genes between adult and fetal tenocytes cultured in 2D versus 3D. Summary of the significantly enriched GO biological process terms. The panther GO-slim statistical overrepresentation test tool was used to determine over representation of defined GO classification for the 183 genes that were commonly DE between adult and fetal cells in 2D versus 3D culture.

PANTHER GO-Slim Overrepresented Biological Process	REFLIST COUNT (14707)	INPUT COUNT	INPUT (expected)	INPUT (Fold Enrichment)	INPUT (FDR)
Cell Adhesion (GO:0007155)	191	13	2.55	5.09	2.57E-03
Cell Surface Receptor Signalling (GO:0007166)	350	16	4.68	3.42	1.54E-02

Degradation of the ECM was a common pathway which was differentially regulated in both adult and fetal tenocytes as a result of 2D or 3D culture, with differences in collagens, matrix metalloproteinases, and integrins (Table 3.6). Muscle contraction was a predominant pathway which was found to be enriched in monolayer cultures, whereas TGF-β, ERK, PAK and Akt signalling was enriched in 3D cultured cells.

Table 3.6. GeneAnalytics pathway analysis of DE genes in 2D versus 3D cultured tenocytes. **A)** The GeneAnalytics pathway analysis tool used to determine the top pathways which are upregulated in monolayer cultures of fetal and adult tenocytes compared to 3D fetal and adult cultures respectively and the top pathways which are upregulated in 3D cultures of fetal and adult tenocytes compared to monolayer fetal and adult cultures respectively.

Source	SuperPath	Score	Source	SuperPath	Score
Upregulated in Adult Monolayer Culture	Cardiac Conduction	22.84	Upregulated in Fetal Monolayer Culture	Diseases of Glycosylation	22.04
	Vascular Smooth Muscle Contraction	18.99		Phospholipase-C Pathway	20.44
	Smooth Muscle Contraction	15.84		Degradation of the Extracellular Matrix	18.94
	Muscular Dystrophies and Dystrophin Glycoprotein Complex	15.3		ERK Signalling	17.99
	Peptide Ligand Binding Receptors	13.63		Integrin Pathway	17.51
	Myometrial Relaxation and Contraction Pathways	12.95		Dilated Cardiomyopathy	16.95
	Cytoskeleton Remodelling	11.93		Vascular Smooth Muscle Contraction	16.95
	Degradation of the Extracellular Matrix	11.83		Striated Muscle Contraction	15.79
	G Alpha Signalling Events	11.73		Cardiac Conduction	14.18
	EPHA Forward Signalling	11.67		Amino Acid Synthesis and Interconversion	14.1
Upregulated in Adult 3D Culture	ERK Signalling	24.9	Upregulated in Fetal 3D Culture	Cytokine Immune System	47.14
	Degradation of the Extracellular Matrix	20.22		PAK Pathway	39.74
	Integrin Pathway	19.09		NF-kappaB Signalling	38.68
	Akt Signalling	18.31		Akt Signalling	36.16
	PAK Pathway	18.27		ERK Signalling	34.8
	Phospholipase-C Pathway	18.19		Innate Immune System	32.83
	Apoptotic Pathways in Synovial Fibroblasts	16.78		TGF-Beta Pathway	31.09
	ECM-Receptor Interactions	16.16		Pathways in Cancer	27.11

3.3 Discussion

The results in this chapter outline the transcriptional profiling of adult, fetal and ESC-tenocytes cultured in a 3D environment and show that ESC-tenocytes are transcriptomically closer to fetal as opposed to adult tenocytes. It demonstrates that culturing adult and fetal cells in 3D results in a large divergence of their gene expression profiles in comparison to 2D static monolayer culture. This result indicates that 3D culture is a more robust method to assess differences in the same cell types from different developmental stages, which would otherwise be lost in conventional culture systems. Collectively, these results indicate that 3D differentiated ESC-tenocytes may be a useful cell source for the treatment of tendon injuries in the future. The results in this chapter have been published (376).

3.3.1. RNA-sequencing pipelines for differential expression analysis

Current knowledge regarding the entire transcriptome of equine tendon cells or ESC-derived tenocytes is limited, with information only being available from a few studies in adult equine tendon cells (240,377) or via quantitative PCR of small numbers of genes in both adult (368) and fetal tenocytes (267). Here, I report for the first time the use of RNA sequencing to carry out deep transcriptional profiling of adult and fetal tenocytes and compare them to tenocytes which have been differentiated from ESCs. By using this approach, we can start to look at the molecular signatures which define adult and fetal tenocytes, which may help reveal why early gestation fetal tendon wounds repair rapidly without any scar tissue production (255,259). This in turn will allow us to start to determine if ESC-derived tenocytes are a viable source of cells for regenerative cellular therapies.

This sequencing methodology was chosen based on its ability to investigate all present RNAs in a sample with extremely high resolution, allowing for both characterisation of their sequence and quantification of their abundances. Although RNA-seq is fast becoming standard practice in biological research, in order to obtain reliable results good study design is crucial, and all efforts have been made within this thesis to achieve this. I have ensured that our RNA is of high quality with minimal degradation (indicated by the RIN numbers), that the size of the final fragments are long enough to provide accurate

sequencing (longer paired-end reads used), that we have a good sequencing depth (designated 20 million reads) and have adequate replicates as determined by power calculations (3 biological replicates) (246). Quality control checking has also been carried out throughout (FastQC, FastQC Screen, DESeq2).

The analysis pipeline chosen to both map the generated reads to the transcript and subsequently normalise and determine differential gene expression can also have a large effect on the overall study results (378). Whilst many comparative studies on different RNA-seq analysis tools have been performed (378–385), each study needs to be tailored to determine the most suitable workflow. This includes the sequencing technology used, sample size, availability of genomic resources for the species being studied, desired analysis type and computation resources available (379). As such I decided to compare both an alignment-based and alignment-free tool (HISAT2 and Salmon respectively), choosing those which had proven most consistent and efficient across multiple studies and were computationally less demanding to perform (379,384,385).

Overall both mappers provided comparable percentage mapping results of between 60-70% for all three groups. Unfortunately, even though transcriptomics is constantly evolving, providing fine-tuned annotated gene details in well studied organisms such as mouse and human, less well characterised species such as the horse still lack sufficient annotation of basic structures such as untranslated regions, protein-coding regions, non-protein coding regions and splice variants, all of which can affect downstream differential expression analysis (386). Given that in human RNA-seq runs, 70-90% of reads are predicted to map to the human genome, with a significant number of reads being predicted to map to multiple loci (246), a 60-70% alignment is an indicator of fairly good quality mapping when considering the limitations associated with the less well annotated horse genome.

The differential expression analysis in this thesis has been conducted using DESeq2, however many other statistical methods are available which rely on different normalisation strategies to correct for sequencing depth and count bias. Using different normalisation strategies can result in quite different lists of differentiated genes being produced. DESeq2 was chosen due to its proven consistency in comparative studies, being one of the more conservative tools when determining DE genes (95% true positive rate) (253,387). Using this approach, I obtained a 79% corroboration between the RNA-

sequencing data obtained using the Salmon alignment-free pipeline, and qPCR data from a larger cohort highlighting the suitability of this approach for our data set.

3.3.2. Determining if ESC-derived tenocytes more closely resemble adult or fetal tenocytes

The data presented in this thesis suggests that the differentiation protocol used, like others (140,154,159,187,388,389), mimics normal tenocyte development. As previously described, the contraction rates and survival of 3D adult, fetal and ESC-tenocyte constructs showed no significant differences, with histological analysis showing similar cellular morphology and alignment of the collagen fibres (154). Quantitative methods to analyse the H&E stained 3D construct alignment could have included the analysis of nuclear angular deviations, where the angles between the longitudinal axis of the 3D construct and the long axis of the tenocyte nuclei are determined, with the smaller the angular deviation showing higher quality alignment similar to the healthy tendon. Collagen type I and type III, which are the major components in tendon tissue, did not significantly differ in gene expression and no qualitative differences were determined histologically. Additional quantification of the precise collagen content and fibre alignments would be needed to confirm this. Although there are many differences in gene expression between ESC-derived, fetal and adult tenocytes (suggesting all three groups represent unique populations), this study shows that of the 26,991 genes mapped ESC-tenocytes have fewer DE genes when compared to fetal tenocytes (2,708 genes) as opposed to adult tenocytes (2,940 genes), using the Salmon pipeline analysis. Results similar to this have been described in ESC-derived human neural stem cells, where 2,041 genes were DE compared to fetal neural stem cells (390), and ESC-derived human pancreatic β-cells, where 755 genes were DE compared to adult pancreatic β-cells (391).

One of the main challenges in assessing tendon differentiation is the lack of definitive markers to identify tendon populations (183) and a panel of tendon related genes is usually used. Yet, many of these tendon-related genes are widely expressed in various tissues (183,259,392). Similarly, Zhang *et al.*, 2018 highlighted the lack of available microarray and RNA-seq datasets documenting the transition from fetal to adult tendon, with most datasets only comprising of the initial stages of embryonic limb development (183), therefore what stage of tendon development differentiated progeny represent is not

always apparent. This study further highlights the issues in this form of assessment. Of the 12 tendon related genes commonly investigated, four were found to be DE between adult and fetal tenocytes. Three of these genes *THBS4*, *SCX* and *MKX* (168,218) are some of the most commonly cited "tendon" genes and interestingly all show a clear gradient of expression, with adult tenocytes having the highest expression, followed by the fetal and then ESC-tenocytes. *SCX* and *THBS4* are also found to be rapidly downregulated in 2D culture and the response of all three of these putative marker genes to 2D and 3D culture differs between adult and fetal cells. They may therefore not be the most suitable markers of a regenerative cell type.

This work does not however address the heterogeneity of our sample populations. Although it is believed that 3D culture is a potent driver of ESC differentiation into tenocytes, quantification of the percentage of desired cell fate achieved has not been conducted (154). Yet even in very optimised differentiation protocols in human ESCs significant variation in differentiation efficiencies are found, with certain lines more readily differentiating down certain lineages than others due to epigenetic, cell cycle patterns and genetic differences between lines (393–395). To try and counteract this problem cell sorting is typically performed (396), however this relies on a suitable marker being available. Similarly, I have not measured the heterogeneity within the tendon population itself. Studies using single-cell RNA-seq suggest that different sub-populations of tenocytes exist (397), with multiple progenitor populations having been derived (398). Therefore, further study to identify sub-populations of cultured tenocytes is required. The heterogeneous nature of the ESC-tenocyte population is therefore likely, in part, to explain why the musculoskeletal gene expression profile is less robust in ESC-tenocytes compared to both adult and fetal tenocytes.

3.3.3. Investigating differences in gene expression in adult reparative and fetal regenerative tenocyte

Wound healing occurs firstly via an acute and local inflammatory response, this leads to cellular proliferation and ECM deposition to remodel the injured tissue (36). In adults, there is rapid cellular proliferation and a delayed but excessive accumulation of unorganised ECM resulting in scar tissue. In contrast, fetal wounds regenerate with non-disrupted collagen ECM through simultaneous proliferation and synthesis of organised

collagen (41). Although the exact mechanisms of fetal scar-less healing are unknown, various studies suggest this regenerative ability is partly explained by intrinsic differences between adult and fetal fibroblasts themselves. Comparative studies have indicated that differences in the migratory activity, inflammatory responses, cellular mediated expression of chemokine, cytokines and growth factors, and deposition of components of the ECM may play a vital role (41–44).

One of the top DE genes between adult and fetal tenocytes was *LOXL4,* a member of the lysyl oxidase gene family which are responsible for initiating collagen and elastin crosslinking in the ECM via signalling through the TGF-β pathway (399). *LOXL4* has been heavily implicated in fibrosis in skin and vascular tissue (400) and is downregulated in Murphy Roth Large (MRL) mice which heal without scarring (401). Interestingly, this gene is significantly downregulated in both fetal, and ESC-tenocytes (-5.03 and -9.68 Log2FC respectively) compared to adult tenocytes, a result which was confirmed at the protein level using immunofluorescence assays. Other genes within this top cluster (Figure 3.10.A) that are downregulated in both fetal and ESC-tenocytes, compared to adult tenocytes include the Integrin Subunit Beta Like 1 (*ITGBL1)* gene which can promote chondrogenesis (402) and *ANKH*, an inorganic pyrophosphate transport regulator, which has been linked to calcification in articular cartilage. The relevance of other genes within this cluster, *WSCD2, FRMD7* and *PYCR1* are not yet clear. Heatmap clusters 2 and 3 (Figure 3.10.A) contain genes that are significantly higher in fetal tenocytes compared to both adult and ESC-tenocytes and include *ADGRL3*, which play a role in cell adhesion, and *LURAP1L* which is involved in cell migration. *FNDC3A,* is involved in extremity development and fin regeneration (403), but its role in mammalian limb development is still to be determined. Other genes in these clusters have no clear role in tendon development.

Interestingly, the expression patterns of many chemokines, cytokines and growth factors, involved in cell migration were also found to differ between adult and fetal tenocytes, all of which have been shown to play a role in cellular migration during wound healing (372–375). Several of these genes are upregulated in the injured tendon at both the gene and protein level, including IGF-1 (insulin-like growth factor 1), bFGF (basic fibroblast growth factor), PDGF (platelet derived growth factor) and SDF-1 (stromal cell derived factor 1) (404–407), which can influence cell migration (407–411). To confirm this

immunofluorescence and ELISA analysis was performed. IGF-1 showed similar results at the protein level to the sequencing results, whereas regardless of the over 7-fold change in *IL-10* expression, secretion was not found to differ between adult, fetal and ESC-tenocytes. IL-10 ELISAs were however performed on 3D cell culture supernatant only and it is unknown if this lack of difference is due to the IL-10 being retained within the 3D constructs themselves which would not have been detectable using this method. Further ELISA's to test digested and extracted medium held within the constructs should be performed to determine this. Further ELISA's on other chemokines, namely IL-8 and RANTES, as well as further replicates were due to be performed however could not be completed due to the COVID19 pandemic as described in the preface section of this thesis.

Research performed by several students in our group was also conducted to investigate the differences in adult and fetal cells' migratory response to growth factors. Of those tested TGF-β3, which is heavily involved in the wound repair process (306,412,413), significantly inhibited fetal tenocyte migration, yet had no effect on adult tenocytes (376). This observation confirms previous reports in skin and oral mucosa fibroblasts (44,374,375). Interestingly, TGF-β3 has been implicated as a "critical traffic controller" which can selectively halt the migration of certain cell types during skin wound repair to ensure proper wound closure (414). Further investigations to underpin the potential mechanism behind this differing response to TGF-β3, and the effect of TGF-β3 on ESC-tenocytes are warranted.

3.3.4. The effect of culture conditions on tenocyte gene expression profiles

One limitation of the migration studies performed is that investigations were conducted on conventional plastic substratum. It has previously been reported that cytokine and growth factor actions are substratum-dependant (374,415,416) which highlights the need to develop assay systems which more closely resemble the *in vivo* environment. Our results highlight this point, with only ten genes being found to be significantly different between the 2D cultured adult and fetal tenocytes, compared to the 542 genes which were DE in 3D culture. This supports previous studies showing that distinct gene expression profiles between cell types isolated from different stages (417), and different tissues

(362), are better preserved in 3D culture. What was more surprising was that adult and fetal tenocytes appeared to modulate gene expression differently when exposed to a 3D culture environment, with very few DE genes overlapping when comparing the two. Unfortunately, I was unable to compare these results to the native tissue, therefore further research is necessary to confirm whether this change in expression under 3D culture mimics that of their true *in vivo* counterpart.

Similar studies investigating the effect of 2D versus 3D culture have been conducted on adult cells alone, with one report highlighting that when human foreskin fibroblasts are cultured in 3D versus monolayer culture there is upregulation of a subset of skin-specific genes that resemble that of the native tissue (417). Evidence of convergence of gene expression profiles as a result of monolayer culturing has also been described. Mueller, *et al*., 2016 showed that when chondrocytes, tenocytes and dermal fibroblasts are cultured in 2D and compared to their respective native tissues, all three cultured cell types clustered together showing very few DE genes, whereas significantly more genes are DE between the native tissues (362). They also compared this to 3D alginate and fibrin models, which although did not completely recapitulate the native gene expression profiles, did have significantly less DE genes compared to the monolayer cultures.

Another factor which must be considered is how long-term passaging may affect gene expression. Over-subculturing on conventional plastic substratum has been documented to place selective pressure on many cell types leading to morphological, developmental and gene expression changes which ultimately alter the original functional characteristics of the cells (418–421). This phenotypic drift has been demonstrated in tendon cell cultures, with studies showing rapid changes in gene expression of several tendon associated genes from native tissue through to the 10th passage (240,422,423). Similarly, in this study *TNMD* and *THBS4* were found to dramatically decrease following the first passage *in vitro*. *COL1A1* and *SCX* also showed a decrease in expression, although this was more gradual with significance only determined from passage 3 and 4 respectively. However, this decreased expression was not observed for all genes with some remaining variable from the first passage through to the tenth passage (*COL1A2* and *COL3A1)*. Although all efforts were made to use low passage cells it is not typically possible to obtain enough cells for experimental use below passage 3, the stage in which many of

these gene expression changes have already occurred. Methods to improve the efficiency of cell isolation from tissue should be examined.

3.3.5. Summary

In summary, this chapter demonstrates that there are significant differences in tenocyte populations cultured in 3D at different developmental stages. ESC-tenocytes were transcriptomically closer to fetal as opposed to adult tenocytes. I was also able to add further evidence to the benefits of 3D culture compared to conventional monolayer passaging. Future studies to optimise this 3D model to allow study of the wound healing environment in adult and fetal cells is likely to prove fruitful, and our transcriptomic data may help to identify key modulators involved in the scarring process as well as highlight if ESC-tenocytes will indeed prove a useful therapeutic.

Chapter 4 – Investigating Transcriptional Changes Resulting from Scleraxis Knockdown

4.1 Introduction

Transcription factors ability to regulate the expression of multiple target genes allows them to play a powerful role in the pathophysiology of many cells, tissues and organs. Identifying how transcription factors act to alter target gene expression may unlock crucial information on disease progression and potential therapeutics. This chapter will focus on scleraxis (SCX), a bHLH transcription factor which, as previously described, is essential for the formation of force transmitting tendons and is believed to play a role in tissue fibrosis.

4.1.1. SCX function in injury repair

The SCX protein is highly conserved between species, with the equine SCX protein having over 90% identity to that of humans, mice and rats (Figure 4.1). This high level of conservation indicates the critical developmental role it plays, with it being shown to be essential not only for normal tendon development in mice, as indicated in SCX knockout studies, but also in a number of other species including chicken and zebrafish (163,424–426). SCX expression is thought to be regulated primarily through TGF-β signalling, with SCX being upregulated in response to TGF-β addition, the effects of which are mediated through the canonical TGF-β-Smad pathway (163,175,182,242). Mechanotransduction has also been shown to be a key regulator of SCX expression, with mechanical loading causing upregulation of SCX expression and proliferation of SCX expressing cells (388,427).

Figure 4.1. SCX protein sequence alignment. NCBI protein sequences from equine (NP_001098620.1), human (NP_001073983.1), mouse (NP_942588.1) and rat (NP_001123980.1) were aligned using COBALT (https://www.ncbi.nlm.nih.gov/tools/cobalt). Red text shows conserved amino acid residues and grey where there are alignment mismatches or gaps. Insert shows the BLAST sequence alignment identity between the equine SCX protein and human, mouse and rat SCX protein sequences. Figure design adapted from Bagchi *et al*., 2011 (428).

SCX is expressed in a wide variety of tissues, however its mechanisms of action in each tissue type are still not thoroughly defined. SCX has however been implicated in several disease and pathological processes, playing a central role in tendon healing in adult (140,162,429) and neonatal animals (430). One study in an adult mouse wound healing model showed that, using a SCX-GFP tracking system, SCX positive cells were the first to migrate to the injury site, increasing production of ECM in order to bridge the wound gap (429). In comparison SCX-null wounds had impaired ECM assembly, with tendon progenitors displaying increased chondrogenic potential resulting in the formation of cartilage-like tissue at the wound site (429). This was further validated in another SCX lineage tracing model of murine flexor tendon repair which similarly showed SCX positive cells localising to the injury site leading to organisation of the wound bridging scar tissue (431).

SCX has also been implicated in the induction of cardiac fibrosis, being found to significantly increase in expression in surgically induced myocardium infarct scar tissue, an increase which was not detected in non-infarcted or sham-operated myocardium (428,432). Similarly, SCX was also shown to be upregulated in a transgenic mouse model of acute heart failure (433). This upregulation occurred several days prior to the increase in fibrillar collagen expression which gives rise to the fibrotic scar tissue, suggesting a role of SCX in fibrotic induction (428,433). In accordance with this, SCX expression is

also strongly upregulated in dermal keloids, which are enlarged fibrotic scars of the skin characterised by the excessive accumulation of fibrillar collagens (434). Taken together SCX therefore seems to be heavily involved in tissue injury repair and fibrosis, highlighting it as an important candidate for the development of novel anti-fibrotic therapies.

Although SCX appears to have a key role in both early embryonic development as well as in adult injury repair, less is known about the role of SCX in fetal development and in young, postnatal tendons. Tendon tissue continues to grow and develop, with fibrillogenesis and remodelling continuing after birth (11,435). As described in chapter 3, fetal tissues including tendons have also been shown to exhibit regenerative capacities following injury (254,255,279,436–438) and young animals generally undergo better tissue regeneration than mature animals (439–441). However, it has not yet been demonstrated if SCX has alternative roles in different stages of tendon development and ageing.

4.1.2. SCX transcriptional regulation

How exactly SCX functions to enable tenocyte differentiation and ECM remodelling during tendon healing remains unclear, and there is limited information on its downstream regulatory effects. Currently *COLIA1* and *TNMD* are the most well documented genes which have been shown to be directly regulated by SCX in adult tenocytes (442,443). However, emerging evidence suggests that SCX has a key role in driving ECM production during development and remodelling in others tissue types including the heart and periodontal ligaments (444,445). In cardiac fibroblasts, genes including *COL1A2, Snai1, Twist1, MMP2* and *FN1* have been identified as direct targets of SCX (242,446–448) but the large-scale identification of SCX regulated genes is still lacking. Table 4.1 shows a number of genes which have, at the time of writing this thesis, been suggested to be under SCX regulatory control, however direct causal relationships have not in many cases been properly demonstrated. A more detailed description of those genes which have been identified as under the direct control of SCX will be described in chapter 5.

Table 4.1. Genes effected by altering SCX expression. Asterisk (*) represents those which have been demonstrated to be under direct control of SCX.

Gene Effected by altering SCX expression (*Gene Names* or Protein Names)	Study Design	Effect	Tissue/Cells	Reference
ACAN*, *COL II*, *OP*, *COL I*, *AP	SCX overexpression	Enhanced expression of ACAN via binding of SCX to E-box within its promoter, increased mRNA levels of type II collagen and osteopontin while suppressing expression of osteoblast phenotype-related genes encoding type I collagen and alkaline phosphatase	Rat Osteoblastic ROS17/2.8 Cells	(449)
COL1A2*	SCX-mediated regulation determined using ChIP and luciferase assays	SCX-mediated regulation of *COL1A2*	Mouse Cardiac Fibroblasts	(446)
MMP2*	SCX-mediated regulation determined using ChIP and luciferase assays	SCX-mediated regulation of *MMP2*	Mouse and Rat Cardiac Fibroblasts	(447)
FNC*	SCX-mediated regulation determined using ChIP and EMSA	SCX-mediated regulation of *FNC*	Mouse and Rat Cardiac Fibroblasts	(448)
Twist1*, *Snai1*	SCX-mediated regulation determined using ChIP, luciferase assay and EMSA	SCX-mediated regulation of *Twist1* and *Snai1*	Mouse and Rat Cardiac Fibroblasts	(450)
COL1A2*	SCX overexpression and luciferase assay	SCX-mediated regulation of COL1A2	Mouse and Rat Cardiac Fibroblasts	(451)
***COL I*, F-actin, Vinculin**	SCX overexpression and knockdown	SCX overexpression increased *COL I* gene expression and F-actin, ITGb1 and Vinculin protein expression (adhesion genes), and decreased cell migration. SCX knockdown increased cell migration	Mouse and Rat Cardiac Fibroblasts	(452)
COL1A1, COL1A2, COL3A1, COL5A1, Fmod, LUM, DNC, MMP2, MMP3, MMP9, MMP11	SCX overexpression and SCX knockdown	SCX upregulation significantly increases *COL1A1, COL1A2, COL3A1, COL5A1, Fmod, LUM, DNC, MMP2, MMP3* and decreases *MMP9* and *MMP11* expression. SCX knockdown significantly decreases C*OL1A1, COL1A2, COL3A1, COL5A1, Fmod, LUM, DNC, BGN, MMP2, MMP3* and increases *MMP9 and MMP11* gene expression	Rat Cardiac Fibroblasts	(242)

COL2A1*	SCX knockdown, luciferase reporter, EMSA and ChIP	SCX-coactivation with SOX9 and p300 to regulate *COL2A1*	Human Chondrosarcoma Cells	(453)
SMA*, BMP4	SCX overexpression, EMSA, ChIP, luciferase assay, Co-IP	SCX physically associated with E12 and bound the E-box in the promoter of SMA and negatively regulated the advanced glycation end product (AGE)-induced SMA expression. SCX induced expression and secretion of bone morphogenetic protein 4 (BMP4)	Mouse Glomerular MC line	(454)
COL1, TNC	SCX overexpression	Increased COL I and TNC protein and gene expression	Human ESC-derived MSCs	(177)
COL1A1, COLXIV	SCX overexpression	qPCR analysis of SCX-overexpression clones showing higher expression of collagens I and XIV than in control	Human ESC-derived MSCs	(455)
***DNC, Fmod, LUM, SMA, SOX9*, COL I, TNMD**	SCX overexpression	Increased DNC, Fmod, LUM and ACTA1 gene expression and decreased SOX9 gene expression, increased collagen I secretion and TNMD protein expression.	Human MSCs	(176)
TNMD, SOX9	Inactivation of endogenous SCX using SCX^{cre} mouse	TNMD absent in tendon and ligament, SOX9 decreased expression in developing cartilage, patella and deltoid tuberosity	Mouse Model	(456)
LUM, Fmod, Brevican, Neuroncam, DNC, BGN	Investigation of Atrioventricular canal regions SCX-null mice	Decreased *LUM, Fmod, Brevican, Neuroncam, DNC, BGN* in postnatal atrioventricular canal regions SCX-null mice	Mouse Model	(457)
BMP4*	SCX null mice, SCX overexpression, luciferase assay and ChIP	*BMP4* decreased in SCX null mice, *BMP4* increased in C3H10T1/2 cell overexpressing SCX, SCX directly binds to E-box in BMP4 promoter	Mouse Model and C3H10T1/2 Cells	(458)
Osteocalcin	SCX overexpression and knockdown	osteocalcin, a marker for bone formation was downregulated and upregulated by SCX overexpression and knockdown of endogenous SCX in PDL cells, respectively	Mouse and Rat Periodontal Ligament Cells	(459)
1,247 DE genes	RNA-seq of remodelling heart valves isolated from E15.5 SCX null mice and overexpression mice	Immuno-validation of decreased levels of COL4A1, COL4A2, Fmod, Hspg2, 1,247 genes thought to be regulated in a SCX-dependent manner	Mouse Remodelling Heart Valves	(460)
Transferrin*, ABP*	SCX overexpression and luciferase assay	SCX regulated the transferrin promoter and androgen binding protein (ABP) promoter activity	Rat Sertoli Cells	(461)

COL1A1*	SCX overexpression studies and EMSA	SCX-mediated regulation of *COL1A1*	Mouse Tendon Fibroblasts	(442)
SOX9, COL II	SCX-null murine tendon progenitor cell lines	Increased SOX9 and COL II following chondrogenic differentiation of SCX-null progenitors	Mouse Tendon progenitors	(429)
COL I, TNMD	SCX overexpression and knockdown	COL I and TNMD were downregulated and upregulated by SCX overexpression and knockdown of endogenous SCX in TSCs	Rat Tendon Stem Progenitor Cells	(462)
COL XIV, TNMD, Col I	SCX null mice	Complete loss of expression of COL XIV and TNMD and slight decrease of COL I	Mouse Tendons	(163)
TNMD*	SCX knockdown	*TNMD* gene expression significantly decreased, SCX directly transactivates *TNMD* via two E-boxes in TNMD promoter	Rat Tenocytes	(422)
COL1A1, COMP, SOX9	SCX knockdown and overexpression	Reduced COL1A1, COMP, SOX9 gene expression in fetal tenocytes only, no change noted in tendon genes in adult tenocytes	Equine Adult and Fetal Tenocytes	(267)
1,002 DE Genes	RNA-seq of SCX knockdown	changes to focal adhesion related genes however not significant upon qPCR validation	Equine Adult Tenocytes	(377)
TNMD, ACAN, ChM-I	SCX overexpression	*TNMD* significantly upregulated in SCX overexpressing tenocytes, upregulation of ACAN and ChM-I in chondrocytes	Chick Tenocytes and Chondrocytes	(443)
COL I	SCX knockdown	siRNA-mediated knockdown of scleraxis completely eliminated upregulation of collagen-1 induced by aldosterone	Mouse Vascular Aortic Smooth Muscle Cells	(463)
2,136 DE Genes	RNA-seq of SCX null zebrafish dorsal tissue	*TNMD, MKX, TNC, FGF4, FGF8b, COL1A1, COL1A2, SP7, ENTP5, BMP2, BMP4, BMP9, Smad1, Smad5/8, Smad4* SCX null compared to control - validated with qPCR	Zebrafish Dorsal Tissue	(424)

4.1.3. Chapter aims

Previous work from our group has shown that knocking down SCX expression in adult equine tenocytes has no effect on their ability to re-organise a 3D matrix to generate artificial tendons whereas SCX knockdown in fetal tenocytes completely prevents their ability to form 3D tendons (267). SCX knockdown also caused considerably different effects on tendon related gene expression in fetal and adult tenocytes further suggesting that SCX regulates gene expression differently during different developmental stages. Therefore, the aim of this chapter is to expand on this work by:-

1) Using a global RNA-sequencing approach to analyse the transcriptome of equine adult and fetal tenocytes following SCX knockdown.

2) Compare DE genes in adult and fetal tenocytes as a result of SCX depletion to tenocytes from young postnatal foals and ESCs in which SCX expression has also been reduced.

4.2 Results

4.2.1. Optimisation of SCX knockdown using a lentiviral system

In order to identify downstream target genes of SCX, a retroviral delivery system to express a short hairpin RNA (shRNA) was used to generate stable SCX knockdown lines (shSCX) or non-target controls (NT) in four biological replicates of fetal and adult tenocytes. Alongside, GFP-Turbo lines were also generated as a positive control allowing visualisation of transduction efficiency and puromycin selection. In doing so it was important to ensure that the process was optimised to ensure all lines had as similar a level of knockdown as possible. To do so batches of lentivirus were made and the titer tested before optimisation commenced. A drop in titer was detected when comparing freshly harvested virus to that stored at -70^{o}C. Batch-to-batch variation was also observed, with it being apparent that each lentiviral plasmid (NT, GFP, shSCX) yielded different viral titers (Figure 4.2). Although in the previous chapter (chapter 3) it was demonstrated that 3D culture was a superior method for analysing transcriptional changes between adult and fetal tenocytes, it is important to note that this work was conducted in conventional 2D culture due to the poor survival of fetal tenocytes in 3D gels following SCX knockdown.

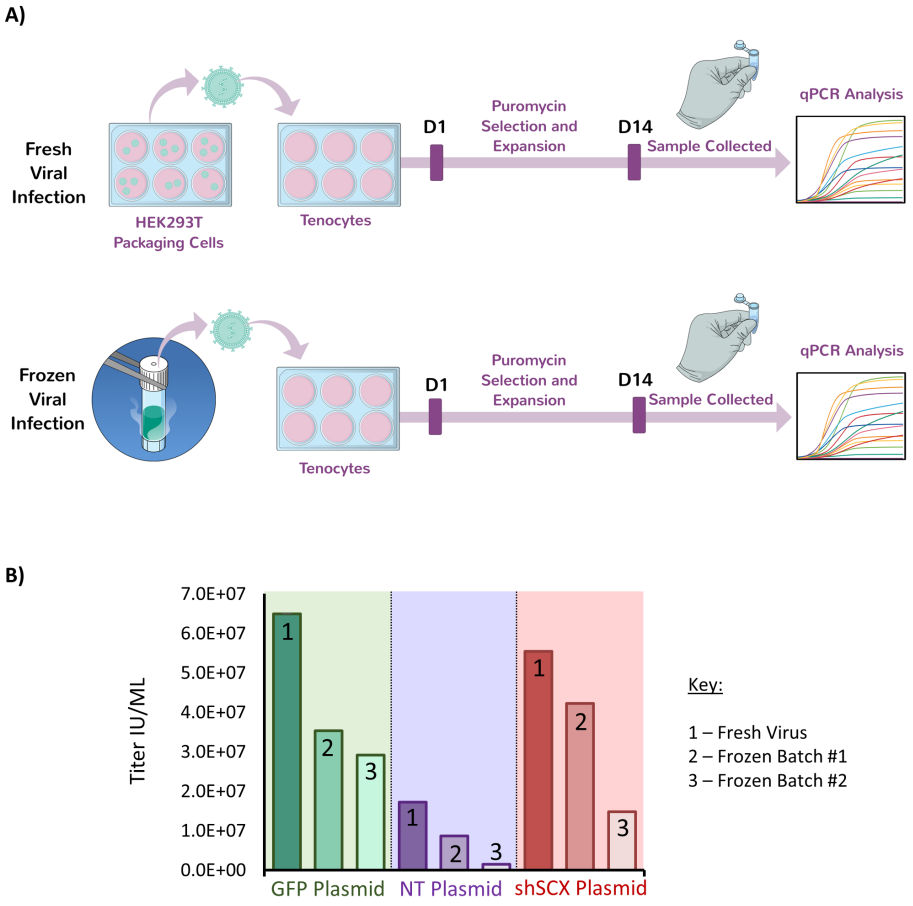

Figure 4.2. Lentiviral infection methods comparing freshly isolated versus frozen virus. A) Lentiviral titer testing using the three plasmids Turbo-GFP shRNA (GFP), non-target, scrambled shRNA (NT) and scleraxis shRNA (shSCX). Fresh lentiviral supernatant was harvested (Fresh) with some being frozen at -70°C (Frozen) before titer testing via qPCR. **B)** The titer of fresh viral supernatant was compared to two different batches of frozen viral preparation (Batch 1 & Batch 2) for each of the three plasmids.

Subsequently frozen lentiviral titers ranging from $5x10^5$ IU/ml to $3x10^7$ IU/ml, as well as fresh virus (> $1x10^8$ IU/ml), were tested on one line of fetal tenocytes and the percentage knockdown of scleraxis gene expression (Figure 4.3.A) and copy number integrations (Figure 4.3.B) recorded in order to determine the most effective titer for subsequent cell line generation. A titer of $1x10^7$ IU/ml was found to provide a good percentage knockdown (84.12%) and cells proliferated well during puromycin selection. Viral titers below $5x10^6$ IU/ml did not produce enough infected cells to successfully expand following puromycin selection. Viral titers above $1x10^8$ IU/ml led to toxic effects where cell death occurred prior to any puromycin selection (Figure 4.3.C).

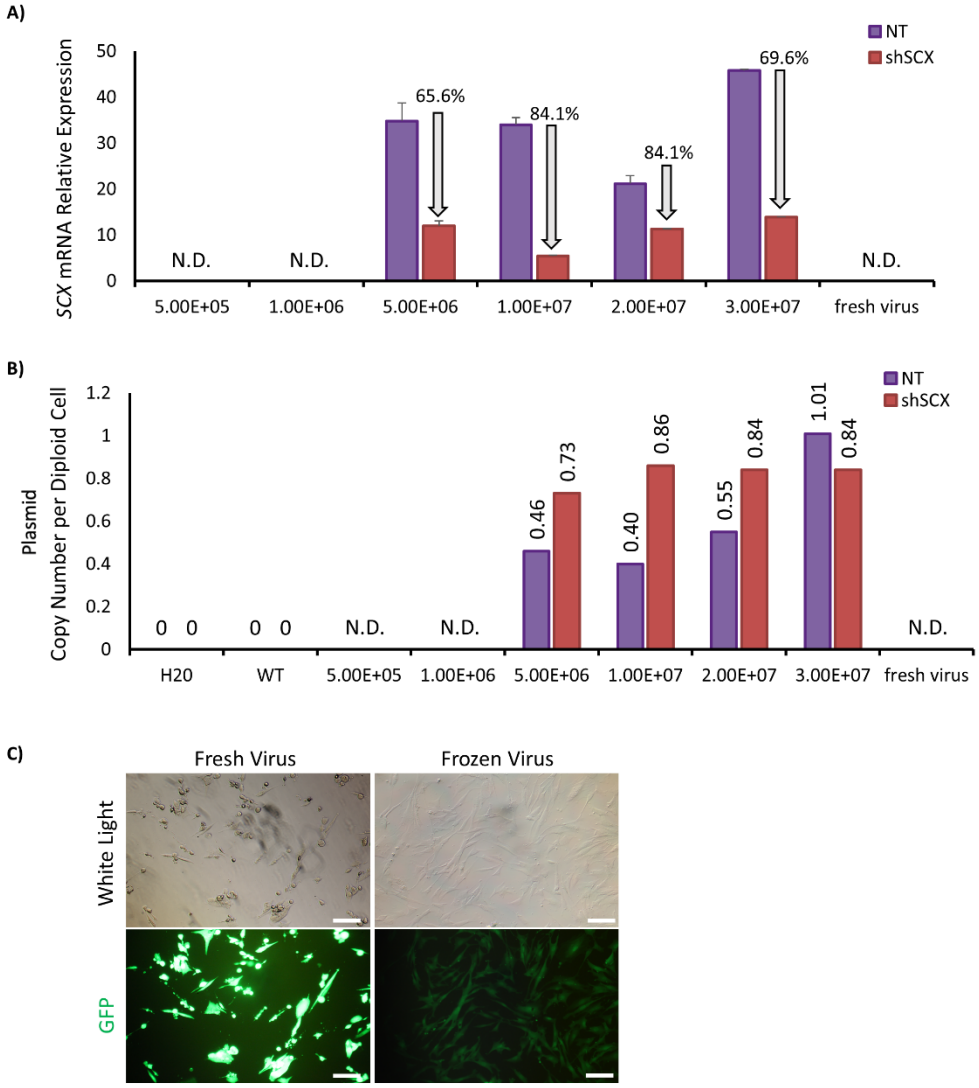

Figure 4.3. Lentiviral optimisation. A) Scleraxis gene expression in one line of fetal tenocytes stably transfected with shRNA to scleraxis. No data (N.D) could be collected for titers of $5x10^5$ or $1x10^6$ as cells did not survive puromycin selection following infection. Similarly, no data could be collected from cells infected with fresh virus (> $1x10^8$) as cells died prior to puromycin infection. *SCX* knockdown was detected in those cells infected with $5x10^6$ to $3x10^7$. Error bars show the standard deviation of two technical replicates. **B)** DNA was collected from tenocytes infected with varying titers of NT shRNA or SCX shRNA, following puromycin antibiotic selection. No data (N.D) could be collected for titers of $5x10^5$ or $1x10^6$ as cells did not survive puromycin selection following infection. Similarly, no data could be collected from cells infected with fresh virus (> $1x10^8$) as cells died prior to puromycin infection. Cell lines with titers ranging from $5x10^6$ to $3x10^7$ in either NT shRNA infected or SCX shRNA infected cells, had approximately 0.5-1 copy of plasmid per diploid cell. Water (H20) and wild type (WT) non infected DNA were used as negative controls. **C)** GFP control infection of one line of fetal tenocytes with fresh HEK293T viral supernatant (Left) vs frozen viral supernatant (Right) prior to selection with puromycin antibiotic. Cells infected with fresh virus show very high levels of GFP expression with cells showing morphological signs of cellular stress, compared to frozen virus where GFP levels were much lower, and no cellular stress was observed. Scale bar = 40 µm.

4.2.2. SCX knockdown cell line generation for RNA-sequencing analysis

The optimised protocol was used to generate four biological replicates of fetal and adult tenocyte SCX knockdown and NT control lines for subsequent RNA-seq analysis. The average percentage of *SCX* mRNA knockdown was 72.6% in adult tenocytes and 80% in fetal tenocytes, which did not significantly differ (p-value = 0.336) (Figure 4.4.A). Viral copy number integration was measured in each line of shSCX and NT expressing tenocytes and approximately one copy number event was detected per diploid cell across all cell lines (Figure 4.4.B). RNA extracted from each line passed quality control checking using an Agilent 2200 TapeStation performed by Cambridge Genomics Services (CGS) (Figure 4.4.C).

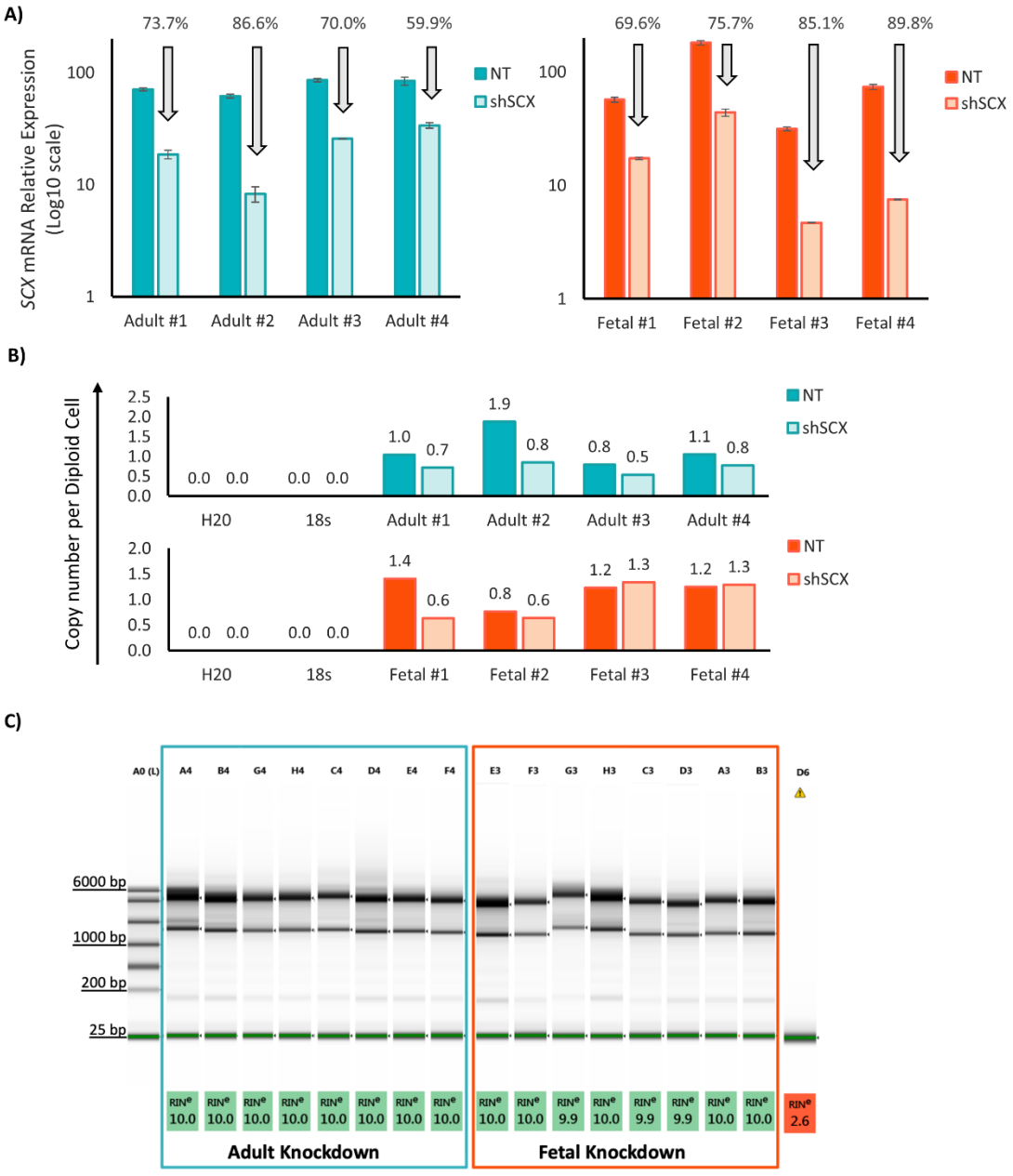

Figure 4.4. SCX knockdown in each biological line of adult and fetal tenocytes. A) Four biological replicates of adult and fetal tenocytes exhibit consistent and comparable reduction in *SCX* mRNA expression following viral transduction with a specific shRNA against SCX (shSCX) when compared to cells transduced with a control non-target scrambled shRNA (NT). Arrows highlight the percentage decrease between the NT control and shSCX expressing cells. Using a two-tailed Student's *t*-test no significant difference between percentage knockdown is detected between the adult and fetal lines ($p = 0.336$). Error bars represent the SD of two qPCR replicates. **B)** Adult and fetal shSCX or NT copies per diploid cell determined by copy number assays in each biological line. Water (H20) and wild type (WT) non infected DNA were used as negative controls. Using a two-tailed Student's *t*-test no significant difference in copy number was detected between fetal NT and shSCX lines ($p = 0.462$), between adult NT and shSCX lines ($p = 0.101$) or between the adult and fetal infected lines ($p = 0.548$). **C)** RNA integrity for all lines was between 9.9-10, indicating high quality RNA. Lane A0 shows the electronic ladder and D6 the no sample control.

A reduction in SCX protein expression was also confirmed using immunocytochemistry (Figure 4.5). In some shSCX lines, SCX protein was reduced but still detectable, in other lines SCX protein was no longer detectable.

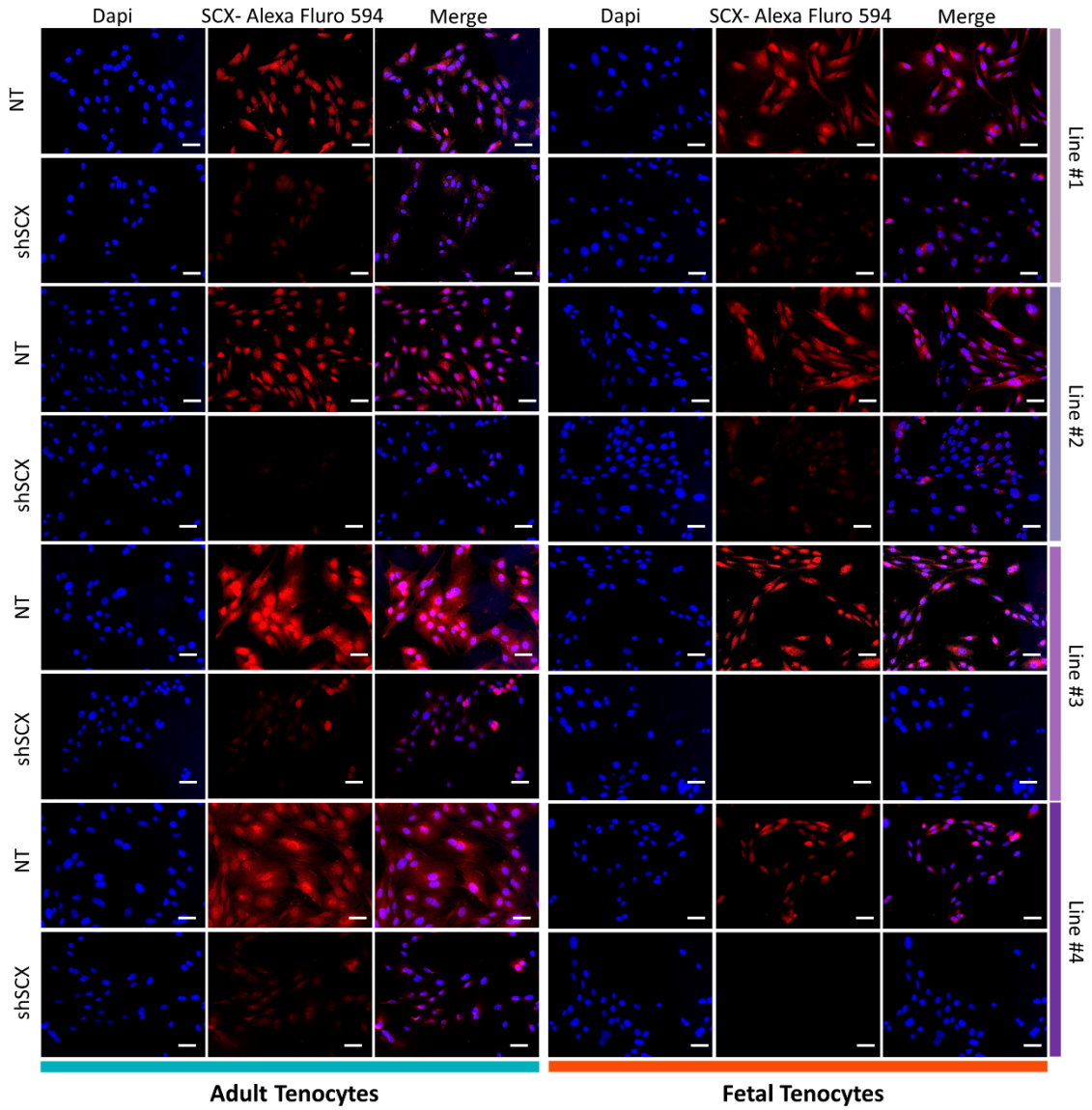

Figure 4.5. Comparing SCX protein expression following SCX knockdown. Immunocytochemistry confirms a reduction in SCX protein (red) in both adult and fetal tenocytes following shSCX expression. Scale bar = 40 μm. DAPI staining of the nuclei is shown in blue.

4.2.3. Technical validation of SCX knockdown and NT control line RNA-sequencing data

Following the RNA-seq run a total of 50.8 billion reads were generated across all the adult and fetal NT and shSCX cell lines, with an average of 134 million reads per sample group (s.d. 0.35 million read pairs). The average read number was 3.4 billion (1.7 billion read pairs) for the adult NT tenocytes, 3.4 billion (1.7 billion read pairs) for the shSCX adult tenocytes, 3 billion (1.5 billion read pairs) for the NT fetal tenocytes and 2.9 billion (1.45 billion read pairs) for the shSCX fetal tenocytes. Detailed analysis of the knockdown RNA-seq data set quantity and size distribution of the Illumina sequencing run can be found in Table 4.2.

Table 4.2. Overview of knockdown RNA-seq metrics. The total size and number of read pairs refers to the total read sizes and counts per group (adult NT, adult shSCX, fetal NT and fetal shSCX tenocytes). The same applies for the median and mean values, both of which include four biological replicates.

	Adult NT	**Adult shSCX**
Total size of all reads per group (bp)	13,460,000,000	13,410,000,000
Median size of reads per sample (bp)	3,430,000,000	3,355,000,000
Mean size of reads per sample (bp)	3,365,000,000	3,352,500,000
Total number of all reads per group	134,600,000	134,100,000
Median number of reads per sample	34,300,000	33,550,000
Mean number of reads per sample	33,650,000	33,525,000
Mean phred score per sample	36.05	36.18
	Fetal NT	**Fetal shSCX**
Total size of all reads per group (bp)	12,000,000,000	11,940,000,000
Median size of reads per sample (bp)	3,045,000,000	2,925,000,000
Mean size of reads per sample (bp)	3,000,000,000	2,985,000,000
Total number of all reads per group	120,000,000	119,400,000
Median number of reads per sample	30,450,000	29,250,000
Mean number of reads per sample	30,000,000	29,850,000
Mean phred score per sample	36.02	36.11

All RNA samples passed quality control (QC) carried out using FastQC and FastQC Screen. Trimming of reads was not required due to the high sequence quality and minimal adapter content. A GC content of 50-52% was obtained, with no sequences being flagged as poor quality.

4.2.4. Scleraxis knockdown leads to differential changes in gene expression in adult and fetal tenocytes

RNA-sequencing was performed to measure transcriptional changes in four lines of adult and four lines of fetal tenocytes following SCX knockdown. A total of 13,159 and 13,142 genes were detectable (out of 21,689) in the adult and fetal tenocytes respectively. Of these, 183 genes were DE using a Log2FC±1 p.adj< 0.05 cut off between adult shSCX and NT controls, with 120 genes being upregulated and 63 genes being downregulated (Figure 4.6.A). In comparison, 477 genes were DE between fetal shSCX and NT controls, with 358 genes being upregulated and 119 genes being downregulated (Figure 4.6.A). Of these DE genes only 117 were commonly differentially regulated as a result of SCX knockdown in both adult and fetal tenocytes lines, with 87 genes being upregulated and 30 genes being downregulated. *MMP3* was found to be the most significantly upregulated gene common to both groups. *IGF2BP1* was the most significantly downregulated gene common to both adult and fetal groups following SCX knockdown, however *CLDN16* was the most significantly downregulated gene when looking at the effects of shSCX in adult tenocytes alone. The results of the differential gene expression analysis can be visualized in the volcano plots in Figure 4.6.B. The RNA sequencing data is freely available in the National Centre for Biotechnology Information Gene Expression Omnibus repository (NCBI GEO, www.ncbi.nlm.nih.gov/geo) [accession number GSE149570]. The lists of differentially expressed genes are available in full in (Paterson et al., 2020, Supplementary File 1).

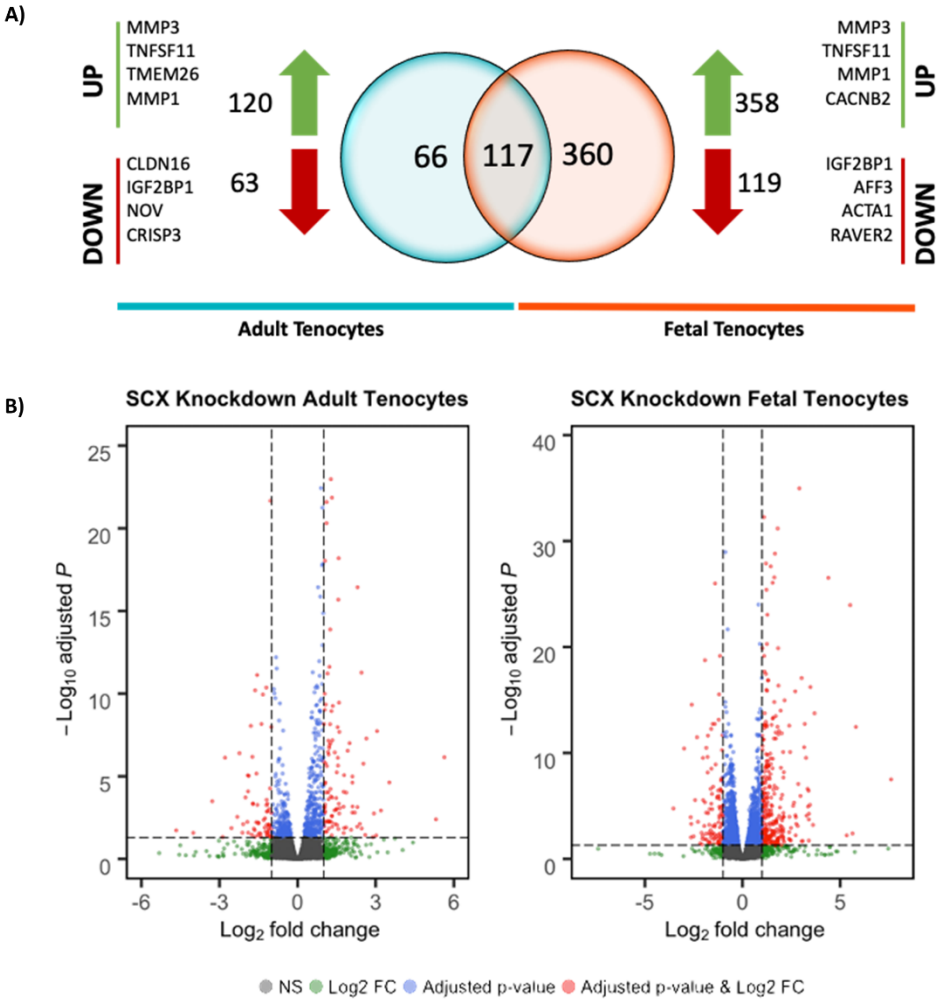

Figure 4.6. Differential expression in adult and fetal tenocytes following SCX knockdown. **A)** VENN diagram showing overlap of DE genes in the adult (teal) and fetal (orange) tenocytes following SCX knockdown. The top 4 upregulated genes with the greatest Log2FC are shown in both groups next to the green arrow and the top 4 downregulated genes are shown in both groups next to the red arrows. **B)** Volcano plot displaying the DE genes between the shSCX and NT control in adult and fetal tenocytes. The x-axis corresponds to the Log2FC and the y-axis the mean expression value of log 10 (p.adj). The red dots represent those genes which are considered DE based a Log2FC±1 p.adj< 0.05 cut off. Positive values on the x-axis represent upregulated genes and negative values represent downregulated genes.

To validate some of the potential direct or indirect targets of SCX, qPCR analysis was conducted using both the original shSCX and NT sequenced lines alongside an additional cohort of two adult and two fetal shSCX and NT tenocyte biological replicates (Figure 4.7). Of the eight genes tested *SCX*, *MMP2* and *MMP3* were significantly DE as a result of SCX knockdown in both adult and fetal tenocytes, corroborating the RNA-sequencing results (Figure 4.7). In the fetal tenocytes, *MMP9, COL14A1* and *COL1A2* had significant adjusted p-values following RNA-seq. However, upon analysis of further biological replicates these genes were no longer significant, whereas *VIM* reached significance with further biological replicates (Figure 4.7). All of the RNA-sequencing data for the adult tenocytes was corroborated by the qPCR analysis. Overall, for all genes in both adult and fetal tenocytes, there was a 75% corroboration between the RNA-sequencing data and the qPCR analysis of the larger cohort.

A)

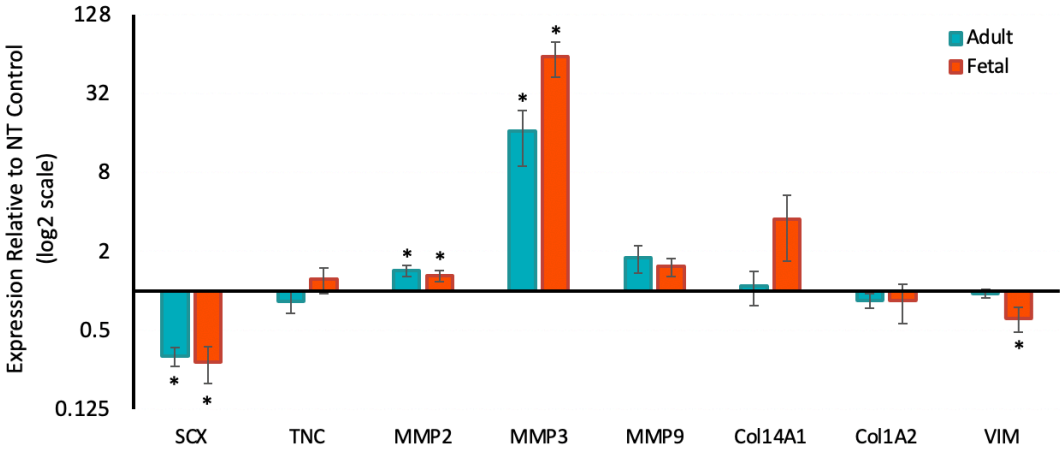

B)

Gene	Adult Knockdown		Fetal Knockdown	
	RNA-seq (p-adj.)	Cohort qPCR (p-value)	RNA-seq (p-adj.)	Cohort qPCR (p-value)
SCX	1.26E-09	1.86E-08	4.89E-07	1.32E-05
TNC	0.9131	0.5411	0.2062	0.4242
MMP2	**0.0013	0.0307	**0.0087	0.0498
MMP3	3.05E-08	0.0471	9.49E-15	0.0089
MMP9	0.6110	0.1990	**0.0038	0.0514
COL14A1	0.8404	0.6729	4.02E-27	0.2023
COL1A2	0.6519	0.1529	**0.0001	0.5768
VIM	0.9208	0.7900	0.5380	0.0145

Figure 4.7. Validation of RNA-seq with an additional biological cohort. A) Validation of 8 DE genes detected from RNA-seq using qPCR on a larger cohort (6x biological replicates) of SCX knockdown lines. Expression shown relative to the NT control on a log 2 scale. * $p < 0.05$ using a two-tailed Student's *t*-test. Error bars represent the SEM of 6 biological replicates. **B)** Comparison of significance in expression following SCX knockdown in RNA-seq and qPCR results from adult and fetal tenocytes. A significance threshold of < 0.05 was used for both RNA-seq p.adj and q-PCR p-values. Red shaded boxes indicate no-significant difference. Yellow shaded boxes with a double asterisk (**) represent a significant p.adj value, but do not meet the fold cut-off (±1). Green shaded boxes indicate there is a significant difference based on both p.adj/p-value and Log2FC±1.

It has previously been demonstrated that SCX either directly or indirectly regulates the expression of several collagens, proteoglycans, matrix metalloproteinases and other transcription factors in both tendon and heart tissue (242,377,442,444,446–448,450,464,465). Using the aforementioned literature available on SCX regulation, a panel of 16 genes previously demonstrated to be affected by SCX knockdown in either tendon or cardiac fibroblasts was collated from the RNA-seq data (Figure 4.8), excluding those already investigated in the qPCR validation (Figure 4.7). In fetal tenocytes 10 of the 16 genes were found to significantly differ as a result of SCX knockdown (p.adj< 0.05). In adult tenocytes only one gene, *MMP1*, was found to significantly differ following SCX knockdown.

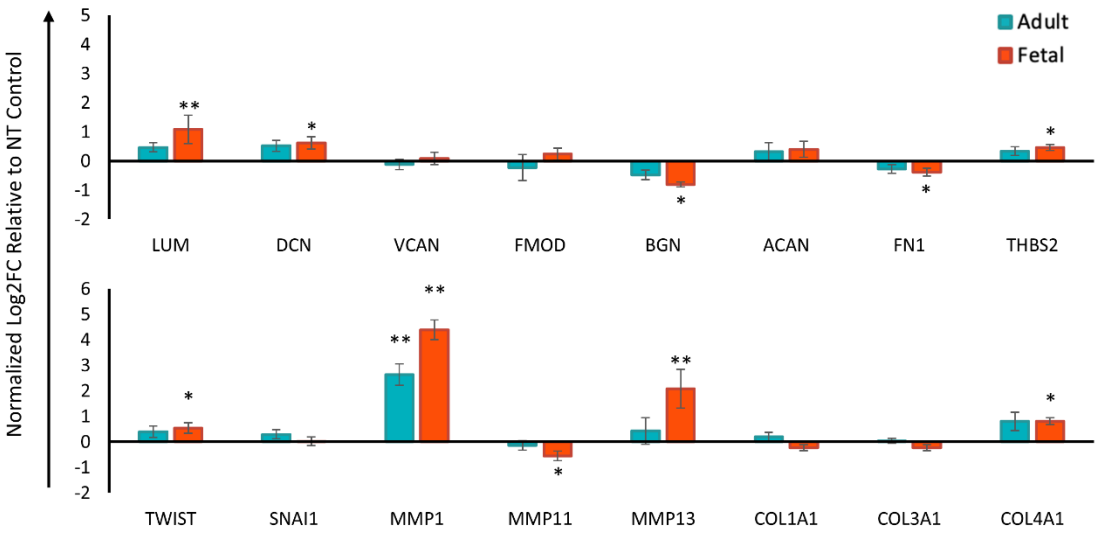

Figure 4.8. RNA-seq data on literature panel of genes thought to be under SCX regulatory control. Bar chart of gene expression of collagens, proteoglycans, matrix metalloproteinases and other transcription factors previously demonstrated to be affected by SCX knockdown in tendon and cardiac fibroblasts in adult (teal) and fetal (orange) shSCX expressing tenocytes. Y-axis shows the normalised Log2FC relative to the NT controlf. Significant differences based on both Log2FC±1 p.adj<0.05 are depicted by a double asterisk (**). Those genes which are significant based on p.adj but not Log2FC are depicted by a single asterisk (*). Error bars represent the SEM of 4 biological replicates.

Validation via immunocytochemistry, although not quantitative, was also performed with ACTA1 and CADM1 antibodies. *ACTA1* gene expression was significantly decreased in fetal shSCX tenocytes compared to the NT control (Log2FC = -2.65, p.adj = 0.0001), but had no difference as a result of SCX knockdown in adult tenocytes. *CADM1* gene expression was significantly decreased in adult and fetal shSCX tenocytes compared to the NT control (Log2FC = -1.89 and –1.85, p.adj = 2.19E-05 and 2.77E-12 respectively). Protein expression of ACTA1 and CADM1 did not corroborate with the sequencing data, and no visible differences were observed between NT and shSCX lines in adult or fetal tenocytes (Figure 4.9). Antibodies for other DE genes including IGF2BP1, TNMD, MMP1, MMP3, Collagen 1, Collagen XIV and RANKL were also due to be tested, however this was not completed due to the COVID19 pandemic (see preface). Similarly, the antibody CADM1 was due to be tested in western blots to confirm its specificity in the horse, however as a result of the COVID19 pandemic this could not be completed (see preface). However, all antibodies were predicted to cross-react with the horse, having over 80% homology to the intended target species.

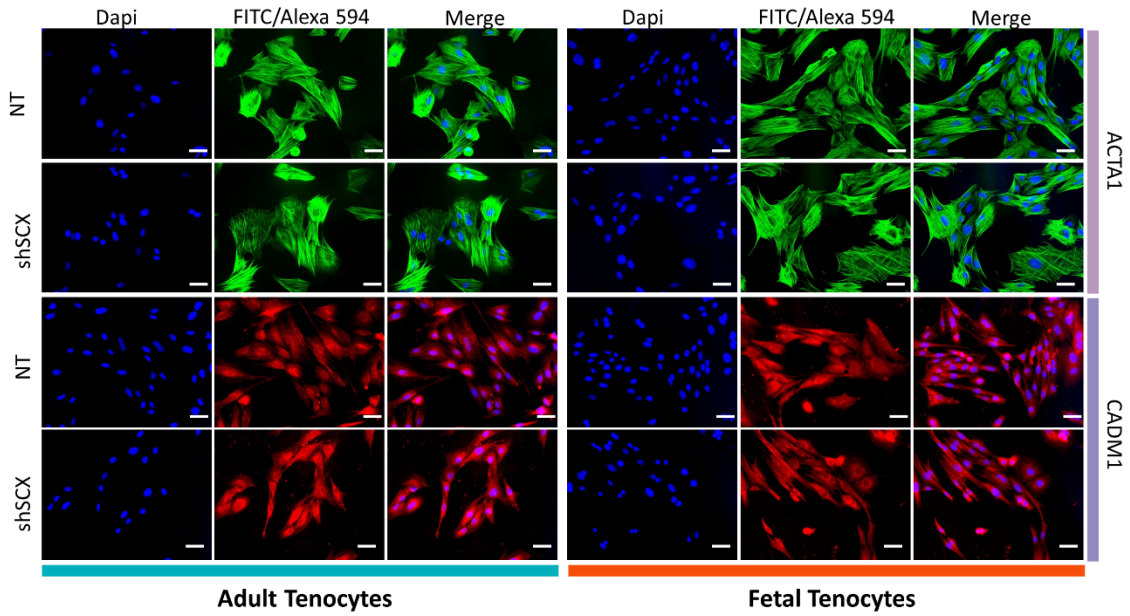

Figure 4.9. Immunocytochemistry validation of SCX knockdown RNA-seq results. Comparison of the corresponding proteins for two significantly DE genes. Images representative of 4 biological lines of 2D cell cultures of adult NT, adult shSCX, fetal NT and fetal shSCX tenocytes. Scale bar = 40 μm. DAPI staining of the nuclei is shown in blue. Anti-ACTA1 is detected using the FITC secondary antibody shown in green. Anti-CADM1 is detected using the Alexa Fluor 594 shown in red.

4.2.5. Gene ontology and pathway analysis of SCX knockdown adult and fetal tenocytes

To determine the biological processes altered as a result of SCX knockdown, gene ontology (GO) analysis was performed. The top ten significantly enriched terms are listed in Table 4.3. In adult tenocytes SCX knockdown resulted in over-representation of genes involved in the regulation of responses to endogenous stimulus, stress, signal transduction and organic substrates. These included several mRNAs from the growth factor protein class as well as g-protein coupled receptors, and membrane traffic proteins. In fetal tenocytes SCX knockdown resulted in over-representation of genes involved in cellular migration and motility as well as tissue development and structure morphogenesis. These included several mRNAs from the growth factor protein class as well as ECM structural proteins, metalloproteases and membrane bound signalling molecules.

Table 4.3. Gene ontology analysis of SCX knockdown RNA-seq data. Summary of the top 10 significantly enriched GO biological process terms for each pairwise comparison of DE genes in adult and fetal tenocytes following SCX knockdown. GO terms have been arranged alphabetically to allow easier comparison between groups. FDR = False Discovery Rate.

PANTHER GO-Slim Overrepresented Biological Process	REFLIST COUNT (14707)	INPUT COUNT	INPUT (Expected)	INPUT (Fold Enrichment)	INPUT (FDR)
Adult Knockdown					
Cellular response to endogenous stimulus (GO:0071495)	638	21	5.32	3.95	6.22E-04
Cellular response to organic substance (GO:0071310)	1503	34	12.53	2.71	8.05E-04
Cellular response to organic substance (GO:0071310)	1178	27	9.82	2.75	6.18E-03
Regulation of response to stimulus (GO:0048583)	2435	42	20.3	2.07	9.41E-03
Regulation of signal transduction (GO:0009966)	1845	35	15.38	2.28	8.59E-03
Regulation of signalling (GO:0023051)	2095	38	17.46	2.18	8.09E-03
Regulation of system process (GO:0044057)	275	12	2.29	5.24	8.79E-03
Response to endogenous stimulus (GO:0009719)	697	23	5.81	3.96	4.29E-04

Response to organic substance (GO:0010033)	1488	32	12.4	2.58	3.02E-03
Response to stress (GO:0006950)	1755	34	14.63	2.32	8.99E-03
Fetal Knockdown					
Anatomical structure morphogenesis (GO:0009653)	1382	67	30.48	2.2	4.86E-06
Cellular response to chemical stimulus (GO:0070887)	1503	67	33.15	2.02	7.52E-05
Positive regulation of response to stimulus (GO:0048584)	1334	62	29.42	2.11	4.80E-05
Positive regulation of signal transduction (GO:0009967)	990	52	21.84	2.38	1.92E-05
Regulation of cell migration (GO:0030334)	558	39	12.31	3.17	2.17E-06
Regulation of cell motility (GO:2000145)	595	39	13.12	2.97	6.39E-06
Regulation of cellular component movement (GO:0051270)	642	41	14.16	2.9	5.64E-06
Regulation of locomotion (GO:0040012)	647	39	14.27	2.73	3.71E-05
Tissue development (GO:0009888)	1072	59	23.64	2.5	9.20E-07
Tube development (GO:0035295)	586	37	12.92	2.86	2.94E-05

In addition to GO analysis, DE genes were also overlaid into the GeneAnalytics Pathway Analysis tool (Table 4.4). Genes DE following SCX knockdown in adult tenocytes resulted in significant enrichment of pathways including metabolism and ECM remodelling. Genes DE following SCX knockdown in fetal tenocytes resulted in significant enrichment of pathways including the TGF-Beta and differentiation pathways.

Table 4.4. GeneAnalytics pathway analysis of SCX knockdown RNA-seq data. Summary of the top 10 Pathways based on entity score for each pairwise comparison of DE genes in adult and fetal tenocytes following SCX knockdown.

GeneAnalytics Pathway Analysis	Entity Score	Number of Genes in Superpath	Number of Genes Matched
Adult Knockdown			
Carbon Metabolism	9.64	143	6
Cell Adhesion_ECM Remodelling	9.2	61	4
GnRH Secretion	8.95	64	4
Metabolism	10.64	2621	37
Nitrogen Metabolism	11.29	17	3
PAK Pathway	9.28	683	14
PPAR Signalling Pathway	11.13	76	5
Statin Pathway	9.03	63	4
Transcription Role of VDR in Regulation of Genes Involved in Osteoporosis	10.81	45	4
Type II Diabetes Mellitus	9.37	59	4
Fetal Knockdown			
Activation of CAMP-Dependant PKA	20.03	630	34
Akt Signalling	21.83	682	37
CREB Pathway	24.1	529	33
Embryonic and Induced Pluripotent Stem Cell Differentiation Pathways and Lineage-specific Markers	17.03	133	13
ERK Signalling	35.5	1179	63
MAPK Signalling Pathway	17.04	321	21
Oxytocin Signalling Pathway	17.49	216	17
PAK Pathway	23.27	683	38
RhoGDI Pathway	18.65	181	16
TGF-Beta Pathway	20.34	653	35

The STRING plugin from Cytoscape was then used to predict interactions between the top DE genes resulting from SCX knockdown, using a less stringent cut off of Log2FC ±0.6 p.adj < 0.05. This approach allowed us to encompass a larger number of DE genes and prevented bias in the network by imposing too high a fold change cut-off (466). This cut-off resulted in a total of 465 DE genes as a result of shSCX expression in the adult tenocytes (305 upregulated and 160 downregulated) and 1149 genes in the fetal tenocytes (803 upregulated and 346 downregulated).

In the adult network 423 genes were recognised by the STRING software which resulted in a network of 332 connected genes and 91 singletons. Within this network the first to third direct neighbouring interactors of SCX can be found in Figure 4.10, with the cytokine CCL26 representing the first direct neighbouring interaction. The top five functional annotations which are common throughout the network are depicted by the coloured bars surrounding each node and include responses to stimulus and cell migration (Figure 4.10).

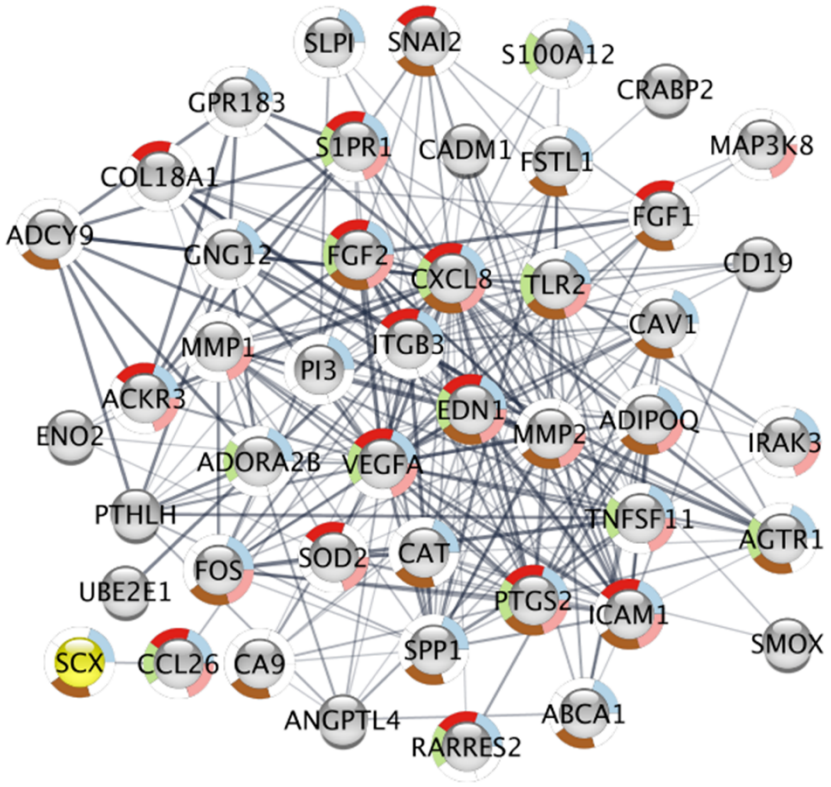

Colour	GO Term	Description	FDR Value
	GO:0009605	Response to external stimulus	2.46E-15
	GO:0030335	Positive regulation of cell migration	2.54E-11
	GO:0032103	Positive regulation of response to external stimulus	3.37E-11
	GO:0009719	Response to endogenous stimulus	6.55E-10
	GO:0034097	Response to cytokines	7.29E-10

Figure 4.10. Adult STRING interaction network. Interaction network showing first to third direct neighbouring interactors for SCX within the DE genes in adult tenocytes following SCX knockdown. The top five functional annotations linking connecting nodes are colour coded and can be visualized around each note in the network. Networks as predicted by STRING and visualized in Cytoscape.

In the fetal network 1060 genes were recognised by the STRING software which resulted in a network of 1001 connected genes and 59 singletons. Within this network the first and second direct neighbouring interactors of SCX can be found in Figure 4.11. In this case only the first and second neighbours were considered in order to reduce the overall size of the network and allow for easier visualisation. This resulted in SOX9, BGN, DCN, GDF6 and CCL26 (the only direct neighbour found in the adult network) representing the first direct neighbouring interactions. The top five functional annotations which are common throughout the fetal network do not overlap with the adult network and include extracellular matrix organisation and skeletal system development (Figure 4.11).

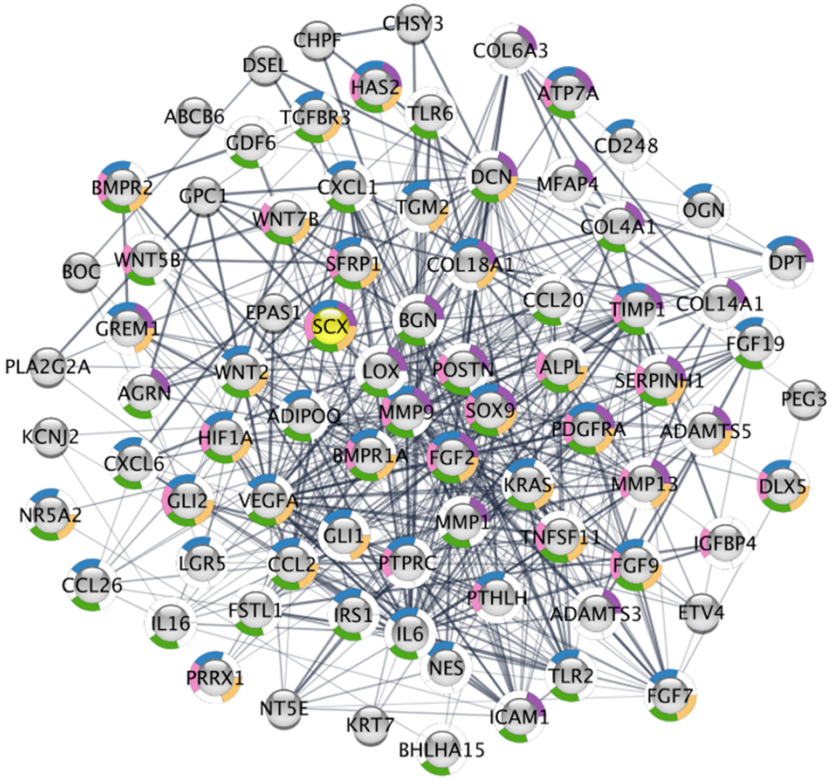

Colour	GO Term	Description	FDR Value
	GO:0030198	Extracellular matrix organisation	2.27E-23
	GO:0042127	Regulation of cell population proliferation	2.48E-21
	GO:0001501	Skeletal system development	8.74E-20
	GO:0010033	Response to organic substance	5.99E-19
	GO:0034097	Animal organ morphogenesis	7.29E-10

Figure 4.11. Fetal STRING interaction network. Interaction network showing first and second direct neighbouring interactors for SCX within the DE genes in fetal tenocytes following SCX knockdown. The top five functional annotations linking connecting nodes are colour coded and can be visualized around each note in the network. Networks as predicted by STRING and visualized in Cytoscape.

4.2.6. Foal tenocytes are differentially affected by scleraxis knockdown compared to both adult and fetal tenocytes

Young postnatal foal tenocytes (aged 54 days – 84 day postpartum) were examined to determine if target genes of SCX are differentially regulated at this developmental stage. Foal tenocytes were capable of remodelling an artificial 3D collagen gel with no significant difference in contraction rate or cell survival observed compared to adult or fetal tenocytes (Figure 4.12.A). Foal tenocytes also express a panel of tendon associated markers with no significant differences compared to adult or fetal cells (Figure 4.12.B).

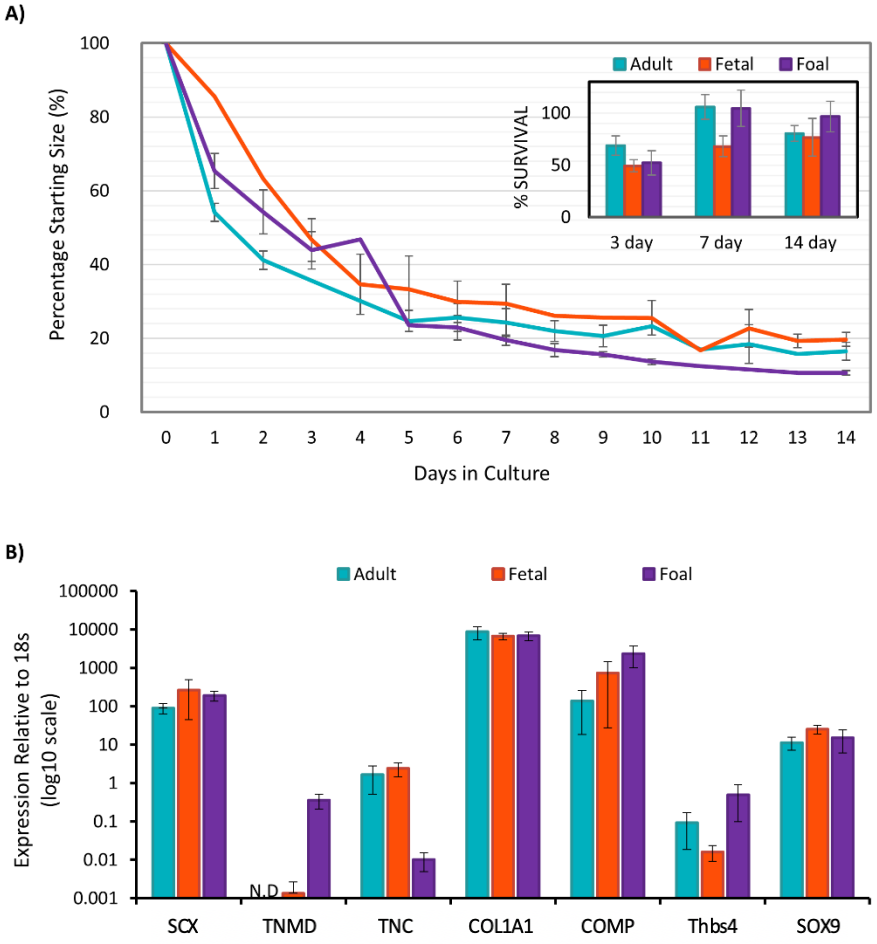

Figure 4.12. Comparison of foal, adult and fetal tenocyte contraction rates and expression of tendon associated markers. A) Adult, fetal and foal tenocytes are capable of contracting a collagen gel to the same degree. Contraction is shown as the percentage of the day 0 value. Similarly, no significant difference in percentage cell survival was detected between the adult, fetal and foal tenocytes. $p > 0.05$ using Welch's ANOVA. Error bars represent the SEM of 3 biological replicates per cell type. **B)** qPCR showed no significant differences in tendon gene expression between adult, fetal and foal tenocytes using Welch's ANOVA. Expression shown relative to the 18s rRNA housekeeping gene. N.D. = expression not detected. Error bars represent the SEM of 3 biological replicates.

SCX expression was knocked down by an average of 79.3% in the foal tenocytes (Figure 4.13.A). SCX knockdown in foal tenocytes did not affect their ability to contract a collagen gel or their cell survival within the collagen gels (Figure 4.13.B).

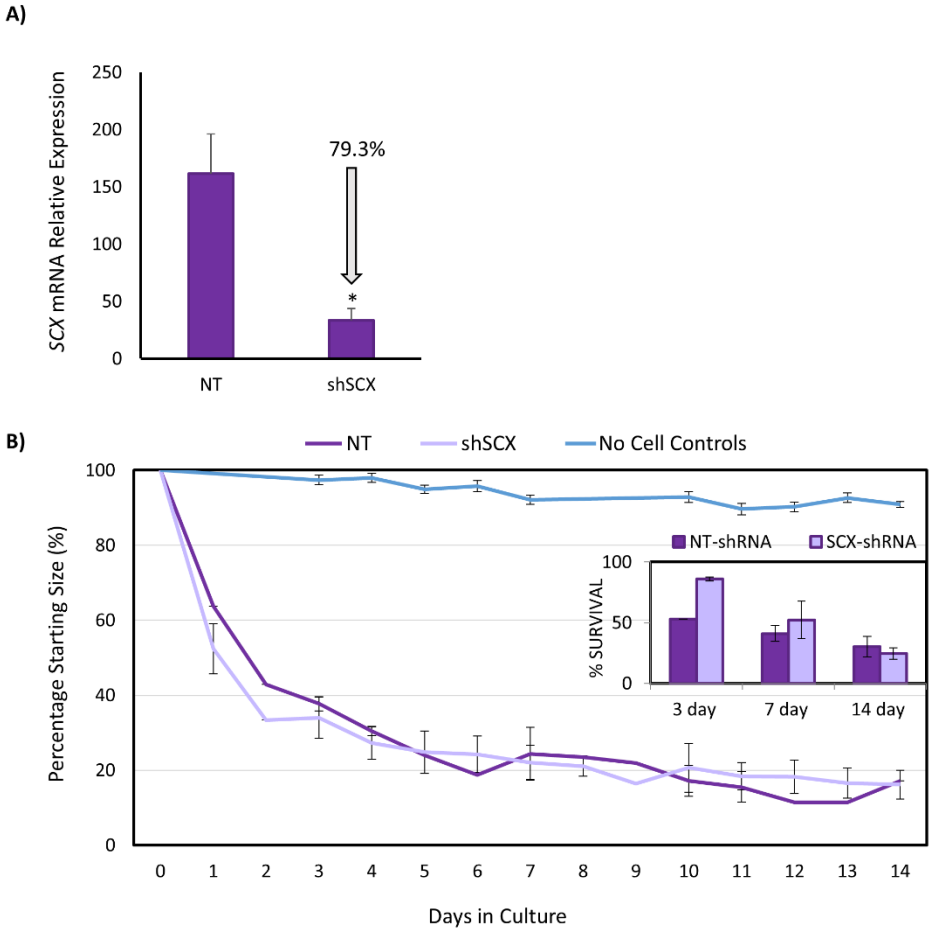

Figure 4.13. SCX knockdown in foal tenocytes does not affect their ability to contract a 3D gel. A) Foal tenocytes exhibit a significant reduction in *SCX* mRNA expression following viral transduction with a specific shRNA against SCX (shSCX) when compared to cells transduced with a control non-target scrambled shRNA (NT). * $p < 0.001$ using a two-tailed Student's *t*-test. Expression shown relative to the 18s rRNA housekeeping gene. Error bars represent the SEM of 3 biological replicates. **B)** Foal tenocytes expressing shSCX can contract a collagen matrix to the same degree as the NT control cells, ~16% of their starting size. Similarly, no significant difference in percentage cell survival was detected. Significance tested between the two conditions (NT vs. shSCX) using a two-tailed Student's *t*-test. Error bars represent the SEM of 3 biological replicates.

Expression of 11 genes were measured by qPCR in shSCX and NT foal tenocytes. Gene selection was based on the results obtained in the adult and fetal knockdown results. Only *COMP* was shown to be significantly DE in the foal tenocytes (Figure 4.14.A). *TNC* and *MMP3* were consistently upregulated to a high degree in all foal replicates (4.76 and 14.66 average fold change relative to NT control), however no significant changes were detected due to the large variation in fold change increase between the biological replicates. Interestingly, of the genes examined *COMP* and *TNC* were not DE in either fetal or adult tenocytes (Figure 4.14.B).

A)

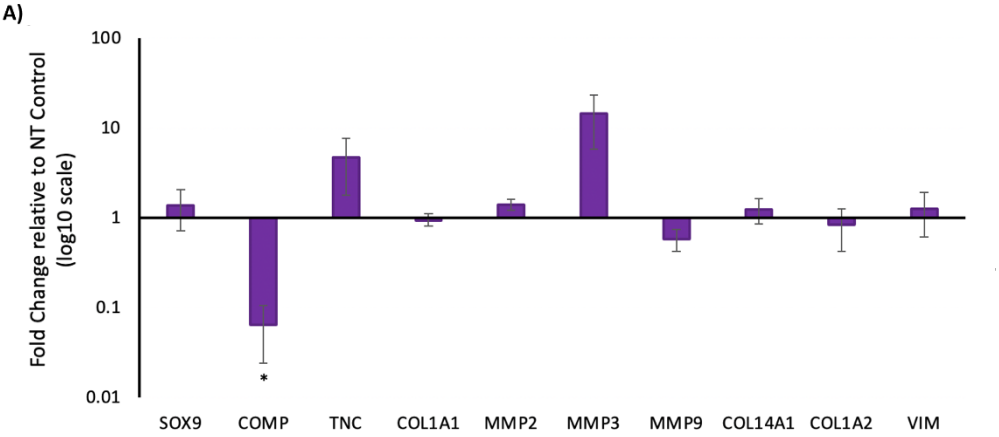

B)

Gene	Adult Knockdown qPCR (p-value)	Fetal Knockdown qPCR (p-value)	Foal Knockdown qPCR (p-value)
SCX	1.86E-08	1.32E-05	0.0005
SOX9	0.4984	0.9022	0.5930
COMP	0.4032	0.8222	2.11E-05
TNC	0.5411	0.4242	0.2725
COL1A1	0.1109	0.0592	0.8093
MMP2	0.0307	0.0498	0.1099
MMP3	0.0471	0.0089	0.1894
MMP9	0.1990	0.0514	0.0588
COL14A1	0.6729	0.2023	0.5681
COL1A2	0.1529	0.5768	0.7355
VIM	0.7900	0.0145	0.6983

Figure 4.14. Effect of knocking down SCX in young postnatal foal tenocytes. A) Gene expression in foal tenocytes following SCX knockdown produces a significant reduction in *COMP*. Error bars represent the SEM of 3 biological replicates. Relative expression is plotted on a log10 scale. * $p < 0.001$ using a two-tailed Student's *t*-test. **B)** Comparison of DE genes in adult, fetal and foal tenocytes using qPCR. Table shows the p-values obtained following Student's *t*-testing of the fold change in gene expression of adult, fetal and foal shSCX expressing tenocytes relative to the NT control. Red shaded boxes indicate no-significant difference and green shaded boxes indicate there is a significant difference $p < 0.05$. Data obtained from 3-6 biological replicates per condition.

4.2.7. Preliminary results on SCX knockdown in ESCs

As described in section 4.2.1, in parallel with the NT and shSCX lentiviral vectors, a GFP-Turbo lentiviral plasmid under the control of the CMV promoter was used to visualize transduction efficiency and the success of puromycin selection in adult and fetal tenocytes. Using this lentiviral vector in ESCs however resulted in no GFP expression. The lack of transcriptional activity of CMV in ESCs has been previously described in mouse ESCs. However why it is inactive is not fully understood, with it being suggested that ESCs might lack all the cofactors necessary for full transcriptional activity (467). As such, using standard cloning techniques, the CMV promoter was removed and replaced with either the EF1a or PGK promoter, both of which have proven superior for stable transgene expression in mouse and human ESCs (467–470). Lentiviral infection of ESCs with GFP-Turbo plasmid under the control of the EF1a promoter resulted in strong GFP expression, whereas no GFP was expressed using the PGK driven plasmid (Figure 4.15.B). The EF1a-GFP-Turbo plasmid was therefore used for subsequent experiments.

The same delivery system as used in the adult, fetal and foal tenocytes, i.e. lentiviral vectors containing shSCX or NT shRNA under the control of the U6 promoter, was then used to generate stable SCX knockdown lines (shSCX) or non-target controls (NT) in one biological line of undifferentiated ESCs, conducted in independent technical triplicates (Figure 4.15.A). Following this, ESC lines underwent 2D tenogenic differentiation and qPCR was subsequently performed. SCX is not expressed in undifferentiated ESCs, but this approach resulted in an average percentage knockdown of *SCX* mRNA of 43.9% following tenogenic differentiation (Figure 4.15.C). Viral copy number integration was measured in each replicate of shSCX and NT expressing tenocyte differentiated ESCs and approximately one copy number event was detected per diploid cell across all technical repeats (Figure 4.15.D).

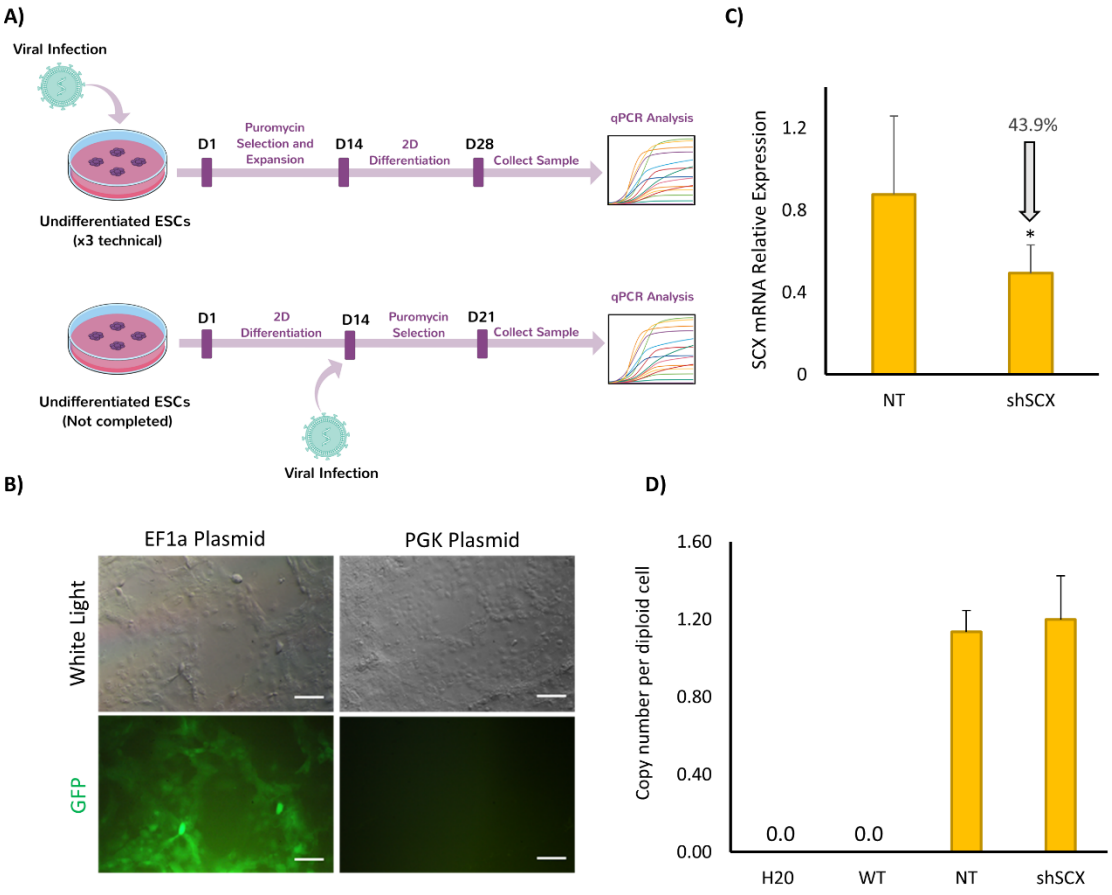

Figure 4.15. Knocking down SCX expression in undifferentiated ESCs. A) Undifferentiated ESCs were transduced with lentivirus before undergoing puromycin section and expansion. Once expanded undifferentiated ESCs were then differentiated into tenocytes in 2D for two weeks before RNA and DNA sample collection and subsequent analysis. This was conducted in one biological line of ESCs in independent technical triplicates. SCX knockdown was also due to be conducted in ESC-derived tenocytes however this could not be completed due to the COVID-19 pandemic (see preface). **B)** GFP control infection of one line of ESCs with GFP-Turbo plasmid driven by the EF1a promoter versus the PGK promoter. Strong GFP expression was found with the EF1a-GFP-Turbo plasmid whereas no GFP was visible with the PGK-GFP-Turbo plasmid. Scale bars = 40μm. **C)** Transduced ESCs following tenogenic differentiation exhibit a significant reduction in SCX mRNA expression following viral transduction with a specific shRNA against SCX (shSCX) when compared to cells transduced with a control non-target scrambled shRNA (NT). * $p < 0.001$ using a two-tailed Student's *t*-test. Expression shown relative to the 18s rRNA housekeeping gene. Error bars represent the SEM of 3 independent technical replicates. **D)** ESC shSCX or NT copies per diploid cell determined by copy number assays in each independent technical replicate. Water (H20) and wild type (WT) non-infected DNA were used as negative controls. Using a two-tailed Student's *t*-test no significant difference in copy number was detected between ESC NT and shSCX lines ($p = 0.81$).

Several genes which were affected by SCX knockdown in adult and fetal tenocytes (*MMP2, MMP3*, *MMP9, LHX9* and *COL1A2*), several tendon associated genes (*MKX, GPRIN3, EYA2, THBS4, TENM4* and *TNC*) and several cartilage associated genes (*COMP, SOX9, CNMD, ACAN* and *COL2A1*) were also investigated using qPCR in the ESC shSCX and NT control lines following tenocyte differentiation (Figure 4.16). *SOX9* and *TENM4* were significantly upregulated following SCX knockdown (p-value = 0.0057 and 0.009 respectively), whereas *GPRIN3* was significantly downregulated (p-value = 9.79E-0.5). *MMP3* and *COMP* also appeared to be upregulated, however they were just above significance (p-values 0.08 and 0.07 respectively). *ACAN* had an over 27-fold increase following SCX knockdown compared to the NT control, and although all replicates showed upregulation the variability between the replicates meant this was not significant. *COL2A1* expression was also induced in shSCX expressing ESC following tenogenic differentiation, whereas it was not expressed in the NT control.

Infection with shSCX was also due to be conducted in ESCs that had been pre-differentiated into tenocytes prior to infection (Figure 4.15.A), however as a result of the COVID19 pandemic further technical and/or biological replicates could not be conducted for either the undifferentiated ESCs or the ESC-tenocytes (see preface).

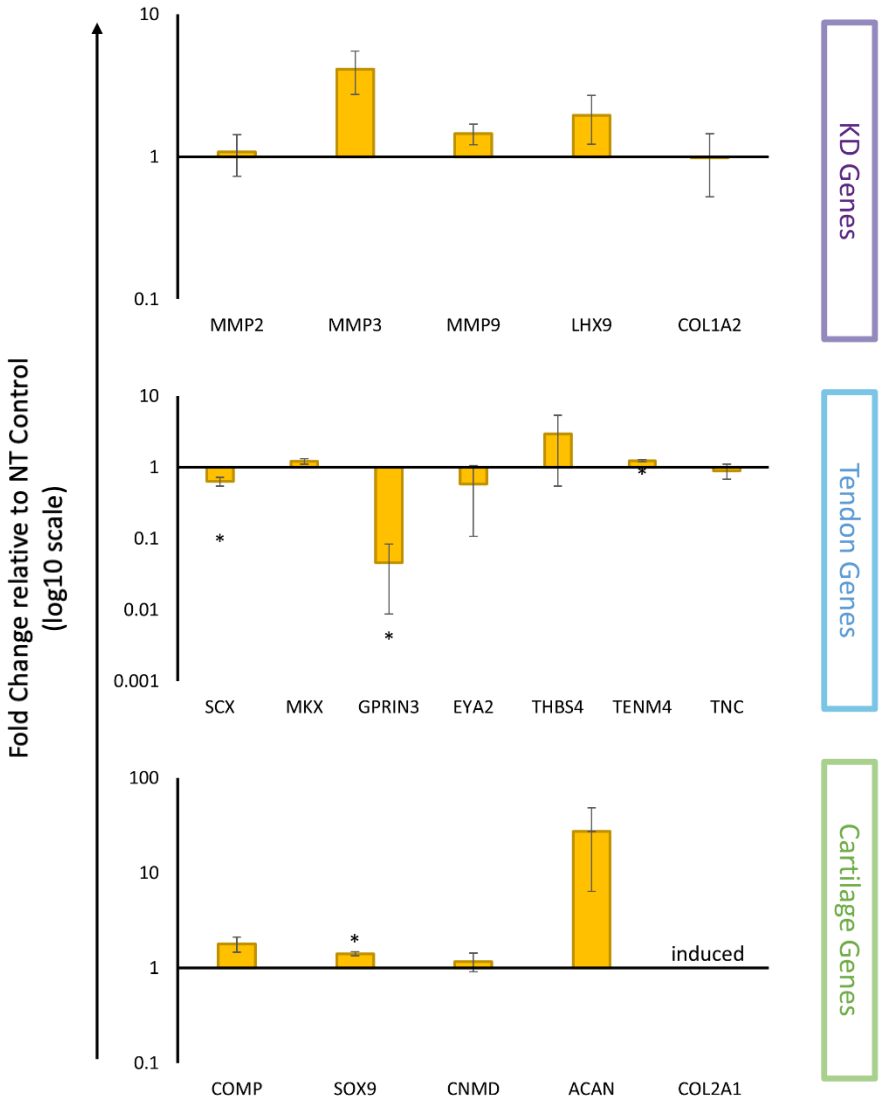

Figure 4.16. SCX knockdown alters ESC-tenocyte gene expression. shSCX ESCs following tenogenic differentiation show significant reduction in *GPRIN3* expression and significant increase in *SOX9* and *TENM4* compared to the NT control. Error bars represent the SEM of 3 independent technical replicates. Relative expression to the NT control is plotted on a log10 scale. * $p < 0.05$ using a two-tailed Student's *t*-test.

4.3 Discussion

The transcription factor SCX is expressed throughout tendon development and plays a key role in directing tendon wound healing. However, little is known regarding its role in fetal or young postnatal tendons, stages in development that are known for their enhanced regenerative capabilities. In this chapter RNA-seq was used to compare the transcriptomes of adult and fetal tenocytes following SCX knockdown. SCX knockdown had a larger effect on gene expression in fetal tenocytes, with gene ontology, network and pathway analysis revealing an overrepresentation of extracellular matrix (ECM) remodelling processes. These included several matrix metalloproteinases, proteoglycans and collagens, some of which were also investigated in SCX knockdown ESCs and tenocytes from young postnatal foals. The results presented indicate a role for SCX in modulating ECM synthesis and breakdown and provides a useful dataset for further study into SCX gene regulation. This results in this chapter have been published (471).

4.3.1. Optimising SCX knockdown via lentiviral infection to improve consistency for RNA-sequencing

To allow identification of downstream target genes of SCX a short-hairpin RNA against the human SCX gene was used, which was introduced using a lentiviral system. This method has previously been used in our lab, producing a significant reduction in endogenous SCX expression with no effect on 2D cellular proliferation or morphology (267). In this study however, care needed to be taken to produce multiple SCX knockdown cell lines from different biological donors for RNA-seq, with the protocol refined to ensure as little technical variability occurred as possible. Poor tissue culture practices have been shown to lead to poor viral titers and low transduction efficiencies (472), therefore producer cells were carefully monitored. Daily medium exchanges were performed to prevent large pH changes which have been linked with cellular stress and destabilisation of the viral envelope (473). Similarly, as factors such as vector inoculum volume, target cell number and vector exposure time to target cells have all been found to influence the transduction results, some varying the final titer by as much as 50-fold difference from the same stock of vector (472), a protocol was generated and rigidly adhered to. A range of lentiviral titers were therefore tested, the percentage of *SCX* knockdown determined as well as the viral copy number integration recorded so as to

ensure that all lines had a similar level of *SCX* knockdown and copy number integrations. Although SCX knockdown was confirmed both using qPCR and immunocytochemistry, it should be noted that quantitative western blotting would be required to give a more accurate reflection of the degree of SCX knockdown at the protein level.

Infection of tenocytes with fresh high titer viral supernatant (> $1x10^8$ IU/ml) resulted in high infection rate with intense GFP signal found in the control cells. These cells underwent apoptosis prior to addition of any antibiotic selection agent. This could suggest that due to high plasmid DNA incorporation, toxic effects may have occurred leading to cell death (474,475). When titers lower than $5x10^6$ IU/ml were used cells did not survive following puromycin selection, suggesting a lack of sufficient virally infected cells to generate stable lines. Optimisation of the viral titer ensured that each line received the same dose of virus and thus minimised the risk of each line having differing copy number integrations which could affect the results. This approach allowed us to study the effects of SCX knockdown on the transcriptome of four biological replicates per group allowing more reliable biological conclusions to be drawn. Limitations in using a single biological replicate for RNA-seq experiments have been extensively documented (476–478) and are highlighted in Nichols et al., 2018. In this study a SCX knockdown of 57% was achieved via siRNA in a single adult equine tenocyte line which resulted in significant downregulation of genes involved in focal adhesions (377). Upon validation of these genes with an additional biological cohort (n = 7), the focal-adhesion genes identified were no longer significant (377). In comparison, in our study a 75% corroboration between the RNA-seq data (n=4) and cohort qPCR (n=6) was found, a result which is similar to that observed in chapter 3 (79% corroboration).

Validation of candidate genes at the protein level was also initiated. Of the two genes tested at the protein level (ACTA1 and CADM1), no corroboration to the sequencing results was determined. Due to the COVID pandemic (see preface) further genes could not be tested, however the data from chapter 3 on protein validation demonstrated that 7 out of the 12 proteins investigated corroborated with the RNA-seq results so it is likely that more genes would need to be tested to get an accurate picture of the true corroboration. TNMD and COL1A1, which were due to be tested, have been robustly demonstrated to be directly under SCX regulatory control in tenocytes, directly transactivating their expression (422,442,446,451). Interestingly in this study, neither

appeared to be augmented at the mRNA level, with TNMD being absent. TNMD is regularly reported as a marker of tendon cells in humans and rats, however its expression in equine tenocytes is less well documented. Regardless of this lack of *TNMD* mRNA, protein expression is still detectable in equine tenocytes suggesting the rate of TNMD protein degradation is different to its mRNA (140). Similarly, collagen I expression has been shown to vary at the mRNA and protein level in SCX overexpression studies (176). It would therefore be of particular interest to examine these two genes at the protein level using qualitative immunocytochemistry and quantitative immunoblotting.

4.3.2. Effect of SCX knockdown in adult and fetal tenocytes

SCX is postulated as being a key mediator in ECM and collagen production in response to matrix building cues in a number of tissue types (242,444). Through gain- or loss-of-function studies several collagens, proteoglycans and matrix metalloproteinases have been shown to be regulated, either directly or indirectly by SCX (242,377,442,444,446–448,450,464,465). In particular, in cardiac fibroblasts SCX has been demonstrated to directly transactivate MMP2, COL1A2 and FN1 expression, following its recruitment to the gene promoter regions via the pro-fibrotic cytokine TGFβ (242,446–448). SCX has therefore been suggested to be a key regulator in maintaining the balance of ECM synthesis and breakdown during injury repair, highlighting its potential as a theraputic target for controlling these processes (447). Our results similarly indicate a significant involvement of SCX in regulating *MMP*s *1, 2, 3, 12* and *13*, *collagens 4A1* and *18A1* as well as ECM proteoglycans *VIM* and *LUM*, with pathway analysis also highlighting ECM remodelling and TGFβ pathway signalling as being significantly overrepresented. It would therefore be of interest to investigate whether SCX is directly regulating these ECM components in equine tenocytes, and as such altering the equilibrium between MMPs and their inhibitors' (tissue inhibitors of metalloproteinases (TIMPs)) activities. This could be assayed firstly using mutagenesis of E-boxes, chromatin immunoprecipitation (ChIP) and electrophoretic mobility shift assay (EMSA) techniques followed by zymography to determine changes in MMP and TIMP activity. Such changes may highlight a role of SCX in the regulation of tendon ECM synthesis and breakdown.

The exact role of scleraxis through fetal to adult development has not been defined. In this study SCX knockdown had a much larger effect on fetal tenocyte gene expression

than adult tenocytes, resulting in 477 DE genes in fetal tenocytes and only 183 DE genes in adult tenocytes. Only 25-35% of the DE genes in both groups were downregulated, with the majority being upregulated as a result of the knockdown. As SCX has only been reported as being a transcriptional activator (453,479), this would suggest that the high proportion of upregulated genes reported are not direct targets of SCX and are instead being affected by some downstream intermediate. However, this traditional view of classifying transcription factors as "activators" or "repressors" is being questioned, and in many cases "activators" often have an indirect repression effect by blocking the binding of other transcriptional activators (480,481). Similarly, this high percentage of upregulated genes may be due to SCX activation of transcriptional repressors, such that when SCX is knocked down this reduced activation of transcriptional repressors may result in de-repression of other genes leading to their upregulation. As SCX has been reported to work with other co-factors (453,479,482), the observed differences in downstream genes in fetal and adult stages, may indicate that there is a difference in the availability of such co-factors at the different stages of development. SCX gene regulation will be explored further in chapter 5.

The fetal tenocytes used in this study were from around 85-90% of the way through gestation, which our group have previously proposed represent a period in which the tendons are still actively developing (267). The large effect on gene expression that was observed following SCX knockdown in fetal tenocytes may indicate that SCX still has a critical role in tendons at this developmental stage. This is supported by previous work from our group which demonstrated that SCX knockdown in fetal tenocytes prevented them from contracting a 3D collagen gel, whereas adult SCX knockdown tenocytes contracted the collagen gels as normal (267). Our data demonstrates that SCX is regulating fewer genes in adult tenocytes. Although SCX is also implicated in adult tendon injury and repair, its expression is thought to be mainly altered through pro-fibrotic TGFβ signalling and via mechanical loading in response to injury (175,388,427), it would therefore be of interest to look at the transcriptome of SCX knockdown adult tenocytes following such stimulus. Similarly, performing SCX overexpression studies on both non-transduced and shSCX expressing adult and fetal tenocytes would be of great benefit to validate the DE genes found as a result of SCX knockdown.

In order to identify potential interactions between the DE genes resulting from SCX knockdown, network analysis was performed in STRING. This form of analysis uses text-mining as well as computational predictions in order to determine protein-protein interactions (483). In the adult network response to stimuli and cellular migration were overrepresented, with only one direct interacting partner of SCX being detected, namely CCL26. CCL26 is a cytokine that displays chemotactic activity to eosinophils and basophils. Why a direct connection between CCL26 and SCX is predicted is unclear. Other genes within this network include MMP 1 and 2, as well as the transcription factor Snai1, a key regulator in the epithelial-to-mesenchymal transition (450). MMP2 and Snai1 have been shown to be directly regulated via SCX in cardiac fibroblasts (447,450). Why no direct connection is made is surprising and highlights the limitations in this form of analysis when investigating less well studied proteins where reference sources are limited. In the fetal tenocyte network a clear overrepresentation of ECM and skeletal system development processes were found with direct connections to SOX9, BGN, DCN, GDF6 and CCL26 being detected. Knockout of BGN and DCN in mouse embryos results in tendon defects and SOX9 and GDF6 are heavily implicated in cartilage development (426,484) suggesting that SCX regulation, or perhaps coordinated expression of these genes, is critical to ensure normal tendon development.

4.3.3. Effect of SCX knockdown in young postnatal tendon

Using a candidate gene approach, it was further demonstrated that SCX-dependent processes differ in young postnatal tenocytes compared to both adult and fetal tenocytes. These tenocytes were isolated from foals of around 3 months of age which represents a period of rapid tendon growth and development (485). Cartilage oligomeric matrix protein (*COMP*), a non-collagenous ECM protein which is primarily present in cartilage but also found in tendons and ligaments, was the only tested gene which significantly differed following SCX knockdown in foal tenocytes. In adult and fetal tenocytes no change in *COMP* expression was observed in shSCX expressing tenocytes. Although *COMP* is not currently a known target of SCX, it does have two E-box binding sites for SCX in its promoter, therefore further investigation into *COMP* regulation by SCX in foal tenocytes is warranted.

SCX has been implicated as an important factor for adaptive changes in postnatal tendons, with it being induced upon mechanical loading (486). This increased SCX expression as a result of mechanical load, leads to an increased proliferation of SCX expressing cells, as well as upregulation of collagen type I and *TNMD* gene expression (486). Whereas in contrast, immobilization results in a decrease in SCX expression and collagen turnover (487). This change in SCX regulation through fetal-to-foal-to-adult development may therefore correlate with this transition from lack of mechanical loading through to weight-bearing and then to increased physical demand and body weight at adulthood. Follow-up studies looking at the transcriptome and direct target genes of SCX in foal tenocytes would be required to make more detailed comparisons, with the integration of mechanotransduction likely to provide further insight into how SCX is regulated during different stages of tendon maturation.

4.3.4. Effect of SCX knockdown in ESCs

The effect of SCX knockdown on ESCs and ESC-tenocytes was also starting to be investigated, however as a result of the COVID-19 pandemic (see preface), it could not be completed. The preliminary data obtained did however indicate a role of SCX in altering the expression of several cartilage genes. These included SOX9, an SRY-Box transcription factor which is essential during multiple steps of chondrogenic differentiation (488), as well as ACAN, a member of the aggrecan/versican proteoglycan family and COL2A1 which are integral parts of the ECM of cartilaginous tissue.

Following tenogenic differentiation of shSCX expressing ESCs, *SOX9* expression was found to significantly increased in the resulting population. During embryonic development SCX and SOX9 have been shown to work in a coordinated manner, with this concerted interaction being required for divergence of precursor cells into either tendon or cartilage progenitors (484). Furthermore, SCX and E47 have been shown to cooperatively bind with SOX9 and p300 to regulate the SOX9-dependent transcription of COL2A1 (453). However, this SOX9-dependent transcription of COL2A1 can also be initiated through SOX9 and p300 alone (453). *COL2A1* expression was induced in tenogenic differentiated shSCX expressing ESCs, which may be the result of increased *SOX9* rather than as a direct result of decreased *SCX* expression. Taken together this suggests that, once SCX expression is repressed in ESCs the SOX9 transcriptional

cascade is activated, thus hampering the switch to a tenogenic phenotype in promotion of a more cartilage-like phenotype. It would therefore be of interest to further investigate the differentiation potential of shSCX expressing ESCs, particularly down the chondrogenic lineage to see if SCX knockdown improves their chondrogenic potential.

In accordance with this hypothesis of impaired tenogenic potential, *GPRIN3* a member of the GPRIN protein family recently identified as an equine specific marker for tendon (240) was significantly decreased in tenogenic differentiated shSCX expressing ESCs. *TENM4,* another gene suggested to be equine tendon specific was also significantly affected, being upregulated in tenogenic differentiated shSCX expressing ESCs which does not fit this hypothesis. TENM4 has however also been implicated as a novel regulator in chondrogenic differentiation, increasing in expression in early differentiation of human BMSCs to chondrocytes (489). This peak in *TENM4* and subsequent decline is coupled with an upregulation of ACAN, COL2A1 and COL10A1, which are common chondrogenic differentiation markers (489). The observed increased *TENM4* may therefore be indicative of early chondrogenic differentiation. Finally, *ACAN* although not significant, had a very high fold increase (27-fold change) in tenogenic differentiated shSCX expressing ESCs. ACAN is a major glycoprotein component in cartilage which has already been shown to be directly regulated by SCX in osteosarcoma cells (449) as well by SOX9 in TC6 chondrocytes (490). Upregulation of ACAN therefore fits with this hypothesis of decreased tenogenic potential in favour of a more cartilage like phenotype.

Caution however must be taken with the results presented on the ESCs as, as mentioned previously, this is only based on three technical repeats using one biological line. Given the interesting results obtained it would be worth repeating this on further lines to see if the hypothesis holds true. Further characterisation of the DE genes at the protein level, as well as looking if they are under direct SCX regulatory control would also be required. In doing so this may shed more light on the complex role SCX plays in embryonic specification of tendon and cartilage lineages.

4.3.5. Summary

In summary, this chapter , as previously reported in cardiac fibroblasts, identifies SCX as a key regulator of ECM gene expression in tendon cells. It is also the first study to confirm that SCX regulation differs during adult and fetal development. Creation of this dataset

provides a crucial resource for directing further studies into SCX regulation which, given the significant role SCX plays in tissue repair, may prove useful for the development of therapeutics for tendon injury and disease. Chapter 5 will start to explore whether some of these identified genes are under the direct transcriptional control of SCX.

Chapter 5 – Identification of Scleraxis Target Genes

5.1 Introduction

Transcription factors fundamentally work through their ability to scan the genome, binding to specific transcription factor binding sites in order to form complexes which guide and control gene expression. In chapter 4, using scleraxis (SCX) knockdown coupled with RNA-seq techniques many potential genes downstream of SCX signalling were identified. However, using these techniques alone doesn't allow for direct causal regulatory mechanisms to be determined. Here I will explore the mechanisms by which transcription factors act to regulate gene expression, and more specifically what is known in regard to SCX gene regulation.

5.1.1. Gene regulation by transcription factors

There are numerous types of regulatory factors which function to control gene expression however, the main regulators are transcription factors. Not only can transcription factors function as "master regulators" to control developmental patterning and cell specification, but they can also act dynamically, with the same transcription factor being able to control distinct regulatory networks across different cell types within the same organism (481,491,492). By binding to short sequence-specific DNA base pair patterns, termed motifs or *cis*-regulator elements, individual transcription factors can control tens, if not hundreds of target genes (480,493). However, more often than not they do not act alone, binding cooperatively with other transcriptional cofactors in order to exert their desired effect.

Transcription factors are typically classified into families based on the specific structural domains which allows them to bind to DNA. These families include, but are not restricted

to, basic helix loop helix (bHLH), basic leucine zipper (bZIP), homeodomain (HD), C2H2-zinc finger (ZF) and nuclear hormone receptor (NHR) DNA binding domains, many of which were first described in the 1980s (494). The mechanisms by which transcription factors can impact transcription are vast, some of which are outlined in Figure 5.1.

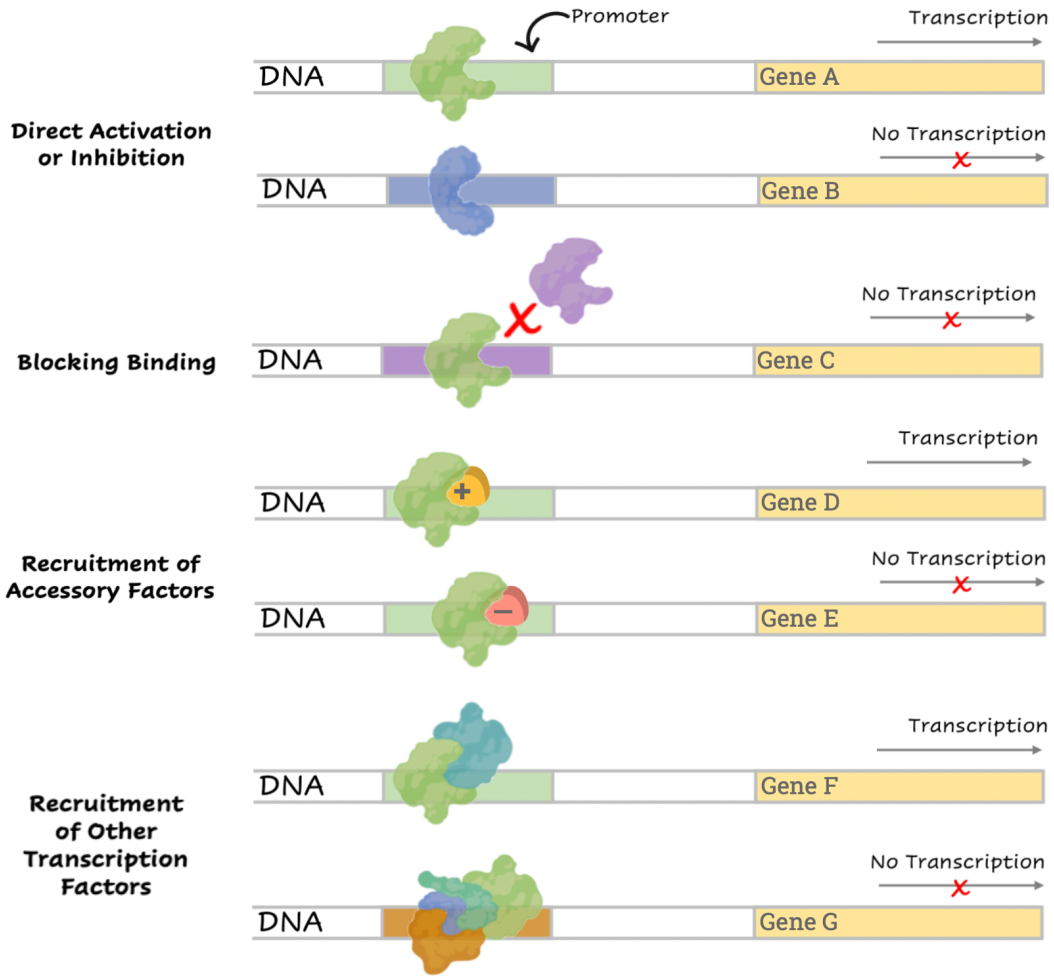

Figure 5.1. Mechanisms of transcription factor actions. Transcription factors can act through a number of mechanisms. They can bind as a monomer, homo- or heterodimer, directly recruiting RNA-polymerase to activate transcription (Gene A). Alternatively, transcription factors can bind as a monomer, homo- or heterodimer and act as repressors, blocking recruitment of RNA-polymerase (Gene B). Transcription factors can also act by simply blocking other proteins from binding to the same sites preventing their ability to activate transcription (Gene C). Most transcription factors however act by recruiting accessory factors. These can be coactivators (Gene D) or corepressors (Gene E), which are frequently large protein complexes which contain domains involved in nucleosome remodelling, chromatin binding or covalent modifications of histones such as p300. Similarly, many transcription factors work cooperatively, with other transcription factors needing to be present in order to allow transcription (Gene F). Equally, transcription factors can recruit multiple cofactors, including transcriptional activators and repressors which can act together to prevent gene transcription (Gene G). Figure inspired from the text in Lambert *et al.*, 2018 (481).

5.1.2. Identification of SCX as a basic helix-loop-helix (bHLH) protein

As described in chapter 4, SCX belongs to the bHLH family of transcriptional regulatory proteins (Figure 5.2), a superfamily which plays important roles in various cellular differentiation and developmental processes (495). Over 240 bHLH transcription factors have been identified thus far and, as such, features including their different protein structure and molecular phylogenetic relationships are used to categorise them into different subfamilies from Class A to F (495,496). All bHLH proteins bind to a specific hexanucleotide DNA motif (CA*NN*TG, where *N* represents any nucleotide), known as E-boxes which are typically located in promoter and enhancer regions of genes (495,497,498).

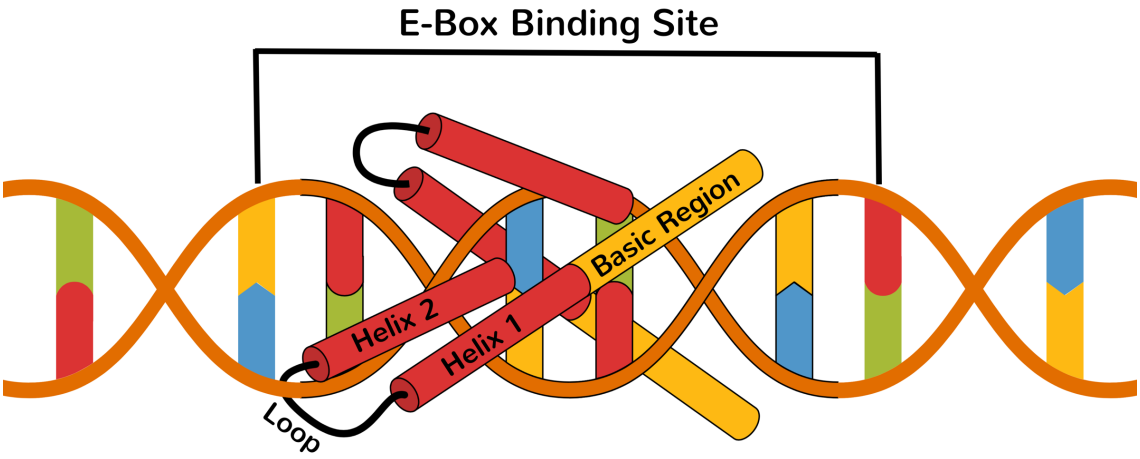

Figure 5.2. Structure of bHLH transcription factors. These proteins contain two highly conserved domains; the basic domain (yellow) located at the amino-terminal end which contains the interface region for DNA interactions and the HLH domain (red) located at the carboxy-terminal end which enables interactions with other protein subunits to occur (498). The HLH domain is composed of two amphipathic alpha-helices separated by a loop, which facilitate folding and packing against other protein subunits to form homo- and heterodimeric complexes (428,479,498). Image represents the SCX protein binding to E-box domain as a homodimer.

SCX was first identified in a yeast two-hybrid screen, developed to uncover potential interacting partners of the *E2A* (also known as *TCF3*) gene product E12 (479). This newly identified 22 kDa protein, SCX, had high homology to other bHLH proteins, having a proline rich region near the carboxyl-terminus like that of several other bHLH activators and was demonstrated to bind specifically to E-boxes as a heterodimer with E12 (479). Similarly, E47, an alternative splice variant of the *E2A* gene, has also been shown to bind

as a heterodimer with SCX, synergistically enhancing transcription of an E-box containing promoter (482). SCX was also revealed to be capable of transactivating aggrecan gene expression without heterodimerization with either E12 or E47 (449). Likewise, when the HLH domain is removed from SCX, which is the region which facilitates protein-protein interactions, it is found to still be capable of transactivating the *COL1A2* promoter, although with approximately 50% reduced activity, demonstrating that heterodimerization is not specifically required for SCX function (428,451). In comparison, when the basic domain, the region required for binding to E-box DNA regions, was removed SCX was no longer capable of transactivating the *COL1A2* promoter highlighting its need to interact with the promoter via direct DNA binding in order to regulate gene expression (428,451). Other SCX binding partners have been identified, for example activating transcription factor 4 (ATF4, part of the cAMP-response element binding protein family) has been demonstrated to repress SCX function in Sertoli cells of the testes (499). However, further work to identify additional binding partners and their effect on SCX function is necessary.

5.1.3. SCX direct gene regulation

Although several studies have identified potential candidate genes which are under SCX regulatory control (Table 4.1), few have demonstrated whether this is via direct or indirect means. In tendon cells, only two genes *COL1A1* and *TNMD* have been demonstrated to be under direct SCX-mediated control (422,442). Using a combination of electrophoretic mobility shift assays (ESMA) and promoter assays, SCX was found to bind as a SCX/E47 heterodimer with the short *cis*-acing element TSE2 (tendon-specific element 2) to promote *COL1A1* transcription via binding to the E-box site CACGTG (442). Similar techniques were used to demonstrate SCX's ability to bind preferentially to two of the five E-boxes (E2:CATCTG and E5:CAGATG) found around the mouse *TNMD* gene promoter, with luciferase promoter assays confirming activation via these two E-boxes (422). In other tissue, SCX has been demonstrated to directly regulate aggrecan (ACAN), a major proteoglycan found in cartilage, in osteoblastic ROS17/2.8, as well as transferrin and androgen binding protein (ABP) in Sertoli cells (449,461). Much work on SCX-mediated regulation has been conducted in cardiac fibroblasts, Table 4.1 in the previous chapter highlights several of the genes which have been demonstrated as under direct SCX control in this cell type, as marked by the asterisk.

5.1.4. Determining and validating transcription factor binding

As discussed in chapter 4, knockdown and overexpression studies are useful tools to allow determination of potential candidate genes which may be downstream of a transcription factor of interest, however a direct causal relationship cannot be determined from this alone. In order to confirm transcription factor binding a number of techniques are available which are broadly categorized as either *in vitro* or *in vivo* based, with the most commonly used being outlined in Table 5.1. *In vitro* approaches generally provide information on intrinsic TF binding sequence preferences and the biophysical parameters controlling these binding events, whereas *in vivo* methods are performed in living cells and can recover information on transcription factor binding events sequence specificity as well as the biological context of those interactions (e.g. cell type, time point, treatment), a concept which is further demonstrated in Figure 5.3 (500,501).

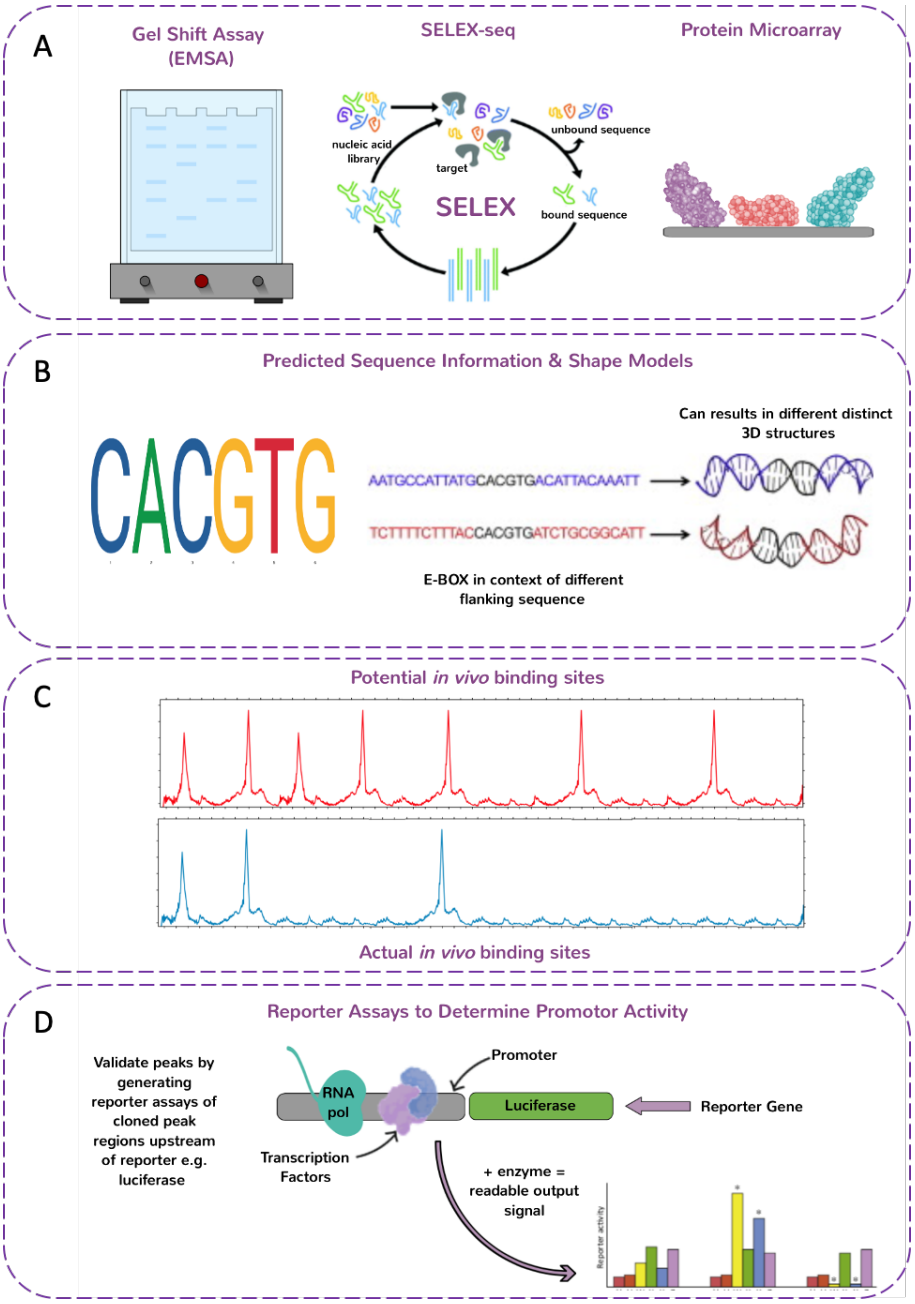

Figure 5.3. Different approaches for determining transcription factor binding. A) Example of *in vitro* methods, which can be low or high throughput, which provide information on the sequence specificities of particular transcription factors. **B)** *In silico* methods use known DNA-protein binding sites to generate computational 'DNA motif models' to predict the specificity of binding to another potential site based on the predicted sequence information and shape models. **C)** *In vivo* methods, which can be low or high throughput, provide information on transcription factor binding within a tissue or cell type at that particular time. However, it must be noted that *in vivo* binding does not necessarily lead to gene regulation, with it being likely that only a small fraction of these binding events impact on gene expression. ChIP-seq peaks displayed represent areas of enrichment, where protein interacts with DNA. **D)** As not all binding events result in gene regulations, functional binding assays are conducted to experimentally validate targets effects on promoter activity, usually by mutating the binding site or conducting overexpression or knockdown studies and determining the effect on the reporter activity. Using Figure adapted from Slattery *et al*., 2014 (502).

Table 5.1. Overview of methods for analysis of transcription factor-DNA binding. TF = Transcription Factor. Table created and inspired by the following review articles:- (481,500,503,504)

	Method	Function	Description	Advantages	Disadvantages
in vitro	DNA-protein-interaction enzyme-linked immunosorbent assay (DPI-ELISA)	Confirming Predicted TF-DNA Binding	Way to determine how specific a known DNA-protein interaction is. Method uses epitope tagged TF which is incubated with binding and non-binding DNA probes in separate wells of an ELISA microplate. Proteins bound to the immobilised DNA are then measured photometrically.	Main method available to allow DNA-motif analysis in a motif-by-motif way to determine DNA-protein interactions, low technical complexity, low cost.	Doesn't work for low protein amounts, prior knowledge on DNA-protein interaction required, low throughput.
in vitro	DNA Footprinting	Confirming Predicted TF-DNA Binding	DNA protection assay where DNA is incubated with TF and subsequently degraded. Pools of DNA fragments are generated. Areas bound by TF with be protected from degradation and can be compared to control pools using gel electrophoresis.	Easy to perform, reliable, inexpensive.	Pre-requisite of known DNA sequence, low throughput.
in vitro	Electrophoretic mobility shift assay (EMSA)	Confirming Predicted TF-DNA Binding	TF and labelled target sequence incubated to test if the specific DNA sequence is bound by the TF by observing a shift in the electrophoretic migration compared to unbound DNA or protein.	Inexpensive, can be used to measure cooperative binding and analysis of mutated versions of a TF.	Pre-requisite of known DNA sequence, not particularly quantitative, low throughput.
in vitro	Mechanical induced trapping of molecular interactions (MITOMI)	Confirming Predicted TF-DNA Binding	A microfluidic device is used to isolate TF-DNA complexes from free DNA instantaneously allowing capture of tens to hundreds of TF-DNA interactions in parallel.	Transient and low affinity interactions better detected.	Limited number of sequences assayed, not as good with TFs which have long target sites.
in vitro	Surface plasmon resonance (SPR)	Confirming Predicted TF-DNA Binding	Optical method to monitor efficiency of binding of TFs to DNA in real time.	Useful for determining TF binding association and dissociation kinetics.	Limited throughput, prior knowledge of TF-DNA binding required.

in vitro	Bacterial one-hybrid (B1H) or yeast one-hybrid (Y1H)	Discovering Novel TF-DNA Binding	TF expressed as a fusion to a subunit of RNA-polymerase and a randomised library of oligonucleotides representing potential TF binding sequence containing selectable markers are cloned into bacterial or yeast cells. Positive and negative selection are then used to enrich for sites that bind the TF tested.	No requirement for specific antibodies, low tech alternative to microarray-based techniques, capable of de novo motif discovery.	Limited capacity to determine binding specificities of TFs with lengthy binding sites, some eukaryotic factors don't function in bacterial or yeast system, not good for low affinity TF binding.
in vitro	DNA affinity purification and sequencing (DAP-seq)	Discovery of Target Regions	TF-binding assay where a DAP-seq guide DNA library, containing adapter DNA sequence, is added to an affinity capture bead-bound TF. Following incubation, the TF bound DNA is then eluted and amplified with PCR primers to introduce an indexed adapter and the DNA is sequenced.	De novo motif discovery, high throughput.	Limited by skewed distribution of genomic sequences, peaks are not necessarily indicative of *in vivo* binding.
in vitro	Systematic evolution of ligands by exponential enrichment (SELEX) based methods	Inferring Novel DNA-binding Motifs	A TF is added to a pool of DNA containing many randomised sequences and allowed to bind. Through a series of selection steps TF-bound-DNA is captured, using methods such as affinity tags, molecular trapping or EMSA, with the subsequently bound DNA fragments amplified by PCR and sequenced.	High throughput, small sample size required, easily automated using liquid handling equipment allowing analysis of hundreds of TFs in parallel.	Expensive, could contain sequence bias.
in vitro	DNA immunoprecipitation (DIP-chip)	Inferring Novel DNA-binding Motifs	Similar to SELEX but uses fragmented genomic DNA rather than synthetic random sequences.	Useful for TFs which have long binding specificities.	Not useful for TFs which bind to short sites.
in vitro	Protein binding microarray (PBM)	Inferring Novel DNA-binding Motifs	Epitope-tagged/labelled TF is bound to double-stranded DNA microarray. Fluorescent-based detection then determines enriched binding motifs.	Efficient and relatively economical, can be used to measure cooperative binding and/or multimers.	Accessibility issues of DNA-binding domains to probe DNA, arrays contain limited numbers of sequence, requires freshly produced and purified proteins.

in vivo	Proteomics of isolated chromatin segments (PICh)	Discovering Novel TF-DNA Binding	Also known as reverse ChIP. Following crosslinking, a desthiobiotin conjugated DNA probe is used to hybridize to a specific genomic region, the associated proteins are isolated and analysed by mass spectrometry.	No prior knowledge about the proteins that bind to the locus of interest required	Unable to distinguish direct from indirect binding, low throughput.
in vivo	Chromatin immunoprecipitation (ChIP) based methods	Discovery of Target Regions	TF-DNA complexes are fixed *in situ* using formaldehyde crosslinking. Crosslinked DNA is sheared into pieces and precipitated with a TF-specific antibody. Bound DNA is the detected using qPCR (ChIP-qPCR), microarray (ChIP-chip), or sequencing (ChIP-seq).	ChIP-qPCR offers a simple, inexpensive method to determine if TF binds certain regions of DNA. ChIP-chip and ChIP-seq offer genome wide profiling of TF binding. Can be used to determine cooperative binding (Co-IP).	For ChIP-qPCR specific probe regions need to be designed to determine binding, hence is low throughput. ChIP-chip and ChIP-seq limited by skewed distribution of genomic sequences.
in vivo	DNA adenine methyltransferase identification (DamID-seq)	Discovery of Target Regions	TF is fused to bacterial DNA adenine methyltransferase and transfected as a hybrid-fusion protein in mammalian cells. The enzyme methylates a consensus sequence near the TF binding sites, which can then be mapped by NGS.	Fewer artifacts than ChIP-based techniques and no need for toxic formaldehyde.	Cannot be used for 'snap-shot' analysis or monitoring dynamic changes in TF binding, need to express DAM hybrid-fusion proteins endogenously as a transgene.
in vivo	Promoter Assays	Identifying TF-DNA binding of regulatory importance	Assay where a TF drives the expression of a given promoter sequence that is fused to a downstream reporter gene. Reporters include galactosidase (GAL), fluorescent reporters (GFP, RFP) or luciferase (LUC) with the activity being detected by means such as photometrically, using flow cytometry or luminescence depending on the reporter system.	Easy to perform, reliable, inexpensive.	Limited to TFs that activate gene expression, variable copy number integrations of the reporter DNA can affect results.

In this chapter chromatin immunoprecipitation (ChIP) techniques are utilised. This is a powerful yet relatively easy and cost-efficient method for identifying transcription factor target gene binding across different cell types or cellular developmental stages at one moment in time. An *in vivo* approach was desired over an *in vitro* one as this would allow for direct comparison of SCX binding in all three of the different cell type of interest; adult, fetal and ESC-derived tenocytes, across the entire genome and, using the RNA-seq results generated in chapter 4, would provide evidence as to whether SCX was directly regulating candidate genes or not. This method was preferred over other *in vivo* techniques such as DamID, in which cells are transfected with plasmid containing the transcription factor of interest fused to the *Escherichia coli* DNA adenine methyltransferase (DAM), as it does not require cell line manipulation with an artificial construct which can be cumbersome and lead to a degree of cellular stress (505). Unfortunately, due to cost reasons and the expense of the RNA-seq conducted throughout this project, ChIP-qPCR was conducted rather than ChIP-ChIP or ChIP-seq, which limits our investigation to only a small number of target genes rather than being genome wide. Further study to look at genome wide SCX binding would therefore be of interest in future work.

5.1.5. Chapter aims

In chapter 4 RNA-seq profiles of SCX knockdown adult and fetal tenocytes were generated, providing an insight into potential genes which may be under SCX regulatory control. However, additional techniques are required to determine if any of the candidate genes are directly bound by SCX, potentially leading to the changes observed. Therefore, the aim of this chapter is to identify novel genes which are the direct targets of SCX regulation in tenocytes isolated from different stages of development.

The specific objectives were to:

1) Optimise a ChIP assay to identify SCX target genes in tenocytes using a candidate gene approach based on known target genes and those identified in chapter 4.

2) Perform ChIP-qPCR on adult, fetal and ESC-derived tenocytes and compare direct SCX targets.

5.2 Results

5.2.1. Optimisation of ChIP-qPCR protocol

Prior to conducting the ChIP experiments several steps needed optimisation. Chromatin shearing, which is one of the most critical steps in the protocol was optimised first, with varying cycle lengths compared to determine the optimum shearing time required to generate fragments between 100-600 base pairs (bp). Three different cycle lengths were tested, namely 23 cycles, 30 cycles and 40 cycles of 20 seconds on and 20 seconds off, and the fragment sizes compared using agarose gel electrophoresis (Figure 5.4.A). Using 23 or 30 cycles resulted in fragments between 100-600 bp as depicted by the strong concentration of DNA in this region. Using 40 cycles produced a weaker smear, likely due to over-sonication leading to fragments of less than 100 bp. Over-sonication can lead to a drop in ChIP-efficiency, therefore the shortest sonication time of 23 cycles was used in the subsequent experiments, with shearing assessments via agarose gel electrophoresis conducted on all replicates prior to their use.

In addition, of upmost importance for successful ChIP experiments is the selection of appropriate antibodies. The successful use of an antibody in another experiment, such as immunocytochemistry or western blotting, does not necessarily mean the antibody will work in ChIP experiments (506). A literature search was therefore conducted to find a SCX antibody which had previously been used in ChIP experiments (termed ChIP-new) (507). This antibody was then compared to a SCX antibody which was routinely used in our laboratory for immunocytochemistry and western blotting (termed ChIP-old) (140) which had not previously been shown to work in ChIP experiments, alongside a histone H3 positive control (Figure 5.4.B). *TNMD* gene specific primers were then designed to encompass the E-box binding sites CAGATG and CATCTG, located around the TATA box of the *TNMD* promoter, which have previously been demonstrated as preferential binding sites for SCX in mature mouse tenocytes (422). qPCR was then conducted using the *TNMD* primers and immunoprecipitated DNA from adult tenocytes, isolated using each of the aforementioned antibodies.

Following qPCR, the data was then normalised. As numerous different normalisation strategies can be found in the literature, including background subtraction (508), fold

enrichment (509), percentage input (%IP) (510), normalisation relative to nucleosome density (511), normalisation to a control sequence (512) as well as combinations of the aforementioned (506), a strategy needed to be determined and used throughout. For this chapter a combinatory normalisation strategy was utilised. Firstly, the data was normalised to the amount of input chromatin (%IP) where the sample precipitation efficiency is measured relative to the total input signal (513). This method is generally preferred over the other commonly used 'fold enrichment over IgG control' method as IgG control reactions can have quite differing levels of background signal (513). However, caution needs to be taken with the handling of input and ChIP samples to ensure the input is a true representation of the amount of chromatin in each reaction. Following this the data was then normalised to the average of a panel of negative control genes (514), consisting of four genes, two of which qPCR assays designed to target intronic regions which contained no E-boxes within a 1.5 Kb span, and assays were also designed for two genes which are known not to be expressed in tenocytes and which had no E-boxes within 500 bp of the promoter region. In doing so this reduced the number of false positives by accounting for background signal which can occur through differences in reproducibility of chromatin washing and purification steps. IgG controls were still performed for all experiments as a further internal negative control however, the data was not normalised to these values.

Following normalisation, no enrichment of the target DNA sequence as a consequence of SCX binding in adult tenocytes was found when using the SCX (old) antibody which binds to the N-terminal region of the SCX protein (Figure 5.4.C), whereas an enrichment of > 5 fold was determined using the SCX (new) antibody, which binds to the C-terminal region. The SCX (new) antibody was therefore used in subsequent experiments. It should be noted, that as a result of the COVID-19 pandemic (see preface) this antibody was not validated by western blotting to determine its specificity in the horse. However, this antibody is made from a keyhole limpet hemocyanin (KLH) carrier protein conjugated with a synthetic peptide made from the 172-201 amino acids located at the C-terminal region of the human SCX protein, which as shown in Figure 4.1 has 100% homology to the equine SCX protein within this region, therefore it is highly likely to be cross-reactive.

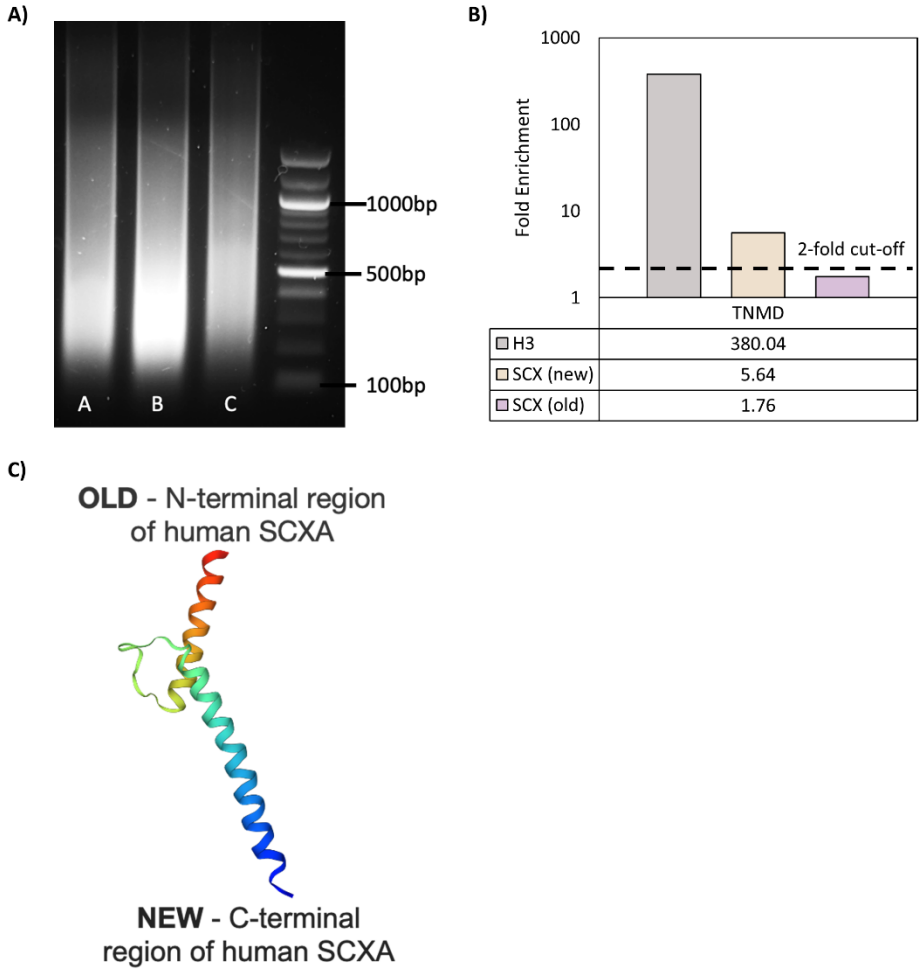

Figure 5.4. ChIP-qPCR protocol optimisation. A) Optimisation of chromatin shearing in one adult tenocyte line as determined by agarose gel electrophoresis. Lane A shows a programme of 23 cycles (20 seconds on, 20 seconds off), lane B a programme of 30 cycles (20 seconds on, 20 seconds off) and lane C a programme of 40 cycles (20 seconds on, 20 seconds off) using a Misonix Sonicator XL2020 Ultrasonic Liquid Processor. **B)** Chromatin immunoprecipitation was performed on adult tenocytes using two different anti-scleraxis antibodies (old vs new) alongside a histone H3 control at a concentration of 2 μg of antibody per reaction, as per the supplier's recommendation. Immunoprecipitates were subjected to qPCR using primers flanking E-box binding sites within the TNMD gene promoter region. Genomic DNA was used as a positive input control. Results represent the fold enrichment of the ratio of SCX- or H3- bound DNA to the average of the negative controls (TEX33, RNASE9, Intronic #1 ad Intronic #2) normalised for input DNA. **C)** Diagram of the SCX bHLH protein demonstrating where the two SCX antibodies (old vs new) bind.

The final optimisation step was to determine the most efficient amount of antibody to use per reaction. It is known that too low a concentration of antibody can lead to failed binding of all the target protein in the immunoprecipitated sample, whereas too high an antibody concentration can result in saturation of the assay leading to lower specific signal and high background noise. Therefore, the SCX antibody concentration was titrated from 1 μg to 10 μg to determine the optimum concentration for use in subsequent reactions. Using an antibody titration curve, 4 μg was determined to be the optimal concentration, giving the lowest signal over background ratio, and was used for subsequent experiments alongside an IgG negative control which was also used at a 4 μg concentration (Figure 5.5).

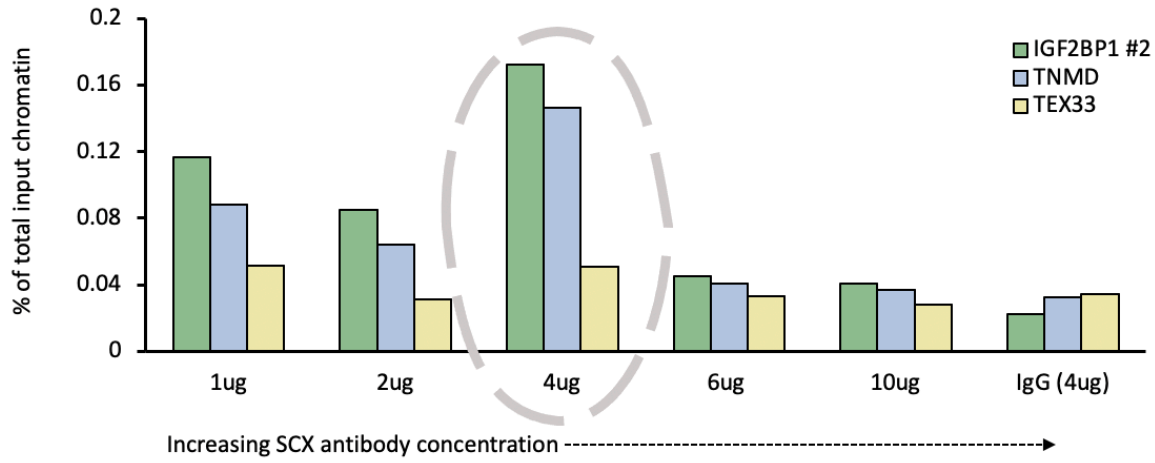

Figure 5.5. SCX antibody titration curve. Immunoprecipitates isolated from reactions using varying antibody concentrations were subjected to qPCR using primers flanking E-box binding sites within the TNMD (positive control), IGF2BP1(candidate gene) and TEX33 (negative control) gene promoter region. Crosslinked chromatin was used as a positive input control. The quantified DNA is expressed as a percentage of the total input chromatin. IgG antibody (4 μg) can be seen on the graph as a negative control. Reactions containing varying IgG concentration were also conducted however for simplicity are not shown.

5.2.2. Identification of SCX targets in adult and fetal tenocytes

Following optimisation ChIP-qPCR was conducted on two genes previously demonstrated to be regulated by SCX, namely *COL1A2*, which has been shown to be directly bound by SCX in cardiac fibroblasts, and *TNMD,* which has been identified as being directly regulated by SCX in adult tenocytes (422,443,446). ChIP-qPCR demonstrated significant enrichment of SCX binding to the *COL1A2* promoter in both adult and fetal tenocytes, despite this gene not being DE in either cell type following SCX knockdown (Figure 5.6). *TNMD* showed significant enrichment in both adult and fetal tenocytes, despite this gene again not being DE in either cell type following SCX knockdown (Figure 5.6).

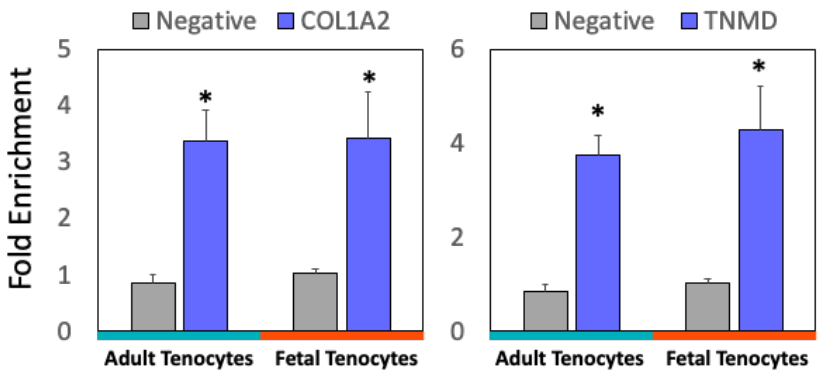

Figure 5.6. ChIP-qPCR on genes unaffected by SCX knockdown. Chromatin immunoprecipitation was performed on adult and fetal tenocytes using an anti-scleraxis antibody (4 μg). Immunoprecipitates were subjected to qPCR using primers flanking E-box binding sites within the gene's promoter regions. Crosslinked chromatin was used as a positive input control. Results of n = 3 biological replicates are presented as a fold enrichment of the ratio of SCX-bound DNA to the average of the negative controls (TEX33, RNASE9, Intronic #1 and Intronic #2) normalised for input DNA, with error bars representing the SEM. Grey bars represent the fold change in enrichment of SCX-bound DNA for the average of the negative control genes. Blue bars represent the fold change in enrichment of SCX-bound DNA for each gene analysed. * $p < 0.05$ using a two-tailed Student's t-test.

Next were tested genes that showed significantly decreased expression in both adult and fetal tenocytes following SCX knockdown (Figure 5.7). *IGF2BP1*, which was the top downregulated gene in both adult and fetal tenocytes was significantly enriched in both adult and fetal tenocytes, however, at different E-box binding sites (*IGF2BP1* #1 in fetal tenocytes and *IGF2BP1* #2 in adult tenocytes). *FGF19*, another gene which was significantly downregulated in both adult and fetal shSCX expressing cells, showed a trend of enrichment (> 2-fold) in fetal tenocytes only, yet this was not significant. *KLF15* and *NOV*, which were significantly downregulated in both fetal and adult tenocytes showed a trend of enrichment (> 2-fold) in both adult and fetal tenocytes however again this was not significant.

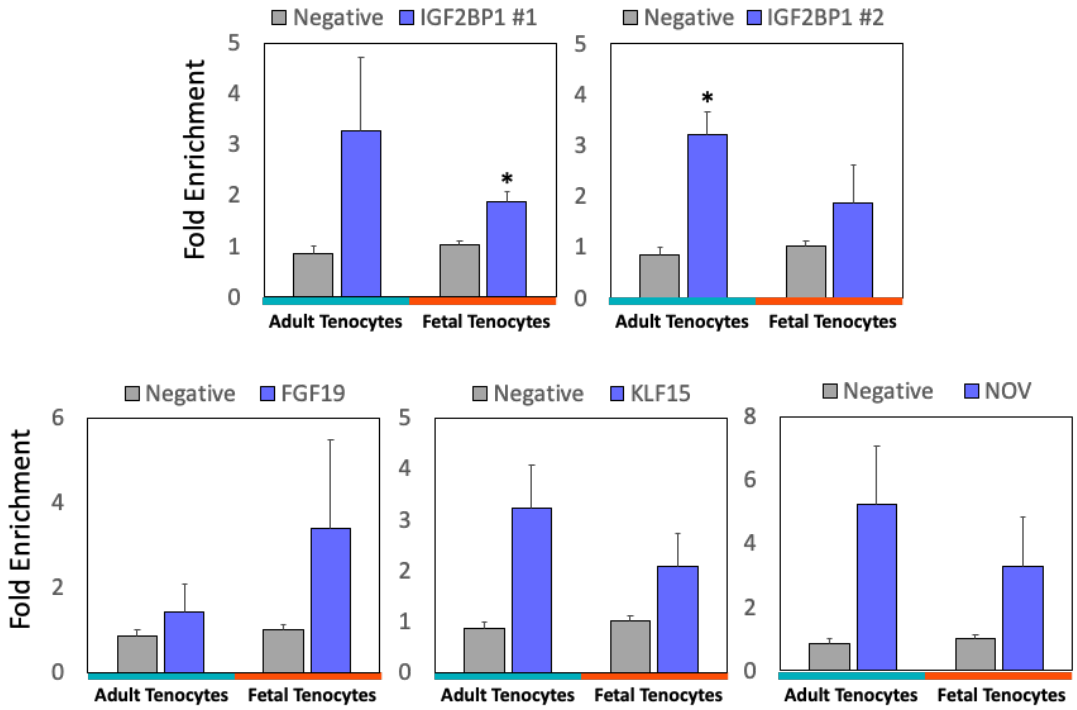

Figure 5.7. ChIP-qPCR on genes downregulated following SCX knockdown in both adult and fetal tenocytes. Chromatin immunoprecipitation was performed on adult and fetal tenocytes using an anti-scleraxis antibody. Immunoprecipitates were subjected to qPCR using primers flanking E-box binding sites within the gene's promoter regions. Crosslinked chromatin was used as a positive input control. Results of n = 3 biological replicates are presented as a fold enrichment of the ratio of SCX-bound DNA to the average of the negative controls (TEX33, RNASE9, Intronic #1 and Intronic #2) normalised for input DNA, with error bars representing the SEM. Grey bars represent the fold change in enrichment of SCX-bound DNA for the average of the negative control genes. Blue bars represent the fold change in enrichment of SCX-bound DNA for each gene analysed. * $p < 0.05$ using a two-tailed Student's t-test.

Following this, genes which were differentially affected by SCX knockdown in adult and fetal tenocytes were then tested (Figure 5.8). *PDGFB*, which was significantly downregulated in fetal tenocytes only following SCX knockdown was significantly enriched in fetal tenocytes. Adult tenocytes also showed substantial enrichment (7.66-fold) however this was not significant due to the high variability between biological replicates. *CLDN16*, which was significantly downregulated in adult tenocytes only following SCX knockdown, showed significant enrichment in SCX binding in adult tenocytes but not fetal tenocytes. *ACTA1*, which was significantly downregulated in fetal shSCX expressing cells only following differential expression analysis, showed no significant enrichment in either cell type (within E-box region #1 or #2). *FGF9* which was similarly significantly decreased in fetal tenocytes only, clearly showed no enrichment of SCX binding.

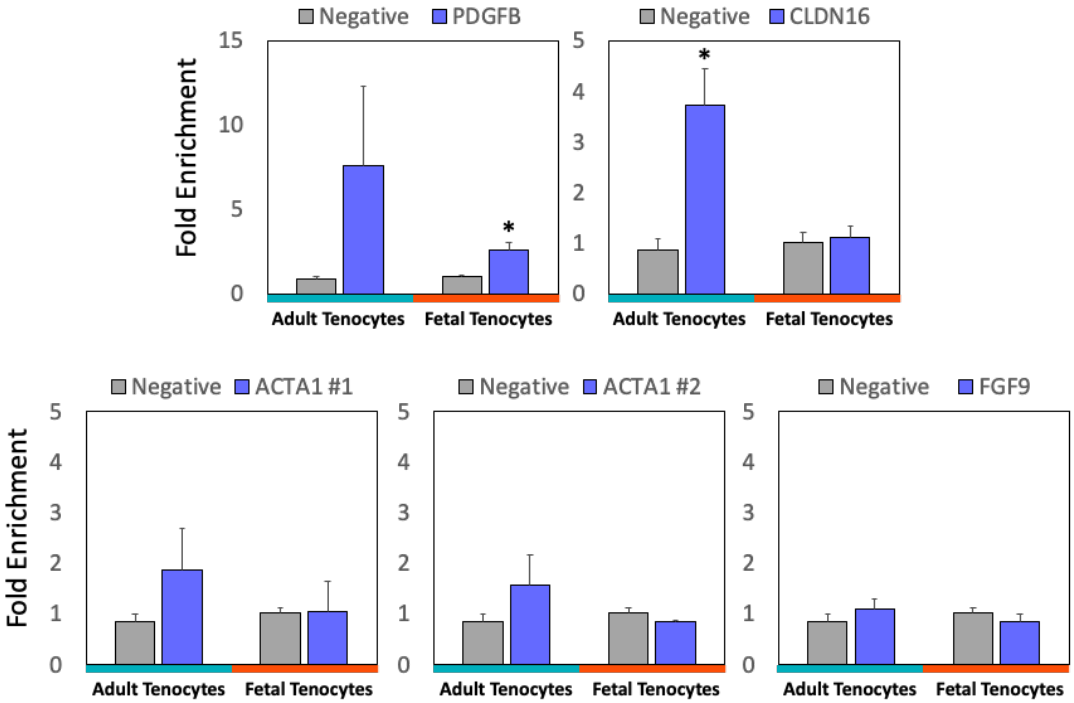

Figure 5.8. ChIP-qPCR on genes differentially affected by SCX knockdown in adult and fetal tenocytes. Chromatin immunoprecipitation was performed on adult and fetal tenocytes using an anti-scleraxis antibody (4 μg). Immunoprecipitates were subjected to qPCR using primers flanking E-box binding sites within the gene's promoter regions. Crosslinked chromatin was used as a positive input control. Results of n = 3 biological replicates are presented as a fold enrichment of the ratio of SCX-bound DNA to the average of the negative controls (TEX33, RNASE9, Intronic #1 and Intronic #2) normalised for input DNA, with error bars representing the SEM. Grey bars represent the fold change in enrichment of SCX-bound DNA for the average of the negative control genes. Blue bars represent the fold change in enrichment of SCX-bound DNA for each gene analysed. * $p < 0.05$ using a two-tailed Student's t-test.

Finally, although SCX has only been demonstrated to be a transcriptional activator, the genes that showed the largest upregulation following SCX knockdown in adult and fetal tenocytes, *MMP3*, was investigated to see if SCX bound within the *MMP3* gene promoter (Figure 5.9). *MMP3* (within E-box region #2) showed a trend of enrichment (> 2-fold) in both adult and fetal tenocytes however this was not significant. No enrichment was found in either of the other E-box regions investigated (#1 or #3).

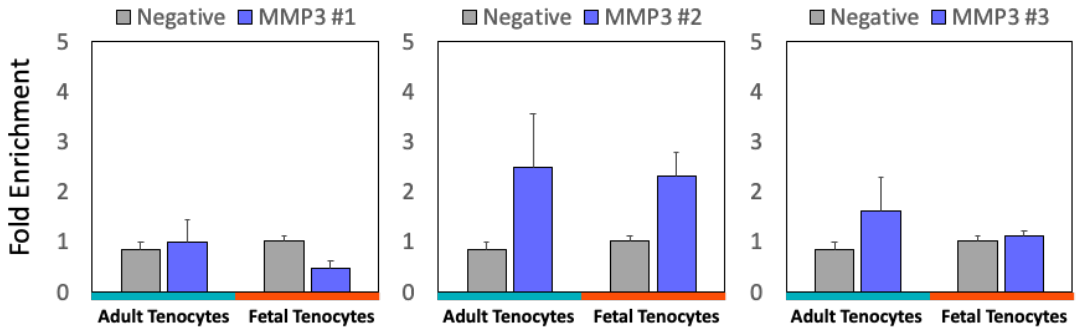

Figure 5.9. ChIP-qPCR on gene upregulated by SCX knockdown in adult and fetal tenocytes. Chromatin immunoprecipitation was performed on adult and fetal tenocytes using an anti-scleraxis antibody (4 μg). Immunoprecipitates were subjected to qPCR using primers flanking E-box binding sites within the gene's promoter regions. Crosslinked chromatin was used as a positive input control. Results of n = 3 biological replicates are presented as a fold enrichment of the ratio of SCX-bound DNA to the average of the negative controls (TEX33, RNASE9, Intronic #1 and Intronic #2) normalised for input DNA, with error bars representing the SEM. Grey bars represent the fold change in enrichment of SCX-bound DNA for the average of the negative control genes. Blue bars represent the fold change in enrichment of SCX-bound DNA for each gene analysed. * $p < 0.05$ using a two-tailed Student's t-test.

5.2.3. Identification of SCX targets in ESC-derived tenocytes

ChIP-qPCR was being conducted to determine the direct targets of SCX in ECS-tenocytes, however as a result of the COVID-19 pandemic this could only be conducted in one biological replicate (see preface). Although no statistically significant conclusions can be drawn from this data, if we consider those with fold enrichment of > 2 to be potentially bound, enrichment of SCX binding was observed in the promoter region of *IGF2BP1* (within E-box region 2), *PDGFB*, *NOV* and *TNMD* in this biological line (Figure 5.10).

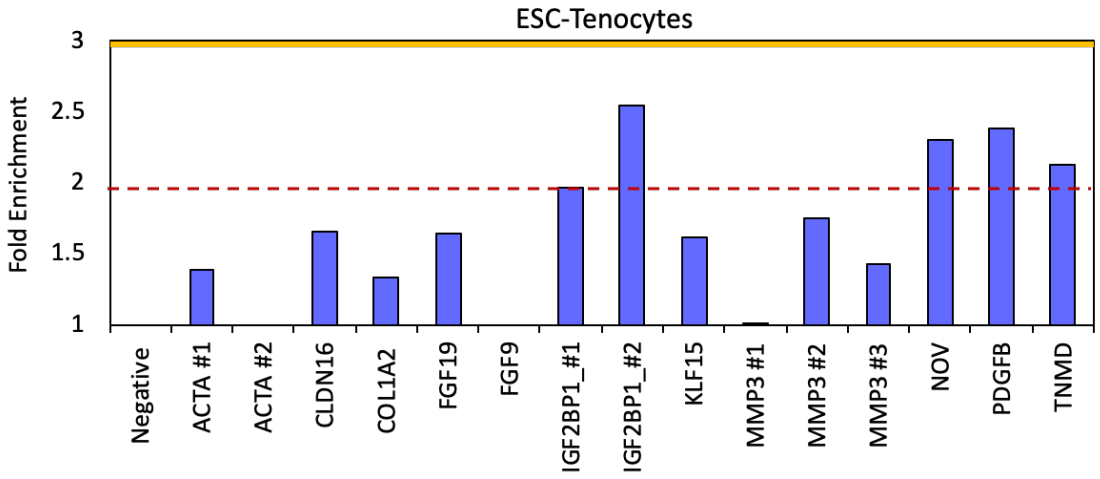

Figure 5.10. ChIP-qPCR in ESC-tenocytes. Chromatin immunoprecipitation was performed on one biological line of ESC-tenocytes using an anti-scleraxis antibody. Immunoprecipitates were subjected to qPCR using primers flanking E-box binding sites within the gene's promoter regions. Crosslinked chromatin was used as a positive input control. Results are presented as a fold enrichment of the ratio of SCX-bound DNA to the average of the negative controls (TEX33, RNASE9, Intronic #1 and Intronic #2 –labelled as negative) normalised for input DNA. Blue bars represent the fold change in enrichment of SCX-bound DNA for each gene analysed.

5.3 Discussion

In the previous chapter, through the generation of SCX knockdown ESCs, fetal, foal and adult tenocytes lines, it was demonstrated that SCX regulation of gene expression differs during different stages of development. However, whether the genes identified were regulated directly via SCX or not was unclear. To further explore this concept, candidate genes which were differentially affected by SCX knockdown were investigated using ChIP-qPCR to determine whether they were directly bound by SCX. Identification of SCX downstream targets at different developmental stages will yield valuable insight into how adult reparative and fetal regenerative tenocytes act to facilitate scleraxis-dependent processes which may provide new targets for therapeutics. The results in this chapter have been published (471).

5.3.1. Differences in SCX binding in adult and fetal tenocytes

Following ChIP optimisation, 11 genes were analysed using ChIP-qPCR in three biological lines of adult and fetal tenocytes. *COL1A2* has been confirmed as a direct downstream target gene of SCX in cardiac fibroblasts (242,446). Yet despite no significant difference in mRNA expression being determined following SCX knockdown in both adult and fetal tenocytes, significant enrichment of SCX binding to the *COL1A2* promoter was detected. This could suggest, that although SCX binds to the *COL1A2* promoter it does not activate transcription in tenocytes. This may be due to the lack of availability of the required SCX interacting partners at this site, which may indicate that SCX directs similar but discrete signalling programs in a tissue-dependant manner that are modified by tissue specific interacting partners (444).

IGF2BP1 expression on the other hand was significantly decreased in both adult and fetal tenocytes following SCX knockdown confirming for the first time that SCX can directly bind to the *IGF2BP1* gene promoter in both adult and fetal tenocytes, although at different E-box binding sites. IGF2BP1 is a member of the IGF-II mRNA binding protein family which regulates the growth factor IGF2. IGF2BP1 knockout (KO) studies in mice have identified its essential role in normal growth and development, with KO mice exhibiting severe dwarfism and impaired gut development (515). KO mice also displayed impaired extracellular matrix formation within the organs tested (intestine, liver, and kidneys) with

reduced expression of *LGALS1*, *LUM*, *TNC* and several other procollagen transcripts. Although IGF2BP1 has not currently been implicated in tendon development, evidence suggests it plays a role in periodontal ligament (PDL) tissue and dental development (516). Further functional studies to determine the effects of altering IGF2BP1 expression in tenocytes would therefore be of interest.

FGF19, KLF15 and *NOV* expression was also significantly decreased in both adult and fetal tenocytes following SCX knockdown. Low levels of enrichment of SCX binding was observed in both adult and fetal tenocytes in the *KLF15* (3.24- and 2.1-fold enrichment in adult and fetal respectively) and *NOV* (3.21- and 2.7-fold enrichment in adult and fetal respectively) E-box promoter regions, although this was not significant. Further biological replicates are therefore required in order to determine if SCX is directly regulating these target genes. *FGF19* E-box showed a trend of enrichment in fetal tenocytes only (3.66-fold enrichment), however this again was not significant and further replicates would be required.

A selection of genes which had differing subsequent expression in adult and fetal tenocytes following SCX knockdown were then investigated. *PDGFB* was significantly decreased following SCX knockdown in fetal tenocytes only. PDGF proteins are produced by a variety of cell types including platelets, macrophages, endothelial cells and smooth muscle cells and are heavily implicated in tendon wound healing (517,518). PDGFB in particular is also proposed to promote ECM production in muscle cells during limb development (519). Significant enrichment of SCX binding to PDGFB was detected in fetal tenocytes, which taken along with the RNA-seq results, provides evidence that SCX directly activates *PDGFB* expression in fetal tenocytes. Enrichment was also detected in adult tenocytes; however, this was not significant due to the large variation in fold changes. This suggests SCX, although bound, may not actively promote transcription in adult tenocytes. *ACTA1* and *FGF9* were also only significantly decreased in fetal tenocytes following SCX knockdown, however no enrichment in SCX binding was detected in either gene in either adult or fetal tenocytes, indicating that the effect on gene expression may be due to an intermediate interactor.

CLDN16 was the most significantly downregulated gene in adult tenocytes following SCX knockdown yet it was unchanged in fetal tenocytes. Little is known in regard to CLDN16, a claudin protein that is an important component of tight junctions between

cells. Direct interaction between SCX and the *CLDN16* gene sequence was confirmed in adult tenocytes, having significant enrichment in SCX binding, whereas no binding was observed in the fetal tenocytes. Functional studies to determine the role of CLDN16 in tendon cells is therefore warranted.

The final investigation focused on whether SCX regulated the expression of *MMP3*, the most significantly upregulated gene in both adult and fetal tenocytes following SCX knockdown. Although SCX has only been reported to be a transcriptional activator, over two-fold enrichment of SCX binding was detected in both adult and fetal tenocytes around one MMP3 E-box binding site (MMP3 #2), although no significant binding was detected to confirm the binding of SCX to any of the three E-box regions within the MMP3 promoter. This could suggest that either SCX has some previously unreported repressive effects, or that it is passively binding the promoter region which is blocking the binding of a different transcriptional activator for *MMP3*. Identifying histone modifications around this promoter site alongside SCX binding may help determine if SCX is indeed involved in *MMP3* regulation.

5.3.2. Differences in SCX binding in ESC-tenocytes

Unfortunately, investigation into SCX binding in ESC-tenocytes could not be completed, with only one biological replicate having been examined. Although this data is preliminary it appears that *IGF2BP1* (around E-box region 2), *PDGFB* and *NOV* show enrichment in SCX binding, like that of the *TNMD* positive control. These genes also all showed enrichment in adult and fetal tenocytes. Although these genes were DE in adult and/or fetal tenocytes following SCX knockdown, whether they would be affected in ESC-tenocyte SCX knockdown lines was not determined and would be worth further investigation. To do so ESCs would first need to be differentiated into tenocytes and SCX knockdown performed on the differentiated cells in order to match that of the adult and fetal tenocyte data.

In chapter 4, several chondrogenic genes were found to differ in their expression following tenogenic differentiation of shSCX expressing ESCs which could signify SCX's role in determining tenogenic versus chondrogenic lineage specification. To investigate this hypothesis high throughput methods could be employed to help decode the temporal changes in gene expression patterns that occur during both tendon and

cartilage differentiation. For example, by combining RNA-seq, histone modification ChIP-seq and transcription factor ChIP-seq experiments; the changes in global gene expression, the chromatin state and transcription factor occupancy at multiple distinct stages of tendon differentiation from ESCs to tenocytes or chondrocytes could be captured. By combining these features, dynamic regulator networks could then be inferred using computational modelling such as that which has been conducted in haematopoietic specification and cardiac differentiation (520,521).

Finally, it should also be noted that ChIP-qPCR was not conducted on the foal tenocytes lines either, which would also be of interest, particularly to look at potential binding of SCX in the *COMP* gene promoter region as this was significantly affected by SCX knockdown in the foal samples alone.

5.3.3. Theoretical mechanisms for differences in SCX binding & gene regulation

When one considers the size of the equine genome, being around 2.7 billion DNA bp in length, searching for potential SCX binding sites using an E-box motif of only 6 bp long will result in hundreds of thousands of potential binding sites. Not all of these sites are actually bound *in vivo* (502,522), so what is it that allows transcription factors to so precisely bind to specific DNA sites and not others? And of those bound sites, as only a small number are suggested to be functional i.e. have an impact on gene expression (502,522,523), what determines this functionality? Predicting and interpreting *in vivo* transcription factor-DNA binding events and their regulatory consequences is therefore quite a sizable task.

It is now recognised that several features contribute to transcription factor-DNA binding preferences beyond that of the core nucleotide sequence, which in this study is the E-box motif. These include the 3D structural features of the binding sites, where variations in DNA groove width or DNA bending for example, as indicated in Figure 5.3.B, can alter the preference for transcription factors to bind to specific DNA sites (502,524,525). Considering this fact, such shape changes at transcription factor binding sites may account for the lack of enrichment in SCX binding observed for many of the primer pairs tested in this study, even though they were designed to encompass E-boxes. Similarly, how accessible the E-box binding regions are could also account for the lack of

enrichment observed. Chromatin accessibility and nucleosome occupancy can impede transcription factor binding and increase transcription factor-DNA dissociation rates, therefore many of the primer pairs generated may have been unknowingly designed to inaccessible E-box regions (Figure 5.11). In order to determine DNA accessibility, methods such as ATAC-seq (assay for transposase-accessible chromatin using sequencing) would need to be conducted, however this was outside the scope of this thesis.

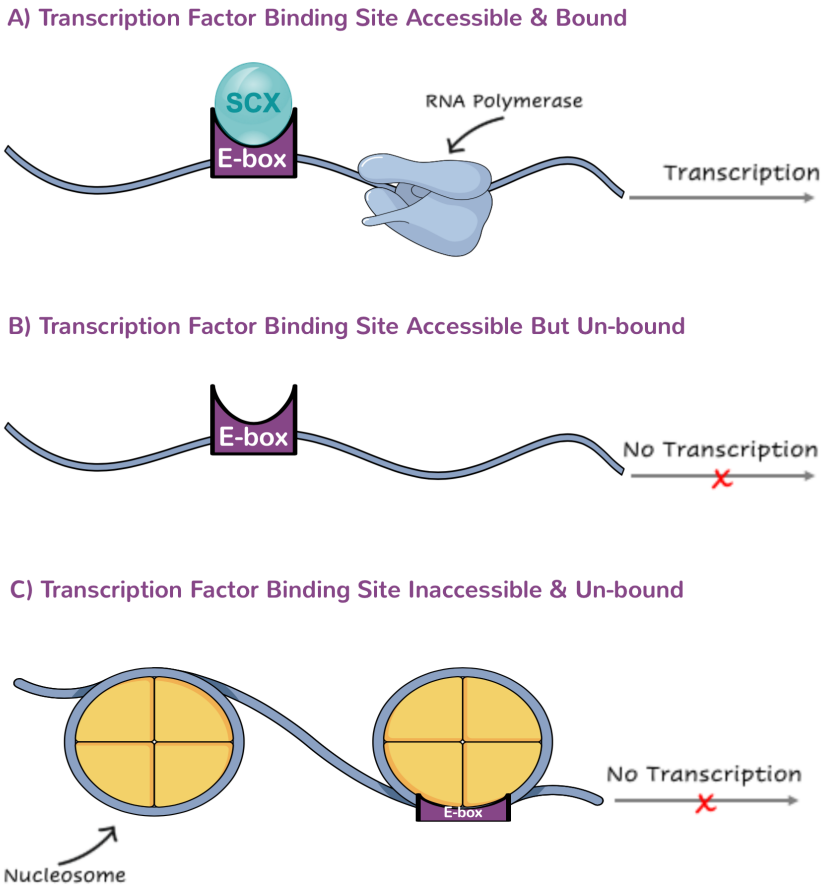

Figure 5.11. Differences in accessibility of E-box binding regions. The accessibility of E-box regions can explain the binding affinity shown. For example, in **A)** the E-box may be accessible therefore SCX can readily bind and result in activation of gene transcription. **B)** However, many E-boxes may be accessible yet remain un-bound due to other factors such as the DNA context surrounding the motif, with it being predicted that on average 99.8% of binding sites in the genome are not bound by their respective transcription factor (526). **C)** One widely accepted reason is due to the accessibility of the binding sites, with many transcription factors preferentially binding to regions of open chromatin rather than inaccessible condensed chromatin (527). Figure inspired by Gomes & Wang *et al.*, 2016 (528).

Consideration should be given to the possibility that SCX might be bound within a particular gene regulatory region in one cell type, or a developmental stage within a cell

type, but not in another. It is well described that gene regulatory networks are plastic, being able to direct distinct patterns of gene regulation in relation to different spatial, temporal and environmental cues (502). One way in which this type of regulatory specificity is achieved is similar to that described previously, where the chromatin environment and DNA accessibility across cell types or developmental stages within a cell type can dynamically change based on the cellular context (502,529–531). Such changes can therefore impact the binding of transcription factors in a context specific manner. For example, BAFT (basic leucine zipper transcription factor) and IRF4 (interferon regulatory factor 4) are two transcription factors which have been demonstrated to be capable of remodelling the chromatin landscape by altering chromatin accessibility for other transcription factor to bind, thus providing T cells with plasticity to differentiate into multiple lineages depending on cytokine environmental cues (532). It may be the case therefore that SCX is able to bind to DNA made accessible in one developmental stage due to other 'pioneer' transcription factors altering the accessibility of the E-box binding site, whereas at another developmental stage it remains inaccessible due to lack of these cooperative transcription factors.

So, what about the case in which SCX is found to bind to a certain gene promoter region in both adult and fetal tenocytes, but only appears to cause a regulatory effect in one of the two? It is well recognised that cell-type or cell-stage specific regulation is likely to occur through binding of a combination of different transcription factors, with differences in combinatorial occupancy resulting in differing effects (533). For example, one study which looked at the binding patterns of three transcription factors, CTCF, RNA polymerase II (RNAPII) and MYC, across 11 different human cell types, revealed the expression level of genes whose promoters were bound by different combinations of the three factors changed depending on the occupancy (533). When certain genes were occupied by both MYC and RNAPII higher expression levels were detected than when the genes were bound by either MYC or RNAPII alone (533). Whereas when these genes were occupied by both MYC and CTCF they exhibited lower expression than those occupied by MYC without CTCF (533). Therefore, by altering the cohort of transcription factors present genes can be regulated differently. It could therefore be hypothesised that SCX is able to regulate, for example, IGFBP1 but not COL1A2 in the same cells due to the presence or absence of other proteins which bind cooperatively to regulate the genes expression in a cell-type specific way. The E2A splice variants E47 and E12 have been

identified as common binding partners of SCX, therefore it would be beneficial to determine whether the DE genes are co-activated with either of these by comparing ChIP-seq profiles or using Co-immunoprecipitation or ESMA techniques.

5.3.4. Summary

Taken together it therefore appears that SCX is developmentally regulated, having age specific transcriptional programmes in tenocytes which lead to differences in gene expression and SCX binding preferences in the developmental stages investigated. Whilst SCX is known to be the first robust marker for tendon progenitor formation, its expression pattern is not limited to tendon, being expressed in many highly ECM rich tissue precursors such as ligaments, bronchial cartilage and pericardium (428,479). It is becoming increasingly apparent that the ECM undergoes age related changes, with such age-related declines in the ECM having a bearing on how wounds heal at different developmental stages (534). Pathway and enrichment analysis of genes whose expression in adult tenocytes changed significantly following SCX knockdown identified an enrichment of genes involved in cell adhesion and ECM remodelling (Section 4.2.5). Consequently, it could therefore be hypothesised that SCX may present as one of the key developmental-specific transcription factors involved in coordinating such changes in the ECM. The specific occupancy of SCX on the promoters of ECM genes may, with interaction with other factors such as E12 and E47, influence the particular pattern of expression of these genes at different developmental stages. As differences in the healing model of adult and fetal tendons have been observed, with many studies indicating changes in ECM constituents between the reparative and regenerative tissues respectively, further understanding of SCX ECM gene regulation and its impact on cell-matrix interactions could be instrumental in understanding these different wound healing mechanisms.

It should be noted that in this chapter only a handful of DE genes were investigated using ChIP-qPCR and thus I was unable to investigate all of the DE genes resulting from the RNA-seq experiment detailed in chapter 4. Using this approach primers were designed within what was determined as the promoter regions of the genes investigated, however evidence is emerging that some genes are regulated by introns with genes still being regulated when promoter regions are deleted (535). This emphasises the need for larger

scale studies such as utilising genome-wide chromatin immunoprecipitation-sequencing or protein binding arrays in order to get a broader picture of SCX downstream regulation.

Chapter 6 – Summary, Discussion and Future Perspectives

6.1 Summary

The overarching goal of this thesis was to explore the suitability of using ESC-derived tenocytes as a cellular therapy. More specifically it aimed to determine if ESC-tenocytes were more similar in their global gene expression profile to fetal or adult tenocytes, as well as to determine how SCX, a key gene in tendon development and healing, regulates gene expression in these different developmental stages. By using an RNA-sequencing approach to tackle both questions, ESC-tenocytes were found to be transcriptomically more similar to fetal as opposed to adult tenocytes, supporting the concept of using them as a cellular therapy and thereby endorsing the need for future *in vivo* efficacy and safety studies. Fetal regenerative and adult reparative cell types were also compared and large distinctions in gene expression were detected. The expression patterns of many chemokine, cytokines, growth factors and ECM proteins, which typically present in the injured adult tendon, differed between these two developmental states. Similarly, SCX was also shown to have differing regulatory effects in these stage specific cell types, differentially interacting with several novel genes involved in ECM remodelling. Taken together this data opens up future avenues of research to determine whether modulation of such factors *in vivo* could enhance adult tendon repair. The transcriptomic data presented in this thesis therefore provides an unprecedented insight into the fundamental differences between regenerative and reparative tendon cells which are likely to be important for future development of novel therapies for treating tendon injuries.

6.2 Discussion

6.2.1. Comparing regenerative and reparative cells

Tendon wound healing is a complex process which has amassed much scientific and financial interest in an effort to try and harness the properties of fetal regenerative healing as a means to improve adult injury repair. Whilst scientific inquiry and the clinical application of mesenchymal stem cell therapies in horses abounds in research labs and veterinary practices worldwide, thus far few adequately powered clinical trials evaluating the clinical outcome of MSC treated SDFT injures has been conducted (39,536,537). In one such study, 113 racehorses considered to have career ending tendinopathy were treated with BMSCs and followed up over a 2-3 year period (39). Of those treated, 98% of horses returned to work, with re-injury rates being lower than those with alternative treatments (39). Although ultrasonographical examination of MSC treated horses showed rapid filling-in of the injured lesion, the longitudinal striated patterns of the tendon architecture did not return to normal suggesting a degree of scarring remained (39,537). Other studies have similarly demonstrated a reduction in re-injury rates following MSC treatment as well as enhanced regeneration (538–540), however completely scarless wound healing like that observed in the fetus remains elusive (541).

Our understanding of fetal scarless healing leaves much to be desired, however as discussed in chapter 3, this appears to be in part due to the intrinsic properties of fetal tenocytes themselves (255). This highlights the need to better characterise fetal and adult cells, as these fundamental differences may be important in uncovering their differing mechanisms of wound repair and may help in the development of cellular or biological therapies. Therefore, in an attempt to better understand the core differences between adult and fetal tenocytes, in this thesis, their transcriptional profiles were compared in both 2D and 3D culture.

Through this work, one finding of particular interest was that the gene expression signature of adult and fetal tenocytes when cultured in a 2D static environment was not significantly different. Only when their environment was perturbed, be that by three-dimensional forces or gene modulation via SCX knockdown, did differences in adult and fetal transcriptional profiles occur. Although no other study to date has compared the

global transcriptome of adult and fetal tenocytes, two studies have demonstrated significant global transcriptional differences in 2D cultured human adult and fetal cardiac and skin fibroblast cells (542,543). Yet these studies compared cells which had a much larger age window, with fetal cells being from around 35-50% of the way through gestation and adult cells being from very elderly patients (50-75 years old). In this thesis I compared equine fetal cells of around 80% of the way through gestation and young, skeletally mature, adult horse (2-10 years old) tenocytes. Although as described in section 3.1.1, regeneration appears not only to be age specific, but also tissue and species specific, it must be noted that the tenocytes used in this study are therefore outside the range typically employed for regenerative studies, which is typically at 60-70% of the way through gestation in fetal sheep models (254,255,544). Similarly the majority of studies published however instead compare cells either directly from adult and fetal tissue collected post-mortem or from 3D cultures, rather than 2D cultures (344,396,545–549). In fact, studies which compare freshly isolated tissue of the limbs (tendon, ligament, cartilage and bone) compared to their 2D cultured counterparts have shown that even between tissues, 2D cultured cells cluster and have fewer differences than their native counterparts further highlighting that, when unperturbed, culturing primary cells in monolayers can result in a loss of their native gene expression profile (240).

Yet despite this lack of transcriptomic difference detected in 2D, the results of previously published research indicate that adult and fetal tenocytes can still respond differently when subjected to different environmental factors when cultured in this manner. For example, when investigating the differences in equine adult and fetal cells' migratory response to growth factors, TGF-β3, which is heavily involved in the wound repair process (306,412,413), is found to significantly inhibit fetal tenocyte migration, yet has no effect on adult tenocytes when cultured in 2D (376). Similarly, sheep fetal tendon fibroblasts were shown to have significantly greater rates of migration, producing more collagen type I when cultured in 2D wound healing scratch assays compared to adult tenocytes (550). The results presented in chapter 4 demonstrated that knocking down the gene SCX results in different global gene expression changes in adult and fetal tenocytes cultured in 2D. Therefore, taken together this suggests that it is how adult and fetal tenocytes respond to different stimuli that is important, and if we can better understand how they act in response to injury we are likely to be able to uncover how fetal tenocytes are able to orchestrate regenerative healing.

Differences in gene expression detected in 3D versus 2D have mainly been attributed to the differences in how the cells are able to form connections between each other, which in 3D is thought to more accurately represent the cell junctions seen *in vivo* which allow for better exchange of molecules between cells (551–555). Cells cultured in 3D have also been demonstrated to have a greater capacity to deposit ECM, with both ECM proteins and growth factors consistently being increased as a result of 3D culture (551–555). In this study significant changes in gene expression were detected between adult and fetal cells cultured in a 3D environment and the results presented demonstrate that ESC-tenocytes have a more similar transcriptomic profile to fetal as opposed to adult tenocytes when cultured in this way. However, to accept that the actions and responses of the cells to an injury environment, and not solely their gene expression profiles, demarcate the regenerative and reparative phenotypes, then more research is required to unequivocally determine if ESC-tenocytes would act in a fetal regenerative manner.

The balance of pro- and anti-inflammatory activity, which is coordinated through cytokines, chemokines and growth factors has been shown to be altered in fetal and adult wounds. Whereas adult wound healing is accompanied by high levels of inflammation (556–561), fetal wounds have minimal inflammation (562). Furthermore, inducing inflammation in fetal wounds, such as through the injection of pro-inflammatory cytokines and growth factors typically present in the adult injury environment, has been shown to stimulate scar formation (330,335,563,564). Although ample evidence exists demonstrating the importance of the local wound environment on wound healing, it appears to not be the major reason for the different healing outcomes of adult and fetal tissue, as in contrast fetal tendons transplanted into an adult environment retain their regenerative capacity (255–259). It has therefore been suggested that instead it is the differences in cellular behaviour in response to injury signals that effects whether scarring ensues, with fetal cells ability to rapidly migrate towards an injury thought to be critical in limiting damaging inflammatory mediator induction that leads to scarring (296,562).

Interestingly, upon comparing the adult and fetal gene expression profiles generated in this thesis, it was apparent that many genes involved in cell migration and inflammatory functions were DE, as indicated by the gene ontology (GO) analysis. Migration of resident cells is an important early tissue injury response that is critical for correct tissue repair (565). In skin, fetal fibroblast migration is increased in response to injury compared

to adult fibroblasts, which is in part due to the differential balance of inflammatory signalling and growth factors within fetal and adult wounds (36,258,373–375,565,566). Chemokines, growth factors and growth factor binding proteins, all of which have been shown to play a role in cellular migration during wound healing (372–375), were amongst the genes associated with the enriched GO terms. In fact several of the genes identified are upregulated in adult tendon injuries including IGF-1 (insulin-like growth factor 1), bFGF (basic fibroblast growth factor), PDGF (platelet derived growth factor) and SDF-1 (stromal cell derived factor 1) (404–407), all of which can influence cell migration (407–411).

Understanding how these factors produced in adult injuries regulate cellular activity is therefore an important next step and would help to determine whether ESC-tenocytes share some of these properties with fetal tenocytes, thereby strengthening the evidence for their clinical use. To do so would require the generation of extensive wound models, which could allow us to determine how adult, fetal and ESC-tenocyte act to close a wound, as well as model if and how an ESC therapy would work in practice. This could be done by determining how adult, fetal and ESC-tenocyte migration rates compare in 2D wound healing assays. The effect of several of the growth factors and inflammatory mediators, identified in this thesis as DE and known to be present in the adult injury environment, on wound closure could then be compared (Figure 6.1).

This could then be developed into a 3D system, where punch wounds could be made in cell seeded 3D collagen artificial tendon gels (154) to represent the typical central core lesion presented (567), and the rate of wound closure again compared with and without the addition of the growth factors and inflammatory mediators (Figure 6.1). Such a system could then be used to model the clinical scenario of applying ESCs to an adult tendon injury, by utilising fluorescently labelled adult tenocytes seeded in co-culture with either ESCs or fetal tenocytes labelled with different fluorophores (46) and the rate and effect on wound closure and matrix remodelling compared. Such *in vitro* tools would minimise the extent of future *in vivo* animal models needed.

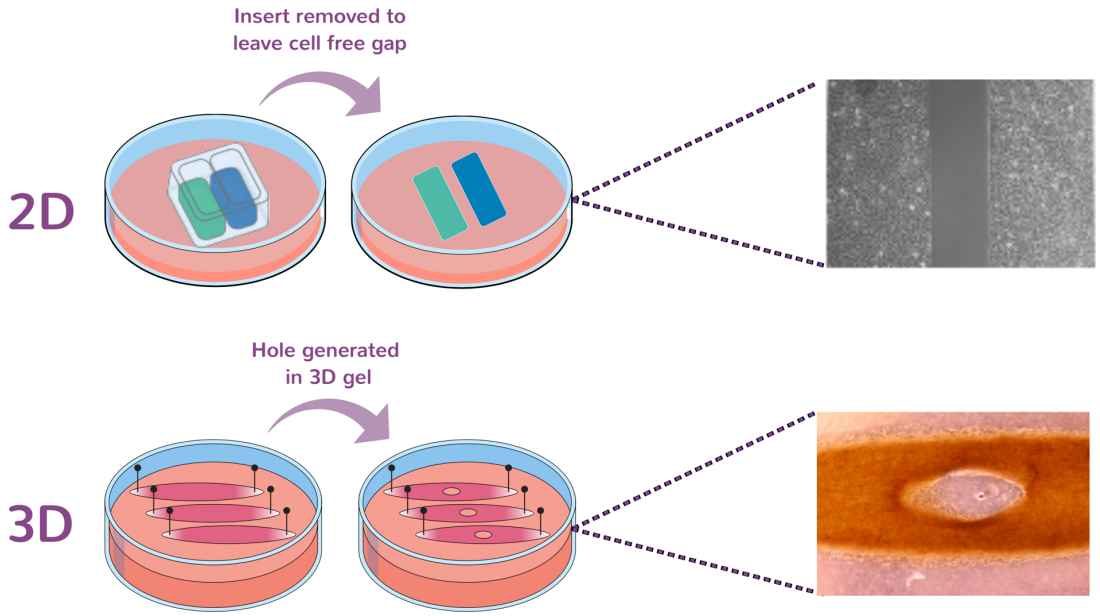

Figure 6.1. Tendon wound modelling. Schematic of potential wound healing assays which could be conducted to better understand the differences in how adult and fetal tenocytes respond to adult injury signals. Assays could be conducted using both 2D scratch assays as well as using 3D collagen gel hole punch assays. The responses could then be compared to that of ESC-tenocytes to give further evidence of their use as a cellular therapy.

However, this simplified wound assay outlined above fails to account for the complexities of the real *in vivo* wound environment. In particular, the effect of immune cells, which play a large role in the wound healing process are not taken into account (568). Therefore, further optimisation of this wound healing assay could be conducted by seeding the assays with stimulated peripheral blood mononuclear cells to better recapitulate the inflamed adult *in vivo* environment. Once this system was established, further alterations could be performed such as looking at the effect of conditions known to alter the rate of healing including altered glucose levels and hypoxia (569,570). The effect of fetal or ESC-tenocytes addition to the adult artificial tendons could again be examined to see how it impacts wound closure. Finally the application of a cyclic external strain could also be investigated to mimic the physical properties experienced in the tendon during healing; another key aspect which is missing in existing *in vitro* wound models (571). This could be done by seeding the 3D collagen gels in a bioreactor and performing the aforementioned punch assay, a system previously utilised in our laboratory (233).

6.2.2. Heterogeneity of the tendon cell population

As discussed in chapter 3, although ESC-tenocytes have fewer DE genes when compared to fetal tenocytes as opposed to adult tenocytes, this study does not account for the heterogeneity of our sample populations. Cellular heterogeneity within various tissue and cell populations is being increasingly recognised as important for understanding how different tissue subpopulations function during development and disease, with studies using single cell RNA-seq (scRNA-seq) rising exponentially within the last decade (572). Prior to the advent of scRNA-seq, the sparse, heterogeneous and auto-fluorescent nature of the tendon cell population limited our ability to interrogate their diversity fully (573). Yet even with the introduction of scRNA-seq, few studies have been conducted using normal adult tendon tissue, with the numbers of bulk RNA-seq data available similarly being limited, particularly in terms of the number of biological replicates, developmental stages and species sequenced (397,573,574). This lack of transcriptomic data available highlights the need for greater collaborative efforts to be made. Having access to larger cohorts of tendon tissue and cellular transcriptomic and proteomic datasets at differing developmental stages would allow for a more accurate picture of tendon cell development and heterogeneity to be obtained. Taken together this could provide vital information for the development of reliable selective markers for key tendon cell populations.

Looking at the limited scRNA-seq studies which have been conducted, it is clear that at least three distinct populations exist within the healthy adult tendon of humans and mice (397,573,574). The first reported scRNA-seq, which was conducted using only 71 individual human tendon cells, isolated from a single healthy adult male which had undergone one passage in culture, described three main populations (397). The first expressed the endothelial cell-specific marker CD3 and *nestin* (*NES*), the second which was also *NES* positive had high tendon-related gene expression (*COL1A1, TNC, Fmod)* suggestive of a progenitor population, and the third, which contained the biggest proportion of cells, was composed of a *NES* negative population which expressed high levels of tendon lineage genes (*THBS4, MKX)* and CD146, suggestive of a mature tenocyte population. A more recent study of human tendon, which contained a data set of over 6,000 cells obtained immediately *ex vivo* from 8 healthy adult tendons, instead found eight distinct transcriptomic clusters, made up of five so called tenocyte populations which expressed collagen matrix genes, monocytes, T cell lymphocytes and endothelial

cells, with *NES* positive cells being predominantly found in the endothelial cell cluster (573). These differing results were suggested to be due to the differences in the numbers of cells analysed, as well as due to potential unintentional preferential selection of cells during monolayer passaging (397,573).

Consistent with this, a study of healthy 6-week old mouse Achilles tendon scRNA-seq identified 11 distinct populations, comprised of three tendon fibroblast-like groups, three endothelial cell groups, two nerve cell groups, immune cells, red blood cells and pericytes based on the analysis of four independent replicate datasets of over 1,000 *ex vivo* tendon cells (574). Interestingly, whilst all of the tendon fibroblast populations expressed *COL1A1* only a small subset expressed the routinely described tendon specific marker *SCX,* a result which was confirmed with RNA *in situ* hybridization and SCX lineage tracing using *SCX:R26*^{tdTomato} mice (574). Similarly, some populations were found to express *TNMD* but not *SCX,* whilst others were found to express both *SCX* and *TNMD* together. Differences in *SCX* expression in tendon subpopulations were also noted in the human scRNA-seq study, with only two out of the five having high *SCX* expression (573).

In this thesis, using bulk RNA-seq data of *in vitro* passaged cells, *SCX* was found to be DE between adult and fetal tenocytes, with *TNMD* not being expressed at the mRNA level in either cell type. Considering, based on the scRNA-seq data available (573,574), that *SCX* and *TNMD* expressing cells appear to be limited to certain subpopulations of tendon cells this could suggest that the proportions of these different subpopulations differ in adult versus fetal tenocytes which could account for the differential expression observed in our bulk RNA-seq data. Similarly, it is unknown how the selective *in vitro* pressures change the ratios of these populations, with some potentially being unintentionally selected for during routine passaging. As our adult and fetal tenocytes were passaged multiple times prior to sequencing, it is unclear whether some populations are overrepresented as a result, which would alter the gene expression profiles obtained. Similarly, the ESC-tenocytes were not passaged following ESC tenogenic differentiation, and given it is likely that only one main population of immature tenocytes would arise following this relatively short differentiation protocol, having access to scRNA-seq data of equine adult and fetal tendon would be of great use to determine which tenogenic population arises following this differentiation protocol.

Computational methods already exist which use deconvolution algorithms to infer scRNA-seq cell type and cellular state compositional information from bulk RNA-seq data (575). The bulk data generated in this study could therefore be of great use to help deconvolve the different cell types present in the adult, fetal and ESC-tenocyte populations (Figure 6.2). Similarly, this data could be used to uncover the cell populations present in RNA-seq profiles of injured tendon tissue from different developmental stages to deconvolve the cell-type gene signature present during injury. Together this information could help determine if different populations respond to injury in fetal regenerative healing, whether a small subset of these cells are present within the adult tendon, and how best to select for this population of interest for use as a cellular therapy. Although the scRNA-seq datasets currently generated are of great value, limitations arise due to technical differences between the donors used, batch variation, anatomical site sequenced, sex of the donors, as well as donor age (573,574). Similarly, concerns have also been raised over the methods required to prepare single cells from tissue, with some suggesting this could result in preferential selection of certain populations over others (573). As cellular heterogeneity is likely to change between individuals as well as throughout tendon development, this further highlights the need for more sequencing data to be generated, with additional insight likely to be obtained by analysing tendons across many different sites, developmental stages and injury timepoints (574) (Figure 6.2).

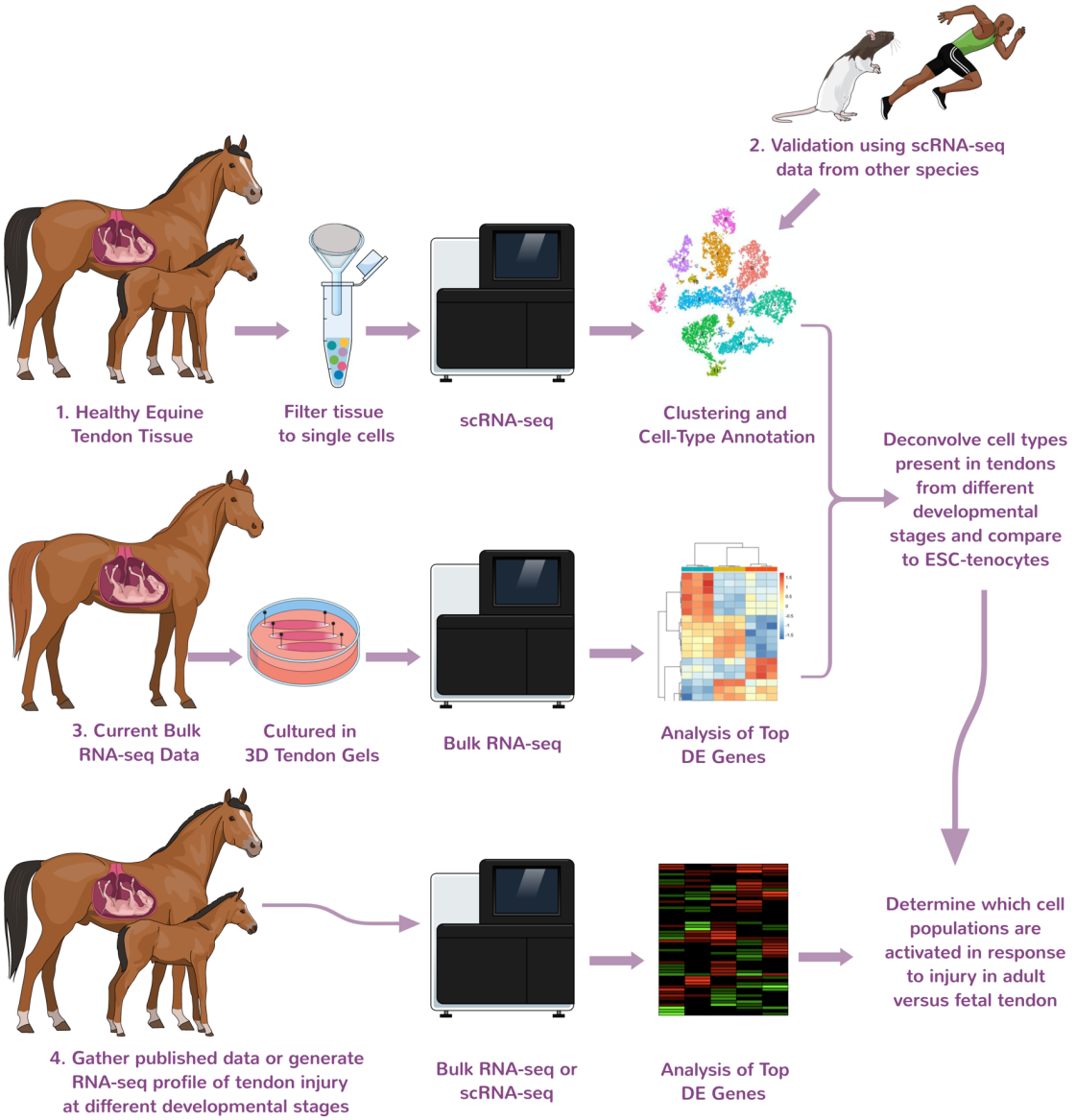

Figure 6.2. Theoretical experiment using scRNA-seq. Schematic showing a theoretical workflow for determining the gene expression signature and population dynamics in different stages of tendon injury and development. 1) A tendon tissue biopsy from the SDFT obtained from fetal, young postnatal and adult horses would be prepared by dissociating the tissue into single cells immediately *ex-vivo*. Resulting cells would then be subjected to scRNA-seq and clustering and cell type annotation performed. 2) The cell type clusters identified would then be validated using data from other scRNA-seq experiments of the same tissue. 3) The bulk RNA-seq data presented in this thesis could then be used to deconvolve and confirm the cell types present in the tendons from the different developmental stages which could then be compared to the ESC-tenocytes to determine which population fraction they appear to be. This could also inform as to which populations may be unintentionally selected for in culture. 4) Previously published datasets or newly published studies looking at the RNA-seq profiles of injured tendon tissue from different developmental stages could then be used to deconvolve the cell-type gene signature present during injury. This information could help determine if different populations respond to injury in adult reparative and fetal regenerative healing. Figure inspired by Rubenstein *et al*., 2020 (576).

6.2.3. SCX as a therapeutic target

As described in section 6.2.2 although SCX has always been thought of as a selectable marker for tendon cells, it is clear that its expression is actually quite heterogeneous within the tendon cell population (573,574). Glimpses of this heterogeneity have also been indicated in adult injury repair models, with various SCX tracking systems showing that SCX positive cells are the main players in the injury repair process (161,429–431,577), playing a key role in the induction of fibrosis in various adult tissue types (see chapter 4). However, the role of SCX in fetal injury repair has not been reported.

In this thesis, using SCX knockdown it was apparent that in adult and fetal tenocytes SCX regulated ECM genes and fibrillar collagens differently. This mechanism of SCX dependant modulation of ECM and collagen gene expression is being increasingly documented, and appears to be conserved across tissues (428,444,578). Changes in the ECM and collagen synthesis are well recognised as important factors in wound healing, the composition and arrangement of which determines if scarring presents (278). Taken together, if SCX differentially regulates ECM production and degradation in adult and fetal injuries, could this affect whether or not tendon fibrosis ensues? If this is the case, the ability to modulate SCX function may therefore provide a mechanism to fine tune the rate of ECM production and degradation to improve wound healing, thereby preventing unwanted tissue fibrosis (578).

A recent study, which has not yet undergone peer-review, has described that SCX depletion in adult mice improves tendon healing, with injured tendons displaying reduced stiffness, increased maximum load to failure and differential expression of matrix related gene expression post injury compared to wild type littermates (579). SCX therefore presents as an interesting target for therapeutic drug design. However, several factors need to be considered when designing drugs to target transcription factors which have historically been considered ‘undruggable’ (578,580,581). These include the fact that transcription factors function via protein-protein or protein-DNA interactions and so typically lack active sites, unlike enzymes for example which have ligand-binding sites which make them more suitable for binding of small molecules (578,582). Similarly transcription factors lack pores or channels and generally have shallow surface involutions which again prohibit small molecule binding (578,582). Strategies to modulate transcription factors are being developed, which include manipulating

transcription factor DNA binding domains using peptidomimetics or blocking protein-DNA binding by compounds that compete with the transcription factor, which may allow SCX to be targeted (581).

However, SCX has the added challenge of being intracellularly expressed, therefore it is likely that any therapeutic would first have to target tenocytes prior to being internalised which, due to the lack of specific markers defining the tendon cell population, is likely to prove difficult (583). This further highlights the need for collaborative efforts to generate more transcriptomic data to allow reliable tendon cell markers to be determined. Another translational barrier includes our limited understanding of the effects of inhibiting or activating SCX *in vivo*. As described in chapter 4 and 5, SCX is highly expressed across a variety of ECM rich tissue types, with its role likely to be highly context specific, therefore off-target effects need to be considered during drug design. Further studies using pre-clinical models of tendon fibrosis are therefore required to evaluate the effects of SCX interference in a clinical setting across tissues.

An alternative strategy for modifying SCX expression therapeutically may be to target another candidate or pathway upstream of SCX. TGF-β is a key mediator of tendon remodelling and has been demonstrated to be an upstream regulator of SCX expression (140,154,175,182,446–448,457,465). Three main TGF-β isoforms are involved in the wound repair process, the expression of which differs in adult versus fetal wounds (41,278,544). In fetal wounds TGF-β3 is elevated in comparison to TGF-β1, whereas in adults TGF-β3 has a delayed expression with TGF-β1 showing more rapid induction and slower clearance from the wound (41,278,544). As such TGF-β3 has been postulated as being anti-fibrotic, with the addition of exogenous TGF-β3 in some animal models showing decreased scar tissue formation (584,585). Conversely, TGF-β1 has been considered as pro-fibrotic, with studies blocking its expression showing some reduction in scar tissue formation (584,586). Attenuation of TGF-β expression, such as through the use of a TGF-β receptor inhibitor, may therefore provide a means to augment SCX expression as described *in vitro* (587). However, due to the huge variety of roles played by TGF-β across many cell and tissue types caution would again need to be exercised.

Considering that alteration of SCX and potential upstream targets of SCX expression may have such wide-ranging effects *in vivo*, the data presented in this thesis acts as a crucial resource to help bridge the gap in our understanding of SCX-dependent gene regulation.

By carefully comparing and contrasting the biology between fetal and adult tendon cells and how SCX may differentially affect gene expression and ECM composition during injury repair it is possible that new targets for therapeutics may be determined (Figure 6.3).

One potential candidate for further investigation is platelet derived growth factor subunit B (*PDGFB)*. *PDGFB* was significantly decreased following SCX knockdown in fetal tenocytes, with SCX being demonstrated to directly bind to an E-box within its promoter region suggesting that SCX directly regulates fetal tenocyte *PDGFB* expression. In adult SCX knockdown tenocytes however, no significant difference in *PDGFB* expression was found. SCX did appear to be bound to the *PDGFB* gene promoter in adult tenocyte, however the lack of effect on *PDGFB* gene expression following SCX knockdown suggests that SCX may only be passively binding, requiring other co-activators to activate its expression. As described in section 6.2.1, growth factors are known to play a key role in tissue healing, having multiple functions including stimulating cell proliferation, aiding angiogenesis, orchestrating cellular differentiation and stimulating chemotaxis (588). PDGF is one such growth factor which is heavily implicated in wound healing, being a potent chemoattractant and mesenchymal cell mitogen (589–592). Furthermore, PDGF has been demonstrated to increase fibroblast proliferation, migration and collagen synthesis, with its *in vivo* application into incised skin wounds showing enhanced ECM deposition during the wound healing process (593–598).

In chapter 3, *PDGFB* mRNA expression was significantly increased in both 3D cultured fetal tenocytes and ESC-tenocytes compared to adult tenocytes. Fetal rat lung fibroblasts and fetal rat skin have also been demonstrated have increased *PDGFB* expression, which decreases with gestational age (589,599). The levels of PDGF and its receptors are similarly decreased in diabetic and aged mice which display delayed wound healing, as well as being reduced in nonhealing human ulcers (600–602). In fact, PDGF-BB, the protein product encoded by the *PDGFB* gene, is already approved for topical treatment of diabetic non-healing foot ulcers (603), with clinical trial data showing as much as a 39% increase in wound healing compared to the placebo (604,605). The use of *PDGFB* gene delivery into rat Achilles tendons has also been investigated, with treated tendons demonstrating accelerated healing compared to untreated controls. *PDGFB* induction resulted in tendons with significantly greater maximum load to failure, maximum stress

and Young's modulus as well as higher structural organisation as observed by histological analysis (606). Likewise *in vivo* induction of the *PDGFB* gene in healing rat ligaments resulted in enhanced collagen and ECM deposition, enhanced angiogenesis and accelerated healing (593).

Taken together with the results demonstrated in this thesis, PDGFB therefore presents as an interesting candidate for future studies. It would therefore be worth further deconvolving this potential pathway between SCX and PDGFB, as well as determining if PDGFB is DE during fetal and adult wound healing. Using the aforementioned wound healing models (section 6.2.1) altering *PDGFB* expression via gene delivery could also be conducted to determine its effect on the rate and degree of wound healing in adult equine tenocytes. As ESC-tenocytes had similar high expression of *PDGFB* compared to adult tenocytes it would also be worth determining if SCX knockdown also alters *PDGFB* expression like that of fetal tenocytes, and whether ESC-tenocyte addition to the wound healing model would result in increased PDGF levels and effect the rate of wound healing.

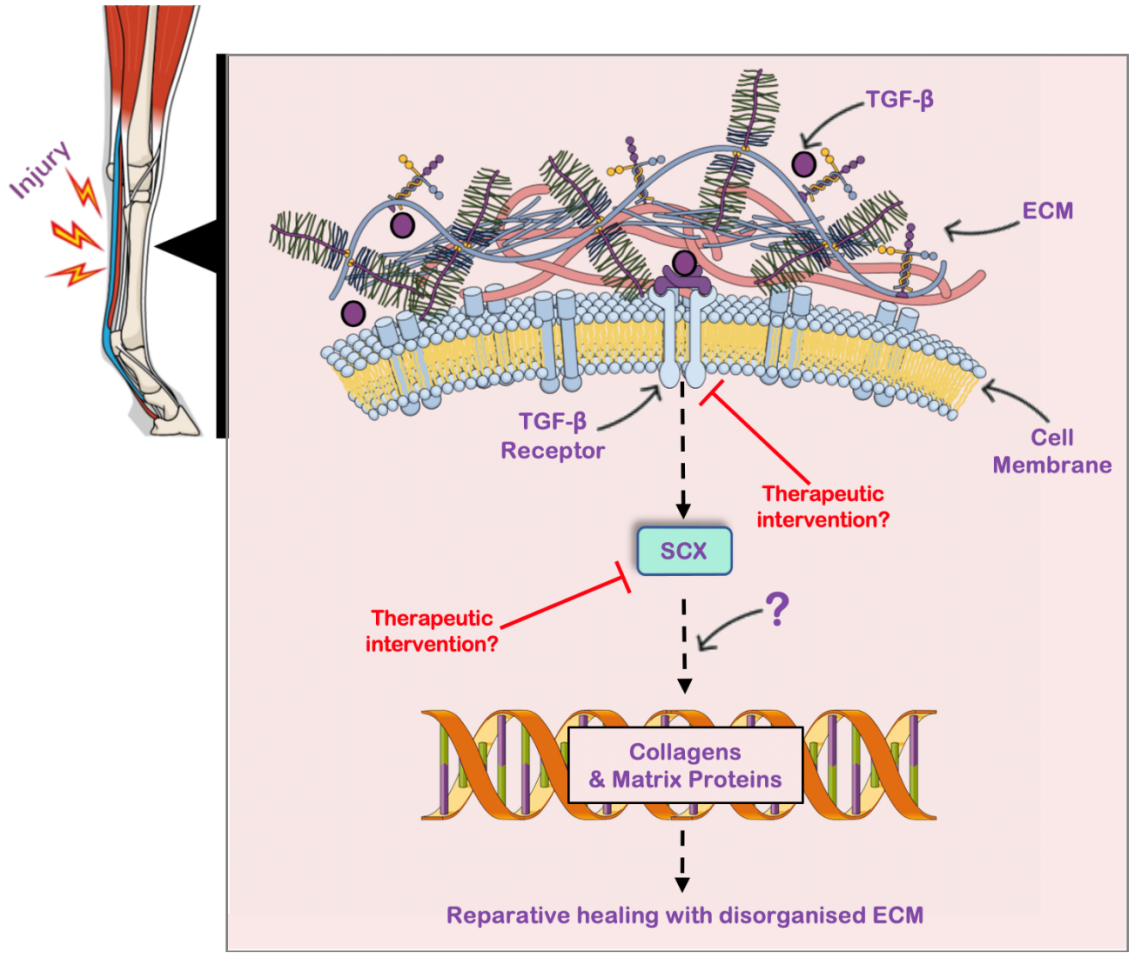

Figure 6.3. Theoretical model of adult injury/repair and potential therapeutic interventions. Damage and physical force have been demonstrated to induce both the expression of growth factors, as well as SCX expression in the injured tendon. How this induction occurs is not fully understood. Injury-induced induction of growth factors, including TGF-β, have been demonstrated to increase SCX expression in tenocytes. Up-regulation of SCX in response to TGF-β, and potentially other factors as represented by the dashed lines, leads to changes in the expression of various downstream target genes, including collagens and ECM proteins. Which collagens and matrix proteins are affected may result in whether scarring ensues. It has therefore been hypothesised that scarring may occur due to inappropriate SCX expression. This indicates SCX or genes upstream of its regulation as potential therapeutic targets. Or similarly, by carefully examining the data produced in this thesis to identify genes that are downstream of SCX regulation in fetal regenerative and adult reparative cells, other potential candidate genes or pathways involved in the scarring phenotype could be determined.

6.2.4. Are ESCs now safe for therapeutic use?

Given the information generated in this thesis, the question remains: Where do we now stand on using ESCs therapeutically? As suggested in section 6.2.1 more work is still required to determine if ESC-tenocytes function like that of fetal tenocytes in a wound injury environment, but there is still another key factor which needs to be considered.

Although tendon injuries have historically been characterised as degenerative conditions devoid of inflammation, our understanding of the disease paradigms have shifted (607). In both horses and humans evidence now indicates a strong inflammatory response is present, with a range of inflammatory cells and cytokines being induced following tendon injury, some of which are described in chapter 1 (558,608–610). In contrast, one of the hallmarks of scarless fetal tendon healing is a dampened inflammatory response, with the fetal wound microenvironment having fewer resident and recruited circulating inflammatory cells as described in chapter 3 (284,324,326–333). Many of these inflammatory cells and released factors have negative impacts on local tendon cells, resulting in the production of inappropriate levels of collagens and matrix proteins which can ultimately results in fibrosis (610). Considering the negative consequences of inflammation on endogenous tendon cells, this leads to the question: Will the same occur to those applied during a cell-based therapy?

Equine ESCs and ESC-derived tenocytes have been demonstrated to be immune privileged, with allogeneic immune cells showing no proliferation in response to their addition *in vitro* (72,107). Similarly, *in vivo* studies in the horse have shown high survival rates of injected ESCs into mechanically induced SDFT injuries with a gradual decrease in leukocytes at the injection site, suggesting that they do not induce immune cell stimulation over a 90 day period (91). More recently they have also been demonstrated to possess a degree of protection from the effects of inflammatory cytokines, including IL-1β, due to a failure to activate the NF-kappa B signalling pathway which regulates multiple aspects of the innate and adaptive immune system (608,611,612). Studies using human and mouse ESCs have also demonstrated that the interferon system, another fundamental component of the innate antiviral immunity in differentiated cells (613), is underdeveloped in ESCs which similarly contributes to the lack of immune response observed by pluripotent cell types (612,614–618).

ESCs lack of inflammatory response is likely due to the fact that during early development any negative changes in proliferation and differentiation, as a result of negative inflammatory regulators, could severely impact embryonic development, and as ESCs reside within the womb the maternal immune system likely acts as the main source of protection (612). The lack of inflammatory response by ESCs and ESC-derivatives may provide an advantage for ESC-derived cellular therapeutics as the implanted cells

would not respond to the inflammatory response already present in the wounded area, thus preventing additional damage caused by the host's immune system (612). However it remains unclear whether over longer periods transplanted ESC-derivatives would develop the ability to respond to inflammation and lose their immune privileged status leading to their rejection (608).

Unlike MSCs, ESCs do not appear to be capable of modulating the immune environment (72,107). As such, although they themselves may be protected from inflammation upon therapeutic injection, the endogenous adult cells will remain unprotected and will therefore likely still contribute to scar tissue formation. It may be the case that therapeutic strategies using cell therapies in conjunction with other pharmaceuticals which can reduce inflammation, may be a better solution for treating tendon injuries. Further characterization of ESC-tenocytes long term response to inflammation, and to what degree the hosts immune response may affect them if they were applied therapeutically is therefore required (612). The data collected in this thesis may help in this objective, allowing immune response pathways which potentially facilitate this immune protection to be uncovered.

Data from this thesis has already assisted other work within our laboratory, looking at the effects of the inflammatory cytokine IL-1β on adult, fetal and ESC-tenocytes. IL-1β is a key inflammatory cytokine which is upregulated rapidly following tendon injury (619) . It has been shown to induce tendon fibroblasts to increase expression of inflammatory and catabolic enzymes including IL-6 and MMP-13 (34), and reduce expression of type I collagen leading to tendons with reduced elastic and tensile strength (620). Molecules which regulate IL-1 signalling include the IL-1 receptor antagonist IL-1RA, encoded by the *IL-1RN* gene. IL-1RA competitively binds to the IL-1R1 receptor, which is responsible for IL-1 signal transduction, preventing IL-1β from inducing an inflammatory, angiogenic or haematopoietic response (621). Interestingly, from the RNA-seq data presented in this thesis, it is evident that ESC-derived tenocytes were found to have significantly lowered expression of the *IL1-R1* receptor gene as well as a significant increase in *IL-1RN* expression, relative to adult tenocytes. This suggested that IL-1β could be being blocked from interacting with the IL-1R1 receptor and thus potentially not eliciting as substantial an inflammatory response through this system. Similarly, the ESC-tenocytes, in comparison to both fetal and adult tenocytes, showed

significantly increased expression of *IL-1R2*, the gene which encodes what is known as the decoy receptor which acts as an endogenous inhibitor of the IL-1 signalling pathway (621). This finding was further explored at the protein level and taken together helped to strengthen the evidence that ESC-tenocytes are protected from the detrimental impact of IL-1β (608). As many other inflammatory genes and receptors including several members of the interferon gamma (IFN-γ) and tumour necrosis factor (TNF) families were also found to be DE in ESC-tenocytes compared to adult tenocytes, further investigation into the effects of such inflammatory factors on these different cells types may shed more light on ESC-tenocytes inflammatory protection.

Other obstacles in the way of clinical translation of ESC-derived cells include concerns about their safety and ability to be produced commercially in line with good manufacturing practice (GMP) (622). Safety and toxicity studies should be carried out to ensure that the stem cell derivatives are nontoxic and clinical trials should be conducted to test for any acute infusion toxicity resulting from the damage at the injection site as well as in the adjacent tissue (622). Similarly karyotyping stability analysis should be conducted on ESCs and ESC-derivatives to minimise potential tumour development (623). The inherent genetic and epigenetic variability of ESCs also needs to be taken into consideration, as it can lead to variability in the differentiation potential and purity of the final cell product. Therefore extensive safety and purity testing would need to be conducted on a cell line to cell line basis (622). Although the clinical requirements for animal and human therapeutics differ, equine pluripotent cell derivatives would likely be held to similar regulatory scrutiny, including adherence to current GMP and rigorous quality control. For human cell therapies, the use of defined culture systems which avoid using chemically undefined materials or those of animal origins are required, which would present an issue for equine ESC culture which relies on the use of fetal bovine serum and mouse embryonic feeder cells to support them (622,623). Ongoing advances to improve equine ESC culture and insurance of reliable cellular differentiation into the desired cell population for therapeutic use are therefore required before considering their use clinically.

6.2.5. Concluding remarks

Overall the data presented in this thesis provides an important insight into the fundamental differences between adult reparative and fetal regenerative cells. Further mining of these data sets alongside comparison to other publicly available data is likely to help identify key factors involved in the scarring process and highlight if ESC-derived tenocytes will indeed be of use as a regenerative therapy.

Appendix A

List of additional data contained in appendix A:

1. List of 441 genes identified as differentially expressed between adult and fetal 3D cultured tenocytes using both HISAT2 and Salmon mapping pipelines.

2. List of 113 genes identified as differentially expressed between adult and fetal 3D cultured tenocytes using HISAT2 mapping only.

3. List of 101 genes identified as differentially expressed between adult and fetal 3D cultured tenocytes using Salmon mapping only.

Table A1. List of DE genes between adult and fetal tenocytes cultured in 3D identified using both alignment-based and alignment-free mapping. 441 genes identified as being DE in adult and fetal tenocytes cultured in 3D using both HISAT2 alignment-based and Salmon alignment-free mapping using a p-adj of < 0.01 and ±2 Log2FC.

		HISAT2 mapping		Salmon mapping	
Ensemble Gene ID	Gene name	Log2 FC	p-adj.	Log2 FC	p-adj.
ENSECAG00000000136	FERMT1	-2.341533	0.00019245	-2.2928457	1.5161E-05
ENSECAG00000000178	RUNX1T1	3.67764308	0.00040125	3.90848913	2.3893E-06
ENSECAG00000000197	TLR3	-4.2669688	0.00129345	-4.2296717	0.00130197
ENSECAG00000000207	ACTA1	4.77285617	0.00014215	4.58471547	0.00047126
ENSECAG00000000239	FNDC1	4.26812098	0.00054429	4.9822643	3.6938E-08
ENSECAG00000000250	CILP2	6.41796104	7.1199E-09	6.23329495	2.8782E-08
ENSECAG00000000353	HPSE2	2.7564817	0.00128162	2.84937111	0.00635759
ENSECAG00000000487	SYNM	3.60778085	8.1415E-16	3.71384156	3.876E-14
ENSECAG00000000599	PCDH7	-2.2547179	1.3041E-06	-2.279693	1.3714E-06
ENSECAG00000000607	TRIB3	2.15943662	0.00037732	2.16287566	0.00012748
ENSECAG00000000627	PDZRN4	4.36965886	0.00093755	4.42726835	0.00229385
ENSECAG00000000734	HMGA1	-3.4200441	5.2784E-16	-3.2671461	2.3321E-14
ENSECAG00000000794	EMB	-3.2597391	0.00015949	-3.4919696	0.00033872
ENSECAG00000001021	ARL4D	2.188635	8.6134E-07	2.07512549	2.3981E-06
ENSECAG00000001688	PCSK6	2.50487687	0.00015877	2.55598718	5.4715E-06
ENSECAG00000001716	PLXNA2	2.76268237	6.4402E-06	2.76037931	5.1934E-07
ENSECAG00000001775	RAB38	-2.1486168	0.00049394	-2.009058	0.00560114
ENSECAG00000001845	P2RY1	5.45203974	0.00530962	4.71114096	0.00823615
ENSECAG00000002211	CD80	-4.0564748	0.00018706	-4.2007679	6.6853E-05
ENSECAG00000002225	SLC6A9	2.25208921	3.5192E-06	2.32291777	5.6812E-08
ENSECAG00000002523	SOWAHB	-3.6340245	0.00220145	-3.7663331	0.00810117
ENSECAG00000002918	BMP7	-5.9741652	5.8711E-08	-5.8157359	1.0491E-07
ENSECAG00000003072	TCIM	-2.9589384	2.8621E-05	-2.995744	4.9934E-08
ENSECAG00000003106	C3AR1	-4.6097727	0.0013045	-4.8672658	0.00041079
ENSECAG00000003201	PRSS35	2.4574136	0.00771137	2.46807185	0.00019981
ENSECAG00000003260	ITIH5	3.82392471	0.00052453	3.79864558	0.00145321
ENSECAG00000003266	PIRT	-3.5618165	4.3714E-05	-4.2829499	0.0037617
ENSECAG00000003277	REL	-2.5969253	7.9618E-11	-2.5127539	5.3694E-10
ENSECAG00000003563	BST2	-6.2736958	0.00090832	-5.8053981	0.00092009
ENSECAG00000003748	PYROXD2	3.30303158	7.4154E-07	4.23272918	3.0215E-07
ENSECAG00000004234	MMP28	3.93778509	4.0577E-07	4.06595303	4.7699E-06
ENSECAG00000004274	IQGAP2	-2.7727862	0.00085209	-2.8559454	0.00186826
ENSECAG00000004408	GPR1	3.78414544	0.00204524	4.28532415	0.00457052
ENSECAG00000004433		-5.835328	0.00807216	-5.0445845	0.00886545
ENSECAG00000004501	FDCSP	-6.6847223	0.00118253	-5.6575216	0.00105275
ENSECAG00000004678	CYSLTR2	-6.5306547	6.8525E-07	-6.2679821	2.5762E-11
ENSECAG00000004913	LPAR6	-3.9495141	7.0539E-06	-3.8467496	1.0309E-12
ENSECAG00000005046	MAB21L2	6.43702054	1.5675E-11	6.58767315	1.2007E-09
ENSECAG00000005302	GJB5	-2.3111674	0.00520971	-2.3417413	0.00238449
ENSECAG00000005384	SPRY4	-2.5111307	3.831E-05	-2.5309516	8.2592E-06
ENSECAG00000005468	PTPRN	-4.6703276	9.662E-05	-4.8962991	2.1748E-07
ENSECAG00000005515	GCNT4	-3.9371659	0.0058059	-4.5854534	0.00019981
ENSECAG00000005573	LOXL4	4.21243948	2.3676E-51	5.03891971	1.0896E-55
ENSECAG00000005574	TMEM51	-2.3843387	0.00143317	-2.498003	0.00015297

ENSECAG00000005704	CARD11	-5.3134338	3.7108E-07	-5.3185911	3.0493E-06
ENSECAG00000005794	MYRIP	-3.5737136	1.4054E-05	-3.7798034	1.2321E-08
ENSECAG00000005814	NEDD9	-2.0598726	0.00013424	-2.0359116	0.00020861
ENSECAG00000005880	RIMKLA	2.76506368	0.00044877	2.65204752	0.00151916
ENSECAG00000006011	RALGPS2	-2.0452634	9.2724E-06	-2.0344183	5.6856E-08
ENSECAG00000006269	SHISAL1	-2.62105	0.00081358	-2.8407084	0.00319114
ENSECAG00000006288		-2.570234	0.00058339	-2.6747484	0.00026787
ENSECAG00000006290	TGM2	-3.5348761	7.2032E-10	-3.6121988	5.1433E-12
ENSECAG00000006338	ANKH	2.95687034	1.9182E-17	3.0175591	1.2121E-17
ENSECAG00000006466	CLDN4	-3.0147664	1.0353E-05	-3.2621497	2.9936E-10
ENSECAG00000006482	CRISP2	-8.1319114	0.00017186	-7.3133794	0.0003983
ENSECAG00000006511	MCHR1	-2.743014	0.00090744	-2.7767734	0.00025378
ENSECAG00000006554	PRRG4	-4.6587619	4.3413E-07	-4.377222	2.5967E-06
ENSECAG00000006567	SLITRK4	-8.3325272	1.2582E-21	-8.5344888	1.8443E-31
ENSECAG00000006646	MUC1	2.11697132	0.00093599	2.14480336	0.00114485
ENSECAG00000006669	ACSM3	3.69286944	1.5798E-07	5.38751195	1.0778E-05
ENSECAG00000006764	CCL20	-2.8715593	8.7989E-09	-2.6258628	7.1817E-05
ENSECAG00000006829	KAZN	-2.0180576	1.8215E-16	-2.0064087	8.1567E-15
ENSECAG00000006867	CDC42EP2	-2.2710903	0.00288405	-2.1874499	0.00618302
ENSECAG00000006880	WNT16	-4.3050993	0.00040771	-4.4414496	0.00097527
ENSECAG00000006914	ELFN2	-2.6759538	4.505E-05	-2.5701959	0.0001013
ENSECAG00000007066	RASSF4	2.59247127	6.7751E-05	3.14052841	0.0006905
ENSECAG00000007242	DUSP2	-4.4615291	0.00523304	-4.6905128	0.00369096
ENSECAG00000007246	CDH8	-4.008536	0.00033632	-3.6375474	0.00246826
ENSECAG00000007379	KCNE3	-5.2660709	1.8237E-11	-5.1955568	4.966E-18
ENSECAG00000007388	ADCYAP1R1	-7.0114935	0.00026051	-6.471501	0.00058952
ENSECAG00000007395	FAM160A1	2.55876033	1.0627E-07	2.48034315	4.9623E-06
ENSECAG00000007432	PTGDR	-5.5693061	0.00022851	-5.5555118	0.00033709
ENSECAG00000007540	CYP7B1	-2.0151221	3.9474E-05	-2.048868	0.00011698
ENSECAG00000007584	HCN1	-5.5369906	0.00095178	-5.5094149	0.00342251
ENSECAG00000007588	EREG	-4.2632313	0.00018887	-4.0866166	1.5956E-06
ENSECAG00000007761	DSC2	-4.3958865	1.0372E-15	-4.5078975	4.1397E-10
ENSECAG00000007825	CALCA	-4.5051221	0.00483056	-4.0089898	0.00690374
ENSECAG00000007918	TNS4	-4.0066786	3.5253E-06	-4.2496032	2.6796E-08
ENSECAG00000007960	LIMD2	-2.4057232	0.00484533	-2.416066	0.00357234
ENSECAG00000007974	GALNT3	-5.0255001	0.00151866	-4.5100546	0.00673051
ENSECAG00000008049	EPOR	2.81617619	9.496E-07	2.84468637	3.3667E-05
ENSECAG00000008193	UPP1	-2.086778	0.00015394	-2.038898	0.00049095
ENSECAG00000008270	FABP5	-2.1524375	0.00075842	-2.3238343	5.6519E-05
ENSECAG00000008330	RIPK4	-2.0948989	0.00031084	-2.0457534	2.0722E-05
ENSECAG00000008335	PDK4	-2.7938745	0.00649576	-2.8267977	0.00384434
ENSECAG00000008425	LURAP1L	5.08907931	1.3715E-13	5.2726881	8.1444E-18
ENSECAG00000008483	GXYLT2	3.34432413	8.0214E-06	3.64031273	2.1748E-07
ENSECAG00000008512	ANKRD33	-3.6948136	0.00130399	-3.7434643	0.0002711
ENSECAG00000008569	TMTC1	3.42818595	0.00274336	3.93095053	5.2856E-06
ENSECAG00000008799	ENPP4	3.02171643	0.00025991	2.9104868	0.00059637
ENSECAG00000008830	WNT5A	-4.0419136	3.0943E-05	-3.8792772	2.7193E-05
ENSECAG00000008871	ALDH1A3	2.6073234	0.00075395	2.51436654	0.00139635
ENSECAG00000008923	THBS1	2.18960517	0.00490194	2.14916222	1.2916E-08
ENSECAG00000008940	TMEM40	3.04498252	0.00128661	3.31016443	0.00169943
ENSECAG00000008993	HIP1R	2.21529678	1.345E-17	2.17187095	8.0079E-19
ENSECAG00000009011	FLRT2	2.24841091	0.00114766	2.45109542	5.8731E-05
ENSECAG00000009038	TMEM255A	2.6311439	0.00017987	2.94093408	4.2899E-06
ENSECAG00000009044	PRDM1	-3.7074327	8.0543E-05	-3.3668736	0.00044769

ENSECAG00000009047	RIBC2	-4.7224658	2.5204E-06	-4.5845932	0.00025694
ENSECAG00000009067	SLC16A6	-5.5676769	3.7676E-07	-5.9149941	8.2221E-07
ENSECAG00000009136	PRXL2A	-4.6277029	9.4944E-14	-4.2801895	7.1607E-19
ENSECAG00000009165	IZUMO1	3.64902062	3.9633E-07	3.33655966	2.387E-05
ENSECAG00000009316	EYA4	3.00456923	0.00804752	3.1398433	0.00333294
ENSECAG00000009375	GASK1A	4.68501483	1.5155E-12	4.72476752	8.8428E-13
ENSECAG00000009398	STS	-2.0444101	1.9376E-09	-2.0081254	2.0003E-07
ENSECAG00000009485	GPT2	2.11337777	0.00109661	2.20648848	0.00013745
ENSECAG00000009515	ATRNL1	2.35322392	0.00147208	2.31114589	0.00205616
ENSECAG00000009668	SCRG1	4.53657908	1.2452E-07	4.18998061	0.00023604
ENSECAG00000009700	ANK3	-3.5194349	1.3541E-14	-3.6583586	8.5835E-16
ENSECAG00000009707	PTGS1	-4.3359346	0.00193875	-4.6026289	0.00030653
ENSECAG00000009723	IGF2BP1	-2.8319188	0.0020927	-2.6387243	0.00352383
ENSECAG00000009742	S100A12	3.0176703	0.00105832	2.83512666	0.00286727
ENSECAG00000009755	EPHB3	3.00741512	3.4378E-08	3.02931323	3.418E-08
ENSECAG00000009779	SORCS2	2.9808972	0.00868468	4.07109889	4.2899E-06
ENSECAG00000009839	VAT1L	3.81505934	6.2386E-06	3.76611532	5.6519E-05
ENSECAG00000009887	COL21A1	-4.4545224	0.00038728	-4.5500276	0.0038423
ENSECAG00000009916	GRIA4	-6.6105951	4.7445E-07	-6.5254339	0.00041079
ENSECAG00000010048	IGSF11	-5.7392746	5.9224E-05	-5.4670265	0.00064118
ENSECAG00000010098	GDPD5	2.17176242	2.4356E-06	2.15792352	1.161E-06
ENSECAG00000010109	IGF1	5.31887202	6.6283E-07	5.70035693	4.9803E-07
ENSECAG00000010118	SRGAP3	3.81657047	0.00015877	3.99716856	0.00176502
ENSECAG00000010145	LPL	-5.7381072	0.00015877	-5.5681756	7.6401E-05
ENSECAG00000010238	CECR2	-4.3201175	1.3706E-17	-4.267903	1.1368E-16
ENSECAG00000010558	PTGFR	2.73634194	6.6408E-06	2.75284184	7.7624E-06
ENSECAG00000010573	CELSR1	-2.2120294	0.001453	-2.1848833	0.00187295
ENSECAG00000010617	VGLL3	2.32801133	0.00077699	2.33876467	1.0732E-07
ENSECAG00000010619	F12	2.42612524	4.7637E-10	2.38144394	1.565E-08
ENSECAG00000010695	FGF21	5.22773832	7.4154E-07	5.09499831	5.0172E-11
ENSECAG00000010700	CREG2	-2.1170458	0.00080862	-2.1167863	0.00523199
ENSECAG00000010739	ITGA2	-3.0156319	0.00128661	-2.7468713	0.00187814
ENSECAG00000010760	MEOX2	3.93970992	3.5408E-09	3.92542584	5.8459E-08
ENSECAG00000010773	PLAG1	-3.811448	2.1066E-08	-3.7144938	1.6585E-08
ENSECAG00000010778	VWF	4.45980086	0.006166	4.74931544	0.00881557
ENSECAG00000010791	LMCD1	4.96197127	1.5667E-05	5.9484775	2.1667E-09
ENSECAG00000010880	SOX6	2.82292549	3.6676E-05	2.59480777	0.00093069
ENSECAG00000010917	HR	3.45912199	3.1047E-20	3.41467206	1.997E-18
ENSECAG00000010928	MMP25	-4.2625304	0.00203897	-3.6161254	0.00881557
ENSECAG00000011217	INHBE	3.74620239	0.00439768	5.12677257	1.9758E-05
ENSECAG00000011229	SLC1A4	2.77792158	7.4501E-09	2.81862572	2.3929E-12
ENSECAG00000011246	GLI1	3.1877193	3.4858E-05	3.36024139	0.0010811
ENSECAG00000011404	SAA1	3.92059635	3.6676E-05	3.14671498	0.00056136
ENSECAG00000011449	ANKS1B	-3.9406144	0.00104941	-3.9969337	0.0019183
ENSECAG00000011626	S1PR1	-4.4899513	0.00085209	-4.5430344	0.00070264
ENSECAG00000011774	APCDD1	-3.6291738	3.5421E-05	-3.6803379	4.4259E-06
ENSECAG00000011994	CYFIP2	-3.7137695	0.00026136	-3.3362598	0.00025378
ENSECAG00000012061	CES2	2.4194751	0.0032751	2.89749544	0.00294133
ENSECAG00000012189	PDE8B	-4.474614	2.6939E-10	-4.6424131	3.3699E-09
ENSECAG00000012212	LRP1B	6.88623685	0.00564666	7.87559141	0.00290038
ENSECAG00000012229	BIRC3	-2.9177185	5.2775E-08	-2.7884153	1.3149E-08
ENSECAG00000012253	CXCL11	-11.082013	0.00340506	-10.170191	0.00714945
ENSECAG00000012282	MPP7	3.21352824	4.5591E-06	3.14332021	0.00014574
ENSECAG00000012327	IL34	2.17463725	1.1446E-06	2.31247856	5.8965E-06

ENSECAG00000012330	LRRC31	4.55384338	0.00148158	5.01789975	0.00261895
ENSECAG00000012370	NPTX2	-5.6616042	0.00130399	-6.0744933	0.00393692
ENSECAG00000012476	PROSER2	2.25472502	1.9074E-05	2.34852927	2.5322E-06
ENSECAG00000012619	CASP14	4.61030456	1.3766E-05	4.97392359	3.9315E-05
ENSECAG00000012662	SEMA3A	-2.1879658	0.00409295	-2.0967904	0.00826553
ENSECAG00000012734	BAIAP2L1	-2.5271569	4.9862E-14	-2.8539484	3.1362E-20
ENSECAG00000012742	CXCL6	-2.8005259	8.1725E-05	-2.7496189	0.00027203
ENSECAG00000012799	COL8A2	2.74091557	1.5798E-07	2.72025264	9.5808E-06
ENSECAG00000012861	TBX3	-2.2270779	7.836E-05	-2.2219292	7.7681E-05
ENSECAG00000012862	LYN	-2.5401625	2.4484E-06	-2.5116837	5.5958E-10
ENSECAG00000012887	CPZ	3.09730212	5.0165E-10	3.12447622	8.0309E-09
ENSECAG00000012955	CD163L1	-6.8621826	0.00330189	-6.8290589	0.00222121
ENSECAG00000013151	RGCC	-2.848275	1.7963E-21	-2.7812529	2.182E-19
ENSECAG00000013176	MEGF6	2.57832397	7.5613E-05	2.57033894	0.00022715
ENSECAG00000013300	CXCL10	-9.1320788	0.00028358	-7.5602863	0.00115525
ENSECAG00000013422	SLC12A2	-2.1150272	1.1343E-07	-2.1118252	3.4961E-07
ENSECAG00000013515	SEMA3B	2.58766669	0.00118766	2.92254743	0.00051024
ENSECAG00000013566	PKP2	5.36293348	1.5798E-07	5.18898846	1.8108E-07
ENSECAG00000013582	DHRS3	3.10205658	5.9779E-09	3.16664357	7.3351E-12
ENSECAG00000013584	PSAPL1	6.09640446	0.00043858	5.63803817	0.00295386
ENSECAG00000013597	DAB2	2.06192089	2.3656E-05	2.20840572	1.7256E-10
ENSECAG00000013677	FRY	-2.8504223	5.2403E-05	-2.9054275	5.8487E-05
ENSECAG00000013749	MBOAT1	2.69040878	1.0049E-07	2.7450555	3.5299E-09
ENSECAG00000013771	PDE4D	-2.1155845	6.8708E-09	-2.2243225	1.2271E-08
ENSECAG00000013788	ARHGDIB	-4.1692158	6.0393E-09	-4.1113517	1.0732E-07
ENSECAG00000013869		3.1217982	0.00338856	3.76415206	0.00018639
ENSECAG00000013952	CADM4	-2.352879	0.00013409	-2.3955103	0.00015165
ENSECAG00000014017	PRKG1	-3.7305763	0.00094603	-3.6554	0.0017102
ENSECAG00000014243	GATM	4.97324108	8.7192E-17	5.05890143	2.3321E-14
ENSECAG00000014287	OMD	3.07235008	0.00311271	3.02817537	0.00316067
ENSECAG00000014295	PI3	-2.6971065	0.0082286	-2.539022	0.00126437
ENSECAG00000014357	DLL1	-3.0370686	1.7193E-12	-3.0183911	4.2929E-13
ENSECAG00000014358	RERG	-4.1697883	0.00044931	-4.4133738	0.00015339
ENSECAG00000014372	SLC9A3R1	-3.7192229	0.00387964	-4.0891085	0.0004864
ENSECAG00000014414	SPI2	7.34623534	0.0002379	7.20655131	0.00814425
ENSECAG00000014504	KIF1A	3.59543011	0.00136511	3.9405549	0.00019101
ENSECAG00000014672	TNFRSF11A	-3.8805198	0.0003906	-4.3222208	0.00015426
ENSECAG00000014708	PTHLH	-2.2279872	1.368E-12	-2.1537588	5.1433E-12
ENSECAG00000014750	ALDH1A2	-4.9608027	0.00439016	-4.8358033	0.00032984
ENSECAG00000014783	FAM43A	-2.677412	0.00166933	-2.7670033	0.00245651
ENSECAG00000014812	KRT23	2.36779776	5.282E-05	3.26439099	5.5958E-10
ENSECAG00000014921	GPRC5A	-2.7257797	0.00640809	-3.2920221	0.00013745
ENSECAG00000014962	FAXDC2	-2.3272309	0.00240682	-2.4827037	0.00192911
ENSECAG00000015029	TGFB3	2.81502591	0.00531843	2.83707647	0.00734538
ENSECAG00000015115	RHBDL1	2.67948903	1.7867E-05	2.77884425	0.00012385
ENSECAG00000015140	LIPG	-4.300185	8.985E-07	-3.8960175	1.5365E-06
ENSECAG00000015189	FAM216B	-7.3302274	2.2393E-10	-7.5929736	6.6394E-08
ENSECAG00000015198	CPM	-5.6139571	5.4363E-06	-5.8724844	0.00042108
ENSECAG00000015255	ARMC4	3.93963389	0.00304154	3.97445895	0.00652436
ENSECAG00000015261	IL18	-2.4406115	0.00018706	-2.3525853	0.00012186
ENSECAG00000015273	IRX1	-3.8023149	0.00022826	-3.5841664	0.00553434
ENSECAG00000015275		4.43513525	0.00568562	3.7530901	0.00030426
ENSECAG00000015342	CXCL8	-4.0728402	2.55E-05	-3.6244808	0.00013216
ENSECAG00000015449	IRF8	-5.5834124	6.2038E-05	-4.7597204	0.00297089

ENSECAG00000015613	SCUBE3	-3.7884725	6.2038E-05	-4.1662414	1.0167E-06
ENSECAG00000015621	ARHGEF16	-3.1102131	0.00259947	-3.5565822	6.3667E-06
ENSECAG00000015692	SERTAD4	2.68347725	9.5526E-05	2.98790501	6.7031E-07
ENSECAG00000015840	PODN	3.05442542	1.6843E-05	3.39806146	4.6168E-09
ENSECAG00000015848	HHIPL2	3.9816694	0.00115401	4.91673451	0.00433019
ENSECAG00000015853	SORT1	2.0442427	0.00070645	2.01272178	0.00119935
ENSECAG00000015958	NKD1	-3.3062348	0.00052769	-3.2884295	0.00094328
ENSECAG00000015959	MYBL1	2.18118485	2.019E-07	2.26605464	1.2343E-07
ENSECAG00000016019	ST6GALNAC2	-5.0467937	1.4617E-08	-5.0709552	1.8871E-07
ENSECAG00000016121	ADAMTS12	-2.2266142	0.00138173	-2.2268432	0.00186727
ENSECAG00000016228	CA2	-3.2351399	0.00706704	-3.3765707	0.00103336
ENSECAG00000016232	IL22RA1	-2.2211795	0.00167849	-2.1677255	0.00768791
ENSECAG00000016251		-3.1989535	2.393E-06	-3.2481457	9.0802E-07
ENSECAG00000016277	SGCD	2.31668385	0.00065092	2.4199453	2.5389E-05
ENSECAG00000016322	CYP24A1	-5.3131645	2.8558E-05	-5.146603	4.2935E-06
ENSECAG00000016339	ADAMTS1	-3.1921274	2.115E-07	-3.0729508	4.0282E-08
ENSECAG00000016362	DUSP16	-2.0251336	1.0372E-15	-2.0344399	2.3593E-15
ENSECAG00000016596	RARG	2.1291855	6.2297E-07	2.18256759	1.1776E-07
ENSECAG00000016661	NR4A1	-2.6733536	0.0003906	-2.7052808	0.00042496
ENSECAG00000016662	MCF2L	-4.3829736	0.00025785	-4.1544271	0.00144421
ENSECAG00000016669	ANGPT1	-3.0764428	0.00137237	-2.9579362	0.00358404
ENSECAG00000016710	UPK3B	3.31417362	2.5213E-07	3.48211803	9.8178E-09
ENSECAG00000016768	GATA2	-2.1757568	6.9123E-07	-2.1779557	4.1397E-10
ENSECAG00000016773	NABP1	-3.0089798	3.2241E-11	-2.9491457	5.1433E-12
ENSECAG00000016778	MKX	4.48814625	1.5358E-05	4.57462131	5.126E-05
ENSECAG00000016784		-3.7465819	0.00810509	-3.112424	0.00018137
ENSECAG00000016797	IGF2BP3	-3.1757805	6.7268E-20	-4.5291167	3.0313E-21
ENSECAG00000016829	ABTB2	2.21790673	0.00167849	2.25752889	0.00335875
ENSECAG00000016997	KIAA1324L	3.5740961	0.00115401	4.21780782	7.4389E-10
ENSECAG00000017059	OTULINL	2.05890446	5.4229E-05	2.0227202	0.0001583
ENSECAG00000017157	IER3	-2.6425156	4.8036E-06	-2.7052895	1.1215E-09
ENSECAG00000017172	IFI27	-3.1501309	0.00126092	-2.9046235	0.0031657
ENSECAG00000017181	PTGS2	-5.9907409	4.2211E-11	-5.7665288	1.5272E-10
ENSECAG00000017185	ZBP1	-7.735991	0.00563246	-7.1258264	0.00888139
ENSECAG00000017294	SNTB1	2.726692	0.00381863	3.11931571	1.265E-08
ENSECAG00000017379	CYP27C1	-2.5469988	0.00378897	-2.6740555	0.00191538
ENSECAG00000017460	ATP12A	-4.1783136	0.00393531	-3.8609243	0.00013207
ENSECAG00000017468	TFAP2A	-3.7010434	0.00011277	-3.8116969	0.00026364
ENSECAG00000017495	NALCN	8.62648614	5.4088E-07	8.5012262	7.2438E-06
ENSECAG00000017566	MVB12B	2.08344532	2.287E-07	2.0195273	2.187E-05
ENSECAG00000017588	MMD	-3.2595323	0.00015877	-3.1874601	3.9207E-05
ENSECAG00000017615	CDH17	-5.1460809	3.4515E-09	-4.8809094	1.0348E-09
ENSECAG00000017625	ITGB3	-2.4053428	0.00611135	-2.3808069	0.00427029
ENSECAG00000017816	ADORA1	-3.330035	0.00197938	-3.4245937	5.8731E-05
ENSECAG00000017826	TMEM26	-2.7942236	9.161E-06	-2.8136503	0.00026861
ENSECAG00000017905	LTBP4	2.45433916	0.00079077	2.65486635	2.2117E-05
ENSECAG00000017921	SUSD1	-2.5843441	3.355E-10	-2.6405919	1.5095E-09
ENSECAG00000017988	FRMD7	4.00113699	2.7332E-06	4.3160619	3.4738E-16
ENSECAG00000018067	ITGBL1	7.84294538	4.245E-17	8.34924268	1.4601E-20
ENSECAG00000018104	IGFBP3	-4.9589598	7.3003E-07	-4.9641739	0.00014791
ENSECAG00000018160	TBX21	-5.3078156	0.00294721	-4.7214316	0.00241451
ENSECAG00000018182	TBX20	2.89190779	0.00097838	2.78345378	0.00504736
ENSECAG00000018218	SYNPO2	3.51498464	2.5726E-05	3.8166235	5.0672E-07
ENSECAG00000018307	TNIK	3.65940666	3.4312E-09	3.61195863	1.8728E-09

ENSECAG00000018472	PDGFB	-5.6669401	9.5924E-12	-5.7883103	3.9319E-08
ENSECAG00000018498	ERMP1	-2.3063207	1.9376E-09	-2.285986	5.1353E-08
ENSECAG00000018514	ADAM23	-3.418859	0.00277703	-3.4105241	0.00238449
ENSECAG00000018533	SALL4	-3.5686032	3.6676E-05	-3.437253	0.00015087
ENSECAG00000018579	F11R	-3.5782062	1.9099E-05	-4.1289729	2.3656E-11
ENSECAG00000018670	ALCAM	-2.2985035	1.0271E-07	-2.3386917	1.4411E-08
ENSECAG00000018716	FGF9	4.68040105	1.563E-05	5.06502884	2.7934E-05
ENSECAG00000018784	NIM1K	2.24362833	0.00257355	2.39199472	6.8E-07
ENSECAG00000018841	CGA	-6.1650069	3.4515E-09	-6.4359983	5.2923E-15
ENSECAG00000018863	ADGRL3	3.31394473	6.4266E-33	3.30640822	5.5044E-34
ENSECAG00000018961	ACTN3	2.18970844	2.9149E-06	2.41495301	7.1171E-07
ENSECAG00000018963	COLEC12	3.28651032	7.7953E-05	3.70323525	1.3395E-06
ENSECAG00000019055	TSGA10	-2.6720524	0.00011659	-3.2893851	1.4376E-05
ENSECAG00000019060	ESYT3	-2.6418899	0.00148875	-2.7338254	0.00071148
ENSECAG00000019148	TNFRSF25	2.17423901	1.4481E-06	2.54910759	0.00626309
ENSECAG00000019193	NCAM1	-2.4898118	0.00123311	-2.2981031	0.00352383
ENSECAG00000019378	KCNV1	-5.9694181	0.00105832	-6.1176314	0.0028497
ENSECAG00000019391	TNFSF10	-3.1088043	0.00088706	-2.6656163	0.00169943
ENSECAG00000019398	TFPI2	-5.4437248	0.00359148	-5.32566	0.00242609
ENSECAG00000019408	CAT	2.83412886	6.8065E-08	2.79457432	7.5397E-08
ENSECAG00000019431	RPS6KA6	-3.0645401	0.0001578	-2.9568484	0.0001583
ENSECAG00000019460	MPPED2	-2.7762209	0.0055796	-3.0549174	0.00440466
ENSECAG00000019549	CERS6	2.1668193	6.6475E-06	2.07605515	2.2969E-06
ENSECAG00000019565	DLX5	2.26748915	0.00032301	2.38401066	8.6492E-07
ENSECAG00000019617	ATP8B4	-2.2220791	1.3741E-07	-2.2032897	1.5634E-08
ENSECAG00000019665	THBS4	5.76774627	2.4339E-06	6.44347205	0.0011023
ENSECAG00000019677	EPHX1	2.83869295	0.00085631	2.90125826	0.00069936
ENSECAG00000019805	WSCD2	6.75530299	1.2528E-16	6.69980512	3.3161E-15
ENSECAG00000019940	AKAP6	-2.463918	0.00025456	-2.5162478	0.00121462
ENSECAG00000019948	TNFRSF4	-4.0967582	0.00093407	-4.0489967	0.00300139
ENSECAG00000019949		2.7061962	1.2856E-05	2.62730017	0.00045342
ENSECAG00000019958	ARHGAP20	-3.5421188	1.3789E-05	-3.4221145	1.797E-06
ENSECAG00000019992	PIP5K1B	4.24182139	0.00047061	3.99378764	0.00124638
ENSECAG00000020129		4.25368184	9.7282E-18	4.34283464	5.1749E-43
ENSECAG00000020311	BCO2	-2.7022472	5.02E-06	-2.7273886	1.7436E-05
ENSECAG00000020407	MYBPC2	3.72171281	2.3319E-08	4.00085065	5.7237E-06
ENSECAG00000020437	BCL2	2.56303207	0.00095178	2.56983569	0.00772621
ENSECAG00000020456	ZBTB7C	3.90278988	5.1661E-10	3.7593439	9.1057E-07
ENSECAG00000020489	SLITRK2	-4.1563859	0.00287016	-4.9622653	0.00244816
ENSECAG00000020685	IGF2BP2	-3.841327	0.00020484	-3.9210676	0.00010719
ENSECAG00000020693	HIF3A	-5.9074552	8.5178E-05	-6.4815614	0.00014485
ENSECAG00000020769	FGF1	-4.5542899	1.3355E-08	-4.6793649	7.2906E-07
ENSECAG00000020810	TNFRSF18	-5.2712075	5.0064E-09	-5.5514838	8.4504E-10
ENSECAG00000020956	SERINC2	-3.2007313	7.0217E-08	-3.2838639	1.8316E-25
ENSECAG00000021009	GUCY1B1	-3.8498584	0.00037722	-3.970919	0.00015424
ENSECAG00000021075	FGD6	-2.9484234	4.9862E-14	-2.9030196	8.3567E-15
ENSECAG00000021108	RASIP1	3.21069958	1.0759E-09	3.01780652	5.9071E-12
ENSECAG00000021125	TFAP2C	-3.9438999	7.1326E-07	-4.2901833	5.2266E-08
ENSECAG00000021326	NRAP	-2.707811	3.0985E-07	-2.7860464	5.9075E-06
ENSECAG00000021413	ADGRG1	-2.0482964	0.00019245	-2.2304588	3.352E-07
ENSECAG00000021446	GRID1	-7.0965265	5.7545E-05	-6.8309753	3.4886E-05
ENSECAG00000021448	PADI1	-2.4051672	0.00105012	-2.3580987	1.2635E-06
ENSECAG00000021545	MTSS1	-2.0997918	5.4829E-07	-2.0676252	1.0916E-06
ENSECAG00000021580		5.88473522	2.3098E-06	9.41975139	1.5989E-07

ENSECAG00000021604	PDGFRL	3.99742933	1.4304E-09	4.21296254	1.4376E-05
ENSECAG00000021634	SLC29A4	-3.7303842	3.089E-06	-3.9358127	1.4508E-06
ENSECAG00000021700	FLT1	-6.1508998	7.8235E-10	-5.5456631	1.456E-10
ENSECAG00000021735	EPHA6	-3.1304639	1.5456E-05	-2.9945099	0.00749362
ENSECAG00000021778	SLC16A7	2.02553444	0.00057212	2.12166712	0.00032441
ENSECAG00000021849	TFPI	-3.690721	7.0593E-05	-3.5357114	3.9629E-05
ENSECAG00000021903	LAMC2	-2.2495481	0.00030142	-2.1065809	0.00034167
ENSECAG00000021914	PDE1C	-3.5081494	0.00040724	-3.4234302	0.00044482
ENSECAG00000022007	SCN9A	-5.9368465	6.1308E-05	-5.9235494	5.4784E-05
ENSECAG00000022015	ALOX12	-6.0709358	3.5674E-11	-7.1280942	2.8351E-26
ENSECAG00000022141	TSLP	-4.6653101	3.4628E-05	-4.5747041	4.0186E-05
ENSECAG00000022232	SASH1	2.20123356	8.3682E-09	2.28112227	1.5635E-12
ENSECAG00000022279	SERPINF1	2.9118206	0.00042524	2.92335337	0.00047418
ENSECAG00000022291	CCDC69	-3.8393631	0.00010545	-3.5878058	0.00069832
ENSECAG00000022333	MFSD4A	-2.3869625	0.00820203	-3.6495821	0.00105375
ENSECAG00000022515	MYO5B	3.25744484	4.54E-05	3.37509913	9.1221E-06
ENSECAG00000022555	KLC3	4.08487287	1.1493E-05	3.87515622	3.9207E-05
ENSECAG00000022618	INAVA	-2.3955029	6.4333E-09	-2.3780334	3.3513E-08
ENSECAG00000022659	CCL26	-4.09336	0.00128661	-4.1479729	3.4886E-05
ENSECAG00000022703	LY5	-4.0154893	7.1326E-07	-3.5199995	3.9319E-08
ENSECAG00000022724	CYP26B1	-2.873045	0.000216	-3.0349599	8.2387E-05
ENSECAG00000022741	CDC42EP3	2.6872654	0.00066342	2.56500986	0.00608059
ENSECAG00000022742	APBB1IP	-2.3521725	0.00411546	-2.3543352	0.00641195
ENSECAG00000022900	RAP1GAP	-2.556878	0.00034106	-2.4670789	0.00130297
ENSECAG00000022919	SIX1	2.27113681	1.4304E-09	2.25900589	2.6229E-10
ENSECAG00000022924	EEF2K	2.0855619	1.6617E-11	2.1301541	4.732E-16
ENSECAG00000022939	S100A1	3.09712772	5.9961E-12	3.08477339	1.0348E-09
ENSECAG00000022944	THSD4	-2.4296467	0.00461336	-2.3030582	0.00088652
ENSECAG00000023134	KCNK5	-4.6899962	2.2301E-08	-4.5607363	7.9194E-25
ENSECAG00000023170	STAT4	-3.5500834	0.000788	-3.5642089	1.4027E-05
ENSECAG00000023264	RTP4	-3.988211	0.00233288	-3.6846611	0.00426569
ENSECAG00000023423	PRX	5.28349385	1.4273E-08	5.39235151	3.7198E-06
ENSECAG00000023458	OLFM2	-5.934918	0.0020927	-5.1852642	0.00386807
ENSECAG00000023472	KCNK2	3.2241896	2.6494E-08	3.18004797	2.9038E-07
ENSECAG00000023607	DOCK5	3.58764123	5.2086E-06	4.00137502	1.5015E-08
ENSECAG00000023663	LRP4	2.97420372	0.00085209	2.98320898	0.00151393
ENSECAG00000023874	SPINT1	-2.343804	0.00011277	-2.4224244	1.3767E-07
ENSECAG00000023888	ALDH1L2	2.04331711	0.000788	2.04672838	2.2986E-05
ENSECAG00000023893	SERPINB5	2.19587457	0.0029746	2.07603771	0.0048333
ENSECAG00000023908	OLFML2A	-2.5125735	8.374E-06	-2.6864469	1.9373E-07
ENSECAG00000023946	SDC3	2.14378568	3.6297E-05	2.11679881	7.1379E-05
ENSECAG00000024011	ADGRF4	-5.8029086	0.00134012	-5.0959245	0.00290038
ENSECAG00000024082	ITGAX	-2.966916	0.00154815	-2.8224583	0.00213905
ENSECAG00000024185	GNG11	-2.5911632	0.00024547	-2.6121683	0.00021977
ENSECAG00000024232	A2ML1	2.20626745	0.00643461	2.38884075	0.00219589
ENSECAG00000024287	MAP3K9	2.3688072	0.00083042	2.20071631	0.00668234
ENSECAG00000024288	SLC27A2	-4.0222032	4.0935E-08	-4.1480246	5.3724E-07
ENSECAG00000024374	ERBB3	-3.2972383	0.00195682	-2.7824123	0.00123976
ENSECAG00000024385	PIWIL4	-4.7981782	0.00246968	-5.1191088	0.00796328
ENSECAG00000024387	PRKG2	-8.2263631	1.4163E-06	-7.2193365	1.5161E-05
ENSECAG00000024399	FGF12	-3.5593341	1.8131E-05	-3.6052741	4.6916E-06
ENSECAG00000024536	NFE2	3.25748473	0.00488029	3.44746426	0.00985863
ENSECAG00000024542	ATP1A4	-2.3630611	0.00175021	-3.6859946	0.00705477
ENSECAG00000024574	GATA3	-2.5350535	0.00018706	-2.7697261	8.5201E-08

ENSECAG00000024588		-4.3474566	0.0006147	-4.0112757	0.00098639
ENSECAG00000024674	TTLL7	2.40487	6.6138E-10	2.50373907	2.3656E-11
ENSECAG00000024705	MAFB	3.26634555	3.4515E-09	3.17012239	1.8233E-08
ENSECAG00000024764	ARHGAP18	-2.4194871	2.7189E-08	-2.3869083	2.8168E-07
ENSECAG00000024810	PLA2G4A	-2.6146686	3.4515E-09	-2.6033319	3.3919E-10
ENSECAG00000024851	EDNRB	-3.5435174	3.831E-05	-3.6295675	1.1269E-05
ENSECAG00000024861	DLX1	-2.9817831	0.0003906	-3.0989414	0.00015339
ENSECAG00000024870	CWH43	2.5816429	0.00044381	2.88495937	9.4669E-06
ENSECAG00000024888	CCL5	-4.1804473	0.00254427	-4.3857992	0.00186958
ENSECAG00000024906	SPOCK3	-7.9372926	2.4339E-06	-7.7998319	2.2158E-05
ENSECAG00000024951	SERPINB7	-5.6165265	0.00129312	-5.6380678	0.00333779
ENSECAG00000024992	HSD17B7	-2.1167203	3.2743E-05	-2.154261	7.1817E-05
ENSECAG00000025020	FHL1	2.47472491	0.00429237	2.90825574	2.2837E-06
ENSECAG00000025109	EEF1A2	-4.6846479	0.00246968	-4.6677601	0.001764
ENSECAG00000025171	HS3ST3A1	-6.7552988	0.00135218	-6.3220018	0.00804473
ENSECAG00000026819	NTN1	3.60482099	3.7728E-08	3.56207493	6.1712E-08
ENSECAG00000026863	EFS	2.1369118	8.7258E-09	2.222296	7.7283E-13
ENSECAG00000026984	GPSM3	-2.9912217	0.0011337	-3.6211824	0.00239279
ENSECAG00000027719		-3.7059477	5.1005E-05	-3.8265987	0.00663305
ENSECAG00000028369	GRIN3B	2.51559851	6.0352E-13	2.58084444	2.3049E-10
ENSECAG00000028889		5.33919832	0.00235867	5.48672777	0.00142053
ENSECAG00000029062	PRNP	-2.8085069	0.00052497	-2.6097475	0.00076656
ENSECAG00000029287		8.0369476	2.4339E-06	7.88559562	0.00069936
ENSECAG00000029428	DLK1	-6.109829	0.00050141	-5.8499562	0.00288007
ENSECAG00000030290	TTC9	6.92811655	6.4984E-06	7.52560989	2.7809E-05
ENSECAG00000030554	LIF	-3.9904499	2.3296E-11	-3.9665182	1.2261E-10
ENSECAG00000030644	PALM3	2.23866059	0.00362624	2.19333134	0.00174301
ENSECAG00000030850	FGF18	2.53965678	0.00049265	2.52884832	0.00205446
ENSECAG00000031322		-8.219668	0.00130399	-6.0515986	0.00162307
ENSECAG00000031442	FGF16	8.44045634	3.6676E-05	8.34984188	0.00042925
ENSECAG00000031983	MTUS1	2.49212065	6.6475E-06	2.634851	4.5421E-09
ENSECAG00000032416	APC2	2.00396644	0.00936522	2.47600749	9.7446E-07
ENSECAG00000032515	CEBPA	2.55601841	0.00363472	2.88770415	0.00408581
ENSECAG00000032623	TMEM158	-3.8230468	2.245E-05	-3.9864453	0.00075747
ENSECAG00000032959		-5.4326121	5.7383E-05	-7.0926593	4.2591E-10
ENSECAG00000032992	TIAM1	-2.7299671	0.00156249	-2.8392356	0.00297582
ENSECAG00000034242		-2.4247444	1.1082E-05	-2.0316611	0.00071148
ENSECAG00000034300	RASD1	-3.4161744	6.2165E-05	-3.5730921	0.00029279
ENSECAG00000034308	TRIM6	-2.0721281	0.00355762	-2.4337465	0.00021615
ENSECAG00000035324	HAS3	-3.6122185	0.00031713	-4.4687797	0.00040641
ENSECAG00000035548		-5.5242707	6.0393E-09	-6.3491358	2.6982E-09
ENSECAG00000035667		2.98994285	1.533E-08	3.00287498	0.00088291
ENSECAG00000035706	SMCO4	-2.217128	1.0071E-06	-2.1279943	1.8233E-08
ENSECAG00000036634	CCDC3	7.58685027	2.4886E-13	7.61328712	1.7657E-11
ENSECAG00000036638	SLC6A12	-3.2719713	0.00068409	-3.4694103	0.00048409
ENSECAG00000036646	FGF19	3.48745894	3.4874E-08	3.2934258	2.6061E-09
ENSECAG00000036997		-2.8411139	0.00210782	-3.02044	0.00414732
ENSECAG00000037060	SCX	2.90519135	0.00053303	3.28870599	3.7439E-06
ENSECAG00000037831	SOX11	-4.5113325	2.7707E-05	-4.7297265	5.6072E-06
ENSECAG00000037859	ERICH4	-2.5068279	0.00420376	-2.5854117	0.00241451
ENSECAG00000038005		-4.6371588	0.00128661	-4.5701944	0.00135646
ENSECAG00000038178	HEY2	-3.0847903	8.546E-07	-3.1208347	2.5876E-05
ENSECAG00000038313	MT2A	2.80863949	0.00058611	2.8115114	0.00065399
ENSECAG00000038853	CCL8	-6.1290135	0.0052412	-5.3797061	0.0052594

ENSECAG00000039651	RNF208	2.05344658	0.00609264	2.14541577	0.00622987
ENSECAG00000039865		-4.9970128	0.0064076	-4.4592034	0.00124768
ENSECAG00000040252		-3.3643973	8.4702E-05	-3.3873436	7.277E-05
ENSECAG00000040532		-7.0614382	0.00106893	-6.1095264	0.00188811
ENSECAG00000040631	GADD45A	2.97598998	6.6156E-07	2.88055323	2.3981E-06

Table A2. List of DE genes between adult and fetal tenocytes cultured in 3D identified using alignment-based mapping. 113 genes identified as being DE in adult and fetal tenocytes using HISAT2 alignment-based mapping only. Based on a p-adj of < 0.01 and ±2 Log2FC.

		HISAT2 mapping		Salmon mapping	
Ensemble Gene ID	Gene name	Log2 FC	p-adj.	Log2 FC	p-adj.
ENSECAG00000000758	CAPN11	3.15496627	0.00224538	3.09830907	0.02176647
ENSECAG00000001481	SAMD9L	-5.2047511	0.00456344	-4.6602804	0.01386661
ENSECAG00000003078	OXGR1	-5.0168761	0.00409423	-5.076409	0.03743207
ENSECAG00000003193	BAMBI	-2.0156985	0.00083641	-1.8890176	0.00156998
ENSECAG00000004942	RGS1	-6.3542033	0.00337147	-6.8050318	0.01598007
ENSECAG00000005126	TRIM22	-9.1744934	0.00531843	-7.3980057	0.01211602
ENSECAG00000005405	BDKRB2	-3.1774411	0.0044009	-3.2466137	0.15885089
ENSECAG00000005577	GPR39	3.70291607	0.00609264	2.3923296	0.03955876
ENSECAG00000006175	PGBD5	-2.2394364	0.00628199	-2.0256107	0.03076012
ENSECAG00000006178	TRH	-3.1586886	0.00845454	-3.4004568	0.04541126
ENSECAG00000006703		-6.8846975	0.00360284	-6.5382462	0.01407504
ENSECAG00000006991	PECAM1	-3.2812738	0.00646998	-3.0118702	0.01788761
ENSECAG00000008059		2.07133801	0.00807216	2.10092386	0.01102352
ENSECAG00000008112	EPGN	-4.981002	0.00349097	-3.7675741	0.06123986
ENSECAG00000008564	MAGI2	4.3350489	0.00409423	3.67277741	0.03032404
ENSECAG00000008624	CCL28	-2.0907807	0.00513794	-1.8497515	0.02226176
ENSECAG00000009660	PLEKHA6	2.07538683	3.4515E-09	1.97239258	2.1631E-08
ENSECAG00000010131	CPLX1	-7.0561848	0.00058594	-6.3104424	0.01390672
ENSECAG00000010206	SMTNL1	-3.3541863	0.00114766	-0.2277101	NA
ENSECAG00000010537	HECW1	-3.7308502	0.00868415	-3.8866447	0.07817924
ENSECAG00000010648	GPR143	-5.0343682	0.00833521	-3.4619438	0.15943615
ENSECAG00000011067	CAPN3	6.19092278	0.003769	5.47839591	0.29120912
ENSECAG00000011406	ST8SIA4	-2.5037637	0.00542982	-2.5741989	0.02285188
ENSECAG00000011439	DHX58	-3.4075018	0.00526951	-2.9065186	0.01879227
ENSECAG00000011794	C20H6orf141	-2.4100135	0.00134346	-1.9407632	0.04408123
ENSECAG00000011854	CFB	3.33787585	0.00173836	3.6591285	0.05507649
ENSECAG00000011934	LGR6	-4.7646084	0.00286369	-4.4256775	0.01964908
ENSECAG00000012150	SHROOM2	-2.013765	8.2604E-06	-1.9138102	8.0022E-06
ENSECAG00000012514		-6.5726344	0.00092689	-5.472098	0.01421732
ENSECAG00000012695	DBX2	7.35191547	5.0721E-05	6.97031326	0.01635939
ENSECAG00000012791	GBP6	-5.5338595	0.00731023	-4.6403105	0.03574442
ENSECAG00000012825	ARHGAP24	-2.3933327	2.9964E-05	-1.4585228	1.2321E-08
ENSECAG00000013681	GRHL2	-2.1182002	0.00259947	-2.0364382	0.01069774
ENSECAG00000013883	ICAM1	-2.1219122	0.00291118	-1.9678908	0.00862649
ENSECAG00000014149	NETO1	-2.9748136	0.00281415	-2.8553719	0.01274405
ENSECAG00000014200	TMEM178B	-4.0274733	0.00414113	-4.337663	0.01654865
ENSECAG00000014992	JAM2	2.26655685	0.00258792	2.23109665	0.01489417
ENSECAG00000015102	MYOZ3	2.51376139	0.00523984	2.48322109	0.04157201
ENSECAG00000015382	NLRP3	-3.7014158	0.00308472	-3.3781294	0.01291967
ENSECAG00000015894	ANGPT2	-4.3283919	0.00233288	-4.4699853	0.02393851
ENSECAG00000016312	CD274	-4.7443637	0.0055796	-4.1456002	0.06648712
ENSECAG00000016564	RPRML	6.09334049	0.0005971	5.35525532	0.02357524
ENSECAG00000016713	TESMIN	5.77049749	0.00105677	4.18396154	0.12196016
ENSECAG00000017450	CMTM8	-3.6785984	0.00612132	-3.2443785	0.02860968
ENSECAG00000018674	CEMIP	2.56811092	0.00706704	2.7727815	0.07011718
ENSECAG00000019084	DLX6	2.93719348	0.00556316	3.22214801	0.03344219
ENSECAG00000019096	CACNA1C	2.27567884	0.00033632	2.35995912	0.01844004

ENSECAG00000019298	FER1L6	-2.1547555	0.00121528	-1.3944155	0.15967857
ENSECAG00000019551	CXCL12	2.40992766	0.00313362	2.77755778	0.04533863
ENSECAG00000020126	LGI3	2.31318306	0.00275405	2.40584765	0.01481823
ENSECAG00000020201	GCNT1	-2.0256484	2.5863E-08	-1.9791658	7.5397E-08
ENSECAG00000020449	PARVG	-4.4467043	4.349E-05	-4.6613435	0.03180037
ENSECAG00000020552	GPR83	-2.237192	0.00300301	-2.3608536	0.01101184
ENSECAG00000020808	TRIL	-3.2019669	0.00734464	-2.7247225	0.03007736
ENSECAG00000020974	RTP3	3.40229862	0.00225973	3.59256623	0.01022927
ENSECAG00000021078	GRB14	-2.1885793	0.0018955	-2.0405071	0.0112897
ENSECAG00000021392	COL26A1	-4.6007733	0.00691737	-4.800369	0.01192905
ENSECAG00000021395	CLDN19	-4.2547343	0.00744684	-3.7053767	0.14535147
ENSECAG00000021654	SLC10A4	-2.5622286	0.00731777	-2.4258814	0.04440647
ENSECAG00000022443	GPR87	-4.8511785	0.00612534	-4.2329937	0.01062557
ENSECAG00000022873	ATP8A1	-3.3897927	0.00975674	-3.2733133	0.04205545
ENSECAG00000023321	ELF5	3.99511829	0.00647054	3.77387669	0.06062318
ENSECAG00000023531	RAD21L1	-4.5907208	0.00718967	-4.3497345	0.01828717
ENSECAG00000023963	NMNAT2	-2.015238	0.00168286	-1.9521989	0.00017472
ENSECAG00000024312	RORB	-6.1999958	0.00445682	-5.191208	0.0202141
ENSECAG00000024358	ZBTB16	3.37335164	0.00576439	3.34476026	0.01766532
ENSECAG00000024389	TEC	-2.1601352	2.3198E-08	-1.9939932	2.4934E-07
ENSECAG00000024599	KIRREL3	2.44204496	0.00568562	2.43956027	0.02703237
ENSECAG00000024961	XAF1	-7.0997631	0.00483482	-5.6398282	0.02853514
ENSECAG00000027765		-4.4045495	0.00282604	#N/A	#N/A
ENSECAG00000028085		-3.4736869	0.0020927	-2.4546557	0.0541678
ENSECAG00000029156		-2.5343909	4.229E-05	#N/A	#N/A
ENSECAG00000029578		-2.2136632	1.4764E-06	#N/A	#N/A
ENSECAG00000031122		-2.9490136	0.00328681	#N/A	#N/A
ENSECAG00000031668		3.21313841	0.00121528	2.63930849	0.09071631
ENSECAG00000032667	INA	-3.6823527	0.003769	-3.6536755	0.01205033
ENSECAG00000033252		4.38380613	0.00093452	#N/A	#N/A
ENSECAG00000033385	LGALS3BP	-5.7343131	0.00798943	-4.8574649	0.01650681
ENSECAG00000033730		-5.0586768	0.00363024	-3.661806	0.19953431
ENSECAG00000033856		-3.9710316	2.8359E-10	#N/A	#N/A
ENSECAG00000034127	CRACR2A	-5.8715142	0.00734513	-5.3840241	0.01952886
ENSECAG00000034535		-2.7986235	0.00530962	#N/A	#N/A
ENSECAG00000035544		4.67384823	0.00479277	#N/A	#N/A
ENSECAG00000036059	FAM155A	-3.9875843	0.00150844	-3.8943619	0.01609996
ENSECAG00000036178	TMEM238	-3.6475014	0.00240682	-0.595895	0.54645876
ENSECAG00000036860	eca-mir-9149	4.713375	0.00845454	#N/A	#N/A
ENSECAG00000037593		-7.1732853	0.00322037	-6.1569948	0.02387106
ENSECAG00000037901		2.53613613	0.00045104	#N/A	#N/A
ENSECAG00000038391		-3.3080144	0.00490194	-2.440336	0.04706489
ENSECAG00000038552		5.09107199	1.9607E-16	#N/A	#N/A

Table A3. List of DE genes between adult and fetal tenocytes cultured in 3D identified using alignment-free mapping. 101 genes identified as being DE in adult and fetal tenocytes using Salmon alignment-free mapping only. Based on a p-adj of < 0.01 and ±2 Log2FC.

		HISAT2 mapping		Salmon mapping	
Ensemble Gene ID	Gene name	Log2 FC	p-adj.	Log2 FC	p-adj.
ENSECAG00000000046	FAM13C	-1.6195041	0.18222154	3.17125249	0.00730174
ENSECAG00000000203	TRPA1	2.1646631	0.08099268	-3.5232629	0.00370842
ENSECAG00000000271	APBA1	-1.8065572	0.30333891	3.56234098	0.00222121
ENSECAG00000000651	SPINK5	3.18019455	0.0104386	-3.989795	0.00986419
ENSECAG00000000852	SGIP1	1.84240495	0.11687374	-2.0474441	0.0004334
ENSECAG00000000903	RASGRF2	-2.5150523	0.01011661	2.50183667	0.00407105
ENSECAG00000001004	TMEM74B	2.93858106	0.00662523	-3.0271051	5.8443E-05
ENSECAG00000002548	RNF182	3.16312232	0.01445254	-2.5000881	0.00835456
ENSECAG00000002867	F2RL1	2.92600133	0.01103188	-3.1685806	0.00016149
ENSECAG00000005379	HPGD	5.35744968	0.04496436	-5.103158	0.00277089
ENSECAG00000006337	RAB11FIP4	1.51444165	0.08369467	-2.0359288	0.00290499
ENSECAG00000006756	MYH14	1.80239384	0.01535388	-2.4475078	0.00632022
ENSECAG00000006853	UBD	7.34828784	NA	-6.2136332	0.00933036
ENSECAG00000007414	SV2A	2.06608734	0.07781021	-2.1665391	0.00436056
ENSECAG00000007647	COL5A3	2.09960722	0.01722894	-2.3739564	0.00096409
ENSECAG00000007985	GOLGA7B	4.07914208	0.00030544	-4.8635145	0.00886039
ENSECAG00000008079	BEND6	-1.4334732	0.03305331	2.03137612	0.00256839
ENSECAG00000008135	TRPM3	2.43795859	0.00262167	-2.9022584	0.00258056
ENSECAG00000008596	THEMIS2	3.73614838	0.00303572	-4.1731665	0.00144851
ENSECAG00000008782	RPH3AL	-1.970219	5.7411E-05	2.35470365	0.00256009
ENSECAG00000009026	CYP2S1	2.28479085	0.06556274	-2.5694729	0.000998
ENSECAG00000009042		NA	NA	-4.0068776	0.00156998
ENSECAG00000009133	ACVRL1	2.76522529	0.03216413	-2.7281562	0.0048333
ENSECAG00000009139	CFTR	3.48826572	0.00523645	-3.2386151	7.1626E-06
ENSECAG00000009306	NECTIN2	2.1646416	0.02263529	-2.5166024	8.4842E-07
ENSECAG00000009989	CHAC1	#N/A	#N/A	2.3427651	0.00307592
ENSECAG00000010120	SNAI2	-1.9139682	0.00067985	2.0093063	0.00051476
ENSECAG00000010178	ITGB4	2.09878486	0.06240864	-2.4954798	2.6127E-05
ENSECAG00000010184		-3.0048909	0.0924961	4.00873623	0.00124638
ENSECAG00000010579		-1.2889062	0.00738851	2.11643134	0.00017701
ENSECAG00000010748	MPZL3	1.7495965	0.01258474	-2.0105522	9.5064E-05
ENSECAG00000010990		1.90261998	NA	-7.4623965	0.00639229
ENSECAG00000011177	TESC	5.22444417	0.18090472	-3.8380927	5.8044E-05
ENSECAG00000011335	ITM2A	-0.1078833	0.99438765	-3.7638186	0.006914
ENSECAG00000012004	PIP4P2	-3.1824575	0.00128917	2.49840814	0.00213905
ENSECAG00000013106	ESM1	5.3933586	0.00652517	-4.9035206	0.00156998
ENSECAG00000013387	WNT7B	2.33097955	0.00345521	-2.6707273	9.0445E-05
ENSECAG00000014486	CADPS	-3.3018163	0.18708899	3.79905652	1.5845E-06
ENSECAG00000014566	CCN5	-2.7399377	0.03684869	4.05688157	2.3163E-05
ENSECAG00000014769	ITPKB	1.92503293	3.9054E-05	-2.0514857	1.1232E-08
ENSECAG00000014891	NRCAM	-3.0816552	0.02074947	3.18643187	0.00482873
ENSECAG00000015194	RHBDL2	0.85112493	0.27911246	-2.0843913	3.6674E-05
ENSECAG00000015758	IRX2	-2.3726504	0.12541428	2.54724085	0.00784876
ENSECAG00000016161	SLPI	-3.2296102	0.10218686	4.60357672	0.00692976
ENSECAG00000016219	KANK1	-1.9695887	1.1943E-05	2.00608053	3.7963E-08
ENSECAG00000016360	PDE3A	3.16358245	0.00583577	-3.1876073	0.00081982
ENSECAG00000016679	GALNT15	-4.7803305	0.02384393	6.0218329	0.00056136

ENSECAG00000017027	SFRP2	-2.9622792	0.1854791	3.57905336	0.0002415
ENSECAG00000017191	SPP1	3.67423204	NA	-3.3416806	0.00054884
ENSECAG00000017274	KRT13	-2.2108775	0.13558616	4.84462662	8.5696E-07
ENSECAG00000017407	MOXD1	2.50573701	0.01080127	-2.724922	0.00033618
ENSECAG00000017793	NGFR	7.2352042	NA	-4.9972198	0.00020873
ENSECAG00000017802	OGN	NA	NA	5.0111161	0.00444675
ENSECAG00000017925	CD200	5.59208777	0.03798189	-5.1950422	2.0052E-05
ENSECAG00000018429	WDFY1	NA	NA	7.45178495	0.00247244
ENSECAG00000018752	APOL6	7.35821682	0.01175625	-6.2500103	0.00096409
ENSECAG00000018814	BCAM	1.91611287	0.00661066	-2.1249601	4.9563E-05
ENSECAG00000018954	NCCRP1	2.33355553	0.02745427	-2.353994	0.00202729
ENSECAG00000019278	GREB1L	1.31211967	0.00168529	-3.6912685	2.5322E-06
ENSECAG00000019637	LGALS12	3.22001286	0.04046191	-4.6844119	3.3873E-06
ENSECAG00000019881	PARP10A	2.86965184	0.03522834	-2.7645911	0.00236697
ENSECAG00000019895	LRRC32	2.76286041	0.04435391	-3.1020272	0.00636883
ENSECAG00000019932		2.6639955	0.04423472	-2.7948001	0.00691739
ENSECAG00000020612	SLC7A3	-2.4386783	0.1419941	3.21409851	0.0003427
ENSECAG00000020778	FBLN7	-2.1186831	0.10409519	2.96054324	0.00143612
ENSECAG00000020869	FGFR4	2.93681835	0.00335286	-2.9972336	0.00714945
ENSECAG00000021277	LAMA3	-2.3801577	0.00720673	2.40472009	0.00020203
ENSECAG00000021796		5.60343379	NA	-4.3705291	0.00910203
ENSECAG00000022166	AKAP12	2.25538142	0.0117464	-2.539386	0.00105505
ENSECAG00000022241	CACNA1H	-2.7208091	NA	3.74362523	0.00025727
ENSECAG00000022263	STC2	-1.8717579	0.00330739	2.05849039	7.1171E-07
ENSECAG00000022420	LSR	1.3665071	0.00294167	-2.1057867	0.00505393
ENSECAG00000022525	AREG	5.18439586	0.01131359	-4.3535474	0.00784876
ENSECAG00000022705	IL16	-2.4271738	0.03956992	3.2734059	8.2994E-05
ENSECAG00000022867	TSPAN18	-1.6664324	0.34736634	2.25746627	0.00210023
ENSECAG00000022950	NDRG2	1.6616239	0.01453637	-2.0800866	5.8872E-05
ENSECAG00000023149	SCIN	4.0219047	0.0070395	-3.640528	0.00302622
ENSECAG00000023241	SCRN1	-1.849233	0.18811295	3.72879837	0.00409267
ENSECAG00000023308		-1.9383997	0.00738851	2.09604288	0.00127729
ENSECAG00000024367	CASP1	5.30741816	0.00414637	-5.1503224	0.00436056
ENSECAG00000024467	SH3RF2	-1.7499529	0.03330243	2.00994316	0.00051413
ENSECAG00000024824	ADGRL2	2.16344977	0.01918242	-2.5757158	0.00011694
ENSECAG00000025065	COL12A1	-2.0296011	0.05650654	2.11338892	0.00275924
ENSECAG00000025098	CRHR2	4.52110424	0.00047195	-6.0095615	0.00737558
ENSECAG00000025101	NELL2	-2.5433028	0.04770242	3.58504878	0.00069319
ENSECAG00000029196		#N/A	#N/A	-5.7282807	0.0038423
ENSECAG00000030119		#N/A	#N/A	2.79196068	0.00433052
ENSECAG00000030636		NA	NA	-2.0104213	3.39E-08
ENSECAG00000030750		#N/A	#N/A	-6.3972951	0.00034055
ENSECAG00000030891		NA	NA	-7.6285948	0.00130927
ENSECAG00000032131		2.41646375	0.01289439	-2.2333961	0.0081493
ENSECAG00000032479		#N/A	#N/A	2.28261287	0.00241451
ENSECAG00000034476		1.71245249	0.329305	-2.6085748	0.00632882
ENSECAG00000034839		#N/A	#N/A	-2.1558908	0.00041765
ENSECAG00000036014		NA	NA	-5.0505276	0.00187259
ENSECAG00000036610	CALY	2.90667392	0.01315119	-3.045238	0.00765603
ENSECAG00000036649		#N/A	#N/A	-6.1491852	0.00714945
ENSECAG00000037853		#N/A	#N/A	2.84437647	0.00567969
ENSECAG00000038379		4.08360737	0.01566214	-3.2178031	0.00382732

Bibliography

1. Ely ER, Verheyen KLP, Wood JLN. Fractures and tendon injuries in National Hunt horses in training in the UK: a pilot study. Equine Vet J. 2010;36(4):365–7.

2. Thorpe CT, Clegg PD, Birch HL. A review of tendon injury: Why is the equine superficial digital flexor tendon most at risk? Equine Vet J. 2010;42(2):174–80.

3. Williams RB, Harkins LS, Hammond CJ, Wood JLN. Racehorse injuries, clinical problems and fatalities recorded on British racecourses from flat racing and National Hunt racing during 1996, 1997 and 1998. Equine Vet J. 2010;33(5):478–86.

4. Gaut L, Duprez D. Tendon development and diseases. Wiley Interdiscip Rev Dev Biol. 2016;5(1):5–23.

5. Aparecida de Aro A, de Campos Vidal B, Pimentel ER. Biochemical and anisotropical properties of tendons. Micron. 2012;43(2–3):205–14.

6. Kastelic J, Galeski A, Baer E. The Multicomposite Structure of Tendon. Connect Tissue Res. 1978;6(1):11–23.

7. Derwin KA, Soslowsky LJ, Kimura JH, Plaas AH. Proteoglycans and glycosaminoglycan fine structure in the mouse tail tendon fascicle. J Orthop Res. 2001;19(2):269–77.

8. Iozzo R V., Murdoch AD. Proteoglycans of the extracellular environment: clues from the gene and protein side offer novel perspectives in molecular diversity and function. FASEB J. 1996;10(5):598–614.

9. Scott JE. Extracellular matrix, supramolecular organisation and shape. J Anat. 1995;187((Pt 2)):259–69.

10. Franchi M, Trirè A, Quaranta M, Orsini E, Ottani V. Collagen Structure of Tendon Relates to Function. Sci World J. 2007;7:404–20.

11. Connizzo BK, Yannascoli SM, Soslowsky LJ. Structure–function relationships of

postnatal tendon development: A parallel to healing. Matrix Biol. 2013;32(2):106–16.

12. Birch HL, Sinclair C, Goodship AE, Smith RKW. Tendon and ligament physiology. In: Equine Sports Medicine and Surgery. Elsevier; 2014. p. 167–88.

13. Smith RKW. Pathophysiology of Tendon Injury. In: Diagnosis and Management of Lameness in the Horse. Elsevier; 2011. p. 694–706.

14. Subramanian A, Kanzaki LF, Galloway JL, Schilling TF. Mechanical force regulates tendon extracellular matrix organization and tenocyte morphogenesis through TGFbeta signaling. Elife. 2018;7:e38069.

15. Bi Y, Ehirchiou D, Kilts TM, Inkson CA, Embree MC, Sonoyama W, et al. Identification of tendon stem/progenitor cells and the role of the extracellular matrix in their niche. Nat Med. 2007;13(10):1219–27.

16. Lee WYW, Lui PPY, Rui YF. Hypoxia-Mediated Efficient Expansion of Human Tendon–Derived Stem Cells In Vitro. Tissue Eng Part A. 2012;18(5–6):484–98.

17. Lovati AB, Corradetti B, Lange Consiglio A, Recordati C, Bonacina E, Bizzaro D, et al. Characterization and differentiation of equine tendon-derived progenitor cells. J Biol Regul Homeost Agents. 2011;25(2):75–84.

18. de Mos M, Koevoet WJLM, Jahr H, Verstegen MMA, Heijboer MP, Kops N, et al. Intrinsic differentiation potential of adolescent human tendon tissue: an in-vitro cell differentiation study. BMC Musculoskelet Disord. 2007;8(1):16.

19. Zhang J, Wang JHC. Characterization of differential properties of rabbit tendon stem cells and tenocytes. BMC Musculoskelet Disord. 2010;11(1):10.

20. Ichim TE, O'Heeron P, Kesari S. Fibroblasts as a practical alternative to mesenchymal stem cells. J Transl Med. 2018;16(1):212.

21. Lee KJ, Clegg PD, Comerford EJ, Canty-Laird EG. A comparison of the stem cell characteristics of murine tenocytes and tendon-derived stem cells. BMC Musculoskelet Disord. 2018;19(1):116.

22. Williamson KA, Lee KJ, Humphreys WJE, Comerford EJV, Clegg PD, Canty-Laird EG. Restricted differentiation potential of progenitor cell populations obtained from the equine superficial digital flexor tendon (SDFT). J Orthop Res. 2015;33(6):849–58.

23. Patterson-Kane JC, Rich T. Achilles Tendon Injuries in Elite Athletes: Lessons in Pathophysiology from Their Equine Counterparts. ILAR J. 2014;55(1):86–99.

24. Patterson-Kane JC, Becker DL, Rich T. The Pathogenesis of Tendon Microdamage in Athletes: the Horse as a Natural Model for Basic Cellular Research. J Comp Pathol. 2012;147(2–3):227–47.

25. Biewener AA. Muscle-tendon stresses and elastic energy storage during locomotion in the horse. Comp Biochem Physiol Part B Biochem Mol Biol. 1998;120(1):73–87.

26. Minetti AE, Ardigò LP, Reinach E, Saibene F. The relationship between mechanical work and energy expenditure of locomotion in horses. J Exp Biol. 1999;202(Pt 17):2329–38.

27. Birch HL, Wilson AM, Goodship AE. The effect of exercise-induced localised hyperthermia on tendon cell survival. J Exp Biol. 1997;200(Pt 11):1703–8.

28. Snedeker JG, Foolen J. Tendon injury and repair – A perspective on the basic mechanisms of tendon disease and future clinical therapy. Acta Biomater. 2017;63:18–36.

29. Stephens PR, Nunamaker DM, Butterweck DM. Application of a Hall-effect transducer for measurement of tendon strains in horses. Am J Vet Res. 1989;50(7):1089–95.

30. RiemersmaI DJ, Bogert AJ, Jansen MO, Schamhardt HC. Tendon strain in the forelimbs as a function of gait and ground characteristics and in vitro limb loading in ponies. Equine Vet J. 1996;28(2):133–8.

31. Dakin SG. A review of the healing processes in equine superficial digital flexor tendinopathy. Equine Vet Educ. 2017;29(9):516–20.

32. Thorpe CT, Chaudhry S, Lei II, Varone A, Riley GP, Birch HL, et al. Tendon overload results in alterations in cell shape and increased markers of inflammation and matrix degradation. Scand J Med Sci Sports. 2015;25(4):e381–91.

33. Spiesz EM, Thorpe CT, Chaudhry S, Riley GP, Birch HL, Clegg PD, et al. Tendon extracellular matrix damage, degradation and inflammation in response to in vitro overload exercise. J Orthop Res. 2015;33(6):889–97.

34. Tsuzaki M, Guyton G, Garrett W, Archambault JM, Herzog W, Almekinders L, et al. IL-1β induces COX2, MMP-1, -3 and -13, ADAMTS-4, IL-1β and IL-6 in human tendon cells. J Orthop Res. 2003;21(2):256–64.

35. Docheva D, Müller SA, Majewski M, Evans CH. Biologics for tendon repair. Adv Drug Deliv Rev. 2015;84:222–39.

36. Yagi LH, Watanuki LM, Isaac C, Gemperli R, Nakamura YM, Ladeira PRS. Human fetal wound healing: a review of molecular and cellular aspects. Eur J Plast Surg. 2016;39(4):239–46.

37. Molloy A, Wood E V. Complications of the Treatment of Achilles Tendon Ruptures. Foot Ankle Clin. 2009;14(4):745–59.

38. Richardson LE, Dudhia J, Clegg PD, Smith R. Stem cells in veterinary medicine – attempts at regenerating equine tendon after injury. Trends Biotechnol. 2007;25(9):409–16.

39. Godwin E., Young N., Dudhia J, Beamish I., Smith R. Implantation of bone marrow-derived mesenchymal stem cells demonstrates improved outcome in horses with overstrain injury of the superficial digital flexor tendon. Equine Vet J. 2012;44(1):25–32.

40. Schneider M, Angele P, Järvinen TAH, Docheva D. Rescue plan for Achilles: Therapeutics steering the fate and functions of stem cells in tendon wound healing. Adv Drug Deliv Rev. 2018;129:352–75.

41. Larson BJ, Longaker MT, Lorenz HP. Scarless Fetal Wound Healing: A Basic Science Review. Plast Reconstr Surg. 2010;126(4):1172–80.

42. Ellis IR, Schor SL. Differential Effects of TGF-β1 on Hyaluronan Synthesis by Fetal and Adult Skin Fibroblasts: Implications for Cell Migration and Wound Healing. Exp Cell Res. 1996;228(2):326–33.

43. Longaker MT, Whitby DJ, Ferguson MWJ, Lorenz HP, Harrison MR, Adzick NS. Adult Skin Wounds in the Fetal Environment Heal with Scar Formation. Ann Surg. 1994;219(1):65–72.

44. Schor S, Ellis I, Irwin C, Banyard J, Seneviratne K, Dolman C, et al. Subpopulations of fetal-like gingival fibroblasts: characterisation and potential significance for wound healing and the progression of periodontal disease. Oral Dis. 2008;2(2):155–66.

45. Dyson SJ. Medical management of superficial digital flexor tendonitis: a comparative study in 219 horses (1992-2000). Equine Vet J. 2010;36(5):415–9.

46. Guest DJ, Smith MRW, Allen WR. Monitoring the fate of autologous and allogeneic mesenchymal progenitor cells injected into the superficial digital flexor tendon of horses: Preliminary study. Equine Vet J. 2008;40(2):178–81.

47. Witte S, Dedman C, Harriss F, Kelly G, Chang Y-M, Witte TH. Comparison of treatment outcomes for superficial digital flexor tendonitis in National Hunt racehorses. Vet J. 2016;216:157–63.

48. Henninger RW, Bramlage LR, Bailey M, Bertone AL, Weisbrode SE. Effects of Tendon Splitting on Experimentally-Induced Acute Equine Tendinitis. Vet Comp Orthop Traumatol. 1992;5(1):1–9.

49. Hu AJ, Bramlage LR. Racing performance of Thoroughbreds with superficial digital flexor tendonitis treated with desmotomy of the accessory ligament of the superficial digital flexor tendon: 332 cases (1989–2003). J Am Vet Med Assoc. 2014;244(12):1441–8.

50. Gibson K, Burbridge H, Pfeiffer D. Superficial digital flexor tendonitis in Thoroughbred race horses: outcome following non-surgical treatment and superior check desmotomy. Aust Vet J. 1997;75(9):631–5.

51. Alexander GR, Gibson KT, Day RE, Robertson ID. Effects of superior check desmotomy on flexor tendon and suspensory ligament strain in equine cadaver limbs. Vet Surg. 2001;30(6):ajvet0300522.

52. Leong NL, Kator JL, Clemens TL, James A, Enamoto-Iwamoto M, Jiang J. Tendon and Ligament Healing and Current Approaches to Tendon and Ligament Regeneration. J Orthop Res. 2020;38(1):7–12.

53. Hamada Y, Katoh S, Hibino N, Kosaka H, Hamada D, Yasui N. Effects of Monofilament Nylon Coated With Basic Fibroblast Growth Factor on Endogenous Intrasynovial Flexor Tendon Healing. J Hand Surg Am. 2006;31(4):530–40.

54. Uggen C, Dines J, McGarry M, Grande D, Lee T, Limpisvasti O. The Effect of Recombinant Human Platelet-Derived Growth Factor BB–Coated Sutures on Rotator Cuff Healing in a Sheep Model. Arthrosc J Arthrosc Relat Surg. 2010;26(11):1456–62.

55. Thomopoulos S, Das R, Silva MJ, Sakiyama-Elbert S, Harwood FL, Zampiakis E, et al. Enhanced flexor tendon healing through controlled delivery of PDGF-BB. J Orthop Res. 2009;27(9):1209–15.

56. Chan BP, Chan KM, Maffulli N, Webb S, Lee KKH. Effect of Basic Fibroblast Growth Factor; An In Vitro Study of Tendon Healing. Clin Orthop Relat Res. 1997;342:239–47.

57. Costa MA, Wu C, Pham BV, Chong AKS, Pham HM, Chang J. Tissue Engineering of Flexor Tendons: Optimization of Tenocyte Proliferation Using Growth Factor Supplementation. Tissue Eng. 2006;12(7):1937–43.

58. Liu C-F, Aschbacher-Smith L, Barthelery NJ, Dyment N, Butler D, Wylie C. What We Should Know Before Using Tissue Engineering Techniques to Repair Injured Tendons: A Developmental Biology Perspective. Tissue Eng Part B Rev. 2011;17(3):165–76.

59. de Vos R-J, Windt J, Weir A. Strong evidence against platelet-rich plasma injections for chronic lateral epicondylar tendinopathy: a systematic review. Br J Sports Med. 2014;48(12):952–6.

60. Shojaee A, Parham A. Strategies of tenogenic differentiation of equine stem cells for tendon repair: current status and challenges. Stem Cell Res Ther. 2019;10(1):181.

61. Smith RKW. Mesenchymal stem cell therapy for equine tendinopathy. Disabil Rehabil. 2008;30(20–22):1752–8.

62. Ouyang HW, Goh JCH, Thambyah A, Teoh SH, Lee EH. Knitted Poly-lactide-co-glycolide Scaffold Loaded with Bone Marrow Stromal Cells in Repair and Regeneration of Rabbit Achilles Tendon. Tissue Eng. 2003;9(3):431–9.

63. Young RG, Butler DL, Weber W, Caplan AI, Gordon SL, Fink DJ. Use of mesenchymal stem cells in a collagen matrix for achilles tendon repair. J Orthop Res. 1998;16(4):406–13.

64. Nourissat G, Diop A, Maurel N, Salvat C, Dumont S, Pigenet A, et al. Mesenchymal Stem Cell Therapy Regenerates the Native Bone-Tendon Junction after Surgical Repair in a Degenerative Rat Model. Rannou FP, editor. PLoS One. 2010;5(8):e12248.

65. Crovace A, Lacitignola L, De siena R, Rossi G, Francioso E. Cell Therapy for Tendon Repair in Horses: An Experimental Study. Vet Res Commun. 2007;31(Suppl 1):281–3.

66. Awad HA, Boivin GP, Dressler MR, Smith FNL, Young RG, Butler DL. Repair of patellar tendon injuries using a cell–collagen composite. J Orthop Res. 2003;21(3):420–31.

67. Hankemeier S, van Griensven M, Ezechieli M, Barkhausen T, Austin M, Jagodzinski M, et al. Tissue engineering of tendons and ligaments by human bone marrow stromal cells in a liquid fibrin matrix in immunodeficient rats: Results of a histologic study. Arch Orthop Trauma Surg. 2007;127(9):815–21.

68. Hankemeier S, Hurschler C, Zeichen J, van Griensven M, Miller B, Meller R, et al. Bone Marrow Stromal Cells in a Liquid Fibrin Matrix Improve the Healing Process of Patellar Tendon Window Defects. Tissue Eng Part A. 2009;15(5):1019–30.

69. Beerts C, Suls M, Broeckx SY, Seys B, Vandenberghe A, Declercq J, et al. Tenogenically Induced Allogeneic Peripheral Blood Mesenchymal Stem Cells in Allogeneic Platelet-Rich Plasma: 2-Year Follow-up after Tendon or Ligament Treatment in Horses. Front Vet Sci. 2017;4:158.

70. Nixon AJ, Dahlgren LA, Haupt JL, Yeager AE, Ward DL. Effect of adipose-derived nucleated cell fractions on tendon repair in horses with collagenase-induced tendinitis. Am J Vet Res. 2008;69(7):928–37.

71. Koerner J, Nesic D, Romero JD, Brehm W, Mainil-Varlet P, Grogan SP. Equine Peripheral Blood-Derived Progenitors in Comparison to Bone Marrow-Derived Mesenchymal Stem Cells. Stem Cells. 2006;24(6):1613–9.

72. Paterson YZ, Rash N, Garvican ER, Paillot R, Guest DJ. Equine mesenchymal stromal cells and embryo-derived stem cells are immune privileged in vitro. Stem Cell Res Ther. 2014;5(4):90.

73. Le Blanc K, Tammik C, Rosendahl K, Zetterberg E, Ringdén O. HLA expression and immunologic propertiesof differentiated and undifferentiated mesenchymal stem cells. Exp Hematol. 2003;31(10):890–6.

74. Bartholomew A, Sturgeon C, Siatskas M, Ferrer K, McIntosh K, Patil S, et al. Mesenchymal stem cells suppress lymphocyte proliferation in vitro and prolong skin graft survival in vivo. Exp Hematol. 2002;30(1):42–8.

75. Di Nicola M, Carlo-Stella C, Magni M, Milanesi M, Longoni PD, Matteucci P, et al. Human bone marrow stromal cells suppress T-lymphocyte proliferation induced by cellular or nonspecific mitogenic stimuli. Blood. 2002;99(10):3838–43.

76. Berglund AK, Fortier LA, Antczak DF, Schnabel L V. Immunoprivileged no more: measuring the immunogenicity of allogeneic adult mesenchymal stem cells. Stem Cell Res Ther. 2017;8(1):288.

77. Lalu MM, McIntyre L, Pugliese C, Fergusson D, Winston BW, Marshall JC, et al. Safety of Cell Therapy with Mesenchymal Stromal Cells (SafeCell): A Systematic Review and Meta-Analysis of Clinical Trials. Beltrami AP, editor. PLoS One.

2012;7(10):e47559.

78. Pig JH, Ishihara A, Wellman ML, Russell DS, Bertone AL. Inflammatory effects of autologous, genetically modified autologous, allogeneic, and xenogeneic mesenchymal stem cells after intra-articular injection in horses. Vet Comp Orthop Traumatol. 2013;26(6):453–60.

79. Joswig A-J, Mitchell A, Cummings KJ, Levine GJ, Gregory CA, Smith R, et al. Repeated intra-articular injection of allogeneic mesenchymal stem cells causes an adverse response compared to autologous cells in the equine model. Stem Cell Res Ther. 2017;8(1):42.

80. Eliopoulos N, Stagg J, Lejeune L, Pommey S, Galipeau J. Allogeneic marrow stromal cells are immune rejected by MHC class I– and class II–mismatched recipient mice. Blood. 2005;106(13):4057–65.

81. Nauta AJ, Westerhuis G, Kruisselbrink AB, Lurvink EGA, Willemze R, Fibbe WE. Donor-derived mesenchymal stem cells are immunogenic in an allogeneic host and stimulate donor graft rejection in a nonmyeloablative setting. Blood. 2006;108(6):2114–20.

82. Badillo AT, Beggs KJ, Javazon EH, Tebbets JC, Flake AW. Murine Bone Marrow Stromal Progenitor Cells Elicit an In Vivo Cellular and Humoral Alloimmune Response. Biol Blood Marrow Transplant. 2007;13(4):412–22.

83. Poncelet AJ, Vercruysse J, Saliez A, Gianello P. Although Pig Allogeneic Mesenchymal Stem Cells Are Not Immunogenic In Vitro, Intracardiac Injection Elicits an Immune Response In Vivo. Transplantation. 2007;83(6):783–90.

84. Zangi L, Margalit R, Reich-Zeliger S, Bachar-Lustig E, Beilhack A, Negrin R, et al. Direct Imaging of Immune Rejection and Memory Induction by Allogeneic Mesenchymal Stromal Cells. Stem Cells. 2009;27(11):2865–74.

85. Pezzanite LM, Fortier LA, Antczak DF, Cassano JM, Brosnahan MM, Miller D, et al. Equine allogeneic bone marrow-derived mesenchymal stromal cells elicit antibody responses in vivo. Stem Cell Res Ther. 2015;6(1):54.

86. Isakova IA, Lanclos C, Bruhn J, Kuroda MJ, Baker KC, Krishnappa V, et al. Allo-Reactivity of Mesenchymal Stem Cells in Rhesus Macaques Is Dose and Haplotype Dependent and Limits Durable Cell Engraftment In Vivo. PLoS One. 2014;9(1):e87238.

87. Saville V. Status of equine stem cell-based veterinary medicine in the UK. Vet Rec. 2019;185(18):575.

88. Arti-cell Forte stem cell-based veterinary product | boehringer-ingelheim.com [Internet]. Available from: https://www.boehringer-ingelheim.com/press-release/arti-cell-forte-stem-cell-based-veterinary-product

89. HorStem | European Medicines Agency [Internet]. Available from: https://www.ema.europa.eu/en/medicines/veterinary/EPAR/horstem

90. Hoogduijn MJ, Lombardo E. Mesenchymal Stromal Cells Anno 2019: Dawn of the Therapeutic Era? Concise Review. Stem Cells Transl Med. 2019;8(11):1126–34.

91. Guest DJ, Smith MR, Allen WR. Equine embryonic stem-like cells and mesenchymal stromal cells have different survival rates and migration patterns following their injection into damaged superficial digital flexor tendon. Equine Vet J. 2010;42(7):636–42.

92. Moya A, Paquet J, Deschepper M, Larochette N, Oudina K, Denoeud C, et al. Human Mesenchymal Stem Cell Failure to Adapt to Glucose Shortage and Rapidly Use Intracellular Energy Reserves Through Glycolysis Explains Poor Cell Survival After Implantation. Stem Cells. 2018;36(3):363–76.

93. Eggenhofer E, Benseler V, Kroemer A, Popp FC, Geissler EK, Schlitt HJ, et al. Mesenchymal stem cells are short-lived and do not migrate beyond the lungs after intravenous infusion. Front Immunol. 2012;3:297.

94. Weiss ARR, Dahlke MH. Immunomodulation by Mesenchymal Stem Cells (MSCs): Mechanisms of Action of Living, Apoptotic, and Dead MSCs. Front Immunol. 2019;10:1191.

95. da Silva Meirelles L, Fontes AM, Covas DT, Caplan AI. Mechanisms involved in the therapeutic properties of mesenchymal stem cells. Cytokine Growth Factor Rev. 2009;20(5–6):419–27.

96. Chen L, Tredget EE, Wu PYG, Wu Y. Paracrine Factors of Mesenchymal Stem Cells Recruit Macrophages and Endothelial Lineage Cells and Enhance Wound Healing. PLoS One. 2008;3(4):e1886.

97. Paterson YZ, Kafarnik C, Guest DJ. Characterization of companion animal pluripotent stem cells. Cytom Part A. 2018;93(1):137–48.

98. Becker AJ, McCulloch EA, Till JE. Cytological Demonstration of the Clonal Nature of Spleen Colonies Derived from Transplanted Mouse Marrow Cells. Nature. 1963;197(4866):452–4.

99. Evans MJ, Kaufman MH. Establishment in culture of pluripotential cells from mouse embryos. Nature. 1981;292(5819):154–6.

100. Martin GR. Isolation of a pluripotent cell line from early mouse embryos cultured in medium conditioned by teratocarcinoma stem cells (embryonic stem cells/inner cell masses/differentiation in vsitro/embryonal carcinoma cells/growth factors). Dev Biol. 1981;78(12):7634–8.

101. Thomson JA. Embryonic Stem Cell Lines Derived from Human Blastocysts. Science (80-). 1998;282(5391):1145–7.

102. Romito A, Cobellis G. Pluripotent Stem Cells: Current Understanding and Future Directions. Stem Cells Int. 2016;2016:9451492.

103. Buzzard JJ, Gough NM, Crook JM, Colman A. Karyotype of human ES cells during extended culture. Nat Biotechnol. 2004;22(4):381–2.

104. Mitalipova MM, Rao RR, Hoyer DM, Johnson JA, Meisner LF, Jones KL, et al. Preserving the genetic integrity of human embryonic stem cells. Nat Biotechnol. 2005;23(1):19–20.

105. Robertson NJ, Brook FA, Gardner RL, Cobbold SP, Waldmann H, Fairchild PJ. Embryonic stem cell-derived tissues are immunogenic but their inherent immune

privilege promotes the induction of tolerance. Proc Natl Acad Sci. 2007;104(52):20920–5.

106. Li L, Baroja M., Majumdar A, Chadwick K, Rouleau A, Gallacher L, et al. Human Embryonic Stem Cells Possess Immune-Privileged Properties. Stem Cells. 2004;22:448–56.

107. McClellan A, Paterson YZ, Paillot R, Guest DJ. Equine Fetal, Adult, and Embryonic Stem Cell-Derived Tenocytes Are All Immune Privileged but Exhibit Different Immune Suppressive Properties In Vitro. Stem Cells Dev. 2019;28(21):1413–23.

108. Okita K, Ichisaka T, Yamanaka S. Generation of germline-competent induced pluripotent stem cells. Nature. 2007;448(7151):313–7.

109. Ginis I, Luo Y, Miura T, Thies S, Brandenberger R, Gerecht-Nir S, et al. Differences between human and mouse embryonic stem cells. Dev Biol. 2004;269(2):360–80.

110. Saito S, Ugai H, Sawai K, Yamamoto Y, Minamihashi A, Kurosaka K, et al. Isolation of embryonic stem-like cells from equine blastocysts and their differentiation in vitro 1. FEBS Lett. 2002;531(3):389–96.

111. Li X, Zhou SG, Imreh MP, Ährlund-Richter L, Allen WR. Horse Embryonic Stem Cell Lines from the Proliferation of Inner Cell Mass Cells. Stem Cells Dev. 2006;15(4):523–31.

112. Abavisani A, McKinnon A, Tecirlioglu RT, Trounson AO, Guo J. Maintenance of horse embryonic stem cells in different conditions. Iran J Vet Res. 2010;11(3):239–48.

113. Mascetti VL, Pedersen RA. Human-Mouse Chimerism Validates Human Stem Cell Pluripotency. Cell Stem Cell. 2016;18(1):67–72.

114. Buta C, David R, Dressel R, Emgård M, Fuchs C, Gross U, et al. Reconsidering pluripotency tests: Do we still need teratoma assays? Stem Cell Res. 2013;11(1):552–62.

115. Prokhorova TA, Harkness LM, Frandsen U, Ditzel N, Schrøder HD, Burns JS, et al. Teratoma Formation by Human Embryonic Stem Cells Is Site Dependent and Enhanced by the Presence of Matrigel. Stem Cells Dev. 2009;18(1):47–54.

116. Smith KP, Luong MX, Stein GS. Pluripotency: Toward a gold standard for human ES and iPS cells. J Cell Physiol. 2009;220(1):21–9.

117. Chung Y, Klimanskaya I, Becker S, Li T, Maserati M, Lu S-J, et al. Human Embryonic Stem Cell Lines Generated without Embryo Destruction. Cell Stem Cell. 2008;2(2):113–7.

118. Takahashi K, Tanabe K, Ohnuki M, Narita M, Ichisaka T, Tomoda K, et al. Induction of Pluripotent Stem Cells from Adult Human Fibroblasts by Defined Factors. Cell. 2007;131(5):861–72.

119. Takahashi K, Yamanaka S. Induction of Pluripotent Stem Cells from Mouse Embryonic and Adult Fibroblast Cultures by Defined Factors. Cell. 2006;126(4):663–76.

120. Nagy K, Sung H-K, Zhang P, Laflamme S, Vincent P, Agha-Mohammadi S, et al. Erratum to: Induced Pluripotent Stem Cell Lines Derived from Equine Fibroblasts. Stem Cell Rev Reports. 2012;8(2):546–546.

121. Bavin EP, Smith O, Baird AEG, Smith LC, Guest DJ. Equine Induced Pluripotent Stem Cells have a Reduced Tendon Differentiation Capacity Compared to Embryonic Stem Cells. Front Vet Sci. 2015;2(55):1–12.

122. Breton A, Sharma R, Diaz AC, Parham AG, Graham A, Neil C, et al. Derivation and characterization of induced pluripotent stem cells from equine fibroblasts. Stem Cells Dev. 2013;22(4):611–21.

123. Khodadadi K, Sumer H, Pashaiasl M, Lim S, Williamson M, Verma PJ. Induction of Pluripotency in Adult Equine Fibroblasts without c-MYC. Stem Cells Int. 2012;2012:429160.

124. Sharma R, Livesey MR, Wyllie DJA, Proudfoot C, Whitelaw CBA, Hay DC, et al. Generation of Functional Neurons from Feeder-Free, Keratinocyte-Derived

Equine Induced Pluripotent Stem Cells. Stem Cells Dev. 2014;23(13):1524–34.

125. Whitworth DJ, Ovchinnikov DA, Sun J, Fortuna PRJ, Wolvetang EJ. Generation and Characterization of Leukemia Inhibitory Factor-Dependent Equine Induced Pluripotent Stem Cells from Adult Dermal Fibroblasts. Stem Cells Dev. 2014;23(13):1515–23.

126. Lee E-M, Kim A-Y, Lee E-J, Park J-K, Park S-I, Cho S-G, et al. Generation of Equine-Induced Pluripotent Stem Cells and Analysis of Their Therapeutic Potential for Muscle Injuries. Cell Transplant. 2016;25(11):2003–16.

127. Quattrocelli M, Giacomazzi G, Broeckx SY, Ceelen L, Bolca S, Spaas JH, et al. Equine-Induced Pluripotent Stem Cells Retain Lineage Commitment Toward Myogenic and Chondrogenic Fates. Stem Cell Reports. 2016;6(1):55–63.

128. Hotta A, Ellis J. Retroviral vector silencing during iPS cell induction: An epigenetic beacon that signals distinct pluripotent states. J Cell Biochem. 2008;105(4):940–8.

129. Liu X, Li W, Fu X, Xu Y. The Immunogenicity and Immune Tolerance of Pluripotent Stem Cell Derivatives. Front Immunol. 2017;8:645.

130. Boyd AS, Wood KJ. Variation in MHC Expression Between Undifferentiated Mouse ES Cells and ES Cell-derived Insulin-producing Cell Clusters. Transplantation. 2009;87(9):1300–4.

131. Jaffe L, Robertson EJ, Bikoff EK. Distinct patterns of expression of MHC class I and β2-microglobulin transcripts at early stages of mouse development. J Immunol. 1991;147(8):2740–9.

132. Guest DJ, Allen WR. Expression of Cell-Surface Antigens and Embryonic Stem Cell Pluripotency Genes in Equine Blastocysts. Stem Cells Dev. 2007;16(5):789–96.

133. Draper JS, Pigott C, Thomson JA, Andrews PW. Surface antigens of human embryonic stem cells: changes upon differentiation in culture*. J Anat. 2002;200(3):249–58.

134. English K, Wood KJ. Immunogenicity of embryonic stem cell-derived progenitors after transplantation. Curr Opin Organ Transplant. 2011;16(1):90–5.

135. Drukker M, Katchman H, Katz G, Even-Tov Friedman S, Shezen E, Hornstein E, et al. Human Embryonic Stem Cells and Their Differentiated Derivatives Are Less Susceptible to Immune Rejection Than Adult Cells. Stem Cells. 2006;24(2):221–9.

136. Dressel R, Nolte J, Elsner L, Novota P, Guan K, Streckfuss-Bömeke K, et al. Pluripotent stem cells are highly susceptible targets for syngeneic, allogeneic, and xenogeneic natural killer cells. FASEB J. 2010;24(7):2164–77.

137. Perez-Cunningham J, Ames E, Smith RC, Peter AK, Naidu R, Nolta JA, et al. Natural Killer Cell Subsets Differentially Reject Embryonic Stem Cells Based on Licensing. Transplantation. 2014;97(10):992–8.

138. Kofidis T, DeBruin JL, Tanaka M, Zwierzchoniewska M, Weissman I, Fedoseyeva E, et al. They are not stealthy in the heart: embryonic stem cells trigger cell infiltration, humoral and T-lymphocyte-based host immune response☆. Eur J Cardio-Thoracic Surg. 2005;28(3):461–6.

139. Swijnenburg R-J, Schrepfer S, Cao F, Pearl JI, Xie X, Connolly AJ, et al. In Vivo Imaging of Embryonic Stem Cells Reveals Patterns of Survival and Immune Rejection Following Transplantation. Stem Cells Dev. 2008;17(6):1023–9.

140. Barsby T, Guest D. Transforming Growth Factor Beta3 Promotes Tendon Differentiation of Equine Embryo-Derived Stem Cells. Tissue Eng Part A. 2013;19(19–20):2156–65.

141. Menendez P, Bueno C, Wang L, Bhatia M. Human Embryonic Stem Cells: Potential Tool for Achieving Immunotolerance? Stem Cell Rev. 2005;1(2):151–8.

142. Buja LM, Vela D. Immunologic and Inflammatory Reactions to Exogenous Stem Cells. J Am Coll Cardiol. 2010;56(21):1693–700.

143. Xian B, Huang B. The immune response of stem cells in subretinal transplantation. Stem Cell Res Ther. 2015;6(1):161.

144. Tzameret A, Sher I, Belkin M, Treves AJ, Meir A, Nagler A, et al. Transplantation of human bone marrow mesenchymal stem cells as a thin subretinal layer ameliorates retinal degeneration in a rat model of retinal dystrophy. Exp Eye Res. 2014;118:135–44.

145. Haworth R, Sharpe M. The issue of immunology in stem cell therapies: a pharmaceutical perspective. Regen Med. 2015;10(3):231–4.

146. Hentze H, Soong PL, Wang ST, Phillips BW, Putti TC, Dunn NR. Teratoma formation by human embryonic stem cells: Evaluation of essential parameters for future safety studies. Stem Cell Res. 2009;2(3):198–210.

147. Kroon E, Martinson LA, Kadoya K, Bang AG, Kelly OG, Eliazer S, et al. Pancreatic endoderm derived from human embryonic stem cells generates glucose-responsive insulin-secreting cells in vivo. Nat Biotechnol. 2008;26(4):443–52.

148. Laflamme MA, Gold J, Xu C, Hassanipour M, Rosler E, Police S, et al. Formation of Human Myocardium in the Rat Heart from Human Embryonic Stem Cells. Am J Pathol. 2005;167(3):663–71.

149. Reubinoff BE, Itsykson P, Turetsky T, Pera MF, Reinhartz E, Itzik A, et al. Neural progenitors from human embryonic stem cells. Nat Biotechnol. 2001;19(12):1134–40.

150. Tomescot A, Leschik J, Bellamy V, Dubois G, Messas E, Bruneval P, et al. Differentiation In Vivo of Cardiac Committed Human Embryonic Stem Cells in Postmyocardial Infarcted Rats. Stem Cells. 2007;25(9):2200–5.

151. Guo XM, Zhao YS, Chang HX, Wang CY, En LL, Zhang XA, et al. Creation of engineered cardiac tissue in vitro from mouse embryonic stem cells. Circulation. 2006;113(18):2229–37.

152. Kumashiro Y, Asahina K, Ozeki R, Shimizu-Saito K, Tanaka Y, Kida Y, et al. Enrichment of hepatocytes differentiated from mouse embryonic stem cells as a transplantable source. Transplantation. 2005;79(5):550–7.

153. Schwartz SD, Hubschman J-P, Heilwell G, Franco-Cardenas V, Pan CK, Ostrick

RM, et al. Embryonic stem cell trials for macular degeneration: a preliminary report. Lancet. 2012;379(9817):713–20.

154. Barsby T, Bavin EP, Guest DJ. Three-dimensional culture and transforming growth factor beta3 synergistically promote tenogenic differentiation of equine embryo-derived stem cells. Tissue Eng - Part A. 2014;20(19–20):2604–13.

155. Schweitzer R, Chyung JH, Murtaugh LC, Brent AE, Rosen V, Olson EN, et al. Analysis of the tendon cell fate using Scleraxis, a specific marker for tendons and ligaments. Development. 2001;128(19):3855–66.

156. Nguyen PK, Pan XS, Li J, Kuo CK. Roadmap of molecular, compositional, and functional markers during embryonic tendon development. Connect Tissue Res. 2018;59(5):495–508.

157. Liu H, Zhu S, Zhang C, Lu P, Hu J, Yin Z, et al. Crucial transcription factors in tendon development and differentiation: their potential for tendon regeneration. Cell Tissue Res. 2014;356(2):287–98.

158. Brent AE, Schweitzer R, Tabin CJ. A somitic compartment of tendon progenitors. Cell [Internet]. 2003;113(2):235–48. Available from: http://www.ncbi.nlm.nih.gov/pubmed/12705871

159. Havis E, Bonnin M-A, Olivera-Martinez I, Nazaret N, Ruggiu M, Weibel J, et al. Transcriptomic analysis of mouse limb tendon cells during development. Development. 2014;141(19):3683–96.

160. Subramanian A, Schilling TF. Tendon development and musculoskeletal assembly: emerging roles for the extracellular matrix. Development. 2015;142(24):4191–204.

161. Pryce BA, Brent AE, Murchison ND, Tabin CJ, Schweitzer R. Generation of transgenic tendon reporters, ScxGFP and ScxAP, using regulatory elements of the scleraxis gene. Dev Dyn. 2007;236(6):1677–82.

162. Scott A, Sampaio A, Abraham T, Duronio C, Underhill TM. Scleraxis expression is coordinately regulated in a murine model of patellar tendon injury. J Orthop Res.

2011;29(2):289–96.

163. Murchison ND, Price BA, Conner DA, Keene DR, Olson EN, Tabin CJ, et al. Regulation of tendon differentiation by scleraxis distinguishes force-transmitting tendons from muscle-anchoring tendons. Development. 2007;134(14):2697–708.

164. Anderson DM, Arredondo J, Hahn K, Valente G, Martin JF, Wilson-Rawls J, et al. Mohawk is a novel homeobox gene expressed in the developing mouse embryo. Dev Dyn. 2006;235(3):792–801.

165. Liu W, Watson SS, Lan Y, Keene DR, Ovitt CE, Liu H, et al. The Atypical Homeodomain Transcription Factor Mohawk Controls Tendon Morphogenesis. Mol Cell Biol. 2010;30(20):4797–807.

166. Zhang J, Wang JHC. The Effects of Mechanical Loading on Tendons - An In Vivo and In Vitro Model Study. Roeder RK, editor. PLoS One. 2013;8(8):e71740.

167. Kayama T, Mori M, Ito Y, Matsushima T, Nakamichi R, Suzuki H, et al. Gtf2ird1-Dependent Mohawk Expression Regulates Mechanosensing Properties of the Tendon. Mol Cell Biol. 2016;36(8):1297–309.

168. Ito Y, Toriuchi N, Yoshitaka T, Ueno-Kudoh H, Sato T, Yokoyama S, et al. The Mohawk homeobox gene is a critical regulator of tendon differentiation. Proc Natl Acad Sci. 2010;107(23):10538–42.

169. Kimura W, Machii M, Xue X, Sultana N, Hikosaka K, Sharkar MTK, et al. Irxl1 mutant mice show reduced tendon differentiation and no patterning defects in musculoskeletal system development. genesis. 2011;49(1):2–9.

170. Anderson DM, George R, Noyes MB, Rowton M, Liu W, Jiang R, et al. Characterization of the DNA-binding Properties of the Mohawk Homeobox Transcription Factor. J Biol Chem. 2012;287(42):35351–9.

171. Chuang H-N, Hsiao K-M, Chang H-Y, Wu C-C, Pan H. The homeobox transcription factor Irxl1 negatively regulates MyoD expression and myoblast differentiation. FEBS J. 2014;281(13):2990–3003.

172. Lejard V, Blais F, Guerquin M-J, Bonnet A, Bonnin M-A, Havis E, et al. EGR1

and EGR2 Involvement in Vertebrate Tendon Differentiation. J Biol Chem. 2011;286(7):5855–67.

173. Guerquin M-J, Charvet B, Nourissat G, Havis E, Ronsin O, Bonnin M-A, et al. Transcription factor EGR1 directs tendon differentiation and promotes tendon repair. J Clin Invest. 2013;123(8):3564–76.

174. Havis E, Duprez D. EGR1 Transcription Factor is a Multifaceted Regulator of Matrix Production in Tendons and Other Connective Tissues. Int J Mol Sci. 2020;21(5):1664.

175. Pryce BA, Watson SS, Murchison ND, Staverosky JA, Dünker N, Schweitzer R. Recruitment and maintenance of tendon progenitors by TGFB signaling are essential for tendon formation. Development. 2009;136(8):1351–61.

176. Alberton P, Popov C, Prägert M, Kohler J, Shukunami C, Schieker M, et al. Conversion of Human Bone Marrow-Derived Mesenchymal Stem Cells into Tendon Progenitor Cells by Ectopic Expression of Scleraxis. Stem Cells Dev. 2012;21(6):846–58.

177. Chen X, Yin Z, Chen J, Shen W, Liu H, Tang Q, et al. Force and scleraxis synergistically promote the commitment of human ES cells derived MSCs to tenocytes. Sci Rep. 2012;2(1):977.

178. Gulotta L V., Kovacevic D, Packer JD, Deng XH, Rodeo SA. Bone Marrow–Derived Mesenchymal Stem Cells Transduced With Scleraxis Improve Rotator Cuff Healing in a Rat Model. Am J Sports Med. 2011;39(6):1282–9.

179. Otabe K, Nakahara H, Hasegawa A, Matsukawa T, Ayabe F, Onizuka N, et al. Transcription factor Mohawk controls tenogenic differentiation of bone marrow mesenchymal stem cells in vitro and in vivo. J Orthop Res. 2015;33(1):1–8.

180. Liu H, Zhang C, Zhu S, Lu P, Zhu T, Gong X, et al. Mohawk Promotes the Tenogenesis of Mesenchymal Stem Cells Through Activation of the TGFβ Signaling Pathway. Stem Cells. 2015;33(2):443–55.

181. Tao X, Liu J, Chen L, Zhou Y, Tang K. EGR1 Induces Tenogenic Differentiation

of Tendon Stem Cells and Promotes Rabbit Rotator Cuff Repair. Cell Physiol Biochem. 2015;35(2):699–709.

182. Tan G-K, Pryce BA, Stabio A, Brigande J V., Wang C, Xia Z, et al. Tgfβ signaling is critical for maintenance of the tendon cell fate. Elife. 2020;9:e52695.

183. Zhang Y-J, Chen X, Li G, Chan K-M, Heng BC, Yin Z, et al. Concise Review: Stem Cell Fate Guided By Bioactive Molecules for Tendon Regeneration. Stem Cells Transl Med. 2018;7(5):404–14.

184. Farhat YM, Al-Maliki AA, Chen T, Juneja SC, Schwarz EM, O'Keefe RJ, et al. Gene Expression Analysis of the Pleiotropic Effects of TGF-β1 in an In Vitro Model of Flexor Tendon Healing. Agarwal S, editor. PLoS One. 2012;7(12):e51411.

185. Rajpar I, Barrett JG. Optimizing growth factor induction of tenogenesis in three-dimensional culture of mesenchymal stem cells. J Tissue Eng. 2019;10:204173141984877.

186. Falcon ND, Riley GP, Saeed A. Induction of Tendon-Specific Markers in Adipose-Derived Stem Cells in Serum-Free Culture Conditions. Tissue Eng Part C Methods. 2019;25(7):389–400.

187. Kapacee Z, Yeung C-YC, Lu Y, Crabtree D, Holmes DF, Kadler KE. Synthesis of embryonic tendon-like tissue by human marrow stromal/mesenchymal stem cells requires a three-dimensional environment and transforming growth factor β3. Matrix Biol. 2010;29(8):668–77.

188. Leung M, Jana S, Tsao C-T, Zhang M. Tenogenic differentiation of human bone marrow stem cells via a combinatory effect of aligned chitosan–poly-caprolactone nanofibers and TGF-β3. J Mater Chem B. 2013;1(47):6516.

189. Lee CH, Moioli EK, Mao JJ. Fibroblastic Differentiation of Human Mesenchymal Stem Cells using Connective Tissue Growth Factor. In: 2006 International Conference of the IEEE Engineering in Medicine and Biology Society. 2006. p. 775–8.

190. Lee CH, Shah B, Moioli EK, Mao JJ. CTGF directs fibroblast differentiation from human mesenchymal stem/stromal cells and defines connective tissue healing in a rodent injury model. J Clin Invest. 2010;120(9):3340–9.

191. Ni M, Rui YF, Tan Q, Liu Y, Xu LL, Chan KM, et al. Engineered scaffold-free tendon tissue produced by tendon-derived stem cells. Biomaterials. 2013;34(8):2024–37.

192. Lui PPY, Wong OT, Lee YW. Transplantation of tendon-derived stem cells pre-treated with connective tissue growth factor and ascorbic acid in vitro promoted better tendon repair in a patellar tendon window injury rat model. Cytotherapy. 2016;18(1):99–112.

193. Park A, Hogan M V., Kesturu GS, James R, Balian G, Chhabra AB. Adipose-Derived Mesenchymal Stem Cells Treated with Growth Differentiation Factor-5 Express Tendon-Specific Markers. Tissue Eng Part A. 2010;16(9):2941–51.

194. Mazzocca AD, McCarthy MBR, Chowaniec D, Cote MP, Judson CH, Apostolakos J, et al. Bone Marrow–Derived Mesenchymal Stem Cells Obtained During Arthroscopic Rotator Cuff Repair Surgery Show Potential for Tendon Cell Differentiation After Treatment With Insulin. Arthrosc J Arthrosc Relat Surg. 2011;27(11):1459–71.

195. Tan S-L, Ahmad RE, Ahmad TS, Merican AM, Abbas AA, Ng WM, et al. Effect of Growth Differentiation Factor 5 on the Proliferation and Tenogenic Differentiation Potential of Human Mesenchymal Stem Cells in vitro. Cells Tissues Organs. 2012;196(4):325–38.

196. Govoni M, Berardi AC, Muscari C, Campardelli R, Bonafè F, Guarnieri C, et al. An Engineered Multiphase Three-Dimensional Microenvironment to Ensure the Controlled Delivery of Cyclic Strain and Human Growth Differentiation Factor 5 for the Tenogenic Commitment of Human Bone Marrow Mesenchymal Stem Cells. Tissue Eng Part A. 2017;23(15–16):811–22.

197. Wang D, Jiang X, Lu A, Tu M, Huang W, Huang P. BMP14 induces tenogenic differentiation of bone marrow mesenchymal stem cells in vitro. Exp Ther Med.

2018;16:1165–74.

198. Berasi SP, Varadarajan U, Archambault J, Cain M, Souza TA, Abouzeid A, et al. Divergent activities of osteogenic BMP2, and tenogenic BMP12 and BMP13 independent of receptor binding affinities. Growth Factors. 2011;29(4):128–39.

199. Chai W, Ni M, Rui YF, Zhang KY, Zhang Q, Xu LL, et al. Effect of growth and differentiation factor 6 on the tenogenic differentiation of bone marrow-derived mesenchymal stem cells. Chin Med J (Engl). 2013;126(8):1509–16.

200. Violini S, Ramelli P, Pisani LF, Gorni C, Mariani P. Horse bone marrow mesenchymal stem cells express embryo stem cell markers and show the ability for tenogenic differentiation by in vitro exposure to BMP-12. BMC Cell Biol. 2009;10(1):29.

201. Lee JY, Zhou Z, Taub PJ, Ramcharan M, Li Y, Akinbiyi T, et al. BMP-12 Treatment of Adult Mesenchymal Stem Cells In Vitro Augments Tendon-Like Tissue Formation and Defect Repair In Vivo. PLoS One. 2011;6(3):e17531.

202. Ni M, Rui Y, Chen Q, Wang Y, Li G. Effect of growth differentiation factor 7 on tenogenic differentiation of bone marrow mesenchymal stem cells of rat in vitro. Chinese J reparative Reconstr Surg. 2011;25(6):1103–9.

203. Shen H, Gelberman RH, Silva MJ, Sakiyama-Elbert SE, Thomopoulos S. BMP12 induces tenogenic differentiation of adipose-derived stromal cells. PLoS One. 2013;8(10):e77613.

204. Gulati BR, Kumar R, Mohanty N, Kumar P, Somasundaram RK, Yadav PS. Bone Morphogenetic Protein-12 Induces Tenogenic Differentiation of Mesenchymal Stem Cells Derived from Equine Amniotic Fluid. Cells Tissues Organs. 2013;198(5):377–89.

205. Mohanty N, Gulati BR, Kumar R, Gera S, Kumar P, Somasundaram RK, et al. Immunophenotypic characterization and tenogenic differentiation of mesenchymal stromal cells isolated from equine umbilical cord blood. Vitr Cell Dev Biol - Anim. 2014;50(6):538–48.

206. Liu J, Tao X, Chen L, Han W, Zhou Y, Tang K. CTGF Positively Regulates BMP12 Induced Tenogenic Differentiation of Tendon Stem Cells and Signaling. Cell Physiol Biochem. 2015;35(5):1831–45.

207. Zarychta-Wiśniewska W, Burdzinska A, Kulesza A, Gala K, Kaleta B, Zielniok K, et al. Bmp-12 activates tenogenic pathway in human adipose stem cells and affects their immunomodulatory and secretory properties. BMC Cell Biol. 2017;18(1):13.

208. Hankemeier S, Keus M, Zeichen J, Jagodzinski M, Barkhausen T, Bosch U, et al. Modulation of Proliferation and Differentiation of Human Bone Marrow Stromal Cells by Fibroblast Growth Factor 2: Potential Implications for Tissue Engineering of Tendons and Ligaments. Tissue Eng. 2005;11(1–2):41–9.

209. Sahoo S, Ang L-T, Cho-Hong Goh J, Toh S-L. Bioactive nanofibers for fibroblastic differentiation of mesenchymal precursor cells for ligament/tendon tissue engineering applications. Differentiation. 2010;79(2):102–10.

210. Durgam SS, Stewart AA, Pondenis HC, Gutierrez-Nibeyro SM, Evans RB, Stewart MC. Comparison of equine tendon- and bone marrow–derived cells cultured on tendon matrix with or without insulin-like growth factor-I supplementation. Am J Vet Res. 2012;73(1):153–61.

211. Gomiero C, Bertolutti G, Martinello T, Van Bruaene N, Broeckx SY, Patruno M, et al. Tenogenic induction of equine mesenchymal stem cells by means of growth factors and low-level laser technology. Vet Res Commun. 2016;40(1):39–48.

212. Raabe O, Shell K, Fietz D, Freitag C, Ohrndorf A, Christ HJ, et al. Tenogenic differentiation of equine adipose-tissue-derived stem cells under the influence of tensile strain, growth differentiation factors and various oxygen tensions. Cell Tissue Res. 2013;352(3):509–21.

213. Dale TP, Mazher S, Webb WR, Zhou J, Maffulli N, Chen G-Q, et al. Tenogenic Differentiation of Human Embryonic Stem Cells. Tissue Eng Part A. 2018;24(5–6):361–8.

214. Stanco D, Caprara C, Ciardelli G, Mariotta L, Gola M, Minonzio G, et al.

Tenogenic differentiation protocol in xenogenic-free media enhances tendon-related marker expression in ASCs. Papaccio G, editor. PLoS One. 2019;14(2):e0212192.

215. Yin Z, Guo J, Wu T, Chen X, Xu L, Lin S, et al. Stepwise Differentiation of Mesenchymal Stem Cells Augments Tendon-Like Tissue Formation and Defect Repair In Vivo. Stem Cells Transl Med. 2016;5(8):1106–16.

216. Shwartz Y, Blitz E, Zelzer E. One load to rule them all: Mechanical control of the musculoskeletal system in development and aging. Differentiation. 2013;86(3):104–11.

217. Bonnin M-A, Laclef C, Blaise R, Eloy-Trinquet S, Relaix F, Maire P, et al. Six1 is not involved in limb tendon development, but is expressed in limb connective tissue under Shh regulation. Mech Dev. 2005;122(4):573–85.

218. Jelinsky SA, Archambault J, Li L, Seeherman H. Tendon-selective genes identified from rat and human musculoskeletal tissues. J Orthop Res. 2010;28(3):289–97.

219. Egerbacher M, Arnoczky SP, Caballero O, Lavagnino M, Gardner KL. Loss of Homeostatic Tension Induces Apoptosis in Tendon Cells: An In Vitro Study. Clin Orthop Relat Res. 2008;466(7):1562–8.

220. Almekinders LC, Baynes AJ, Bracey LW. An In Vitro Investigation Into the Effects of Repetitive Motion and Nonsteroidal Antiinflammatory Medication on Human Tendon Fibroblasts. Am J Sports Med. 1995;23(1):119–23.

221. Barkhausen T, van Griensven M, Zeichen J, Bosch U. Modulation of cell functions of human tendon fibroblasts by different repetitive cyclic mechanical stress patterns. Exp Toxicol Pathol. 2003;55(2–3):153–8.

222. Bayer ML, Yeung C-YC, Kadler KE, Qvortrup K, Baar K, Svensson RB, et al. The initiation of embryonic-like collagen fibrillogenesis by adult human tendon fibroblasts when cultured under tension. Biomaterials. 2010;31(18):4889–97.

223. Kessler D, Dethlefsen S, Haase I, Plomann M, Hirche F, Krieg T, et al. Fibroblasts in Mechanically Stressed Collagen Lattices Assume a “Synthetic” Phenotype. J

Biol Chem. 2001;276(39):36575–85.

224. Tanaka H, Manske PR, Pruitt DL, Larson BJ. Effect of cyclic tension on lacerated flexor tendons in vitro. J Hand Surg Am. 1995;20(3):467–73.

225. Yang G, Crawford RC, Wang JHC. Proliferation and collagen production of human patellar tendon fibroblasts in response to cyclic uniaxial stretching in serum-free conditions. J Biomech. 2004;37(10):1543–50.

226. Zeichen J, van Griensven M, Bosch U. The Proliferative Response of Isolated Human Tendon Fibroblasts to Cyclic Biaxial Mechanical Strain. Am J Sports Med. 2000;28(6):888–92.

227. Elsdale T, Bard J. Collagen substrata for studies on cell behaviour. J Cell Biol. 1972;54(3):626–37.

228. Butler DL, Gooch C, Kinneberg KRC, Boivin GP, Galloway MT, Nirmalanandhan VS, et al. The use of mesenchymal stem cells in collagen-based scaffolds for tissue-engineered repair of tendons. Nat Protoc. 2010;5(5):849–63.

229. Kuo CK, Tuan RS. Mechanoactive Tenogenic Differentiation of Human Mesenchymal Stem Cells. Tissue Eng Part A. 2008;14(10):1615–27.

230. Chen X, Song X-H, Yin Z, Zou X-H, Wang L-L, Hu H, et al. Stepwise Differentiation of Human Embryonic Stem Cells Promotes Tendon Regeneration by Secreting Fetal Tendon Matrix and Differentiation Factors. Stem Cells. 2009;27(6):1276–87.

231. Yang G, Rothrauff BB, Lin H, Gottardi R, Alexander PG, Tuan RS. Enhancement of tenogenic differentiation of human adipose stem cells by tendon-derived extracellular matrix. Biomaterials. 2013;34(37):9295–306.

232. Altman GH, Horan RL, Martin I, Farhadi J, Stark PRH, Volloch V, et al. Cell differentiation by mechanical stress. FASEB J. 2002;16(2):1–13.

233. Atkinson F, Evans R, Guest JE, Bavin EP, Cacador D, Holland C, et al. Cyclical strain improves artificial equine tendon constructs in vitro. J Tissue Eng Regen Med. 2020;14(5):690–700.

234. Breidenbach AP, Dyment NA, Lu Y, Rao M, Shearn JT, Rowe DW, et al. Fibrin Gels Exhibit Improved Biological, Structural, and Mechanical Properties Compared with Collagen Gels in Cell-Based Tendon Tissue-Engineered Constructs. Tissue Eng Part A. 2015;21(3–4):438–50.

235. Subramanian G, Stasuk A, Elsaadany M, Yildirim-Ayan E. Effect of Uniaxial Tensile Cyclic Loading Regimes on Matrix Organization and Tenogenic Differentiation of Adipose-Derived Stem Cells Encapsulated within 3D Collagen Scaffolds. Stem Cells Int. 2017;2017:6072406.

236. Beldjilali-Labro M, Garcia Garcia A, Farhat F, Bedoui F, Grosset J-F, Dufresne M, et al. Biomaterials in Tendon and Skeletal Muscle Tissue Engineering: Current Trends and Challenges. Materials (Basel). 2018;11(7):1116.

237. Hissnauer TN, Baranowsky A, Pestka JM, Streichert T, Wiegandt K, Goepfert C, et al. Identification of molecular markers for articular cartilage. Osteoarthr Cartil. 2010;18(12):1630–8.

238. Embree MC, Kilts TM, Ono M, Inkson CA, Syed-Picard F, Karsdal MA, et al. Biglycan and Fibromodulin Have Essential Roles in Regulating Chondrogenesis and Extracellular Matrix Turnover in Temporomandibular Joint Osteoarthritis. Am J Pathol. 2010;176(2):812–26.

239. Cheng T, Maddox NC, Wong AW, Rahnama R, Kuo AC. Comparison of gene expression patterns in articular cartilage and dedifferentiated articular chondrocytes. J Orthop Res. 2012;30(2):234–45.

240. Kuemmerle J, Theiss F, Okoniewski M, Weber F, Hemmi S, Mirsaidi A, et al. Identification of Novel Equine (Equus caballus) Tendon Markers Using RNA Sequencing. Genes (Basel). 2016;7(11):97.

241. Soliman H, Rossi FMV. Cardiac fibroblast diversity in health and disease. Matrix Biol. 2020;91–92:75–91.

242. Bagchi RA, Roche P, Aroutiounova N, Espira L, Abrenica B, Schweitzer R, et al. The transcription factor scleraxis is a critical regulator of cardiac fibroblast phenotype. BMC Biol. 2016;14(1):21.

243. Ewis AA, Zhelev Z, Bakalova R, Fukuoka S, Shinohara Y, Ishikawa M, et al. A history of microarrays in biomedicine. Expert Rev Mol Diagn. 2005;5(3):315–28.

244. Stefano GB. Comparing Bioinformatic Gene Expression Profiling Methods: Microarray and RNA-Seq. Med Sci Monit Basic Res. 2014;20:138–42.

245. Anamika K, Verma S, Jere A, Desai A. Transcriptomic Profiling Using Next Generation Sequencing - Advances, Advantages, and Challenges. In: Next Generation Sequencing - Advances, Applications and Challenges. InTech; 2016.

246. Conesa A, Madrigal P, Tarazona S, Gomez-Cabrero D, Cervera A, McPherson A, et al. A survey of best practices for RNA-seq data analysis. Genome Biol. 2016;17(1):13.

247. Wang Z, Gerstein M, Snyder M. RNA-Seq: a revolutionary tool for transcriptomics. Nat Rev Genet. 2009;10(1):57–63.

248. Finotello F, Di Camillo B. Measuring differential gene expression with RNA-seq: challenges and strategies for data analysis. Brief Funct Genomics. 2015;14(2):130–42.

249. Garber M, Grabherr MG, Guttman M, Trapnell C. Computational methods for transcriptome annotation and quantification using RNA-seq. Nat Methods. 2011;8(6):469–77.

250. Soneson C, Delorenzi M. A comparison of methods for differential expression analysis of RNA-seq data. BMC Bioinformatics. 2013;14(1):91.

251. Spies D, Renz PF, Beyer TA, Ciaudo C. Comparative analysis of differential gene expression tools for RNA sequencing time course data. Brief Bioinform. 2019;20(1):288–98.

252. Tang M, Sun J, Shimizu K, Kadota K. Evaluation of methods for differential expression analysis on multi-group RNA-seq count data. BMC Bioinformatics. 2015;16(1):360.

253. Seyednasrollah F, Laiho A, Elo LL. Comparison of software packages for detecting differential expression in RNA-seq studies. Brief Bioinform.

2015;16(1):59–70.

254. Beredjiklian PK, Favata M, Cartmell JS, Flanagan CL, Crombleholme TM, Soslowsky LJ. Regenerative Versus Reparative Healing in Tendon: A Study of Biomechanical and Histological Properties in Fetal Sheep. Ann Biomed Eng. 2003;31(10):1143–52.

255. Favata M, Beredjiklian PK, Zgonis MH, Beason DP, Crombleholme TM, Jawad AF, et al. Regenerative properties of fetal sheep tendon are not adversely affected by transplantation into an adult environment. J Orthop Res. 2006;24(11):2124–32.

256. Coolen NA, Schouten KCWM, Middelkoop E, Ulrich MMW. Comparison between human fetal and adult skin. Arch Dermatol Res. 2010;302(1):47–55.

257. Lin KY, Posnick JC, Al-Qattan MM, Vajsar J, Becker LE. Fetal Nerve Healing: An experimental study. Plast Reconstr Surg. 1994;93(7):1323.

258. Stalling SS, Nicoll SB. Fetal ACL Fibroblasts Exhibit Enhanced Cellular Properties Compared with Adults. Clin Orthop Relat Res. 2008;466(12):3130–7.

259. Tang Q-M, Chen JL, Shen WL, Yin Z, Liu HH, Fang Z, et al. Fetal and adult fibroblasts display intrinsic differences in tendon tissue engineering and regeneration. Sci Rep. 2015;4(1):5515.

260. Grognuz A, Scaletta C, Farron A, Raffoul W, Applegate LA. Human Fetal Progenitor Tenocytes for Regenerative Medicine. Cell Transplant. 2016;25(3):463–79.

261. Han S-H, Yang B-C, Ko M-S, Oh H-S, Lee S-S. Length difference between equine ZFX and ZFY genes and its application for molecular sex determination. J Assist Reprod Genet. 2010;27(12):725–8.

262. Zuker M. Mfold web server for nucleic acid folding and hybridization prediction. Nucleic Acids Res. 2003;31(13):3406–15.

263. Pear WS, Nolan GP, Scott ML, Baltimore D. Production of high-titer helper-free retroviruses by transient transfection. Proc Natl Acad Sci. 1993;90(18):8392–6.

264. Joshi MU, Keith Pittman H, Haisch CE, Verbanac KM. Real-time PCR to determine transgene copy number and to quantitate the biolocalization of adoptively transferred cells from EGFP-transgenic mice. Biotechniques. 2008;45(3):247–58.

265. Barczak W, Suchorska W, Rubiś B, Kulcenty K. Universal Real-Time PCR-Based Assay for Lentiviral Titration. Mol Biotechnol. 2015;57(2):195–200.

266. Sanger F, Nicklen S, Coulson AR. DNA sequencing with chain-terminating inhibitors. Proc Natl Acad Sci. 1977;74(12):5463–7.

267. Bavin EP, Atkinson F, Barsby T, Guest DJ. Scleraxis Is Essential for Tendon Differentiation by Equine Embryonic Stem Cells and in Equine Fetal Tenocytes. Stem Cells Dev. 2017;26(6):441–50.

268. Livak KJ, Schmittgen TD. Analysis of Relative Gene Expression Data Using Real-Time Quantitative PCR and the 2−ΔΔCT Method. Methods. 2001;25(4):402–8.

269. Hart SN, Therneau TM, Zhang Y, Poland GA, Kocher J-P. Calculating Sample Size Estimates for RNA Sequencing Data. J Comput Biol. 2013;20(12):970–8.

270. Kim D, Langmead B, Salzberg SL. HISAT: a fast spliced aligner with low memory requirements. Nat Methods. 2015;12(4):357–60.

271. Li H, Handsaker B, Wysoker A, Fennell T, Ruan J, Homer N, et al. The Sequence Alignment/Map format and SAMtools. Bioinformatics. 2009;25(16):2078–9.

272. Liao Y, Smyth GK, Shi W. featureCounts: an efficient general purpose program for assigning sequence reads to genomic features. Bioinformatics. 2014;30(7):923–30.

273. Love MI, Huber W, Anders S. Moderated estimation of fold change and dispersion for RNA-seq data with DESeq2. Genome Biol. 2014;15(12):550.

274. Patro R, Duggal G, Love MI, Irizarry RA, Kingsford C. Salmon provides fast and bias-aware quantification of transcript expression. Nat Methods. 2017;14(4):417–9.

275. Soneson C, Love MI, Robinson MD. Differential analyses for RNA-seq: transcript-level estimates improve gene-level inferences. F1000Research. 2015;4:1521.

276. Zhao A, Qin H, Fu X. What Determines the Regenerative Capacity in Animals? Bioscience. 2016;66(9):735–46.

277. Rowlatt U. Intrauterine wound healing in a 20 week human fetus. Virchows Arch A Pathol Anat Histol. 1979;381(3):353–61.

278. Rolfe KJ, Grobbelaar AO. A Review of Fetal Scarless Healing. ISRN Dermatol. 2012;2012:698034.

279. Porrello ER, Mahmoud AI, Simpson E, Hill JA, Richardson JA, Olson EN, et al. Transient Regenerative Potential of the Neonatal Mouse Heart. Science (80-). 2011;331(6020):1078–80.

280. Mast BA, Albanese CT, Kapadia S. Tissue Repair in the Fetal Intestinal Tract Occurs With Adhesions, Fibrosis, and Neovascularization. Ann Plast Surg. 1998;41(2):140–7.

281. Block M. Wound Healing in the New-Born Opossum (Didelphis virginianam). Nature. 1960;187(4734):340–1.

282. Lorenz HP, Longaker MT, Perkocha LA, Jennings RW, Harrison MR, Adzick NS. Scarless wound repair: a human fetal skin model. Development. 1992;114(1):253–9.

283. Bagchi D, Das A, Roy S. Wound Healing, Tissue Repair, and Regeneration in Diabetes. Elsevier; 2020. 1–638 p.

284. Armstrong JR, Ferguson MWJ. Ontogeny of the Skin and the Transition from Scar-Free to Scarring Phenotype during Wound Healing in the Pouch Young of a Marsupial, Monodelphis domestica. Dev Biol. 1995;169(1):242–60.

285. Beanes SR, Hu F-Y, Soo C, Dang CMH, Urata M, Ting K, et al. Confocal Microscopic Analysis of Scarless Repair in the Fetal Rat. Plast Reconstr Surg. 2002;109(1):160–70.

286. Longaker MT, Whitby DJ, Adzick NS, Crombleholme TM, Langer JC, Duncan BW, et al. Studies in fetal wound healing VI. Second and early third trimester fetal wounds demonstrate rapid collagen deposition without scar formation. J Pediatr Surg. 1990;25(1):63–9.

287. Whitby DJ, Ferguson MWJ. The extracellular matrix of lip wounds in fetal, neonatal and adult mice. Development. 1991;112(2):651–68.

288. Lovvorn HN, Cheung DT, Nimni ME, Perelman N, Estes JM, Adzick NS. Relative distribution and crosslinking of collagen distinguish fetal from adult sheep wound repair. J Pediatr Surg. 1999;34(1):218–23.

289. Cuttle L, Nataatmadja M, Fraser JF, Kempf M, Kimble RM, Hayes MT. Collagen in the scarless fetal skin wound: Detection with Picrosirius-polarization. Wound Repair Regen. 2005;13(2):198–204.

290. Epstein EH. (Alpha1(3))3 human skin collagen. Release by pepsin digestion and preponderance in fetal life. J Biol Chem. 1974;249(10):3225–31.

291. Merkel JR, DiPaolo BR, Hallock GG, Rice DC. Type I and Type III Collagen Content of Healing Wounds in Fetal and Adult Rats. Exp Biol Med. 1988;187(4):493–7.

292. Hallock GG, Rice DC, Merkel JR, DiPaolo BR. Analysis of Collagen Content in the Fetal Wound. Ann Plast Surg. 1988;21(4):310–5.

293. Knight KR, Lepore DA, Horne RSC, Ritz M, Hurley J V., Kumta S, et al. Collagen content of uninjured skin and scar tissue in foetal and adult sheep. Int J Exp Pathol. 1993;74(6):583–91.

294. Goldberg SR, Quirk GL, Sykes VW, Kordula T, Lanning DA. Altered Procollagen Gene Expression in Mid-Gestational Mouse Excisional Wounds. J Surg Res. 2007;143(1):27–34.

295. Whitby DJ, Longaker MT, Harrison MR, Adzick NS, Ferguson MW. Rapid epithelialisation of fetal wounds is associated with the early deposition of tenascin. J Cell Sci. 1991;99(Pt 3):583–6.

296. Cass D., Bullard K., Slyverster K., Yang E., Sheppard D, Herlyn M, et al. Epidermal Integrin Expression Is Upregulated Rapidly in Human Fetal Wound Repair. J Pediatr Surg. 1998;33(2):312–6.

297. Colwell AS, Krummel TM, Longaker MT, Lorenz HP. Early-Gestation Fetal Scarless Wounds Have Less Lysyl Oxidase Expression. Plast Reconstr Surg. 2006;118(5):1125–9.

298. Beanes SR, Dang C, Soo C, Wang Y, Urata M, Ting K, et al. Down-regulation of decorin, a transforming growth factor–beta modulator, is associated with scarless fetal wound healing. J Pediatr Surg. 2001;36(11):1666–71.

299. Scott PG, Dodd CM, Ghahary A, Shen YJ, Tredget EE. Fibroblasts from Post-Burn Hypertrophic Scar Tissue Synthesize Less Decorin than Normal Dermal Fibroblasts. Clin Sci. 1998;94(5):541–7.

300. Sayani, Dodd, Nedelec, Shen, Ghahary, Tredget, et al. Delayed appearance of decorin in healing burn scars. Histopathology. 2000;36(3):262–72.

301. Peled ZM, Phelps ED, Updike DL, Chang J, Krummel TM, Howard EW, et al. Matrix Metalloproteinases and the Ontogeny of Scarless Repair: The Other Side of the Wound Healing Balance. Plast Reconstr Surg. 2002;110(3):801–11.

302. Soo C, Hu F-Y, Zhang X, Wang Y, Beanes SR, Lorenz HP, et al. Differential Expression of Fibromodulin, a Transforming Growth Factor-β Modulator, in Fetal Skin Development and Scarless Repair. Am J Pathol. 2000;157(2):423–33.

303. Zheng Z, Zhang X, Dang C, Beanes S, Chang GX, Chen Y, et al. Fibromodulin Is Essential for Fetal-Type Scarless Cutaneous Wound Healing. Am J Pathol. 2016;186(11):2824–32.

304. Wilgus TA, Ferreira AM, Oberyszyn TM, Bergdall VK, DiPietro LA. Regulation of scar formation by vascular endothelial growth factor. Lab Investig. 2008;88(6):579–90.

305. Rolfe KJ, Irvine LM, Grobbelaar AO, Linge C. Differential gene expression in response to transforming growth factor-β1 by fetal and postnatal dermal

fibroblasts. Wound Repair Regen. 2007;15(6):897–906.

306. Soo C, Beanes SR, Hu FY, Zhang X, Dang C, Chang G, et al. Ontogenetic Transition in Fetal Wound Transforming Growth Factor-β Regulation Correlates with Collagen Organization. Am J Pathol. 2003;163(6):2459–76.

307. Martin P, Dickson MC, Millan FA, Akhurst RJ. Rapid induction and clearance of TGFβ1 is an early response to wounding in the mouse embryo. Dev Genet. 1993;14(3):225–38.

308. Weissleder R, Lee AS, Fischman AJ, Reimer P, Shen T, Wilkinson R, et al. Polyclonal human immunoglobulin G labeled with polymeric iron oxide: antibody MR imaging. Radiology. 1991;181(1):245–9.

309. Cowin AJ, Holmes TM, Brosnan P, Ferguson MWJ. Expression of TGF-beta and its receptors in murine fetal and adult dermal wounds. Eur J Dermatol. 2001;11(5):424–31.

310. Chen W, Fu X, Ge S, Sun T, Zhou G, Jiang D, et al. Ontogeny of expression of transforming growth factor-β and its receptors and their possible relationship with scarless healing in human fetal skin. Wound Repair Regen. 2005;13(1):68–75.

311. Haynes JH, Johnson DE, Mast BA, Diegelmann RF, Salzberg DA, Cohen IK, et al. Platelet-derived growth factor induces fetal wound fibrosis. J Pediatr Surg. 1994;29(11):1405–8.

312. Chen W, Fu X-B, Ge S-L, Sun T-Z, Sheng Z-Y. Ontogeny of expression of basic fibroblast growth factor and its receptors in human fetal skin. Chinese J Traumatol. 2005;8(6):332–8.

313. Dang CM, Beanes SR, Soo C, Ting K, Benhaim P, Hedrick MH, et al. Decreased expression of fibroblast and keratinocyte growth factor isoforms and receptors during scarless repair. Plast Reconstr Surg. 2003;111(6):1969–79.

314. Rolfe KJ, Cambrey AD, Richardson J, Irvine LM, Grobbelaar AO, Linge C. Dermal fibroblasts derived from fetal and postnatal humans exhibit distinct responses to insulin like growth factors. BMC Dev Biol. 2007;7(1):124.

315. Krummel TM, Nelson JM, Diegelmann RF, Lindblad WJ, Salzberg AM, Greenfield LJ, et al. Fetal response to injury in the rabbit. J Pediatr Surg. 1987;22(7):640–4.

316. Lawrence Depalma R, Krummel TM, Durham LA, Michna BA, Thomas BL, Nelson JM, et al. Characterization and Quantitation of Wound Matrix in the Fetal Rabbit. Matrix. 1989;9(3):224–31.

317. Estes JM, Scott Adzick N, Harrison MR, Longaker MT, Stern R. Hyaluronate metabolism undergoes and ontogenic transition during fetal development: Implications for Scar-free wound healing. J Pediatr Surg. 1993;28(10):1227–31.

318. Longaker MT, Chiu ES, Adzick NS, Stern M, Harrison MR, Stern R. Studies in Fetal Wound Healing V. A Prolonged Presence of Hyaluronic Acid Characterizes Fetal Wound Fluid. Ann Surg. 1991;213(4):292–6.

319. Longaker MT, Chiu ES, Harrison MR, Crombleholme TM, Langer JC, Duncan BW, et al. Studies in Fetal Wound Healing IV. Hyaluronic Acid-Stimulating Activity Distinguishes Fetal Wound Fluid from Adult Wound Fluid. Ann Surg. 1989;210(5):667–72.

320. West DC, Shaw DM, Lorenz P, Adzick NS, Longaker MT. Fibrotic healing of adult and late gestation fetal wounds correlates with increased hyaluronidase activity and removal of hyaluronan. Int J Biochem Cell Biol. 1997;29(1):201–10.

321. Mast BA, Haynes JH, Krummel TM, Diegelmann RF, Cohen IK. In Vivo Degradation of Fetal Wound Hyaluronic Acid Results in Increased Fibroplasia, Collagen Deposition, and Neovascularization. Plast Reconstr Surg. 1992;89(3):503–9.

322. Iocono JA, Ehrlich HP, Keefer KA, Krummel TM. Hyaluronan induces scarless repair in mouse limb organ culture. J Pediatr Surg. 1998;33(4):564–7.

323. Walraven M, Talhout W, Beelen RHJ, van Egmond M, Ulrich MMW. Healthy human second-trimester fetal skin is deficient in leukocytes and associated homing chemokines. Wound Repair Regen. 2016;24(3):533–41.

324. Wulff BC, Parent AE, Meleski MA, DiPietro LA, Schrementi ME, Wilgus TA. Mast Cells Contribute to Scar Formation during Fetal Wound Healing. J Invest Dermatol. 2012;132(2):458–65.

325. Wulff BC, Wilgus TA. Examining the Role of Mast Cells in Fetal Wound Healing Using Cultured Cells In Vitro. Methods Mol Biol. 2013;1037:495–506.

326. Olutoye OO, Alaish SM, Carr ME, Paik M, Yager DR, Cohen IK, et al. Aggregatory characteristics and expression of the collagen adhesion receptor in fetal porcine platelets. J Pediatr Surg. 1995;30(12):1649–53.

327. Olutoye O., Yager D., Cohen I., Diegelmann R. Lower cytokine release by fetal porcine platelets: A possible explanation for reduced inflammation after fetal wounding. J Pediatr Surg. 1996;31(1):91–5.

328. Cowin AJ, Brosnan MP, Holmes TM, Ferguson MWJ. Endogenous inflammatory response to dermal wound healing in the fetal and adult mouse. Dev Dyn. 1998;212(3):385–93.

329. Hopkinson-Woolley J, Hughes D, Gordon S, Martin P. Macrophage recruitment during limb development and wound healing in the embryonic and foetal mouse. J Cell Sci. 1994;107(Pt 5):1159–67.

330. Adolph VR, DiSanto SK, Bleacher JC, Dillon PW, Krummel TM. The potential role of the lymphocyte in fetal wound healing. J Pediatr Surg. 1993;28(10):1316–20.

331. Burrington JD. Wound healing in the fetal lamb. J Pediatr Surg. 1971;6(5):523–8.

332. Scott Adzick N, Harrison MR, Glick PL, Beckstead JH, Villa RL, Scheuenstuhl H, et al. Comparison of fetal, newborn, and adult wound healing by histologic, enzyme-histochemical, and hydroxyproline determinations. J Pediatr Surg. 1985;20(4):315–9.

333. Julia MV, Albert A, Morales L, Miro D, Sancho MA, Garcia X. Wound healing in the fetal period: The resistance of the scar to rupture. J Pediatr Surg. 1993;28(11):1458–62.

334. Olutoye OO, Zhu X, Cass DL, Smith CW. Neutrophil Recruitment by Fetal Porcine Endothelial Cells: Implications in Scarless Fetal Wound Healing. Pediatr Res. 2005;58(6):1290–4.

335. Liechty KW, Adzick NS, Crombleholme TM. IDiminished interleukin 6 (IL-6) production during scarless human fetal wound repair. Cytokine. 2000;12(6):671–6.

336. Liechty KW, Crombleholme TM, Cass DL, Martin B, Adzick NS. Diminished Interleukin-8 (IL-8) Production in the Fetal Wound Healing Response. J Surg Res. 1998;77(1):80–4.

337. Morris MW, Allukian M, Herdrich BJ, Caskey RC, Zgheib C, Xu J, et al. Modulation of the inflammatory response by increasing fetal wound size or interleukin-10 overexpression determines wound phenotype and scar formation. Wound Repair Regen. 2014;22(3):406–14.

338. Gordon A, Kozin ED, Keswani SG, Vaikunth SS, Katz AB, Zoltick PW, et al. Permissive environment in postnatal wounds induced by adenoviral-mediated overexpression of the anti-inflammatory cytokine interleukin-10 prevents scar formation. Wound Repair Regen. 2008;16(1):70–9.

339. Liechty KW, Kim HB, Adzick NS, Crombleholme TM. Fetal wound repair results in scar formation in interleukin-10–deficient mice in a syngeneic murine model of scarless fetal wound repair. J Pediatr Surg. 2000;35(6):866–73.

340. Peranteau WH, Zhang L, Muvarak N, Badillo AT, Radu A, Zoltick PW, et al. IL-10 Overexpression Decreases Inflammatory Mediators and Promotes Regenerative Healing in an Adult Model of Scar Formation. J Invest Dermatol. 2008;128(7):1852–60.

341. Wulff BC, Pappa NK, Wilgus TA. Interleukin-33 encourages scar formation in murine fetal skin wounds. Wound Repair Regen. 2019;27(1):19–28.

342. Wulff BC, Yu L, Parent AE, Wilgus TA. Novel differences in the expression of inflammation-associated genes between mid- and late-gestational dermal fibroblasts. Wound Repair Regen. 2013;21(1):103–12.

343. Hu MS, Januszyk M, Hong WX, Walmsley GG, Zielins ER, Atashroo DA, et al. Gene expression in fetal murine keratinocytes and fibroblasts. J Surg Res. 2014;190(1):344–57.

344. Colwell AS, Longaker MT, Peter Lorenz H. Identification of differentially regulated genes in fetal wounds during regenerative repair. Wound Repair Regen. 2008;16(3):450–9.

345. Estes JM, Berg JS Vande, Adzick NS, MacGillivray TE, Desmoulière A, Gabbiani G. Phenotypic and functional features of myofibroblasts in sheep fetal wounds. Differentiation. 1994;56(3):173–81.

346. McCluskey J, Martin P. Analysis of the Tissue Movements of Embryonic Wound Healing—DiI Studies in the Limb Bud Stage Mouse Embryo. Dev Biol. 1995;170(1):102–14.

347. Brink HE, Bernstein J, Nicoll SB. Fetal dermal fibroblasts exhibit enhanced growth and collagen production in two- and three-dimensional culture in comparison to adult fibroblasts. J Tissue Eng Regen Med. 2009;3(8):623–33.

348. Jerrell RJ, Leih MJ, Parekh A. The altered mechanical phenotype of fetal fibroblasts hinders myofibroblast differentiation. Wound Repair Regen. 2019;27(1):29–38.

349. Parekh A, Sandulache VC, Singh T, Cetin S, Sacks MS, Dohar JE, et al. Prostaglandin E2 differentially regulates contraction and structural reorganization of anchored collagen gels by human adult and fetal dermal fibroblasts. Wound Repair Regen. 2009;17(1):88–98.

350. Sandulache VC, Parekh A, Dohar JE, Hebda PA. Fetal Dermal Fibroblasts Retain a Hyperactive Migratory and Contractile Phenotype Under 2-and 3-Dimensional Constraints Compared to Normal Adult Fibroblasts. Tissue Eng. 2007;13(11):2791–801.

351. Schor SL, Schor AM, Rushton G, Smith L. Adult, foetal and transformed fibroblasts display different migratory phenotypes on collagen gels: evidence for an isoformic transition during foetal development. J Cell Sci. 1985;73:221–34.

352. Martin P, Lewis J. Actin cables and epidermal movement in embryonic wound healing. Nature. 1992;360(6400):179–83.

353. Brock J, Midwinter K, Lewis J, Martin P. Healing of incisional wounds in the embryonic chick wing bud: characterization of the actin purse-string and demonstration of a requirement for Rho activation. J Cell Biol. 1996;135(4):1097–107.

354. McCallion RL, Ferguson MWJ. Fetal Wound Healing and the Development of Antiscarring Therapies for Adult Wound Healing. Mol Cell Biol Wound Repair. 1988;4(1):561–600.

355. Longaker MT, Whitby DJ, Jennings RW, Duncan BW, Ferguson MWJ, Harrison MR, et al. Fetal diaphragmatic wounds heal with scar formation. J Surg Res. 1991;50(4):375–85.

356. De Buys Roessingh AS, Hohlfeld J, Scaletta C, Hirt-Burri N, Gerber S, Hohlfeld P, et al. Development, Characterization, and Use of a Fetal Skin Cell Bank for Tissue Engineering in Wound Healing. Cell Transplant. 2006;15(8–9):823–34.

357. Hohlfeld J, de Buys Roessingh A, Hirt-Burri N, Chaubert P, Gerber S, Scaletta C, et al. Tissue engineered fetal skin constructs for paediatric burns. Lancet (London, England). 2005;366(9488):840–2.

358. von der Mark K, Gauss V, von der Mark H, Müller P. Relationship between cell shape and type of collagen synthesised as chondrocytes lose their cartilage phenotype in culture. Nature. 1977;267(5611):531–2.

359. Lee KS, Cha S-H, Kang HW, Song J-Y, Lee KW, KO KB, et al. Effects of Serial Passage on the Characteristics and Chondrogenic Differentiation of Canine Umbilical Cord Matrix Derived Mesenchymal Stem Cells. Asian-Australasian J Anim Sci. 2013;26(4):588–95.

360. Wall ME, Bernacki SH, Loboa EG. Effects of Serial Passaging on the Adipogenic and Osteogenic Differentiation Potential of Adipose-Derived Human Mesenchymal Stem Cells. Tissue Eng. 2007;13(6):1291–8.

361. Mouriaux F, Zaniolo K, Bergeron M-A, Weidmann C, De La Fouchardière A, Fournier F, et al. Effects of Long-term Serial Passaging on the Characteristics and Properties of Cell Lines Derived From Uveal Melanoma Primary Tumors. Investig Opthalmology Vis Sci. 2016;57(13):5288.

362. Mueller AJ, Tew SR, Vasieva O, Clegg PD, Canty-Laird EG. A systems biology approach to defining regulatory mechanisms for cartilage and tendon cell phenotypes. Sci Rep. 2016;6(1):33956.

363. Stawinski P, Sachidanandam R, Chojnicka I, Płoski R. Basic Bioinformatic Analyses of NGS Data. In: Clinical Applications for Next-Generation Sequencing. Elsevier; 2016. p. 19–37.

364. Mitra A, Skrzypczak M, Ginalski K, Rowicka M. Strategies for Achieving High Sequencing Accuracy for Low Diversity Samples and Avoiding Sample Bleeding Using Illumina Platform. Oudejans C, editor. PLoS One. 2015;10(4):e0120520.

365. Deng G, Li K, Chen S, Chen P, Zheng H, Yu B, et al. Interleukin-10 promotes proliferation and migration, and inhibits tendon differentiation via the JAK/Stat3 pathway in tendon-derived stem cells in vitro. Mol Med Rep. 2018;

366. Ricchetti ET, Reddy SC, Ansorge HL, Zgonis MH, Van Kleunen JP, Liechty KW, et al. Effect of Interleukin-10 Overexpression on the Properties of Healing Tendon in a Murine Patellar Tendon Model. J Hand Surg Am. 2008;

367. Saxena A, Khosraviani S, Noel S, Mohan D, Donner T, Hamad ARA. Interleukin-10 paradox: A potent immunoregulatory cytokine that has been difficult to harness for immunotherapy. Cytokine. 2015;74(1):27–34.

368. Taylor SE, Vaughan-Thomas A, Clements DN, Pinchbeck G, Macrory LC, Smith RK, et al. Gene expression markers of tendon fibroblasts in normal and diseased tissue compared to monolayer and three dimensional culture systems. BMC Musculoskelet Disord. 2009;10(1):27.

369. Kusafuka K, Hiraki Y, Shukunami C, Kayano T, Takemura T. Cartilage-specific matrix protein, chondromodulin-I (ChM-I), is a strong angio-inhibitor in endochondral ossification of human neonatal vertebral tissues in vivo: relationship

with angiogenic factors in the cartilage. Acta Histochem. 2002;104(2):167–75.

370. Delany AM, Hankenson KD. Thrombospondin-2 and SPARC/osteonectin are critical regulators of bone remodeling. J Cell Commun Signal. 2009;3(3–4):227–38.

371. Chen J, Zhang E, Zhang W, Liu Z, Lu P, Zhu T, et al. Fos Promotes Early Stage Teno-Lineage Differentiation of Tendon Stem/Progenitor Cells in Tendon. Stem Cells Transl Med. 2017;6(11):2009–19.

372. Złotkowska A, Andronowska A. Chemokines as the modulators of endometrial epithelial cells remodelling. Sci Rep. 2019;9(1):12968.

373. Balaji S, Watson CL, Ranjan R, King A, Bollyky PL, Keswani SG. Chemokine Involvement in Fetal and Adult Wound Healing. Adv Wound Care. 2015;4(11):660–72.

374. Ellis I, Banyard J, Schor SL. Differential response of fetal and adult fibroblasts to cytokines: Cell migration and hyaluronan synthesis. Development. 1997;124(8):1593–600.

375. Ellis IR, Schor SL. Differential motogenic and biosynthetic response of fetal and adult skin fibroblasts to TGF-β isoforms. Cytokine. 1998;10(4):281–9.

376. Paterson YZ, Cribbs A, Espenel M, Smith EJ, Henson FMD, Guest DJ. Genome-wide transcriptome analysis reveals equine embryonic stem cell-derived tenocytes resemble fetal, not adult tenocytes. Stem Cell Res Ther. 2020;11(1):184.

377. Nichols AEC, Settlage RE, Werre SR, Dahlgren LA. Novel roles for scleraxis in regulating adult tenocyte function. BMC Cell Biol. 2018;19(1):14.

378. Rapaport F, Khanin R, Liang Y, Pirun M, Krek A, Zumbo P, et al. Comprehensive evaluation of differential gene expression analysis methods for RNA-seq data. Genome Biol. 2013;14(9):95.

379. Sahraeian SME, Mohiyuddin M, Sebra R, Tilgner H, Afshar PT, Au KF, et al. Gaining comprehensive biological insight into the transcriptome by performing a broad-spectrum RNA-seq analysis. Nat Commun. 2017;8(1):59.

380. Dillies M-A, Rau A, Aubert J, Hennequet-Antier C, Jeanmougin M, Servant N, et al. A comprehensive evaluation of normalization methods for Illumina high-throughput RNA sequencing data analysis. Brief Bioinform. 2013;14(6):671–83.

381. Schaarschmidt S, Fischer A, Zuther E, Hincha DK. Evaluation of Seven Different RNA-Seq Alignment Tools Based on Experimental Data from the Model Plant Arabidopsis thaliana. Int J Mol Sci. 2020;21(5):1720.

382. Mortazavi A, Williams BA, McCue K, Schaeffer L, Wold B. Mapping and quantifying mammalian transcriptomes by RNA-Seq. Nat Methods. 2008;5(7):621–8.

383. Benjamin AM, Nichols M, Burke TW, Ginsburg GS, Lucas JE. Comparing reference-based RNA-Seq mapping methods for non-human primate data. BMC Genomics. 2014;15(1):570.

384. Baruzzo G, Hayer KE, Kim EJ, Di Camillo B, FitzGerald GA, Grant GR. Simulation-based comprehensive benchmarking of RNA-seq aligners. Nat Methods. 2017;14(2):135–9.

385. Zhang C, Zhang B, Lin L-L, Zhao S. Evaluation and comparison of computational tools for RNA-seq isoform quantification. BMC Genomics. 2017;18(1):583.

386. Mansour TA, Scott EY, Finno CJ, Bellone RR, Mienaltowski MJ, Penedo MC, et al. Tissue resolved, gene structure refined equine transcriptome. BMC Genomics. 2017;18(1):103.

387. Costa-Silva J, Domingues D, Lopes FM. RNA-Seq differential expression analysis: An extended review and a software tool. Wei Z, editor. PLoS One. 2017;12(12):e0190152.

388. Maeda T, Sakabe T, Sunaga A, Sakai K, Rivera AL, Keene DR, et al. Conversion of Mechanical Force into TGF-β-Mediated Biochemical Signals. Curr Biol. 2011;21(11):933–41.

389. Sharma RI, Snedeker JG. Biochemical and biomechanical gradients for directed bone marrow stromal cell differentiation toward tendon and bone. Biomaterials.

2010;31(30):7695–704.

390. Shin S, Sun Y, Liu Y, Khaner H, Svant S, Cai J, et al. Whole Genome Analysis of Human Neural Stem Cells Derived from Embryonic Stem Cells and Stem and Progenitor Cells Isolated from Fetal Tissue. Stem Cells. 2007;25(5):1298–306.

391. Eguizabal C, Aran B, Chuva de Sousa Lopes SM, Geens M, Heindryckx B, Panula S, et al. Two decades of embryonic stem cells: a historical overview. Hum Reprod Open. 2019;2019(1).

392. Liu H, Xu J, Liu C-F, Lan Y, Wylie C, Jiang R. Whole transcriptome expression profiling of mouse limb tendon development by using RNA-seq. J Orthop Res. 2015;33(6):840–8.

393. Doi A, Park I-H, Wen B, Murakami P, Aryee MJ, Irizarry R, et al. Differential methylation of tissue- and cancer-specific CpG island shores distinguishes human induced pluripotent stem cells, embryonic stem cells and fibroblasts. Nat Genet. 2009;41(12):1350–3.

394. Hu B-Y, Weick JP, Yu J, Ma L-X, Zhang X-Q, Thomson JA, et al. Neural differentiation of human induced pluripotent stem cells follows developmental principles but with variable potency. Proc Natl Acad Sci. 2010;107(9):4335–40.

395. Osafune K, Caron L, Borowiak M, Martinez RJ, Fitz-Gerald CS, Sato Y, et al. Marked differences in differentiation propensity among human embryonic stem cell lines. Nat Biotechnol. 2008;26(3):313–5.

396. Hrvatin S, O'Donnell CW, Deng F, Millman JR, Pagliuca FW, DiIorio P, et al. Differentiated human stem cells resemble fetal, not adult, β cells. Proc Natl Acad Sci. 2014;111(8):3038–43.

397. Yin Z, Hu J, Yang L, Zheng Z-F, An C, Wu B, et al. Single-cell analysis reveals a nestin + tendon stem/progenitor cell population with strong tenogenic potentiality. Sci Adv. 2016;2(11):e1600874.

398. Mienaltowski MJ, Adams SM, Birk DE. Tendon proper- and peritenon-derived progenitor cells have unique tenogenic properties. Stem Cell Res Ther.

2014;5(4):86.

399. Busnadiego O, Gonzalez-Santamaria J, Lagares D, Guinea-Viniegra J, Pichol-Thievend C, Muller L, et al. LOXL4 Is Induced by Transforming Growth Factor 1 through Smad and JunB/Fra2 and Contributes to Vascular Matrix Remodeling. Mol Cell Biol. 2013;33(12):2388–401.

400. Huang M, Cai G, Baugh LM, Liu Z, Smith A, Watson M, et al. Systemic Sclerosis Dermal Fibroblasts Induce Cutaneous Fibrosis Through Lysyl Oxidase–like 4: New Evidence From Three-Dimensional Skin-like Tissues. Arthritis Rheumatol. 2020;72(5):791–801.

401. Gourevitch D, Kossenkov A V., Zhang Y, Clark L, Chang C, Showe LC, et al. Inflammation and Its Correlates in Regenerative Wound Healing: An Alternate Perspective. Adv Wound Care. 2014;3(9):592–603.

402. Song EK, Jeon J, Jang DG, Kim HE, Sim HJ, Kwon KY, et al. ITGBL1 modulates integrin activity to promote cartilage formation and protect against arthritis. Sci Transl Med. 2018;10(462):eaam7486.

403. Liedtke D, Orth M, Meissler M, Geuer S, Knaup S, Köblitz I, et al. ECM alterations in Fndc3a (Fibronectin Domain Containing Protein 3A) deficient zebrafish cause temporal fin development and regeneration defects. Sci Rep. 2019;9(1):13383.

404. Dahlgren LA, Mohammed HO, Nixon AJ. Temporal expression of growth factors and matrix molecules in healing tendon lesions. J Orthop Res. 2005;23(1):84–92.

405. Chen CH, Cao Y, Wu YF, Bais AJ, Gao JS, Tang JB. Tendon Healing In Vivo: Gene Expression and Production of Multiple Growth Factors in Early Tendon Healing Period. J Hand Surg Am. 2008;33(10):1834–42.

406. Molloy T, Wang Y, Murrell GAC. The Roles of Growth Factors in Tendon and Ligament Healing. Sport Med. 2003;33(5):381–94.

407. Shimode K, Iwasaki N, Majima T, Funakoshi T, Sawaguchi N, Onodera T, et al. Local Upregulation of Stromal Cell–Derived Factor-1 After Ligament Injuries Enhances Homing Rate of Bone Marrow Stromal Cells in Rats. Tissue Eng Part

A. 2009;15(8):2277–84.

408. Sharma M, Afrin F, Satija N, Tripathi RP, Gangenahalli GU. Stromal-Derived Factor-1/ CXCR4 Signaling: Indispensable Role in Homing and Engraftment of Hematopoietic Stem Cells in Bone Marrow. Stem Cells Dev. 2011;20(6):933–46.

409. Schreier T, Degen E, Baschong W. Fibroblast migration and proliferation during in vitro wound healing. Res Exp Med. 1993;193(1):195–205.

410. Kitaori T, Ito H, Schwarz EM, Tsutsumi R, Yoshitomi H, Oishi S, et al. Stromal cell-derived factor 1/CXCR4 signaling is critical for the recruitment of mesenchymal stem cells to the fracture site during skeletal repair in a mouse model. Arthritis Rheum. 2009;60(3):813–23.

411. Ponte AL, Marais E, Gallay N, Langonné A, Delorme B, Hérault O, et al. The In Vitro Migration Capacity of Human Bone Marrow Mesenchymal Stem Cells: Comparison of Chemokine and Growth Factor Chemotactic Activities. Stem Cells. 2007;25(7):1737–45.

412. Helmo FR, Machado JR, Guimarães CSDO, Teixeira VDPA, Reis MA Dos, Corrêa RRM. Fetal wound healing biomarkers. Dis Markers. 2013;35(6):939–44.

413. Goldberg SR, McKinstry RP, Sykes V, Lanning DA. Rapid closure of midgestational excisional wounds in a fetal mouse model is associated with altered transforming growth factor-β isoform and receptor expression. J Pediatr Surg. 2007;42(6):966–73.

414. Han A, Bandyopadhyay B, Jayaprakash P, Lua I, Sahu D, Chen M, et al. The anti-motility signaling mechanism of TGFβ3 that controls cell traffic during skin wound healing. Biol Open. 2012;1(12):1169–77.

415. Ellis I, Schor SL. The interdependent modulation of hyaluronan synthesis by TGF-β1 and extracellular matrix: Consequences for the control of cell migration. Growth Factors. 1995;12(3):211–22.

416. Schor SL. Cytokine control of cell motility: Modulation and mediation by the extracellular matrix. Prog Growth Factor Res. 1994;5(2):223–48.

417. Chen H, Seaman L, Liu S, Ried T, Rajapakse I. Chromosome conformation and gene expression patterns differ profoundly in human fibroblasts grown in spheroids versus monolayers. Nucleus. 2017;8(4):383–91.

418. Neumann E, Riepl B, Knedla A, Lefèvre S, Tarner IH, Grifka J, et al. Cell culture and passaging alters gene expression pattern and proliferation rate in rheumatoid arthritis synovial fibroblasts. Arthritis Res Ther. 2010;12(3):R83.

419. Hughes P, Marshall D, Reid Y, Parkes H, Gelber C. The costs of using unauthenticated, over-passaged cell lines: how much more data do we need? Biotechniques. 2007;43(5):575–86.

420. Briske-Anderson MJ, Finley JW, Newman SM. The Influence of Culture Time and Passage Number on the Morphological and Physiological Development of Caco-2 Cells. Exp Biol Med. 1997;214(3):248–57.

421. Chang-Liu C-M, Woloschak GE. Effect of passage number on cellular response to DNA-damaging agents: cell survival and gene expression. Cancer Lett. 1997;113(1–2):77–86.

422. Shukunami C, Takimoto A, Nishizaki Y, Yoshimoto Y, Tanaka S, Miura S, et al. Scleraxis is a transcriptional activator that regulates the expression of Tenomodulin, a marker of mature tenocytes and ligamentocytes. Sci Rep. 2018;8(1):3155.

423. Yao L, Bestwick CS, Bestwick LA, Maffulli N, Aspden RM. Phenotypic Drift in Human Tenocyte Culture. Tissue Eng. 2006;12(7):1843–9.

424. Nie C, Wan S, Chen Y, Zhu D, Wang X, Dong X, et al. Loss of scleraxis leads to distinct reduction of mineralized intermuscular bone in zebrafish. Aquac Fish [Internet]. 2020; Available from: https://linkinghub.elsevier.com/retrieve/pii/S2468550X20300484

425. Edom-Vovard F, Duprez D. Signals regulating tendon formation during chick embryonic development. Dev Dyn. 2004;229(3):449–57.

426. Delgado Caceres M, Pfeifer CG, Docheva D. Understanding Tendons: Lessons

from Transgenic Mouse Models. Stem Cells Dev. 2018;27(17):1161–74.

427. Eliasson P, Andersson T, Aspenberg P. Rat Achilles tendon healing: mechanical loading and gene expression. J Appl Physiol. 2009;107(2):399–407.

428. Bagchi RA, Czubryt MP. Scleraxis: A New Regulator of Extracellular Matrix Formation. In: Genes and Cardiovascular Function. Springer; 2011. p. 57–65.

429. Sakabe T, Sakai K, Maeda T, Sunaga A, Furuta N, Schweitzer R, et al. Transcription factor scleraxis vitally contributes to progenitor lineage direction in wound healing of adult tendon in mice. J Biol Chem. 2018;293(16):5766–80.

430. Howell K, Chien C, Bell R, Laudier D, Tufa SF, Keene DR, et al. Novel Model of Tendon Regeneration Reveals Distinct Cell Mechanisms Underlying Regenerative and Fibrotic Tendon Healing. Sci Rep. 2017;7(1):45238.

431. Best KT, Loiselle AE. Scleraxis lineage cells contribute to organized bridging tissue during tendon healing and identify a subpopulation of resident tendon cells. FASEB J. 2019;33(7):8578–87.

432. Espira L, Czubryt MP. Emerging concepts in cardiac matrix biologyThis article is one of a selection of papers published in a special issue on Advances in Cardiovascular Research. Can J Physiol Pharmacol. 2009;87(12):996–1008.

433. Czubryt MP, McAnally J, Fishman GI, Olson EN. Regulation of peroxisome proliferator-activated receptor coactivator 1 (PGC-1) and mitochondrial function by MEF2 and HDAC5. Proc Natl Acad Sci. 2003;100(4):1711–6.

434. Naitoh M, Kubota H, Ikeda M, Tanaka T, Shirane H, Suzuki S, et al. Gene expression in human keloids is altered from dermal to chondrocytic and osteogenic lineage. Genes to Cells. 2005;10(11):1081–91.

435. Theodossiou SK, Schiele NR. Models of tendon development and injury. BMC Biomed Eng. 2019;1(1):32.

436. Yates CC, Hebda P, Wells A. Skin Wound Healing and Scarring: Fetal Wounds and Regenerative Restitution. Birth Defects Res Part C Embryo Today Rev. 2012;96(4):325–33.

437. Cox BC, Chai R, Lenoir A, Liu Z, Zhang L, Nguyen D-H, et al. Spontaneous hair cell regeneration in the neonatal mouse cochlea in vivo. Development. 2014;141(4):816–29.

438. Ansorge HL, Hsu JE, Edelstein L, Adams S, Birk DE, Soslowsky LJ. Recapitulation of the Achilles tendon mechanical properties during neonatal development: A Study of differential healing during two stages of development in a mouse model. J Orthop Res. 2012;30(3):448–56.

439. Ballas CB, Davidson JM. Delayed wound healing in aged rats is associated with increased collagen gel remodeling and contraction by skin fibroblasts, not with differences in apoptotic or myofibroblast cell populations. Wound Repair Regen. 2001;9(3):223–37.

440. Chen J, Zhang W, Liu Z, Zhu T, Shen W, Ran J, et al. Characterization and comparison of post-natal rat Achilles tendon-derived stem cells at different development stages. Sci Rep. 2016;6(1):22946.

441. Iismaa SE, Kaidonis X, Nicks AM, Bogush N, Kikuchi K, Naqvi N, et al. Comparative regenerative mechanisms across different mammalian tissues. NPJ Regen Med. 2018;3(1):6.

442. Léjard V, Brideau G, Blais F, Salingcarnboriboon R, Wagner G, Roehrl MHA, et al. Scleraxis and NFATc Regulate the Expression of the Pro-α1(I) Collagen Gene in Tendon Fibroblasts. J Biol Chem. 2007;282(24):17665–75.

443. Shukunami C, Takimoto A, Oro M, Hiraki Y. Scleraxis positively regulates the expression of tenomodulin, a differentiation marker of tenocytes. Dev Biol. 2006;298(1):234–47.

444. Czubryt MP. A tale of 2 tissues: the overlapping role of scleraxis in tendons and the heart. Can J Physiol Pharmacol. 2014;92(9):707–12.

445. Roguljic H, Matthews BG, Yang W, Cvija H, Mina M, Kalajzic I. In vivo Identification of Periodontal Progenitor Cells. J Dent Res. 2013;92(8):709–15.

446. Bagchi RA, Czubryt MP. Synergistic roles of scleraxis and Smads in the regulation

of collagen 1α2 gene expression. Biochim Biophys Acta - Mol Cell Res. 2012;1823(10):1936–44.

447. Nagalingam RS, Safi HA, Al-Hattab DS, Bagchi RA, Landry NM, Dixon IMC, et al. Regulation of cardiac fibroblast MMP2 gene expression by scleraxis. J Mol Cell Cardiol. 2018;120:64–73.

448. Bagchi RA, Lin J, Wang R, Czubryt MP. Regulation of fibronectin gene expression in cardiac fibroblasts by scleraxis. Cell Tissue Res. 2016;366(2):381–91.

449. Liu Y, Watanabe H, Nifuji A, Yamada Y, Olson EN, Noda M. Overexpression of a Single Helix-Loop-Helix-type Transcription Factor, Scleraxis, Enhances Aggrecan Gene Expression in Osteoblastic Osteosarcoma ROS17/2.8 Cells. J Biol Chem. 1997;272(47):29880–5.

450. Al-Hattab DS, Safi HA, Nagalingam RS, Bagchi RA, Stecy MT, Czubryt MP. Scleraxis regulates Twist1 and Snai1 expression in the epithelial-to-mesenchymal transition. Am J Physiol Circ Physiol. 2018;315(3):H658–68.

451. Espira L, Lamoureux L, Jones SC, Gerard RD, Dixon IMC, Czubryt MP. The basic helix–loop–helix transcription factor scleraxis regulates fibroblast collagen synthesis. J Mol Cell Cardiol. 2009;47(2):188–95.

452. Roche PL, Nagalingam RS, Bagchi RA, Aroutiounova N, Belisle BMJ, Wigle JT, et al. Role of scleraxis in mechanical stretch-mediated regulation of cardiac myofibroblast phenotype. Am J Physiol Physiol. 2016;311(2):297–307.

453. Furumatsu T, Shukunami C, Amemiya-Kudo M, Shimano H, Ozaki T. Scleraxis and E47 cooperatively regulate the Sox9-dependent transcription. Int J Biochem Cell Biol. 2010;42(1):148–56.

454. Abe H, Tominaga T, Matsubara T, Abe N, Kishi S, Nagai K, et al. Scleraxis Modulates Bone Morphogenetic Protein 4 (BMP4)-Smad1 Protein-Smooth Muscle α-Actin (SMA) Signal Transduction in Diabetic Nephropathy. J Biol Chem. 2012;287(24):20430–42.

455. Chen X, Yin Z, Chen J, Liu H, Shen W, Fang Z, et al. Scleraxis-overexpressed human embryonic stem cell-derived mesenchymal stem cells for tendon tissue engineering with knitted silk-collagen scaffold. Tissue Eng Part A. 2014;20(11–12):1583–92.

456. Yoshimoto Y, Takimoto A, Watanabe H, Hiraki Y, Kondoh G, Shukunami C. Scleraxis is required for maturation of tissue domains for proper integration of the musculoskeletal system. Sci Rep. 2017;7(1):45010.

457. Barnette DN, Hulin A, Ahmed ASI, Colige AC, Azhar M, Lincoln J. Tgfβ-Smad and MAPK signaling mediate scleraxis and proteoglycan expression in heart valves. J Mol Cell Cardiol. 2013;65:137–46.

458. Blitz E, Viukov S, Sharir A, Shwartz Y, Galloway JL, Pryce BA, et al. Bone Ridge Patterning during Musculoskeletal Assembly Is Mediated through SCX Regulation of Bmp4 at the Tendon-Skeleton Junction. Dev Cell. 2009;17(6):861–73.

459. Takimoto A, Kawatsu M, Yoshimoto Y, Kawamoto T, Seiryu M, Takano-Yamamoto T, et al. Scleraxis and osterix antagonistically regulate tensile force-responsive remodeling of the periodontal ligament and alveolar bone. Development. 2015;142(4):787–96.

460. Barnette DN, VandeKopple M, Wu Y, Willoughby DA, Lincoln J. RNA-Seq Analysis to Identify Novel Roles of Scleraxis during Embryonic Mouse Heart Valve Remodeling. PLoS One. 2014;9(7):e101425.

461. Muir T, Sadler-Riggleman I, Skinner MK. Role of the Basic Helix-Loop-Helix Transcription Factor, Scleraxis, in the Regulation of Sertoli Cell Function and Differentiation. Mol Endocrinol. 2005;19(8):2164–74.

462. Chen W, Tang H, Zhou M, Hu C, Zhang J, Tang K. Dexamethasone inhibits the differentiation of rat tendon stem cells into tenocytes by targeting the scleraxis gene. J Steroid Biochem Mol Biol. 2015;152:16–24.

463. Chen K, Zhou X, Sun Z. Haplodeficiency of Klotho Gene Causes Arterial Stiffening via Upregulation of Scleraxis Expression and Induction of Autophagy. Hypertension. 2015;66(5):1006–13.

464. Bagchi RA, Wang R, Jahan F, Wigle JT, Czubryt MP. Regulation of scleraxis transcriptional activity by serine phosphorylation. J Mol Cell Cardiol. 2016;92:140–8.

465. Havis E, Bonnin M-A, Esteves de Lima J, Charvet B, Milet C, Duprez D. TGFβ and FGF promote tendon progenitor fate and act downstream of muscle contraction to regulate tendon differentiation during chick limb development. Development. 2016;143(20):3839–51.

466. Evans TG. Considerations for the use of transcriptomics in identifying the "genes that matter" for environmental adaptation. J Exp Biol. 2015;218(12):1925–35.

467. Chung S, Andersson T, Sonntag K-C, Björklund L, Isacson O, Kim K-S. Analysis of Different Promoter Systems for Efficient Transgene Expression in Mouse Embryonic Stem Cell Lines. Stem Cells. 2002;20(2):139–45.

468. Liew C-G, Draper JS, Walsh J, Moore H, Andrews PW. Transient and Stable Transgene Expression in Human Embryonic Stem Cells. Stem Cells. 2007;25(6):1521–8.

469. Norrman K, Fischer Y, Bonnamy B, Wolfhagen Sand F, Ravassard P, Semb H. Quantitative Comparison of Constitutive Promoters in Human ES cells. PLoS One. 2010;5(8):e12413.

470. Wang R, Liang J, Jiang H, Qin L-J, Yang H-T. Promoter-Dependent EGFP Expression during Embryonic Stem Cell Propagation and Differentiation. Stem Cells Dev. 2008;17(2):279–90.

471. Paterson YZ, Evans N, Kan S, Cribbs A, Henson FMD, Guest DJ. The transcription factor scleraxis differentially regulates gene expression in tenocytes isolated at different developmental stages. Mech Dev. 2020;163:103635.

472. Zhang B, Metharom P, Jullie H, Ellem KA, Cleghorn G, West MJ, et al. The significance of controlled conditions in lentiviral vector titration and in the use of multiplicity of infection (MOI) for predicting gene transfer events. Genet Vaccines Ther. 2004;2(1):6.

473. Holic N, Seye AK, Majdoul S, Martin S, Merten OW, Galy A, et al. Influence of Mildly Acidic pH Conditions on the Production of Lentiviral and Retroviral Vectors. Hum Gene Ther Clin Dev. 2014;25(3):178–85.

474. Liu H-S, Jan M-S, Chou C-K, Chen P-H, Ke N-J. Is Green Fluorescent Protein Toxic to the Living Cells? Biochem Biophys Res Commun. 1999;260(3):712–7.

475. Taghizadeh RR, Sherley JL. CFP and YFP, but Not GFP, Provide Stable Fluorescent Marking of Rat Hepatic Adult Stem Cells. J Biomed Biotechnol. 2008;2008:453590.

476. Lamarre S, Frasse P, Zouine M, Labourdette D, Sainderichin E, Hu G, et al. Optimization of an RNA-Seq Differential Gene Expression Analysis Depending on Biological Replicate Number and Library Size. Front Plant Sci. 2018;9:108.

477. Baccarella A, Williams CR, Parrish JZ, Kim CC. Empirical assessment of the impact of sample number and read depth on RNA-Seq analysis workflow performance. BMC Bioinformatics. 2018;19(1):423.

478. Son K, Yu S, Shin W, Han K, Kang K. A Simple Guideline to Assess the Characteristics of RNA-Seq Data. Biomed Res Int. 2018;2018:2906292.

479. Cserjesi P, Brown D, Ligon KL, Lyons GE, Copeland NG, Gilbert DJ, et al. Scleraxis: a basic helix-loop-helix protein that prefigures skeletal formation during mouse embryogenesis. Development. 1995;121(4):1099–110.

480. Hobert O. Gene Regulation by Transcription Factors and MicroRNAs. Science (80-). 2008;319(5871):1785–6.

481. Lambert SA, Jolma A, Campitelli LF, Das PK, Yin Y, Albu M, et al. The Human Transcription Factors. Cell. 2018;172(4):650–65.

482. Carlberg AL, Tuan RS, Hall DJ. Regulation of Scleraxis Function by Interaction with the bHLH Protein E47. Mol Cell Biol Res Commun. 2000;3(2):82–6.

483. Szklarczyk D, Gable AL, Lyon D, Junge A, Wyder S, Huerta-Cepas J, et al. STRING v11: protein–protein association networks with increased coverage, supporting functional discovery in genome-wide experimental datasets. Nucleic

Acids Res. 2019;47(1):607–13.

484. Asou Y, Nifuji A, Tsuji K, Shinomiya K, Olson EN, Koopman P, et al. Coordinated expression ofscleraxis andSox9 genes during embryonic development of tendons and cartilage. J Orthop Res. 2002;20(4):827–33.

485. Firth EC. The response of bone, articular cartilage and tendon to exercise in the horse. J Anat. 2006;208(4):513–26.

486. Mendias CL, Gumucio JP, Bakhurin KI, Lynch EB, Brooks S V. Physiological loading of tendons induces scleraxis expression in epitenon fibroblasts. J Orthop Res. 2012;30(4):606–12.

487. Dideriksen K, Boesen AP, Reitelseder S, Couppé C, Svensson R, Schjerling P, et al. Tendon collagen synthesis declines with immobilization in elderly humans: no effect of anti-inflammatory medication. J Appl Physiol. 2017;122(2):273–82.

488. Akiyama H. The transcription factor Sox9 has essential roles in successive steps of the chondrocyte differentiation pathway and is required for expression of Sox5 and Sox6. Genes Dev. 2002;16(21):2813–28.

489. Suzuki N, Mizuniwa C, Ishii K, Nakagawa Y, Tsuji K, Muneta T, et al. Teneurin-4, a transmembrane protein, is a novel regulator that suppresses chondrogenic differentiation. J Orthop Res. 2014;32(7):915–22.

490. Sekiya I, Tsuji K, Koopman P, Watanabe H, Yamada Y, Shinomiya K, et al. SOX9 Enhances Aggrecan Gene Promoter/Enhancer Activity and Is Up-regulated by Retinoic Acid in a Cartilage-derived Cell Line, TC6. J Biol Chem. 2000;275(15):10738–44.

491. Gertz J, Reddy TE, Varley KE, Garabedian MJ, Myers RM. Genistein and bisphenol A exposure cause estrogen receptor 1 to bind thousands of sites in a cell type-specific manner. Genome Res. 2012;22(11):2153–62.

492. Lee TI, Young RA. Transcriptional Regulation and Its Misregulation in Disease. Cell. 2013;152(6):1237–51.

493. Mitsis T, Efthimiadou A, Bacopoulou F, Vlachakis D, Chrousos G, Eliopoulos E.

Transcription factors and evolution: An integral part of gene expression (Review). World Acad Sci J. 2020;2:3–8.

494. Johnson PF, McKnight SL. Eukaryotic Transcriptional Regulatory Proteins. Annu Rev Biochem. 1989;58(1):799–839.

495. Massari ME, Murre C. Helix-Loop-Helix Proteins: Regulators of Transcription in Eucaryotic Organisms. Mol Cell Biol. 2000;20(2):429–40.

496. Gyoja F. Basic helix-loop-helix transcription factors in evolution: Roles in development of mesoderm and neural tissues. genesis. 2017;55(9):e23051.

497. Murre C, Bain G, van Dijk MA, Engel I, Furnari BA, Massari ME, et al. Structure and function of helix-loop-helix proteins. Biochim Biophys Acta - Gene Struct Expr. 1994;1218(2):129–35.

498. Jones S. An overview of the basic helix-loop-helix proteins. Genome Biol. 2004;5(6):226.

499. Muir T, Wilson-Rawls J, Stevens JD, Rawls A, Schweitzer R, Kang C, et al. Integration of CREB and bHLH transcriptional signaling pathways through direct heterodimerization of the proteins: role in muscle and testis development. Mol Reprod Dev. 2008;75(11):1637–52.

500. Geertz M, Maerkl SJ. Experimental strategies for studying transcription factor-DNA binding specificities. Brief Funct Genomics. 2010;9(5–6):362–73.

501. Inukai S, Kock KH, Bulyk ML. Transcription factor–DNA binding: beyond binding site motifs. Curr Opin Genet Dev. 2017;43:110–9.

502. Slattery M, Zhou T, Yang L, Dantas Machado AC, Gordân R, Rohs R. Absence of a simple code: how transcription factors read the genome. Trends Biochem Sci. 2014;39(9):381–99.

503. Jolma A, Taipale J. Methods for Analysis of Transcription Factor DNA-Binding Specificity In Vitro. Subcell Biochem. 2011;52:155–73.

504. Brand LH, Satbhai SB, Kolukisaoglu Ü, Wanke D. Limits And Prospects Of

Methods For The Analysis Of DNA-Protein Interaction. Anal Regul DNA Curr Dev Knowl Appl Uncovering Gene Regul. 2013;2013:124–48.

505. Liu ET, Pott S, Huss M. Q&A: ChIP-seq technologies and the study of gene regulation. BMC Biol. 2010;8(1):56.

506. Haring M, Offermann S, Danker T, Horst I, Peterhansel C, Stam M. Chromatin immunoprecipitation: optimization, quantitative analysis and data normalization. Plant Methods. 2007;3(1):11.

507. Teo Z, Chan JSK, Chong HC, Sng MK, Choo CC, Phua GZM, et al. Angiopoietin-like 4 induces a β-catenin-mediated upregulation of ID3 in fibroblasts to reduce scar collagen expression. Sci Rep. 2017;7(1):6303.

508. Mutskov V, Felsenfeld G. Silencing of transgene transcription precedes methylation of promoter DNA and histone H3 lysine 9. EMBO J. 2004;23(1):138–49.

509. Tariq M, Saze H, Probst A V., Lichota J, Habu Y, Paszkowski J. Erasure of CpG methylation in Arabidopsis alters patterns of histone H3 methylation in heterochromatin. Proc Natl Acad Sci. 2003;100(15):8823–7.

510. Nagaki K, Talbert PB, Zhong CX, Dawe RK, Henikoff S, Jiang J. Chromatin immunoprecipitation reveals that the 180-bp satellite repeat is the key functional DNA element of Arabidopsis thaliana centromeres. Genetics. 2003;163(3):1221–5.

511. Kristjuhan A, Svejstrup JQ. Evidence for distinct mechanisms facilitating transcript elongation through chromatin in vivo. EMBO J. 2004;23(21):4243–52.

512. Mathieu O, Probst A V., Paszkowski J. Distinct regulation of histone H3 methylation at lysines 27 and 9 by CpG methylation in Arabidopsis. EMBO J. 2005;24(15):2783–91.

513. Asp P. The chromatin immunoprecipitation (ChIP) assay and ChIP-qPCR. In: Epigenetics Methods. Elsevier; 2020. p. 281–96.

514. Keller DM, McWeeney S, Arsenlis A, Drouin J, Wright CVE, Wang H, et al.

Characterization of Pancreatic Transcription Factor Pdx-1 Binding Sites Using Promoter Microarray and Serial Analysis of Chromatin Occupancy. J Biol Chem. 2007;282(44):32084–92.

515. Hansen TVO, Hammer NA, Nielsen J, Madsen M, Dalbaeck C, Wewer UM, et al. Dwarfism and Impaired Gut Development in Insulin-Like Growth Factor II mRNA-Binding Protein 1-Deficient Mice. Mol Cell Biol. 2004;24(10):4448–64.

516. Song JS, Hwang DH, Kim S-O, Jeon M, Choi B-J, Jung H-S, et al. Comparative Gene Expression Analysis of the Human Periodontal Ligament in Deciduous and Permanent Teeth. PLoS One. 2013;8(4):e61231.

517. Kendall RT, Feghali-Bostwick CA. Fibroblasts in fibrosis: novel roles and mediators. Front Pharmacol. 2014;5:123.

518. Yang G, Rothrauff BB, Tuan RS. Tendon and ligament regeneration and repair: Clinical relevance and developmental paradigm. Birth Defects Res Part C Embryo Today Rev. 2013;99(3):203–22.

519. Tozer S, Bonnin M-A, Relaix F, Di Savino S, Garcia-Villalba P, Coumailleau P, et al. Involvement of vessels and PDGFB in muscle splitting during chick limb development. Development. 2007;134(14):2579–91.

520. Goode DK, Obier N, Vijayabaskar MS, Lie-A-Ling M, Lilly AJ, Hannah R, et al. Dynamic Gene Regulatory Networks Drive Hematopoietic Specification and Differentiation. Dev Cell. 2016;36(5):572–87.

521. Gong W, Koyano-Nakagawa N, Li T, Garry DJ. Inferring dynamic gene regulatory networks in cardiac differentiation through the integration of multi-dimensional data. BMC Bioinformatics. 2015;16(1):74.

522. Li X, MacArthur S, Bourgon R, Nix D, Pollard DA, Iyer VN, et al. Transcription Factors Bind Thousands of Active and Inactive Regions in the Drosophila Blastoderm. PLoS Biol. 2008;6(2):e27.

523. Fisher WW, Li JJ, Hammonds AS, Brown JB, Pfeiffer BD, Weiszmann R, et al. DNA regions bound at low occupancy by transcription factors do not drive

patterned reporter gene expression in Drosophila. Proc Natl Acad Sci. 2012;109(52):21330–5.

524. Stella S, Cascio D, Johnson RC. The shape of the DNA minor groove directs binding by the DNA-bending protein Fis. Genes Dev. 2010;24(8):814–26.

525. Chen Y, Zhang X, Dantas Machado AC, Ding Y, Chen Z, Qin PZ, et al. Structure of p53 binding to the BAX response element reveals DNA unwinding and compression to accommodate base-pair insertion. Nucleic Acids Res. 2013;41(17):8368–76.

526. Wang J, Zhuang J, Iyer S, Lin X, Whitfield TW, Greven MC, et al. Sequence features and chromatin structure around the genomic regions bound by 119 human transcription factors. Genome Res. 2012;22(9):1798–812.

527. Dror I, Golan T, Levy C, Rohs R, Mandel-Gutfreund Y. A widespread role of the motif environment in transcription factor binding across diverse protein families. Genome Res. 2015;25(9):1268–80.

528. Gomes ALC, Wang HH. The Role of Genome Accessibility in Transcription Factor Binding in Bacteria. Przytycka TM, editor. PLOS Comput Biol. 2016;12(4):e1004891.

529. Stergachis AB, Neph S, Reynolds A, Humbert R, Miller B, Paige SL, et al. Developmental Fate and Cellular Maturity Encoded in Human Regulatory DNA Landscapes. Cell. 2013;154(4):888–903.

530. Thomas S, Li X-Y, Sabo PJ, Sandstrom R, Thurman RE, Canfield TK, et al. Dynamic reprogramming of chromatin accessibility during Drosophila embryo development. Genome Biol. 2011;12(5):43.

531. Thurman RE, Rynes E, Humbert R, Vierstra J, Maurano MT, Haugen E, et al. The accessible chromatin landscape of the human genome. Nature. 2012;489(7414):75–82.

532. Ciofani M, Madar A, Galan C, Sellars M, Mace K, Pauli F, et al. A Validated Regulatory Network for Th17 Cell Specification. Cell. 2012;151(2):289–303.

533. Lee B-K, Bhinge AA, Battenhouse A, McDaniell RM, Liu Z, Song L, et al. Cell-type specific and combinatorial usage of diverse transcription factors revealed by genome-wide binding studies in multiple human cells. Genome Res. 2012;22(1):9–24.

534. Kular JK, Basu S, Sharma RI. The extracellular matrix: Structure, composition, age-related differences, tools for analysis and applications for tissue engineering. J Tissue Eng. 2014;5:204173141455711.

535. Rose AB. Introns as Gene Regulators: A Brick on the Accelerator. Front Genet. 2019;9:672.

536. Smith RKW, McIlwraith CW. Consensus on equine tendon disease: Building on the 2007 Havemeyer symposium. Equine Vet J. 2012;44(1):2–6.

537. Smith RKW. Regenerative medicine in equine orthopaedics: what and when? UK-Vet Equine. 2020;4(1):8–13.

538. Smith RKW, Werling NJ, Dakin SG, Alam R, Goodship AE, Dudhia J. Beneficial Effects of Autologous Bone Marrow-Derived Mesenchymal Stem Cells in Naturally Occurring Tendinopathy. Laird EG, editor. PLoS One. 2013;8(9):e75697.

539. Dyson SJ. Medical management of superficial digital flexor tendonitis: a comparative study in 219 horses (1992-2000). Equine Vet J. 2004;36(5):415–9.

540. O'Meara B, Bladon B, Parkin TDH, Fraser B, Lischer CJ. An investigation of the relationship between race performance and superficial digital flexor tendonitis in the Thoroughbred racehorse. Equine Vet J. 2010;42(4):322–6.

541. Wu F, Nerlich M, Docheva D. Tendon injuries. EFORT Open Rev. 2017;2(7):332–42.

542. Jonsson MKB, Hartman RJG, Ackers-Johnson M, Tan WLW, Lim B, van Veen TAB, et al. A Transcriptomic and Epigenomic Comparison of Fetal and Adult Human Cardiac Fibroblasts Reveals Novel Key Transcription Factors in Adult Cardiac Fibroblasts. JACC Basic to Transl Sci. 2016;1(7):590–602.

543. Ramelet A-A, Hirt-Burri N, Raffoul W, Scaletta C, Pioletti DP, Offord E, et al. Chronic wound healing by fetal cell therapy may be explained by differential gene profiling observed in fetal versus old skin cells. Exp Gerontol. 2009;44(3):208–18.

544. Herdrich BJ, Danzer E, Davey MG, Bermudez DM, Radu A, Zhang L, et al. Fetal tendon wound size modulates wound gene expression and subsequent wound phenotype. Wound Repair Regen. 2010;18(5):543–9.

545. Maisel M, Herr A, Milosevic J, Hermann A, Habisch H-J, Schwarz S, et al. Transcription Profiling of Adult and Fetal Human Neuroprogenitors Identifies Divergent Paths to Maintain the Neuroprogenitor Cell State. Stem Cells. 2007;25(5):1231–40.

546. Weber EL, Lai Y-C, Garner W, Chuong CM. Abstract 81. Transcriptome Analysis of Fetal Versus Adult Hair Follicle Dermal Papilla Cells Reveals Key Differences to Explain the Lack of Human Adult Hair Follicle Regenerative Capacity. Plast Reconstr Surg - Glob Open [Internet]. 2017;5:61–2. Available from: http://journals.lww.com/01720096-201704001-00081

547. Camp JG, Badsha F, Florio M, Kanton S, Gerber T, Wilsch-Bräuninger M, et al. Human cerebral organoids recapitulate gene expression programs of fetal neocortex development. Proc Natl Acad Sci. 2015;112(51):15672–7.

548. Baxter M, Withey S, Harrison S, Segeritz C-P, Zhang F, Atkinson-Dell R, et al. Phenotypic and functional analyses show stem cell-derived hepatocyte-like cells better mimic fetal rather than adult hepatocytes. J Hepatol. 2015;62(3):581–9.

549. Blodgett DM, Nowosielska A, Afik S, Pechhold S, Cura AJ, Kennedy NJ, et al. Novel Observations From Next-Generation RNA Sequencing of Highly Purified Human Adult and Fetal Islet Cell Subsets. Diabetes. 2015;64(9):3172–81.

550. Brink HE, Miller GJ, Beredjiklian PK, Nicoll SB. Serum-dependent effects on adult and fetal tendon fibroblast migration and collagen expression. Wound Repair Regen. 2006;14(2):179–86.

551. Yan Z, Yin H, Brochhausen C, Pfeifer CG, Alt V, Docheva D. Aged Tendon Stem/Progenitor Cells Are Less Competent to Form 3D Tendon Organoids Due to

Cell Autonomous and Matrix Production Deficits. Front Bioeng Biotechnol. 2020;8:406.

552. Jensen C, Teng Y. Is It Time to Start Transitioning From 2D to 3D Cell Culture? Front Mol Biosci. 2020;7:33.

553. Hong H, Stegemann JP. 2D and 3D collagen and fibrin biopolymers promote specific ECM and integrin gene expression by vascular smooth muscle cells. J Biomater Sci Polym Ed. 2008;19(10):1279–93.

554. Duval K, Grover H, Han L-H, Mou Y, Pegoraro AF, Fredberg J, et al. Modeling Physiological Events in 2D vs. 3D Cell Culture. Physiology. 2017;32(4):266–77.

555. Rosmark O, Åhrman E, Müller C, Elowsson Rendin L, Eriksson L, Malmström A, et al. Quantifying extracellular matrix turnover in human lung scaffold cultures. Sci Rep. 2018;8(1):5409.

556. Dakin SG, Werling D, Hibbert A, Abayasekara DRE, Young NJ, Smith RKW, et al. Macrophage Sub-Populations and the Lipoxin A4 Receptor Implicate Active Inflammation during Equine Tendon Repair. PLoS One. 2012;7(2):e32333.

557. Dakin SG, Dudhia J, Werling NJ, Werling D, Abayasekara DRE, Smith RKW. Inflamm-Aging and Arachadonic Acid Metabolite Differences with Stage of Tendon Disease. PLoS One. 2012;7(11):e48978.

558. Millar NL, Murrell GAC, McInnes IB. Inflammatory mechanisms in tendinopathy – towards translation. Nat Rev Rheumatol. 2017;13(2):110–22.

559. Dakin SG, Dudhia J, Smith RKW. Science in brief: Resolving tendon inflammation. A new perspective. Equine Vet J. 2013;45(4):398–400.

560. Clegg PD, Strassburg S, Smith RK. Cell phenotypic variation in normal and damaged tendons. Int J Exp Pathol. 2007;88(4):227–35.

561. Hosaka Y, Kirisawa R, Yamamoto E, Ueda H, Iwai H, Takehana K. Localization of Cytokines in Tendinocytes of the Superficial Digital Flexor Tendon in the Horse. J Vet Med Sci. 2002;64(10):945–7.

562. Satish L, Kathju S. Cellular and Molecular Characteristics of Scarless versus Fibrotic Wound Healing. Dermatol Res Pract. 2010;2010:790234.

563. Lin RY, Sullivan KM, Argenta PA, Meuli M, Lorenz HP, Adzick NS. Exogenous Transforming Growth Factor-Beta Amplifies Its Own Expression and Induces Scar Formation in a Model of Human Fetal Skin Repair. Ann Surg. 1995;222(2):146–54.

564. Sullivan KM, Lorenz HP, Meuli M, Lin RY, Adzick NS. A model of scarless human fetal wound repair is deficient in transforming growth factor beta. J Pediatr Surg. 1995;30(2):198–203.

565. Sandulache VC, Dohar JE, Hebda PA. Adult-fetal fibroblast interactions: effects on cell migration and implications for cell transplantation. Cell Transplant. 2005;14(5):331–7.

566. Metcalfe AD, Ferguson MW. Tissue engineering of replacement skin: the crossroads of biomaterials, wound healing, embryonic development, stem cells and regeneration. J R Soc Interface. 2007;4(14):413–37.

567. Bradshaw H, Williams J. Evaluation of equine superficial digital flexor tendon lesions. Vet Nurse. 2012;3(9):578–84.

568. Chisari E, Rehak L, Khan WS, Maffulli N. The role of the immune system in tendon healing: a systematic review. Br Med Bull. 2020;133(1):49–64.

569. Sikes KJ, Li J, Gao S-G, Shen Q, Sandy JD, Plaas A, et al. TGF-b1 or hypoxia enhance glucose metabolism and lactate production via HIF1A signaling in tendon cells. Connect Tissue Res. 2018;59(5):458–71.

570. Izumi S, Otsuru S, Adachi N, Akabudike N, Enomoto-Iwamoto M. Control of glucose metabolism is important in tenogenic differentiation of progenitors derived from human injured tendons. Dong Y, editor. PLoS One. 2019;14(3):e0213912.

571. Freedman BR, Rodriguez AB, Leiphart RJ, Newton JB, Ban E, Sarver JJ, et al. Dynamic Loading and Tendon Healing Affect Multiscale Tendon Properties and ECM Stress Transmission. Sci Rep. 2018;8(1):10854.

572. Svensson V, Vento-Tormo R, Teichmann SA. Exponential scaling of single-cell RNA-seq in the past decade. Nat Protoc. 2018;13(4):599–604.

573. Kendal AR, Layton T, Al-Mossawi H, Appleton L, Dakin S, Brown R, et al. Multi-omic single cell analysis resolves novel stromal cell populations in healthy and diseased human tendon. Sci Rep. 2020;10(1):13939.

574. De Micheli AJ, Swanson JB, Disser NP, Martinez LM, Walker NR, Oliver DJ, et al. Single-cell Transcriptomic Analyses Identifies Extensive Heterogeneity in the Cellular Composition of Mouse Achilles Tendons. Am J Physiol Cell Physiol [Internet]. 2020;Sep 2:Epub ahead of print. Available from: http://www.ncbi.nlm.nih.gov/pubmed/32877217

575. Frishberg A, Peshes-Yaloz N, Cohn O, Rosentul D, Steuerman Y, Valadarsky L, et al. Cell composition analysis of bulk genomics using single-cell data. Nat Methods. 2019;16(4):327–32.

576. Rubenstein AB, Smith GR, Raue U, Begue G, Minchev K, Ruf-Zamojski F, et al. Single-cell transcriptional profiles in human skeletal muscle. Sci Rep. 2020;10(1):229.

577. Dyment NA, Hagiwara Y, Matthews BG, Li Y, Kalajzic I, Rowe DW. Lineage Tracing of Resident Tendon Progenitor Cells during Growth and Natural Healing. Asakura A, editor. PLoS One. 2014;9(4):e96113.

578. Czubryt MP. Common threads in cardiac fibrosis, infarct scar formation, and wound healing. Fibrogenesis Tissue Repair. 2012;5(1):19.

579. Best K, Mora K, Knapp E, Buckley M, Loiselle A. Scleraxis-Lineage Cell Depletion Improves Tendon Healing and Disrupts Adult Tendon Homeostasis. bioRxiv [Internet]. 2020;2020.02.01.930255. Available from: https://doi.org/10.1101/2020.02.01.930255

580. Bushweller JH. Targeting transcription factors in cancer — from undruggable to reality. Nat Rev Cancer. 2019;19(11):611–24.

581. Hagenbuchner J, Ausserlechner MJ. Targeting transcription factors by small

compounds—Current strategies and future implications. Biochem Pharmacol. 2016;107:1–13.

582. Inamoto I, Shin JA. Peptide therapeutics that directly target transcription factors. Pept Sci. 2019;111(1):e24048.

583. Eadie AL, Titus AJ, Brunt KR. Getting to the heart of myofibroblast differentiation: implications for scleraxis in ECM remodeling and therapeutic targeting. Am J Physiol Heart Circ Physiol. 2018;315(5):1232–5.

584. Shah M, Foreman DM, Ferguson MWJ. Neutralisation of TGF-beta 1 and TGF-beta 2 or exogenous addition of TGF-beta 3 to cutaneous rat wounds reduces scarring. J Cell Sci. 1995;108(Pt 3):985–1002.

585. Ferguson MW, Duncan J, Bond J, Bush J, Durani P, So K, et al. Prophylactic administration of avotermin for improvement of skin scarring: three double-blind, placebo-controlled, phase I/II studies. Lancet. 2009;373(9671):1264–74.

586. Shah M, Foreman DM, Ferguson MWJ. Control of scarring in adult wounds by neutralising antibody to transforming growth factor β. Lancet. 1992;339(8787):213–4.

587. Kishimoto Y, Ohkawara B, Sakai T, Ito M, Masuda A, Ishiguro N, et al. Wnt/β-catenin signaling suppresses expressions of Scx, Mkx, and Tnmd in tendon-derived cells. Katoh M, editor. PLoS One. 2017;12(7):e0182051.

588. Maffulli N, Moller HD, Evans CH. Tendon healing: can it be optimised? Br J Sports Med. 2002;36(5):315–6.

589. Peled ZM, Rhee SJ, Hsu M, Chang J, Krummel TM, Longaker MT. The Ontogeny of Scarless Healing II: EGF and PDGF-B Gene Expression in Fetal Rat Skin and Fibroblasts as a Function of Gestational Age. Ann Plast Surg. 2001;47(4):417–24.

590. Pierce GF, Brown D, Mustoe TA. Quantitative analysis of inflammatory cell influx, procollagen type I synthesis, and collagen cross-linking in incisional wounds: influence of PDGF-BB and TGF-beta 1 therapy. J Lab Clin Med. 1991;117(5):373–82.

591. Xu J, Clark RAF. Extracellular matrix alters PDGF regulation of fibroblast integrins. J Cell Biol. 1996;132(1):239–49.

592. Harwood FL, Goomer RS, Gelberman RH, Silva MJ, Amiel D. Regulation of alpha(v)beta3 and alpha5beta1 integrin receptors by basic fibroblast growth factor and platelet-derived growth factor-BB in intrasynovial flexor tendon cells. Wound Repair Regen. 1999;7(5):381–8.

593. Nakamura N, Shino K, Natsuume T, Horibe S, Matsumoto N, Kaneda Y, et al. Early biological effect of in vivo gene transfer of platelet-derived growth factor (PDGF)-B into healing patellar ligament. Gene Ther. 1998;5(9):1165–70.

594. Pierce, Ph.D., M.D GF, Mustoe, M.D TA. Pharacologic enhancement of wound healing. Annu Rev Med. 1995;46(1):467–81.

595. Pierce GF, Tarpley JE, Yanagihara D, Mustoe TA, Fox GM, Thomason A. Platelet-derived growth factor (BB homodimer), transforming growth factor-beta 1, and basic fibroblast growth factor in dermal wound healing. Neovessel and matrix formation and cessation of repair. Am J Pathol. 1992;140(6):1375–88.

596. Pierce GF, Vande Berg J, Rudolph R, Tarpley J, Mustoe TA. Platelet-derived growth factor-BB and transforming growth factor beta1 selectively modulate glycosaminoglycans, collagen, and myofibroblasts in excisional wounds. Am J Pathol. 1991;138(3):629–46.

597. Pierce GF, Mustoe TA, Lingelbach J, Masakowski VR, Griffin GL, Senior RM, et al. Platelet-derived growth factor and transforming growth factor-beta enhance tissue repair activities by unique mechanisms. J Cell Biol. 1989;109(1):429–40.

598. Pierce GF, Mustoe TA, Lingelbach J, Masakowski VR, Gramates P, Deuel TF. Transforming growth factor beta reverses the glucocorticoid-induced wound-healing deficit in rats: possible regulation in macrophages by platelet-derived growth factor. Proc Natl Acad Sci. 1989;86(7):2229–33.

599. Buch S, Jones C, Liu J, Han RNN, Tanswell AK, Post M. Differential Regulation of Platelet-Derived Growth Factor Genes in Fetal Rat Lung Fibroblasts. Exp Cell Res. 1994;211(1):142–9.

600. Werner S, Grose R. Regulation of wound healing by growth factors and cytokines. Physiol Rev. 2003;83(3):835–70.

601. Pierce GF, Tarpley JE, Tseng J, Bready J, Chang D, Kenney WC, et al. Detection of platelet-derived growth factor (PDGF)-AA in actively healing human wounds treated with recombinant PDGF-BB and absence of PDGF in chronic nonhealing wounds. J Clin Invest. 1995;96(3):1336–50.

602. Demidova-Rice TN, Hamblin MR, Herman IM. Acute and Impaired Wound Healing. Adv Skin Wound Care. 2012;25(8):349–70.

603. Kiwanuka E, Junker J, Eriksson E. Harnessing Growth Factors to Influence Wound Healing. Clin Plast Surg. 2012;39(3):239–48.

604. Steed DL, Study Group * the DU. Clinical evaluation of recombinant human platelet – derived growth factor for the treatment of lower extremity diabetic ulcers. J Vasc Surg. 1995;21(1):71–81.

605. Yamakawa S, Hayashida K. Advances in surgical applications of growth factors for wound healing. Burn Trauma. 2019;7:10.

606. Suwalski A, Dabboue H, Delalande A, Bensamoun SF, Canon F, Midoux P, et al. Accelerated Achilles tendon healing by PDGF gene delivery with mesoporous silica nanoparticles. Biomaterials. 2010;31(19):5237–45.

607. Mosca MJ, Rashid MS, Snelling SJ, Kirtley S, Carr AJ, Dakin SG. Trends in the theory that inflammation plays a causal role in tendinopathy: a systematic review and quantitative analysis of published reviews. BMJ Open Sport Exerc Med. 2018;4(1):e000332.

608. McClellan A, Evans R, Sze C, Kan S, Paterson Y, Guest D. A novel mechanism for the protection of embryonic stem cell derived tenocytes from inflammatory cytokine interleukin 1 beta. Sci Rep. 2019;9(1):2755.

609. Dakin SG, Dudhia J, Smith RKW. Resolving an inflammatory concept: The importance of inflammation and resolution in tendinopathy. Vet Immunol Immunopathol. 2014;158(3–4):121–7.

610. Morita W, Dakin SG, Snelling SJB, Carr AJ. Cytokines in tendon disease. Bone Joint Res. 2017;6(12):656–64.

611. Liu T, Zhang L, Joo D, Sun S-C. NF-κB signaling in inflammation. Signal Transduct Target Ther. 2017;2:17023.

612. D'Angelo W, Gurung C, Acharya D, Chen B, Ortolano N, Gama V, et al. The Molecular Basis for the Lack of Inflammatory Responses in Mouse Embryonic Stem Cells and Their Differentiated Cells. J Immunol. 2017;198(5):2147–55.

613. Samuel CE. Antiviral actions of interferons. Clin Microbiol Rev. 2001;14(4):778–809.

614. Wang R, Teng C, Spangler J, Wang J, Huang F, Guo Y-L. Mouse Embryonic Stem Cells Have Underdeveloped Antiviral Mechanisms That Can Be Exploited for the Development of mRNA-Mediated Gene Expression Strategy. Stem Cells Dev. 2014;23(6):594–604.

615. Wang R, Wang J, Paul AM, Acharya D, Bai F, Huang F, et al. Mouse embryonic stem cells are deficient in type I interferon expression in response to viral infections and double-stranded RNA. J Biol Chem. 2013;288(22):15926–36.

616. Wang R, Wang J, Acharya D, Paul AM, Bai F, Huang F, et al. Antiviral Responses in Mouse Embryonic Stem Cells. J Biol Chem. 2014;289(36):25186–98.

617. Chen L-L, Yang L, Carmichael G. Molecular basis for an attenuated cytoplasmic dsRNA response in human embryonic stem cells. Cell Cycle. 2010;9(17):3552–64.

618. Chen G-Y, Hwang S-M, Su H-J, Kuo C-Y, Luo W-Y, Lo K-W, et al. Defective Antiviral Responses of Induced Pluripotent Stem Cells to Baculoviral Vector Transduction. J Virol. 2012;86(15):8041–9.

619. Manning CN, Havlioglu N, Knutsen E, Sakiyama-Elbert SE, Silva MJ, Thomopoulos S, et al. The early inflammatory response after flexor tendon healing: A gene expression and histological analysis. J Orthop Res. 2014;32(5):645–52.

620. Thampatty BP, Li H, Im H-J, Wang JH-C. EP4 receptor regulates collagen type-I, MMP-1, and MMP-3 gene expression in human tendon fibroblasts in response to IL-1β treatment. Gene. 2007;386(1–2):154–61.

621. Peters VA, Joesting JJ, Freund GG. IL-1 receptor 2 (IL-1R2) and its role in immune regulation. Brain Behav Immun. 2013;32:1–8.

622. Neofytou E, O'Brien CG, Couture LA, Wu JC. Hurdles to clinical translation of human induced pluripotent stem cells. J Clin Invest. 2015;125(7):2551–7.

623. Donadeu FX, Esteves CL. Prospects and challenges of induced pluripotent stem cells in equine health. Front Vet Sci. 2015;2:59.